# Self-Assembled Monolayers for Biological Applications: Design, Processing, Characterization and Biological Studies

**Adriana R. Kyvik**

Universitat Autònoma
de Barcelona

# Self-Assembled Monolayers for Biological Applications: Design, Processing, Characterization and Biological Studies

Adriana R. Kyvik

Doctor of Philosophy in Materials Science

Director: Dr. Imma Ratera
Tutor: Dr. Cristina Palet Ballús
Chemistry Department, Science Faculty
December 2018

This thesis is presented for the partial fulfillment of the degree of Doctor of Philosophy by:

Adriana Ruiz Kyvik

Accepted by:

Imma Ratera

Cristina Palet Ballús


**Dr. IMMA RATERA**, Scientific Researcher of the Spanish Research Council at the Materials Science Institute of Barcelona (ICMAB-CSIC)

CERTIFIES

That **Adriana R. Kyvik**, Master in Chemical Engineering and Biotechnology, has performed, under her supervision, the research entitled "Self-Assembled Monolayers for Biological Applications: Design, Processing, Characterization and Biological Studies". This work has been performed under the framework of the Materials Science PhD program of the Chemistry Department of the Autonomous University of Barcelona.

And in witness of this, below this is signed,

Director

Dr. Imma Ratera

December, 2018

# Abstract

Self-assembled monolayers (SAMs) on gold surfaces have been designed, processed, characterized and used for specific biological studies. The studies performed include the control of lipid bilayer diffusion, cell adhesion and vascularization studies and also the creation of antimicrobial surfaces.

More specifically, dynamic SAMs on surfaces whose properties can be modified with an electrochemical external stimulus have been developed and used to interrogate biological systems. The developed platform has been applied to two different applications to overcome present challenges when performing biological studies.

Firstly, in Chapter 2, the design and synthesis of all the molecules needed to develop an electroactive platform, its processing as SAMs and the optimization of the surface confined redox process between a non-reactive Hydroquinone (HQ) termination and its corresponding reactive Benzoquinone (BQ) is reported. Two different interfacial reactions taking place on the electroactivated surfaces were studied in detail; the Diels-Alder (DA) and the Michael Addition (MA) interfacial reactions, with cyclopentadiene (Cp) or thiol tagged molecules, respectively. The comparative study between DA and MA as surface functionalization strategies with a temporal control reveal that even though MA is not commonly used for this purpose it offers an attractive strategy for stimulus activated functionalization for biological applications.

In Chapter 3, the developed platform has been used to achieve a temporal control of cell adhesion and in this way mimic *in vivo* conditions more accurately. Cell adhesion plays fundamental roles in biological functions and as such, it is important to control cell adhesion on materials used for biomedical applications. Towards this aim, the dynamic interface developed has been used to immobilize cell adhesion promoting peptides through the two different interfacial reactions, namely the DA and the MA reaction, and a comparative study has been carried out. Moreover, a study involving immobilized VEGF-mimicking peptide Qk has been conducted demonstrating the possibility of using the novel peptide for directing cell differentiation into tubular networks for *in vitro* platforms, by attaching them on a surface.

In Chapter 4, we have used the developed electroactive interface to control the dynamics of lipid bilayers as cell membrane models, designed for transmembrane protein characterization in a more *in vivo* like environment. Specifically, electroactive SAMs have been used to control the moment in which tethering of lipid bilayer deposited on them occurs and consequently decrease its diffusion. In this way, proteins and lipids can maintain their fluidity until tethering is desired, a useful platform for transmembrane protein characterization.

Finally, in Chapter 5, a surface biofunctionalization strategy also based on SAMs has been used to produce a bactericidal surface by successfully immobilizing novel antimicrobial proteins produced by recombinant DNA technology. This is relevant in view of the verge of an imminent antibiotics crisis. To confirm the antimicrobial activity and biofilm growth prevention of these surfaces, a biofilm assay was performed demonstrating that proteins retain their antimicrobial effect when immobilized.

All these strategies open new possibilities for controlled biomolecule immobilization for fundamental biological studies and for applications in biotechnology, in the interface of materials science and biology.

# Abbreviations

**$[Ru(NH_3)_6)]^{3+}$** Hexaammineruthenium(III) Chloride

**AB** Alamar Blue

**AC** Alternate Current

**AIBN** 2,2'-azobisisobutyronitrile

**AMPs** Antimicrobial Peptides and Proteins

**Au** Gold

**BBB** Biological Breadboard

**BLMs** Black Lipid Membranes

**Boc** tert-Butyloxycarbonyl protecting group

**BQ** Benzoquinone

**BSA** Bovine Serum Albumine

**CAM** Cell Adhesion Molecule

**CA** Contact Angle

**CE** Counter Electrode

**CF** Carboxyfluorescein

**Cp** Cyclopentadiene

**Cu** Copper

**CV** Cyclic Voltammetry

**DA** Diels-Alder

**DCM** Dicloromethane

**DIEA** N, N-Diisopropylethylamine

**DMEM** Dulbecco's Modified Eagle Medium

**DMF** Dimethylformamide

**DPN** Dip-Pen Nanolithography

**DPTTE** 1,2-Dipalmitoyl-sn-Glycero-3-Phosphothioethanol (Sodium Salt)

**ECM** Extracellular Matrix

**EDC** 1-Ethyl-3-(3-dimethylaminopropyl)carbodiimide

**EDTA** Ethylenediaminetetraacetic acid

**EGF** Endothelial Growth Factor

**EGM-2** Endothelial Cell Growth Medium

**EG** Ethylene Glycol

**EtOH** Ethanol

**FA** Focal Adhesion

**FITC** Fluorescein isothiocyanate

**GFP** Green Fluorescent Protein

**Gly** Glycine

**GUV** Giant Unilamellar Vesicle

**HCl** Hydrochloric Acid

**$His_6$** 6-Histidine tag

**HOSu** N-Hydroxysuccinimide

**HQ** Hydroquinone

**IB** Inclusion Body or Aggregate

**ICAM** Intercellular Adhesion Molecule

**ITO** Indium Tin Oxide

**KPi** Buffered Potassium Phosphate Solution

**LUV** Large Unilamellar Vesicle

**Lys** Lysine

**MA** Michael Addition

**MetOH** Methanol

**MHC** Multivalent Chelator Headgroups

**MQ** Milli-Q water

**NaH** Sodium Hydride

**NaOH** Sodium Hydroxide

**Ni-NTA** Nickel(II)-chelated Nitrilotriacetic Acid

**NIL** Nanoimprint Lithography

**Ni** Nickel

**NSCs** Neural Stem Cells

**NVOC** Nitroveratryloxycarbonyl

**OEG** Oligo Ethylene Glycol

**p6** petri dish

**PBS** Phosphate Buffer Saline

**PEG** Polyethyleneglycol

**PFA** Paraformaldehyde

**PMA** Phosphomolybdic Acid

**PMMA** Poly(methyl methacrylate)

**POPC** Phosphatidylcholine

**Pt** Platinum

**QCM** Quartz Crystal Microbalance

**RE** Reference Electrode

**RGD** Arginylglycylaspartic acid

**Rho** Rhodamine

**ROI** Region of Interest

**RT** Room Temperature

**SAMs** Self-Assembled Monolayers

**SEM** Standard Error of the Mean

**SLBs** Supported Lipid Bilayers

**SPFS** Surface Plasmon-enhanced Fluorescence Spectroscopy

**SPR** Surface Plasmon Resonance

**SUV** Small Unilamellar Vesicle

**t-BuLi** tert-Buthyl Lithium

**TFA** Trifluoroacetic Acid

**THF** Tetrahydrofuran

**TIS** Triisopropylsilane

**TKR** Tyrosine Kinase Receptor

**tLBMs** Tethered Lipid Bilayers Membranes

**TLC** Thin Layer Chromatography

**U2-OS** Osteoblastoma Sarcoma cells

**VASP** Vasodilator-Stimulated Phosphoprotein

**VCAM** Vascular-Cell Adhesion Molecule

**VEGFR** VEGF Receptor

**VEGF** Vascular Endothelial Growth Factor

**WE** Working Electrode

**XPS** X-Ray Photoelectron Spectroscopy

# Contents

# Introduction and Objectives

# 1

> *The science of today is the technology of tomorrow.*
>
> — **Edward Teller**

## 1.1 Tailored Surfaces for Biological Applications

With the verge of nanoscience and nanotechnology, the creation of new materials, together with the availability of new experimental tools, new strategies have been created to emulate the *in vivo* conditions with more accuracy. This is to be able to understand better how biological systems work and also to develop new materials which resemble these complex biological environments more closely [1, 2]. With these new methodologies materials can be designed and fabricated to perform highly specific and sophisticated interactions with biological compounds and in this way mimic the natural environment of *in vivo* tissues.

In fact, materials used for biomedical applications range a broad spectrum of different uses, in invasive and non-invasive environments; such as materials for medical implants, materials for drug delivery systems or for molecular diagnostics, such as biosensing platforms, or for surgery and clinical therapy [3].

These materials can be either two dimensional (2D) or three dimensional (3D); 3D systems have been very useful for studying the molecular basis of tissue function, for the creation of drug delivery systems or *in vitro* tissue models; 2D systems are useful as coatings for biomedical devices, for *in vitro* systems in fundamental cell behavior studies or for the creation of biosensors [4].

In 2D approaches, typically, surfaces are modified in a controlled manner and depending on the type of processing performed, particular interaction of the surfaces with different biomolecules can tuned [5].

## 1.2 Dynamic Surfaces for Biological Applications

Dynamic surfaces are those platforms developed in which, upon an external stimulus, their surface properties become modulated (Figure 1.1). This external stimulus can take different forms, systems reactive to electrochemical, photochemical, biochemical, change in pH or temperature have been developed to trigger a certain change in the material surface.

These type of sophisticated platforms present interesting properties which can find use in various fields, ranging from biology and medicine to (bio)electronics and material sciences. In fact, the development of such platforms require interdisciplinary expertise [6].

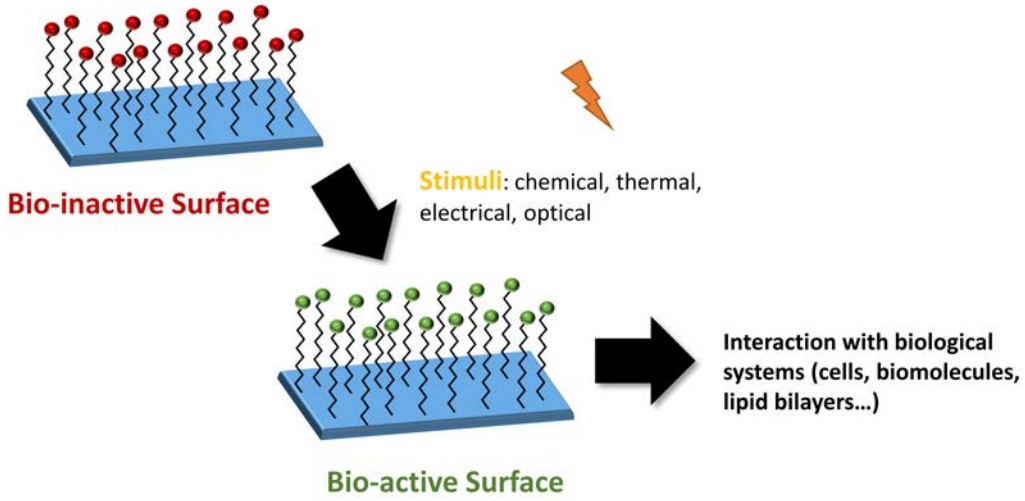


**Figure 1.1:** Schematic representation of a dynamic surface for the use in biological applications. A bio-inactive surface becomes bio-active in presence of an external stimulus, which can be of different nature.

The possibility of modifying the surface of substrates *in vitro* is decisive in order to stimulate the changes in environment recreating those to which a cell would be exposed to during its lifetime within a tissue [7]. Hence, these type of substrates are perfect candidates to accomplish the creation of natural complex systems, emulating *in vivo* conditions in a more accurate manner.

In the field of biology, these type of substrates can provide new insights in several areas, such as new opportunities for mechanistic studies of the pathways by which cells respond to changes in their environments. For example, it is known that dynamic changes in the extracellular matrix (ECM) influence cell behavior in many important contexts, including migration and differentiation of cells during development and also the metastasis of tumor cells. However, studies of these processes are difficult due to the lack of methods that can unambiguously change the properties of the ECM underlying a cell [8].

For these reasons, much research has been done in order to overcome and address this issue, and as a result, different strategies involving stimulus-responsive platforms have been developed to investigate biological systems and obtain more reliable outcomes.

### 1.2.1 Types of Dynamic Substrates

Basically, three different strategies have been used to form dynamic substrates, namely, self-assembled monolayers, polymeric films and hydrogels.

Self-assembled monolayers (SAMs) are highly ordered films that are formed spontaneously on a surface [9] and therefore are widely used for homogeneous surface modification purposes [10]. In addition, the terminal groups of the building blocks of SAMs allow the tuning of the interfacial surface properties, such as its chemical reactivity, conductivity, wettability, adhesion, friction, corrosion resistance and (bio)compatibility, to name some [11].

Polymeric films which are stimulus reactive, suffer a big change in their physicochemical properties in response to a stimulus. To achieve this, responsive moieties are added to different locations of the polymer chain, which in turns yields changes of different nature at the macromolecular level, for example, change in hydrophilicity or solubility [12].

Hydrogels also are interesting since they can be synthesized to change from gel-to-solid or solid-to-gel upon an external stimulus, this being of a physical or chemical nature. They are used in many different platforms especially where 3D matrices are needed, for example in sensing devices or as drug delivery carriers [13].

### 1.2.2 Types of External Stimuli

The main characteristic of these dynamic surfaces is the ability to change the surface properties through the application of an external stimulus, which can be of different nature. This temporal control provides possibilities of gaining insight into fundamental cellular interactions and processes which are still not completely understood, opening up for new biotechnologies [14].

In biomedical sciences these platforms allow the modulation and control of biological interactions and cell behavior in culture [15, 16]. Electrochemical [16, 17], photochemical [18, 19] or biochemical stimulus reactive platforms haven been reported to, for example, turn 'on' and 'off' cell binding *in situ* [20]. In Figure 1.2 different examples or stimulus-responsive interfaces are schematically represented.

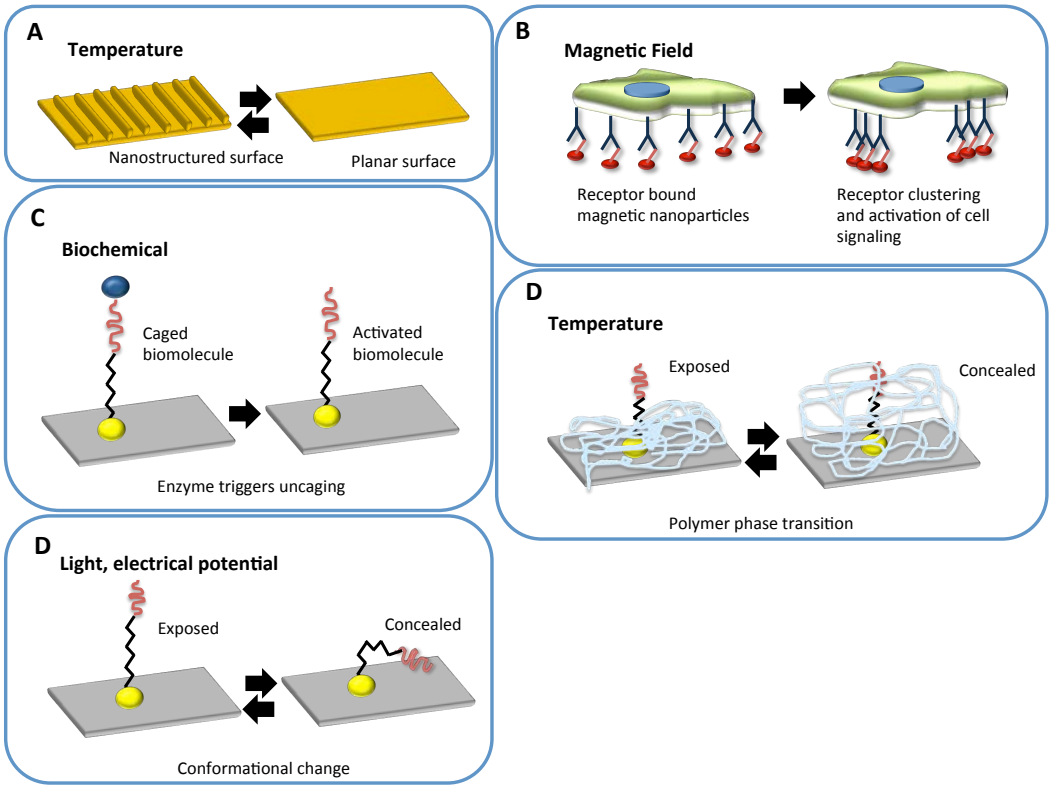


**Figure 1.2:** Schematic representation of examples of stimulus-responsive interfaces used for biological applications. (A) Shape-memory polymer surfaces, which allow the control of the topography via temperature, inducing a certain cell behavior. (B) The use of superparamagnetic nanoparticles (illustrated in color red), linked to a ligand and which bind evenly across the plasma membrane to cell surface receptors. In presence of a magnetic field, the nanoparticles aggregate together forming clusters and this arrangement activates cell signaling. (C) The presence of an enzyme deprotects the caged and immobilized cell adhesion promoting peptide and allows cells to attach. (D) Polymers which are thermo-responsive can be used to cover or uncover a cell adhesion promoting peptide moieties on surface and thereby control cell attachment or detachment. (E) Moieties which are susceptible to electrical potential or exposure to light can be used to control the exposure or the immobilization of biomolecules on surface. Reproduced and modified from [1].

## 1.3 Self-Assembled Monolayers (SAMs)

### 1.3.1 Types of SAMs

SAMs, as previously mentioned, consist of molecular monolayers which form in a spontaneous manner on solid surfaces, either from vapor or liquid [9] (Figure 1.3). This self-assembly phenomenon was firstly observed in 1983 by Nuzzo and Allara, who reported the self-assembly of bifunctional dialkyl disulfides on gold covered surfaces [21].

Different molecules are capable of forming these stable layers on surfaces and depending on the functional group they possess, metals, glass or gold can be used as substrates. For metals, molecules bearing phosphonates are normally used, for glass or hydroxylated surfaces, silanes, and for gold and other metal oxides, thiols [14, 22]. Therefore, SAMs have provided a very useful platform for making fundamental

research in the areas of optoelectronics, environmental monitoring technology, in addition to its use in applications within tissue engineering and for the study of mechanistic cell biology processes [14].

The attracting properties of SAMs are that (i) they allow studies which can probe the dependence of different biological signals in an independent way, especially relevant for stem cell behavior studies, (ii) they can be formed on surfaces which are translucid, allowing the observation of cells with inverted microscopes and thus facilitating time lapse studies, (iii) generally the molecules used for SAMs are commercially available and finally, (iv) SAM preparation is easy and straight forward [23]. In addition, since monolayers can be formed on conducting surfaces this can be exploited for electrochemical modulation of surface molecules by application of a voltage [24].

Importantly, the ability to modify and choose the head and tail group of the molecules forming a SAM, provide a design flexibility and a good model system for studies in different areas [22].

The common features of molecules used for SAM formation consist in (i) a terminal group, which confers the surface specific properties, (ii) a spacer group, generally an alkyl chain which gives place to well ordered monolayers and (iii) the anchoring group, responsible for the interaction between the molecule and the surface, specific for the surface material (Figure 1.3) [14].

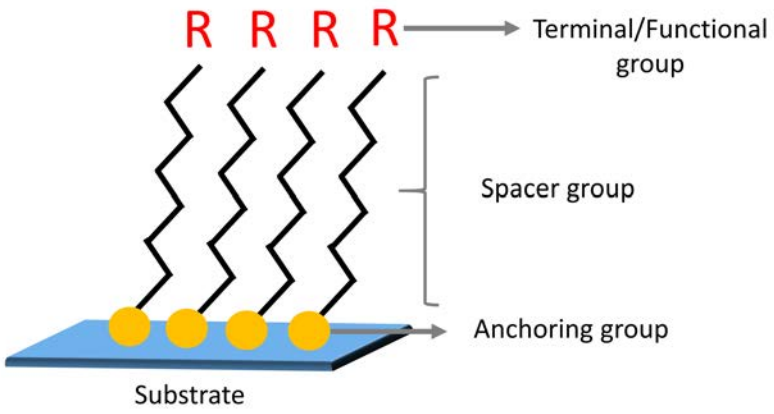


**Figure 1.3:** Schematic representation of an ideal SAM. The terminal group is tunable using organic synthetic procedures, providing a certain surface functionality or reactivity; the alkyl chain enables tight, regular and well ordered molecular packing and the anchoring group immobilizes the molecules on surface and stabilizes the surface atoms and the alkyl chains during packing [14].

**SAMs of Alkanethiols on Gold** One of the most studied platforms are SAMs formed by alkanethiolates on gold: long chain alkanethiolates form densely packed, highly ordered trans-extended monolayers in a rapid and spontaneous manner on gold since the sulfur atoms coordinate to the gold (111) in a densely packed array [24, 25]. Alkanethiolates are readily available from different commercial sources so no previous experience in synthetic chemistry is strictly required to readily form SAMs [23].

### 1.3.2 SAMs for Cell Biology

SAMs have been widely used for studying biological and biochemical processes since they can provide with platforms which mimic more closely *in vivo* conditions, as opposed to traditional cell culture platforms (i.e. petri dishes or flasks). They permit the functionalization of surfaces using molecules containing organic groups with different functionalities, providing cell adhesion or avoiding unspecific adsorption of proteins, nearly with an atomic-level precision [14, 26].

SAMs for biological applications generally need to have three characteristics: (i) they should be able to prevent unspecific adsorption of proteins or other biomolecules, allowing more reliable studies when only the molecules of interest interact with the surface, (ii) SAM molecular composition and density should be controllable and, (iii) molecules immobilized should present the functional groups of interest in a structured manner, in this way minimizing effects of the surface, being these limited mass transport, blocked binding sites or conformational changes [26].

SAMs combined with patterning techniques, so incorporating a way of controlling the spatial distribution of the molecules on surface, have even broadened their usage for biological applications. It has allowed the creation of surfaces which present ligands in a specific manner; having control over the ligand type, the density and the spatial arrangement, and thus being able to perform experiments where effects of molecules can be studied whilst avoiding confounding factors [23].

In addition to this, SAMs are easily characterized using a large number of techniques. These, among many others, have been, x-ray photoelectron spectroscopy (XPS), surface plasmon resonance (SPR), ellipsometry, quartz crystal microbalance (QCM) and mass spectroscopy, to characterize the composition, coverage, thermodynamics and binding processes [14].

#### Protein-Resistant Surfaces

Bio-inert surfaces are those designed to be able to avoid unspecific physical adsorption of biomolecules or cells. These are normally formed using oligo- or poly(ethylene glycol) (OEG or PEG) functional groups. Therefore, alkanethiols incorporating ethylene glycols groups are routinely used in SAMs which are designed for biological and biochemical studies [27, 28], in sight of avoiding unspecific protein adsorption.

The use of pegylated flexible chains creates a hydration layer making protein repealed from the surface (Figure 1.4) [29]. On the contrary, when hydrophobic terminated groups are exposed on the surface, such as methyl groups, protein readily adsorbs onto the surface [26].

Nonetheless, the actual specific requirements for achieving resistance to unspecific adsorption is not yet clear [30], and SAMs with other non-fouling functional groups, such as oligosarcosines, permethylated sorbitol groups, oligosulfoxides, perfluoroalkyls, or oligo(phosphorylcholine) groups have also been used to create bio-inert surfaces [24, 27].

### Mixed SAMs

Generally, to avoid steric hindrance and ensure that the functional groups of interest are properly exposed on the surface, mixed SAMs are used. These are monolayers formed by more than one type of molecule, normally comprising an alkanethiol with a pegylated chain and the alkanethiol with the termination of interest. In biological applications, the termination of interest is normally a reactive site which can act as a linker to a biological ligand [26].

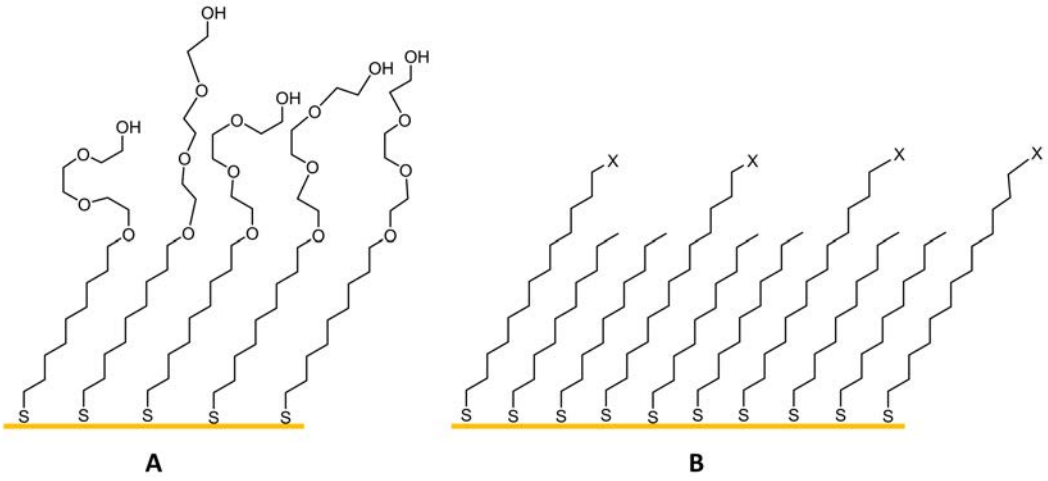


**Figure 1.4:** (A) Pegylated SAM on a gold surface, used as bio-inert surface to avoid unspecific adsorption of protein [24]. (B) Mixed SAM with functional group X exposed on the surface.

### Steps for SAM Formation for Biological Applications

Making SAMs is straight forward, and the standard protocol consists of the following steps: (i) cleansing of the substrate, (ii) SAM formation through liquid or vapor deposition and (iii) conjugation with a biomolecule. Thereafter, depending on the desired application of the system, different steps can be followed. For cell studies, normally cell seeding, cell fixation and immunostaining would proceed. However, DNA, lipid bilayers, antibodies or protein can be conjugated or linked onto the SAM functionalized surface in a controlled manner using different strategies [23].

## 1.4 Patterning Techniques for SAMs

Many different techniques have been used to spatially confine molecules to form SAMs in a determined way. Among these are soft lithography techniques, which have provided the fabrication of elastomeric stamps to use for μCP, one of the most widespread methods for SAM patterning, initially developed by Whitesides [10, 31]. Other techniques used have been microfluidic lithography, photo deprotection, and techniques involving more sophisticated instruments, such as an atomic force microscope.

### 1.4.1 Micro-contact printing

Due to its ease, micro-contact printing (μCP) has been widely used to generate patterned SAMs by stamping alkanethiols onto gold surfaces. In general, a prefabricated polydimethylsiloxane elastomeric stamp (PDMS stamp) is inked with an alkanethiol and then pressed onto a gold surface (Figure 1.5) [32]. This is accomplished by firstly preparing the stamp by making a blend of silicone oligomers with a curing agent that hardens the polymer through cross-linking of the polymer chains. This blend is casted onto a silicon master mold, previously silanized with a hydrophobic silane [10], that has the opposite of the pattern desired. After curing, the flexible PDMS stamp is obtained by peeled it off from the silicon master. Thereafter, the PDMS is inked with the solution containing the SAM forming molecules, either by immersion of the stamp or by coating the stamp with some drops of the molecule solution. Finally, the SAM is formed when the stamp comes into contact with the substrate's surface during a short time. After peeling off the stamp from the substrate, this one presents the pattern transferred from the stamp [33].

#### Backfilling

Bare gold regions of already patterned surfaces can be backfilled with a second type of alkanethiol and in this way create a pattern in which two types of alkanethiols are confined to specific regions. Normally, one of the alkanethiols consists of a pegylated one to avoid unspecific biomolecule adsorption (Figure 1.5). The other molecule sometimes has been a hydrophobic alkanethiol, leading to the adsorption of ECM proteins, such as fibronectin and laminin [23].

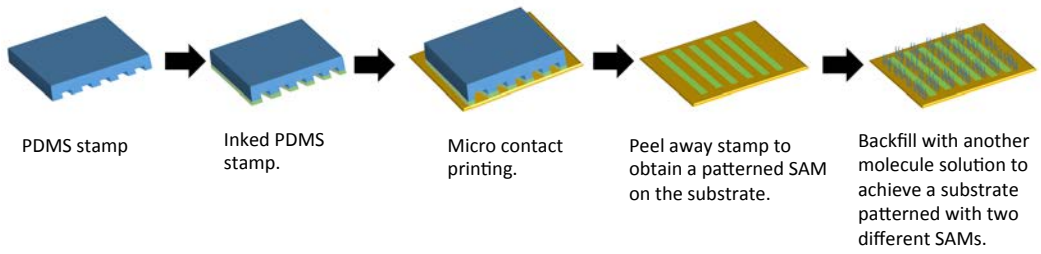


**Figure 1.5:** Schematic representation of the preparation of SAM modified substrates with spatial control of the functionalization. First, μCP is used to pattern a SAM on the bare gold surface and then, subsequently, the non-functionalized areas are backfilled with another SAM.

### 1.4.2 Microfluidic Lithography

Microfluidics has also been used to prepare patterned SAMs in a simple way, by allowing the spatial control of biomolecule conjugation with the use of elastomeric stamps which form channels when in contact with the surface [34]. Basically, a solution of alkanethiol is flowed through the channels formed by the PDMS achieving a spatial arrangement of SAM formation in accordance to the pattern of the channels. Up until now, this technique has been used for the creation of dynamic SAM gradients

for studies of cell polarization, directed cell migration, and contiguous cell co-cultures studies [14, 35].

### 1.4.3 Photochemistry

Photochemistry has been attractive due to its use as a non-invasive way of tailoring the surface composition of SAMs, by using micro-patterned masks to deprotect reactive terminal moieties by their exposure to light [19, 23, 36]. Additionally, to add complexity and create gradients, the use of graded photomasks can be used to immobilize biomolecules with varying density [37].

### 1.4.4 Other Lithographic Techniques

For more sophisticated techniques, more specialized or custom-made equipment is required, however, some advantages are offered by these, which are for example based on atomic force microscopy, such as dip-pen nanolithography [38]. Generally, these techniques are able to create patterms with higher fidelity and resolution, going down to the nano range, and require low sample volumes [14].

## 1.5 Immobilization Strategies using SAMs

As mentioned before, one of the advantages of using SAMs is the versatility offered by the possibility of tailoring molecules with specific anchoring groups using organic chemistry. Nevertheless, when it comes to more complex and bulky molecules, the synthesis becomes challenging and time consuming, as in the case of proteins, carbohydrates or other biomolecules. This can be overcomed by using a second step and immobilizing these biomolecules through a conjugation with the molecules from an already formed SAM. For achieving this, there are different coupling strategies available [14], such as the NTA-Ni SAM strategy for proteins, the carboxylic-amine reactions or the cyclodextrin-biotin interaction. As already mentioned, some developed platforms have been dynamic, which implies that the immobilization of the biomolecule can only take place in presence of an external stimulus, which modifies the initially formed SAM, yielding a reactive surface (Figure 1.6).

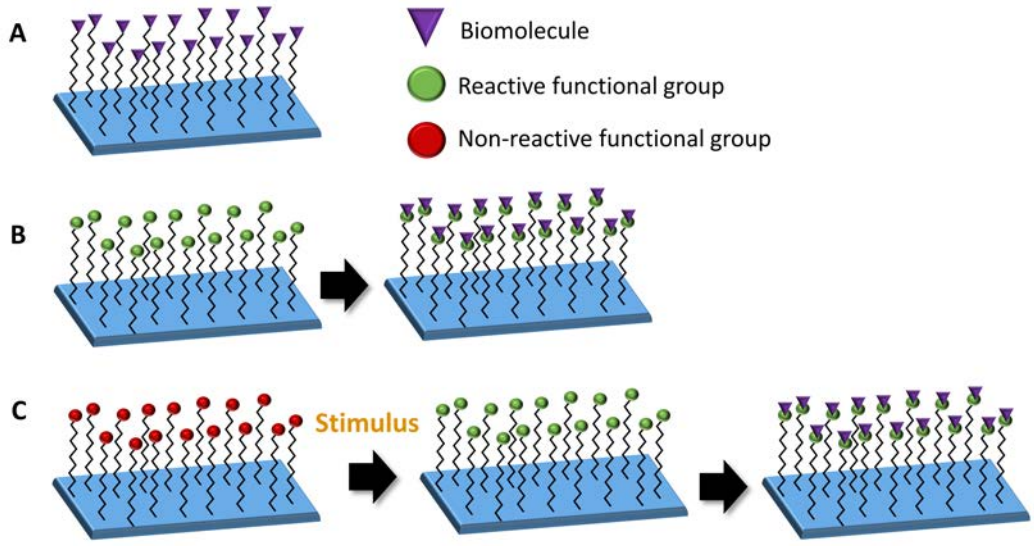


**Figure 1.6:** Schematic representation of different approaches for biomolecule immobilization using SAMs designed for biological applications. (A) Immobilization of the biomolecules directly onto the surface, (B) immobilization of the biomolecules using a preformed SAM and (C) immobilization of the biomolecules using a stimulus responsive SAM.

## 1.6 Analytical Techniques for SAM Characterization

Different techniques have been used to characterize SAMs, evaluating the quality of the films or the chemical nature of these, using techniques which are macroscopic or those that probe the film with molecular resolution [39]. Below, the techniques used in the research presented in this dissertation are briefly introduced.

### 1.6.1 Contact Angle

Contact angle (CA) is used to evaluate the hydrophobicity or hydrophilicity of surfaces. It basically consists in placing a water droplet on a surface to measure the angle between the surface and the liquid. The more hydrophilic the surface, the lower the contact angle measured, as opposed to hydrophobic surfaces, which have high contact angles. CA provides a way to estimate the quality of the functionalization and assess the wettability of the surface [39].

### 1.6.2 Cyclic Voltammetry

Cyclic voltammetry (CV) is an electrochemical technique which is used to investigate the reduction and oxidation processes of electroactive molecular species. The information retrieved from this technique is displayed in cyclic voltammograms: in the x-axis the applied potential is represented, which is the parameter controlled by the user, while in the y-axis, the resulting current is portrayed, which is the response. Following two different types of conventions, the US and the IUPAC, as shown in Figure 1.7, the lower potentials are displayed on the left (IUPAC) or on the right (US). The scan rate determines how fast the potential is scanned and faster scan rates lead to a decrease of the diffusion layer, giving place to higher currents [40].

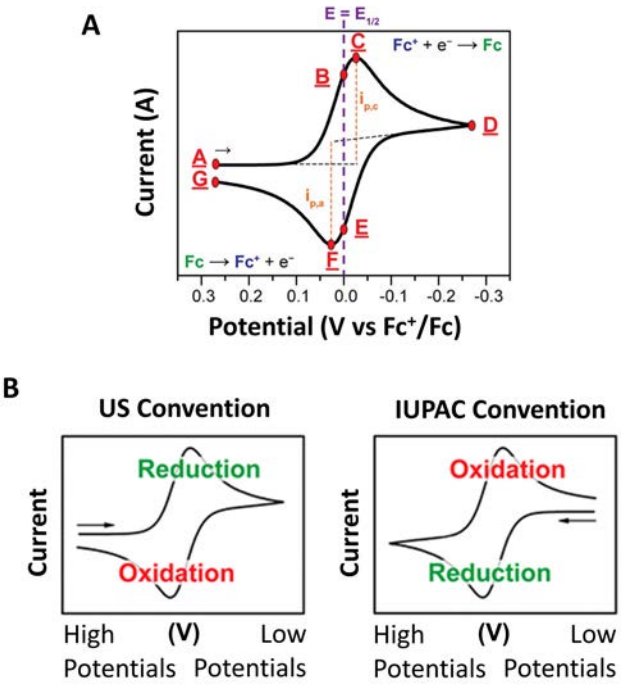


**Figure 1.7:** (A) Characteristic cyclic voltammogram. (B) Voltammograms in the US and the IUPAC convention: the arrow indicates the direction in which the potential is scanned to record the data. Reproduced from [40].

The current peaks observed in voltammograms, as seen in Figure 1.7, are produced as a result of a formed layer of reduced X (species of analysis) at the surface of the electrode, which hinders the diffusion of additional X+ to the electrode, decreasing the current as the scan continues.

The conventional 3-electrode electrochemical cell setup is composed of the following electrodes (Figure 1.8): (i) the reference electrode (RE), which has a well-known and stable equilibrium potential. Its function is to be the reference point against which the potential of other electrodes can be measured. One of the most commonly used is the Ag/AgCl electrode; (ii) the working electrode (WE), in which the reaction of interest takes place. A potentiostat is used to control the applied potential of the WE as a function of the RE potential; (iii) the counter electrode (CE), whose purpose is to complete the electrical circuit. A typical CE is a platinum wire, since it should be made of a material which is as inert as possible. Although there is electron transfer during the duration of the CV, the electrical neutrality is maintained thanks to the migration of ions in solution. The electrolyte solution is the mixture of a solvent and a supporting electrolyte and it should be electrochemically inert in the conditions of the experiment [40].

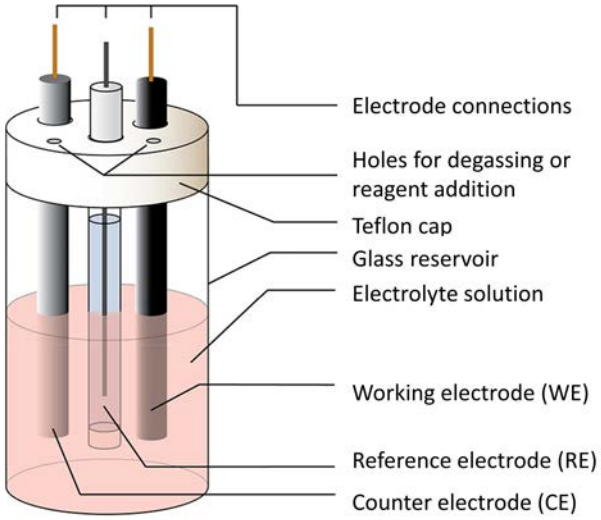


**Figure 1.8:** Conventional 3-electrode setup consisting in a working electrode (WE), a reference electrode (RE) and a counter electrode (CE) immersed within the electrolyte solution.

The use of electrochemistry with SAMs not solely provides a way to analyze the formed monolayer but also gives tools to be able to control the reactivity of surface tethered electroactive molecules by changing their redox state [39].

Commonly, the formation of electroactive SAMs can be characterized by measuring the current intensity versus the scan rate and if a linear relationship is obtained, this indicates that the molecules are surface confined, since the surface tethering of electroactive molecules minimizes the effect of the diffusion of electrons [26]. In fact, this relationship is what is expected for a rapid reversible redox process of an immobilized redox couple on a surface [41, 42].

Furthermore, the surface coverage of electroactive SAMs can be estimated by integrating the oxidation or reduction peak area obtained from a CV and applying the Equation 1.1.

$$Q = nFA\Gamma \tag{1.1}$$

In this equation, Q is the total charge, n is the number of electrons involved in the redox couple, F is Faraday's constant, A is the surface area of the electrode that is in contact with the electrolyte and $\Gamma$ is the surface coverage in mol·cm$^{-2}$.

### 1.6.3 X-Ray Photoelectron Spectroscopy

X-ray photoelectron spectroscopy (XPS) is one of the most widely used techniques to obtain information about the elemental composition and chemical environment of the atoms of the near surface region (less than 10 nm) having a sensitivity in the range of 0.1 (atomic)% [43]. The instrumentation used for this technique is the photoelectron spectrometer (Figure 1.9). The physical principle behind this technique is the photoelectric effect, in which an electron initially bound to an atom/ion is ejected by a photon. Since photons are a massless and chargeless package of energy, they are annihilated during their photo-electron interaction, and

thus, they transfer all their energy to the electron. If this energy is large enough, the electron will be emitted not only from the atom/ion, but from the solid as well [44]. Then, the electron can be detected and its kinetic energy measured. The kinetic energy is a function of the electrons binding energy, which in turn, gives information about the element and chemical environment. Since the binding energy is independent of the X-ray energy, the data is represented in a spectrum as a function of the binding energy, which can be calculated by the initial photon energy and the kinetic energy through the Einstein (1905) expression [45].

Although X-rays can penetrate micrometers below the surface, when a photoelectron is produced at a depth higher than 10 nm, it loses energy and the signal disappears in the background of the spectrum. Hence, this technique ensures that the discrete signals that are displayed come from the surface alone [44].

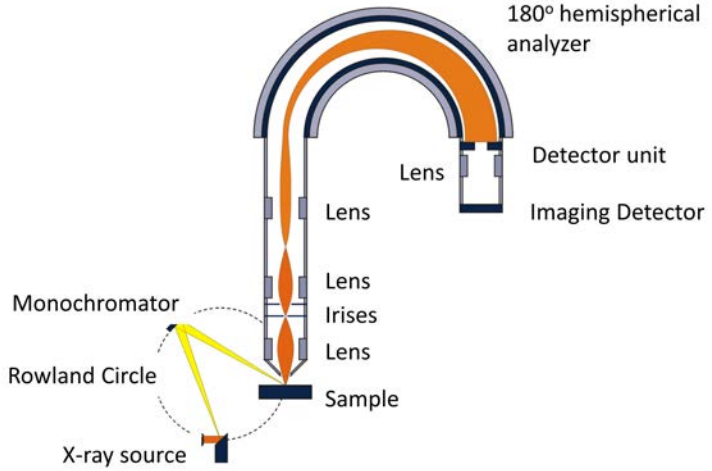


**Figure 1.9:** Main components of a photoelectron spectrometer.

### 1.6.4 Atomic Force Microscopy

Atomic force microscopy (AFM) is one of the techniques used to obtain structural information of the surface with a spatial resolution up to a subnanometer level [46]. It employs a sharp tip to raster the sample by scanning over its surface while sensing the interaction between the tip and the sample [47]. The tip is placed at the end of a flexible cantilever that is mounted on a piezoelectric material that acts as a moving scanner in three dimensions. During the sample analysis, a laser diode emits a laser beam onto the back of the cantilever over the tip. The interaction force between the tip and the sample makes the cantilever deflect to a certain degree, which in turn, causes the angular deflection of the reflected laser beam. The amount of the beam deflection is detected by a position-sensitive photodiode [48]. See Figure 1.10 for a schematic representation.

There are several modes in which AFMs can operate, to create or characterize patterned SAMs at the nanoscale [39]. In contact mode, the movement in the z-axis is used to maintain the force constant, while the movements in the x- and y-axis are used to move the sample so the tip scans the desired surface area. In this mode, the cantilever deflection is the feedback parameter and the resulting data of the

tip's relative distance from the surface at different x-y values can be mapped into a topographical image of the scanned area [49].

On the other hand, non-contact mode employs a small piezoelectric element placed under the cantilever to make it oscillate at, or closer to, its resonance frequency [50]. This oscillation is modified when the cantilever is brought to 10-100 nm from the sample surface due to interaction forces between the tip and the surface, such as Van der Waals, electrostatic, capillary and magnetic forces [51]. This oscillation change implies a decrease in resonant frequency and amplitude in addition to a phase shift. Therefore, this mode is useful to characterize the amplitude modulation, which can provide information about the topography; the frequency modulation, which informs about the sample's properties; and phase shifts, which allows the differentiation of materials. The phase shift imaging is one of the most common AFM methods used because it provides a contrast image based on material properties, such as adhesion, stiffness, dissipation and viscoelasticity [52].

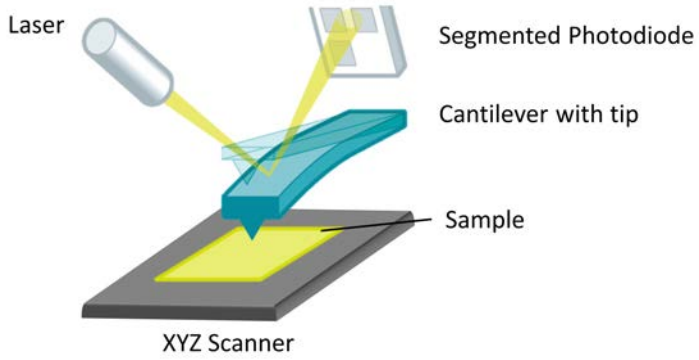


**Figure 1.10:** AFM working basic mechanism.

## 1.7 General Objectives

With the aim of overcoming existing biological challenges such as (i) the creation of surfaces which emulate more precisely *in vivo* environments for fundamental cell behavior studies, (ii) surfaces capable of tethering lipid bilayers as cell membrane models with a temporal control for better characterization of embedded proteins and (iii) the creation of novel antimicrobial surfaces, in this PhD dissertation the main objective is the preparation of SAMs for biological applications.

Towards this aim, a dynamic SAM based on an electroactive building block will be used and its capability for carrying out stimulus responsive interfacial reactions will be investigated. Specifically, two interfacial reactions will be studied and compared, namely the Diels-Alder and the Michael Addition reaction. Once optimized, this platform will be used for two different biologically relevant applications: (i) for the controlled diffusion of lipid bilayers, as cell membrane models, and (ii) for controlled cell adhesion and differentiation studies. Furthermore, using the NTA-Ni SAM strategy, antimicrobial proteins will be immobilized on surfaces and characterized

using a multi-technique approach. Finally, a biofilm assay will be conducted to evaluate the bactericidal properties of the modified surfaces.

To carry out these general objectives, the we will focus on the following specific tasks:

- In Chapter 2, the design, synthesis and characterization of an electroactive SAM for electroactivation of interfacial reactions. Comparison of two interfacial reactions, namely the Diels-Alder and the Michael Addition reactions.
- In Chapter 3, by using the platform obtained in Chapter 2, compare the immobilization of a cell adhesion promoting peptide through the Diels-Alder and the Michael Addition interfacial reactions. Evaluate cell adhesion by quantification of cell density, cell spreading and focal adhesion area.
- In Chapter 4, by using the platform obtained in Chapter 2, study the controlled tethering of lipid bilayers as cell membrane models using an external stimulus. Study the control of diffusion coefficient of electroactivated surface tethered lipid bilayers with the fluorescence recovery after photobleach technique.
- In Chapter 5, preparation and characterization of SAMs with immobilized antimicrobial proteins for the creation of bactericidal surfaces. Evaluation of the activity of the modified surfaces using a biofilm assay.

In Chapter 6 all the experimental details are described.

# References


[1] P. M. Mendes. „Chemical Society Reviews Cellular nanotechnology: making biological interfaces smarter“. In: *Chem. Soc. Rev. Chem. Soc. Rev* 42.42 (2013), pp. 9207–9218 (cit. on pp. 1, 4).

[2] E. Wischerhoff, N. Badi, J. F. Lutz, and A. Laschewsky. „Smart bioactive surfaces“. In: *Soft Matter* 6.4 (2010), pp. 705–713 (cit. on pp. 1, 66).

[3] K. Balani, R. Narayan, and A. Agarwal. „Surface Engineering and Modification for Biomedical Applications“. In: *Biosurfaces, Chapter 7*. 2015, pp. 201–238 (cit. on p. 1).

[4] K. Duval, H. Grover, L. Han, et al. „Modeling Physiological Events in 2D vs. 3D Cell Culture“. In: *Physiology* 32.4 (2017), pp. 266–277 (cit. on p. 1).

[5] R. Hauert. „A review of modified DLC coatings for biological applications“. In: *Diamond and Related Materials* 12 (2003), pp. 583–589 (cit. on p. 1).

[6] J. J. Gooding, S. G. Parker, . Lu, and K. Gaus. „Molecularly Engineered Surfaces for Cell Biology: From Static to Dynamic Surfaces“. In: *Langmuir* 30.12 (2014), pp. 3290–3302 (cit. on p. 1).

[7] F. Meiners, I. Plettenberg, J. Witt, et al. „Local control of protein binding and cell adhesion by patterned organic thin films“. In: *Analytical and Bioanalytical Chemistry* 405.11 (2013), pp. 3673–3691 (cit. on pp. 2, 61, 62).

[8] M. Mrksich. „A surface chemistry approach to studying cell adhesion“. In: *The Royal Society of Chemistry* 29 (2000), pp. 267–273 (cit. on p. 2).

[9] A. Pulsipher and M. N. Yousaf. „Surface chemistry and cell biological tools for the analysis of cell adhesion and migration“. In: *ChemBioChem* 11.6 (2010), pp. 745–753 (cit. on pp. 2, 4, 66).

[10] J. Tien, Y. Xia, and G. M. Whitesides. „Microcontact Printing of SAMs“. In: *Thin Films* 24 (1998) (cit. on pp. 2, 7, 8).

[11] C. D. Bain, J. Evall, and G. M. Whitesides. „Formation of Monolayers by the Coadsorption of Thiols on Gold: Variation in the Head Group, Tail Group, and Solvent“. In: *Journal of the American Chemical Society* 43.2 (1989), pp. 51–45 (cit. on pp. 2, 62).

[12] J.-K. Chen and C.-J. Chang. „Fabrications and Applications of Stimulus-Responsive Polymer Films and Patterns on Surfaces: A Review.“ In: *Materials* 7.2 (2014), pp. 805–875 (cit. on p. 3).

[13] I. Willner. „Stimuli-Controlled Hydrogels and Their Applications“. In: *Accounts of Chemical Research* 50 (2017), p. 50 (cit. on p. 3).

[14] A. Pulsipher and M. N. Yousaf. „Self-Assembled Monolayers as Dynamic Model Substrates for Cell Biology“. In: *Advanced Polymer Science* 240 (2010), pp. 103–134 (cit. on pp. 3–6, 9, 27).

[15] N. Li, A. Tourovskaia, and A. Folch. „Biology on a Chip: Microfabrication for Studying the Behavior of Cultured Cells“. In: *Critical Reviews in Biomedical Engineering* 31 (2003), pp. 423–488 (cit. on p. 3).

[16] W.-S. Yeo, M. N. Yousaf, and M. Mrksich. „Dynamic Interfaces between Cells and Surfaces: Electroactive Substrates that Sequentially Release and Attach Cells“. In: *Journal of the American Chemical Society* 125.49 (2003), pp. 14994–14995 (cit. on pp. 3, 25).

[17] C. Chi Albert Ng, A. Magenau, S. H. Ngalim, et al. „Using an Electrical Potential to Reversibly Switch Surfaces between Two States for Dynamically Controlling Cell Adhesion“. In: *Angewandte Chemie* 51.31 (2012), pp. 7706–10 (cit. on pp. 3, 66).

[18] R. N. Andrews, K.-S. Mun, C. Scott, et al. „Rapid prototyping of heterotypic cell–cell contacts“. In: *Journal of Materials Chemistry B* 1.42 (2013), p. 5773 (cit. on p. 3).

[19] W. S. Dillmore, M. N. Yousaf, and M. Mrksich. „A Photochemical Method for Patterning the Immobilization of Ligands and Cells to Self-Assembled Monolayers“. In: *Langmuir* 20.17 (2004), pp. 7223–7231 (cit. on pp. 3, 9, 31, 36).

[20] A. Pulsipher, S. Park, D. Dutta, W. Luo, and M. N. Yousaf. „*In situ* modulation of cell behavior via smart dual-ligand surfaces.“ In: *Langmuir* 30.45 (2014), pp. 13656–13666 (cit. on p. 3).

[21] R. G. Nuzzo and D. L. Allara. „Adsorption of Bifunctional Organic Disulfides on Gold Surfaces“. In: *Journal of the American Chemical Society* 105.13 (1983), pp. 4481–4483 (cit. on p. 4).

[22] A. Ulman. „Formation and Structure of Self-Assembled Monolayers“. In: *Chemical Reviews* 96.4 (1996), pp. 1533–1554 (cit. on pp. 4, 5).

[23] J. T. Koepsel and W. L. Murphy. „Patterned Self-Assembled Monolayers: Efficient, Chemically Defined Tools for Cell Biology“. In: *Chembiochem* 12.12 (2012), pp. 1717–1724 (cit. on pp. 5–9).

[24] J. S. Rudra, S. H. Kelly, and J. H. Collier. *Self-Assembling Biomaterials*. Elsevier, 2017, pp. 67–89 (cit. on pp. 5–7).

[25] C. Pale-Grosdemange, E. S. Simon, K. L. Prime, and G. M. Whitesides. „Formation of self-assembled monolayers by chemisorption of derivatives of oligo(ethylene glycol) of structure $HS(CH_2)_{11}(OCH_2CH_2)$textsubscriptmOH on gold.“ In: *Journal of the American Chemical Society* 113.1 (1991), pp. 12–20 (cit. on p. 5).

[26] J. C. Love, L. A. Estroff, J. K. Kriebel, N. Ralph G., and G. M. Whitesides. „Self-Assembled Monolayers of Thiolates on Metals as a Form of Nanotechnology“. In: *Chem. Rev.* 105 (2005), pp. 1103–1169 (cit. on pp. 6, 7, 12, 27, 28, 31, 35, 39, 48).

[27] J. Robertus, W. R. Browne, and B. L. Feringa. „Dynamic control over cell adhesive properties using molecular-based surface engineering strategies“. In: *Chemical Society reviews* 39.1 (2010), pp. 354–78 (cit. on pp. 6, 26, 30).

[28] E. Ostuni, R. G. Chapman, M. N. Liang, et al. „Self-Assembled Monolayers That Resist the Adsorption of Proteins and the Adhesion of Bacterial and Mammalian Cells“. In: *Langmuir* 17 (2001), pp. 6336–6343 (cit. on p. 6).

[29] M. Cerruti, S. Fissolo, C. Carraro, et al. „Poly(ethylene glycol) monolayer formation and stability on gold and silicon nitride substrates“. In: *Langmuir* 24.19 (2008), pp. 10646–10653 (cit. on p. 6).

[30] J. D. Cox, M. S. Curry, S. K. Skirboll, P. L. Gourley, and D. Y. Sasaki. „Surface passivation of a microfluidic device to glial cell adhesion: a comparison of hydrophobic and hydrophilic SAM coatings“. In: *Biomaterials* 23.3 (2002), pp. 929–935 (cit. on p. 6).

[31] C. S. Chen, M. Mrksich, S. Huang, G. M. Whitesides, and D. E. Ingber. „Micropatterned Surfaces for Control of Cell Shape, Position, and Function“. In: *Biotechnology Progress* 14.3 (1998), pp. 356–363 (cit. on pp. 7, 65).

[32] V. Santhanam and R. P. Andres. „Microcontact Printing of Uniform Nanoparticle Arrays“. In: *Nano Letters* 4.1 (2004), pp. 41–44 (cit. on p. 8).

[33] F. M. Wisser, B. Schumm, G. Mondin, J. Grothe, and S. Kaskel. „Precursor strategies for metallic nano- and micropatterns using soft lithography“. In: *Journal of Materials Chemistry C* 3.12 (2015), pp. 2717–2731 (cit. on p. 8).

[34] G. A. Hudalla, N. A. Kouris, J. T. Koepsel, B. M. Ogle, and W. L. Murphy. „Harnessing endogenous growth factor activity modulates stem cell behavior“. In: *Integrative Biology* 3.8 (2011), pp. 832–842 (cit. on p. 8).

[35] B. M. Lamb, N. P. Westcott, and M. N. Yousaf. „Microfluidic Lithography to Create Dynamic Gradient SAM Surfaces for Spatio-temporal Control of Directed Cell Migration“. In: *ChemBio* 9 (2008), pp. 2628–2632 (cit. on p. 9).

[36] E. W. L. Chan, S. Park, and M. N. Yousaf. „An electroactive catalytic dynamic substrate that immobilizes and releases patterned ligands, proteins, and cells“. In: *Angewandte Chemie* 47.33 (2008), pp. 6267–6271 (cit. on pp. 9, 30, 66).

[37] E.-J. Lee, E. W. L. Chan, and M. N. Yousaf. „Spatio-Temporal Control of Cell Coculture Interactions on Surfaces“. In: *ChemBioChem* 10.10 (2009), pp. 1648–1653 (cit. on p. 9).

[38] C.-C. Wu, D. N. Reinhoudt, C. Otto, V. Subramaniam, and A. H. Velders. „Strategies for Patterning Biomolecules with Dip-Pen Nanolithography“. In: *Small* 7.8 (2011), pp. 989–1002 (cit. on p. 9).

[39] R. K. Smith, P. A. Lewis, and P. S. Weiss. „Patterning self-assembled monolayers“. In: *Progress in Surface Science* 75.1-2 (2004), pp. 1–68 (cit. on pp. 10, 12, 13).

[40] P. Krysinski, M. R. Moncelli, and F. Tadini-Buoninsegni. „A voltammetric study of monolayers and bilayers self-assembled on metal electrodes“. In: *Electrochimica Acta* 45.12 (2000), pp. 1885–1892 (cit. on pp. 10, 11, 146).

[41] H. Ju and D. Leech. „Effect of electrolytes on the electrochemical behaviour of 11-(ferrocenylcarbonyloxy)undecanethiol SAMs on gold disk electrodes“. In: *Physical Chemistry Chemical Physics* 1.7 (1999), pp. 1549–1554 (cit. on p. 12).

[42] H.-G. Hong and W. Park. „Electrochemical characteristics of hydroquinone-terminated self-assembled monolayers on gold“. In: *Langmuir* 17.8 (2001), pp. 2485–2492 (cit. on pp. 12, 29, 30, 35, 40).

[43] X. Zhang and M. Cresswell. „Materials Characterization of Inorganic Controlled Release“. In: *Inorganic Controlled Release Technology*. Elsevier, 2016, pp. 57–91 (cit. on p. 12).

[44] P. van der Heide. *X-ray Photoelectron Spectroscopy: An introduction to Principles and Practices*. John Wiley & Sons, 2011, p. 264 (cit. on p. 13).

[45] P. G. Zambonin and E. Desimoni. „X-Ray Photoelectron Spectroscopy: Principles, Instrumentation, Data Processing and Molten Salt Applications“. In: *Molten Salt Chemistry*. Dordrecht: Springer Netherlands, 1987, pp. 425–445 (cit. on p. 13).

[46] H. Yang, Y. Wang, S. Lai, et al. „Application of Atomic Force Microscopy as a Nanotechnology Tool in Food Science“. In: *Journal of Food Science* 72.4 (2007), R65–R75 (cit. on p. 13).

[47] Y. F. Dufrêne. „AFM for nanoscale microbe analysis“. In: *The Analyst* 133.3 (2008), pp. 297–301 (cit. on p. 13).

[48] M. H. Fulekar and B. Pathak. *Environmental nanotechnology* (cit. on p. 13).

[49] R. M. Twyman. *Atomic Force Microscopy Methodologies*. 2009 (cit. on p. 14).

[50] Y. Martin, C. C. Williams, and H. K. Wickramasinghe. „Atomic force microscope-force mapping and profiling on a sub 100-Å scale“. In: *Citation: Journal of Applied Physics* 61.10 (1987), p. 4723 (cit. on p. 14).

[51] D. Rugar and P. Hansma. „Atomic Force Microscopy“. In: *Physics Today* 43.10 (1990), pp. 23–30 (cit. on p. 14).

[52] N. F. Martínez and R. García. „Measuring phase shifts and energy dissipation with amplitude modulation atomic force microscopy“. In: *Nanotechnology* 17.7 (2006), S167–S172 (cit. on p. 14).

# 2 Stimuli-Activated Functionalization Strategies to Spatially and Temporally Control Surface Properties: Michael vs. Diels-Alder Type Additions

> *Organic chemistry is the chemistry of carbon compounds. Biochemistry is the study of carbon compounds that crawl.*
>
> — **Mike Adams**

## 2.1 Introduction

### 2.1.1 Electroactive SAMs

With the aim of gaining more control over surface functionalization of materials, the design and synthesis of dynamic SAMs has been one of the strategies pursued by many. Among these, are those which are switched by an external electrochemical stimulus: they present an interesting platform since they allow the modification of surface properties on demand (Figure 2.1). For example, by conferring switchable physical chemical or biological properties which can be tuned in a predictable and accurate way at a given time [16, 53–55].

This strategy requires the use of molecules which bear electroactive groups, since these possess the property of undergoing oxidation and reduction by the application of a positive or negative potential. Actually, redox active SAMs have been extensively used in studies of electron transfer since they provide a robust platform for the investigation of electron transfer kinetics [56]. Some examples are the use of SAMs with ferrocene terminated molecules [57], or those with fullerene [58], porphyrins [59], quinones [53, 60] and also tetrathiafulvalene termination [61]: all these have been used for a wide range of applications including charge transport, protein immobilization and cell guidance. Wettability changes of surfaces when applying a voltage has also been explored by using electroactive SAMs [55].

Basically, the application of a generally low voltage onto surfaces functionalized with electroactive SAMs, induces a change in the terminal functionalities of the SAM [62] thereby allowing, for example, a click reaction to take place on demand [63] or a conformation change which can provide useful information and become the base of biosensing platforms [64, 65].

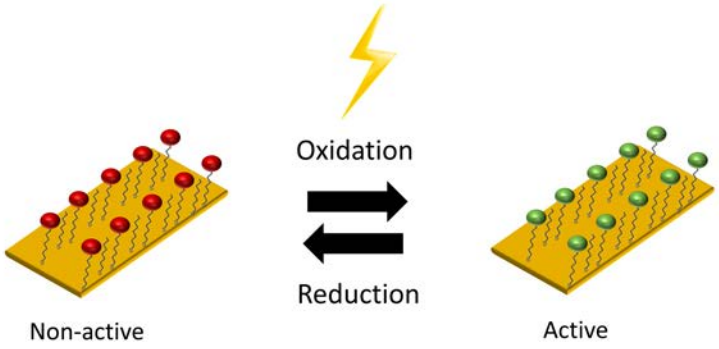


**Figure 2.1:** Schematic representation of the oxidation and reduction process of electroactive SAMs in presence of an external electrochemical stimulus.

### Electrochemical Induced Interfacial Reactions

The simplest approach for the immobilization of biomolecules via the use of SAMs involves surface tethering of the biomolecules of interest by synthesizing thiol-modified biomolecules or taking advantage of the thiols present in the cysteine amino acids, sometimes already present in the biomolecules. However, this presents some inconveniences, such as the lack of a spacer group which normally provides a well compacted and organized monolayer, or the lack of control in the orientation of the biomolecules. A second approach would consist in a two step process: firstly, the creation of monolayers with reactive terminal groups and secondly, performing an interfacial reaction with the biomolecule of interest in order to immobilize it. A third approach, and the one we will exploit, is the creation of a stimulus-responsive monolayer, which in the first instance is non-reactive towards the biomolecule of interest, but upon exposure to an external stimulus, becomes reactive to the biomolecule. See Figure 1.6 for a schematic illustration of these three approaches.

In fact, the ability to immobilize ligands on a surface on demand through a multi-step process using an external stimulus, such as the application of a low voltage, is interesting since the synthesis of large and complex molecules limits the control over surface density. Furthermore, monolayers composed by large molecules are more prone to have defects, which in turn leads to more non-specific biomolecule adsorption [27]. Therefore, the ability to generate small reactive groups on surface on demand, which are capable of immobilizing ligands such as large biomolecules via a second step, is of high interest.

Nonetheless, these stimulus-reactive surfaces are very relevant in biological sciences specially to study cell-material interaction, since the temporal control of the surface modification allows the study of time dependent processes and, in addition, allow the design of time lapse experiments, impossible of performing with static platforms.

For this purpose, different electrochemical reactive SAMs have been studied and used for biological studies, especially those functionalized surfaces based on the Hydroquinone/Benzoquinone redox couple. This platform, developed by Mrksich

and Yousaf, has shown to provide a real time control over molecular interactions between functionalized surfaces, biomolecules and cells [14, 66].

Another strategy for the immobilization of molecules using an electrochemical stimulus has been the use of $Cu^{1}$ catalyzed Huisgen cycloaddtion click reactions, between alkyne and azide (Figure 2.2). Choi et al. have reported a strategy using masked acetylene-terminated alkanethiolates: upon oxidation the acetylene groups become exposed and thus a click reaction can take place with azide functionalized molecules [54].

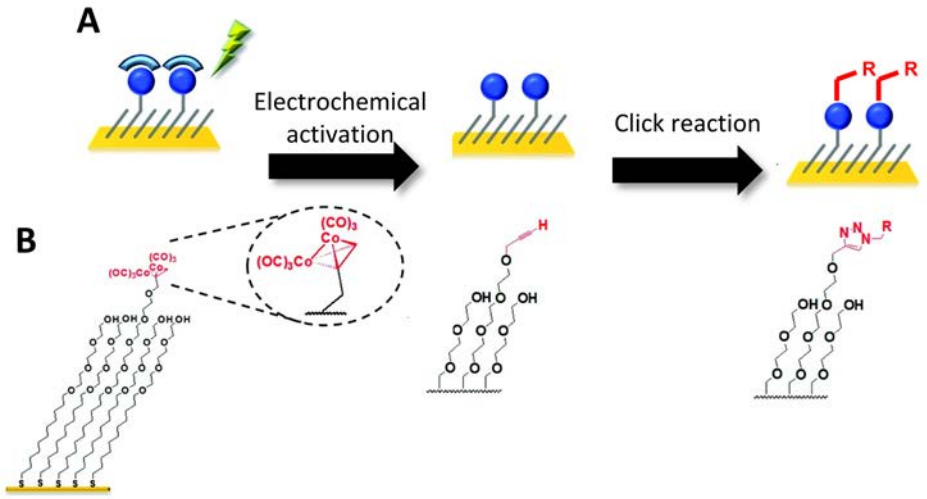


**Figure 2.2:** Schematic representation of the strategy used by Choi et al. for the stimulus responsive stepwise peptide immobilization. (A) On demand activation of the peptide tethering and (B) the chemical structure of the SAM. Reproduced with permission from [54].

Also, aromatic nitro groups on surface have been used to be electrochemically converted to amino groups by applying a negative potential in a selective way for further protein immobilization. This was done by using a homobifunctional linker, reactive with the amino group on surface and with the amino groups in primary antibodies [67].

Another electroactive platform developed by Li et al. [68] consisted in SAMs of trimethoxybenzene moieties, which also allowed a stimulus responsive stepwise surface modulation with the application of a voltage. This allowed not only the immobilization of a peptide, but furthermore, the control of its configuration on surface. The study involved tethering linear arginylglycylaspartic acid (RGD) molecules, a cell adhesion promoting peptide (see Section 3.1.3 for more information), which were, in a second step, converted into its cyclic conformation (Figure 2.3). This was done by using RGD peptides modified with cysteines, since these can react with 1,2-benzoquinones, resulting in a benzothiazine [69].

Potentials used for these applications should not harm cells or compromise the SAM, and therefore, normally these are never higher than 1 V for oxidative processes and lower than -1 V for reductive ones, since the application of lower voltages leads to SAM desorption [26, 70].

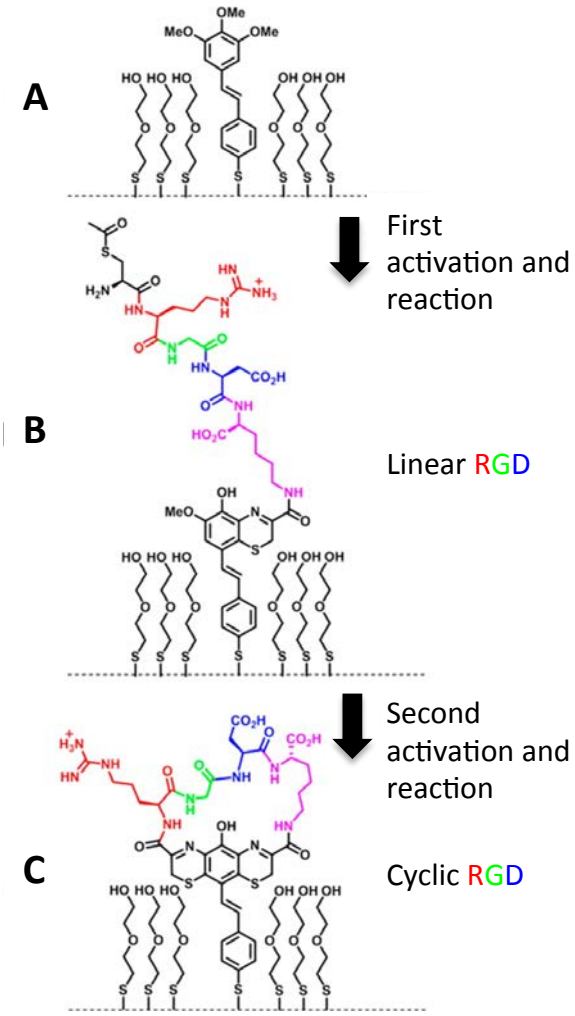


**Figure 2.3:** Immobilization of linear and cyclic RGD peptides upon an electrochemical stimulus. (A) Structure of the mixed SAMs, (B) SAM after electrochemical activation and reaction with the linear RGD peptide, (C) after the second electrochemical activation and reaction the linear RGD peptide can change into its cyclic conformation. Reproduced and modified with permission from [68].

### 2.1.2 SAM Desorption

Interesting for some applications is the use of applied voltage for SAM desorption. Thiols undergo reductive desorption when a negative potential is applied to the supporting substrate (Au-S-R + $H^+$ + $e^-$ → Au + HS-R), this being normally around -1 V or slightly higher [26, 70, 71].

Different factors influence at which potential alkanethiolates desorb, among these are the chain length, the degree of order of the SAM, the number of hydrogen bonds within the SAM and the underlying substrate's crystallinity [72].

Several groups have exploited this phenomenon in the field of biology, for example to detach cell sheets or to be able to pattern cells in specific regions [73]. In Fukuda's group they have developed a gold-coated membrane substrate modified with an oligopeptide layer that can be used to grow and subsequently detach a thick cell sheet through an electrochemically induced desorption [74]. Also, the same group

has engineered an electrochemical approach for the fabrication of capillary-like structures, precisely aligned within micrometer distances, whose internal surfaces are covered with vascular endothelial cells (Figure 2.4) [75].

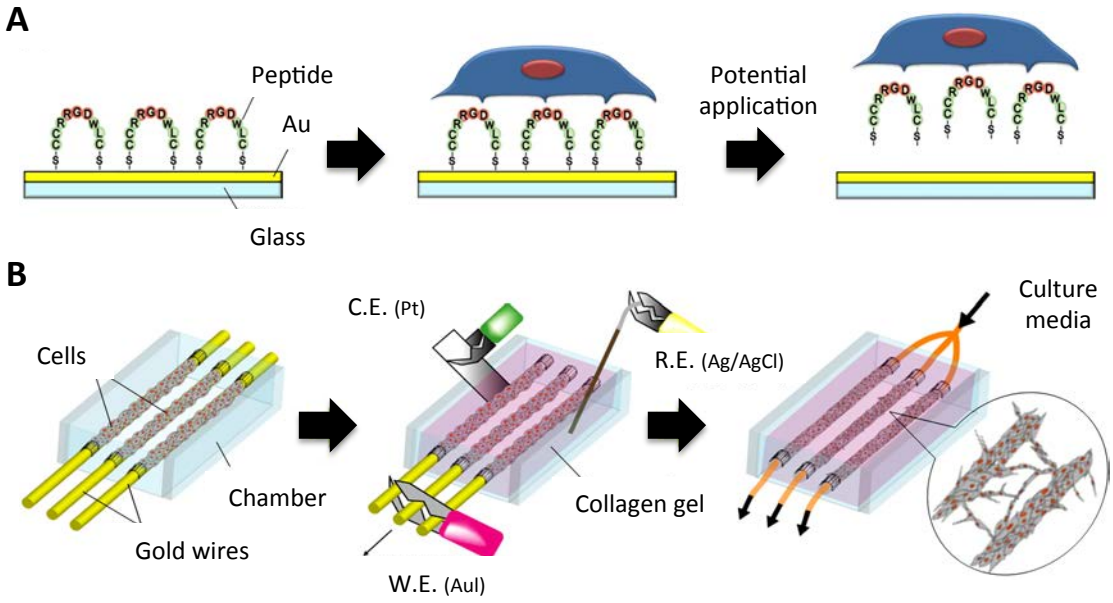


**Figure 2.4:** Schematic representation of the experimental setup used for cell detachment promoted by the reductive desorption of the oligopeptide. (A) The oligopeptide was chemically adsorbed onto the gold coated surfaces with thiol-gold bonds. Cells were allowed to adhere and grow and thereafter detached using the application of a negative voltage to promote desorption. (B) Gold rods functionalized with the oligopeptide and with endothelial cells adhered onto them were placed in a chamber surrounded with collagen. These were desorbed by applying a voltage and the subsequent removal of the rods yielded capillaries formed by cells. By connecting the system to a microsyringe pump to introduce culture medium capillaries were able to interconnect between each other by forming luminal structures. Reproduced and modified with permission from [75].

Published in Nature Protocols is a platform developed by Searson's group for triggering cell detachment from patterned electrode arrays by programmed subcellular release (partial cell detachment) [71]. Yet another platform for cell detachment studies with an electrochemical control has been created: Yoon et al. manufactured an addressable, multifunctional, and reusable platform, termed the biological breadboard (BBB), for spatiotemporal manipulation of cell adhesion and detachment at cellular and subcellular levels [76].

### 2.1.3 The Hydroquinone (HQ)/Benzoquinone (BQ) Chemistry

The Hydroquinone/Benzoquinone (HQ/BQ) redox couple has been extensively studied and used for different applications (Figure 2.5). HQ terminated alkanethiols have been used to functionalize gold substrates to prepare modified electrodes and these SAMs have been thoroughly investigated: the two proton, two electron process of these SAMs has been studied varying the alkyl chain length of the alkanethiols and the pH [42]. In addition, studies of electrochemical scanning tunneling microscopy

and spectroscopy have been done in view of better understanding the mechanism of the interfacial proton coupled electron transfer of HQ terminated SAMs [77].

Exploiting the fact that HQ terminal groups are non-chemically reactive and BQ groups are reactive, HQ surfaces can be activated upon oxidation to BQ by applying a low potential, typically below 0.8 V [42]. In this way, different molecules can easily be immobilized since BQ groups are reactive with azides [65], primary amines [78, 79], thiols, through the Michael-Addition reaction [60, 65, 80, 81] and cyclopentadiene groups, through the Diels-Alder reaction [82]. This platform has been used in various ways for the control and development of smart surfaces useful for the study of cell adhesion, cell co-culture or cell migration [27, 83], to mention some examples.

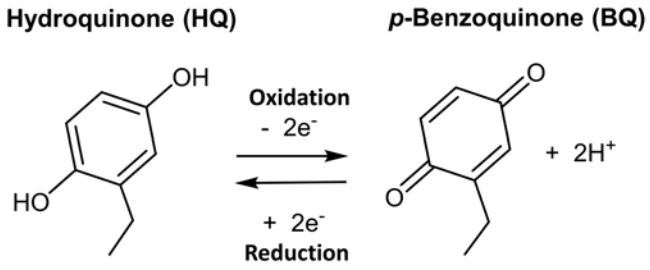


**Figure 2.5:** Schematic representation of the oxidation process of HQ to BQ consisting in a 2 proton 2 electron process.

Yousaf's group has worked extensively on dynamic platforms using the HQ/BQ chemistry: they have developed surfaces which can be switched on inducing different outcomes, such as the immobilization of molecules or the cleavage of surface bound ligands [36, 84]. Cell adhesion and cell migration have been studied using these substrates too, by tethering RGD molecules via the Diels-Alder reaction on selective regions using soft lithography techniques or microfluidics [85] and thus gaining spatial control on top of the temporal control given by the external electrochemical stimulus. Also, cellular activity has been monitored using this platform since an electrical output can be read. For example, in a study carried out by Collier et al., the surface of a cell was engineered to contain cutinase, which can convert a non electroactive hydroxyphenyl ester to an electroactive HQ, and hence, cellular activity was reflected on the redox readout of the electrode [86]. Biosensors have also been made exploiting the HQ/BQ chemistry [56], for example, a novel strategy using epimeric monosaccharide-Q hybrids on gold surfaces has been used to probe specific carbohydrate-protein recognition interactions using electrochemistry [87].

All these studies demonstrate that the control of redox switchable SAM biointerfaces are promising for applications in the field of tissue engineering and material sciences [56].

### 2.1.4 BQ Interfacial Reactions

As mentioned earlier, BQ groups can readily react with many different functional groups, these are portrayed in Figure 2.6. Two of the most used interfacial reactions have been the Diels-Alder and the Michael Addition.

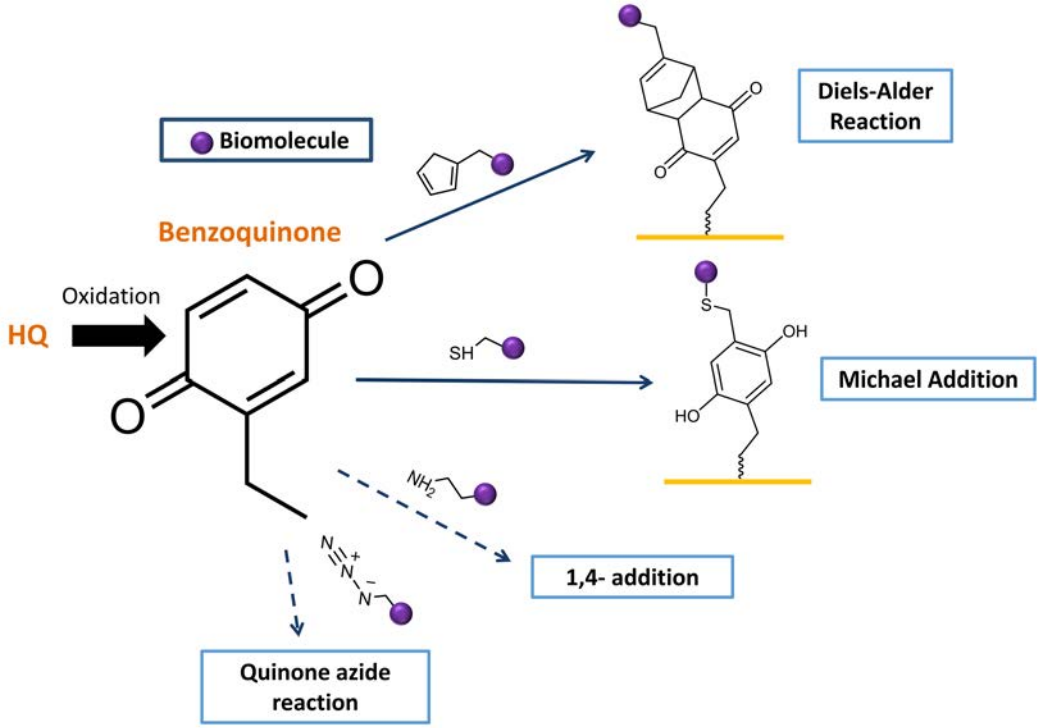


**Figure 2.6:** Schematic representation of the different interfacial reactions BQ can undergo.

### Diels-Alder Reaction

The Diels-Alder (DA) reaction is a reversible cyclo-addition occurring between a conjugated diene (in the cis configuration) and an electron-deficient dienophile. Advantageously, this reaction is orthogonal, efficient, and atom conservative and does not require a catalyst. It is also insensitive to some reaction conditions, such as air and humidity, allowing its use under ambient conditions [84]. The DA reaction is also crucial for the modification of molecular surfaces such as fullerenes [88]. One of the pairs of diene and electron-deficient dienophiles most used for DA reactions are cyclopentadiene (Cp) and BQ derivatives, respectively (Scheme 2.1). When using conjugated Cp, sigmatropic isomerization can take place before the reaction occurs, variating the final position of attachment of the ligand [89].

Mrksich and Yousaf were the first ones to use this reaction for surface functionalization of biological ligands and it has been since then further sophisticated by incorporating light sensitive groups like the nitroveratryloxycarbonyl (NVOC) protecting group, achieving thus, not only an electrochemical temporal control, but also a photochemical spatial control [19].

BQ and Cp react under mild conditions but for interfacial reactions they show some important drawbacks. On one side, the synthesis of the reduced HQ-tagged molecules is complex and not standardized [26]. On the other side, it is also challenging to synthesize Cp-terminated functional derivatives to be used for the DA reactions due to their low stability. Furthermore, low functionalization reproducibility caused by the variability of Cp derivatives on the chemoabsorption process previous to the DA reaction has been previously reported [82].

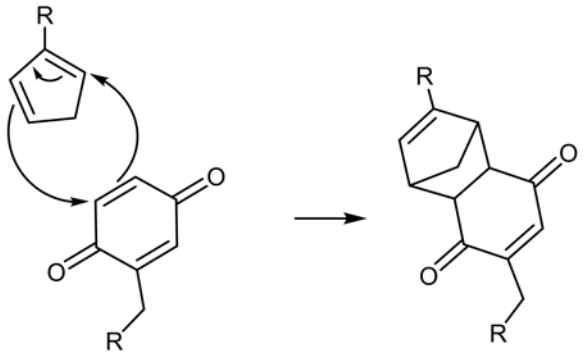


Scheme 2.1: Reaction mechanism of the DA reaction between Cp and HQ.

### Michael Addition Reaction

The Michael Addition (MA) reaction has been widely used and studied since it allows the synthesis of selective products efficiently whilst using environmentally friendly conditions [90]. Basically, it consists in the addition of a nucleophile, which is referred to as the "Michael donor", to an activated electrophilic alkene, named the "Michael acceptor", resulting in a "Michael adduct". More specifically, Michael donors are generally enolate type nucleophiles, which in the presence of a catalyst react with the adduct, an $\alpha$,$\beta$-unsaturated carbonyl [91]. Even though this type of reaction is usually performed with enolate nucleophiles and activated alkenes, there are many other functional groups that possess enough nucleophilicity to undergo this reaction (Scheme 2.2). Indeed, several non-enolate nucleophiles have been previously used, such as amines [60, 79], thiols [65, 80], azides [65, 91], and phosphines [90]. MA rates of thiols reacting with acrylates or vinyl sulfones depend on the pH of the reaction media, and they rely on the particular pKa of each thiol. This is explained by the fact that the reacting species are the thiolates rather than the thiols [92]. Interestingly, MA reactions readily occur under physiological conditions and are selective to thiol containing proteins over amine nucleophiles, for example [91]. Thus, reactions with lysine residues require a higher pH than 9.3 and their rates are still dramatically slower than the reaction with cysteine at a comparable pH. Another important advantage of MA reactions for SAM derivatization is the fact that the synthesis of functional molecules with thiol terminal groups is easier to perform than that of the previously mentioned Cp derivatives for the DA reaction, and the resulting compounds are more stable. Due to the synthetic versatility pathways offered by this reaction, many different reaction chemistries have been discovered and implemented to yield a large range of efficient reactions giving place to highly specific products [91].

The MA reaction between the BQ and the thiol is a strategy used previously in different studies [60, 65, 80, 81]. For example, on surface, the immobilization of glutathione using the HQ/BQ chemistry has been reported in the literature [80] and also, DNA has been immobilized onto indium tin oxide (ITO) surfaces coated with silanes terminated in BQ [65].

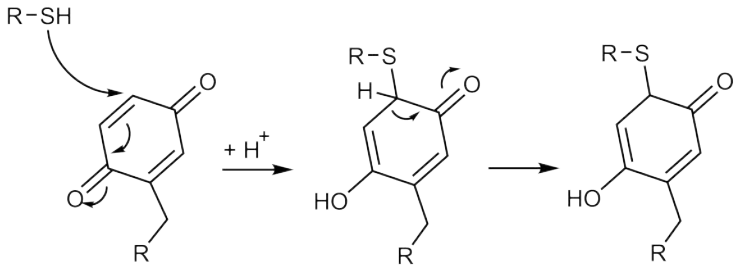


**Scheme 2.2:** Reaction mechanism of the MA reaction, between thiol and HQ.

## 2.2 Objectives and Strategy

Even though both DA and MA reactions have been widely studied, to our knowledge there has been no comparative study between the interfacial DA and MA reactivity of Cp- and thiol-terminated functional molecules, respectively, onto an electrochemically activated BQ SAM. In view of its interest for biological applications, in this Chapter we will study the differences on the spatial and temporal control given by these two surface functionalization strategies. More specifically, the different interfacial reactivities of electrochemically activated BQ SAMs with Cp- and thiol-terminated functional molecules and their implications on the modification of properties of gold substrates will be investigated using a multi-technique approach. This is important to further expand the use of such a versatile strategy for spatial and temporal control of surface functionalization. Also, due to the cumbersome synthesis of Cp and thiol derivatives, we will make an emphasis to accurately report and optimize the synthetic route of the molecules to be used. For the comparative study between both interfacial reactions two molecules consisting in fluorescein modified with Cp and thiol will be synthesized to be able to easily characterize and compare the modified surfaces using fluorescence microscopy.

In order to perform tackle the abovementioned general objectives, we will focus on the following specific objectives:

- Design, synthesis and characterization of the molecules for surface functionalization with an electroactive mixed SAM based on HQ terminated alkanethiols (molecules **1** and **2**, Figure 2.7).
- Synthesis of molecules to be used as probes for the characterization of the interfacial reactions: (i) simple molecules for CV characterization, Cp and thiol groups with an hexyl chain (molecules **16** and **17**, Scheme 2.5) and (ii) molecules to be used as fluorescent probes, thiol and Cp functionalized fluorescein derivatives (molecules **3** and **4**, Figure 2.7) for the comparison of the DA and MA reaction using fluorescence microscopy.[1]

[1]This has been done in collaboration with the Combinatorial Chemistry Unit (Technology Platform of the Barcelona Science Park) in a collaborative framework.

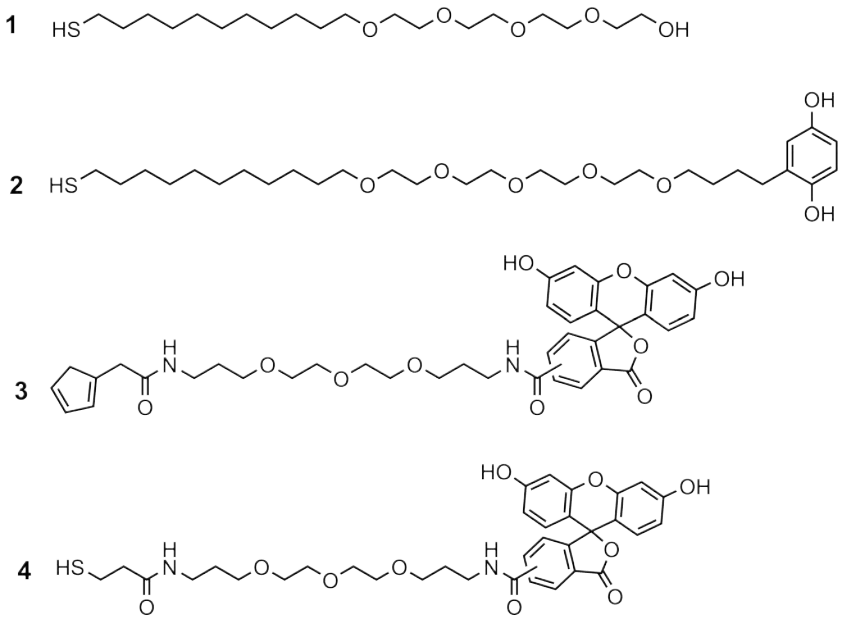


**Figure 2.7:** Molecular structures of the synthesized molecules. All of these molecules contain a polyethylene glycol chain bridging the $\omega$-terminated group and the anchoring unit. In such molecules, the alkyl chain provides structural order to get compact molecular monolayers, whereas the oligo(ethylene glycol) chain prevents unspecific protein and cell adsorption.

- Characterization of the mixed SAM formed with the HQ electroactive molecules and the pegylated alkanethiols (molecules **1** and **2**) using CV, CA and XPS.
- Study and comparison between the DA and MA interfacial reactions using a multi-technique approach. Spatial confinement of fluorescein probes by preparing patterned mixed SAMs of electroactive molecule **2** and molecule **1** using μCP and subsequent fluorescent ligand immobilization through the interfacial reactions.

The work presented here has been published in the Journal of Physical Chemistry B [93]. A schematic representation of the work described in this Chapter is shown through Figure 2.8.

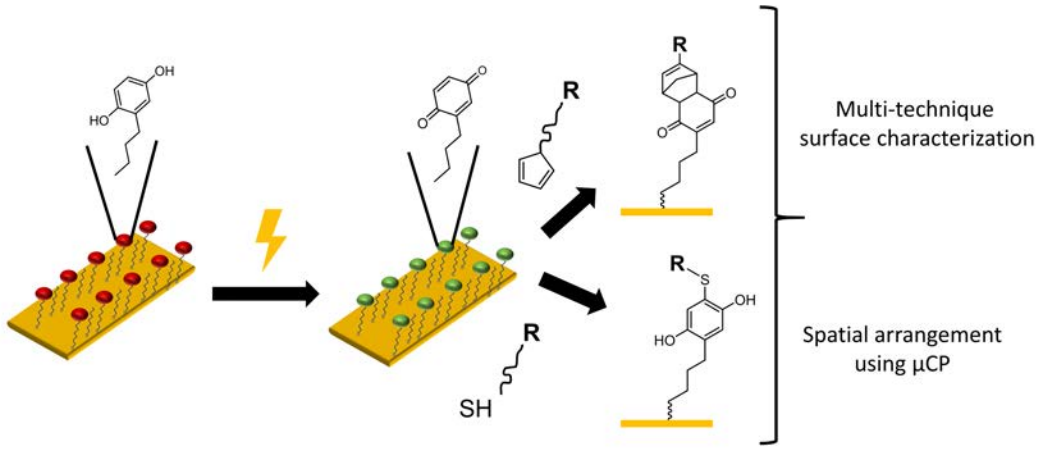


**Figure 2.8:** Schematic representation of the work flow and strategy to achieve the objectives proposed in order to assess the comparison between the MA vs DA interfacial reaction using the HQ/BQ chemistry.

## 2.3 Design and Synthesis of Molecules

### 2.3.1 Molecules for the Mixed SAMs

Firstly, the synthesis of the pegylated alkanethiol (molecule **1**) and the HQ derivative (molecule **2**) were optimized. Some of the main disadvantages of the DA interfacial reaction when using HQ as the dienophile have been attributed to synthetic difficulties to achieve the final HQ compound [26, 82] and to the low chemoabsorption reproducibility of the process [42], which hinder its extended use for a wide range of applications. Therefore, an effort to thoroughly describe the synthetic route for this molecule was done, and details of the synthesis are provided in Section 7.1.1.

Molecules **1** and **2** were designed to have 3 common different functional components (Figure 2.9): (i) the thiol surface anchoring groups, since these molecules were intended for functionalization of gold coated surfaces; (ii) the alkyl chains which confer structural stability to the monolayer through the formation of a compact 2D packing mediated by van der Waals $CH_2$- - -$CH_2$ interactions. This is important since it is known that molecular packing can impact the physicochemical properties of SAMs [94–96]. Finally, (iii) the ethylene glycol (EG) linker units which provide hydrophilicity to the surface and prevent unspecific binding of proteins and cells [97, 98]. Finally, molecule **2** contains a HQ moitey to confer the redox properties to the functionalized surface.

In addition, the number of carbon units and EG units for each molecule were taken into account, considering that for the formation of the mixed SAM the electroactive and reactive HQ moieties must be properly exposed. This is important to avoid steric hindrance and allow the interfacial reaction of exposed the BQ groups with specific ligands to take place [99].

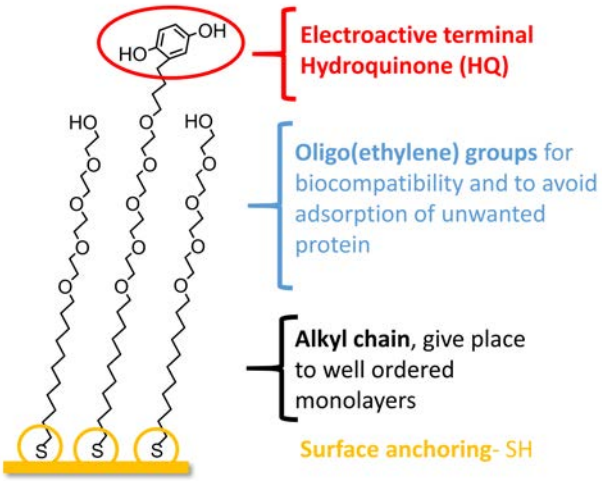


**Figure 2.9:** Schematic representation of the design and structure of the molecules used for electroactive mixed SAM formation, these presenting an electroactive head group (HQ), oligoethylene groups, an alkyl chain and the thiol anchoring group (-SH).

Compound **1**, consisting of an alkanethiol functionalized with a tetra(ethylene glycol) group, the 1-mercaptoundec-11-yl-tetra(ethylene glycol), was synthetized through a three step procedure (Scheme 2.3 (A)). The synthesis of the hydroquinone-tetra(ethylene glycol)alkanethiol **2** consisted of the subsequent modification of the alkanethiol **1** with the protected HQ **8** resulting in a six step procedure (Scheme 2.3 (A)). Briefly, treatment of tetra(ethylene glycol) with 11-bromo-1-undecene in a saturated aqueous NaOH solution afforded the alkene **5**. Subsequent addition of thiolacetic acid in the presence of a radical initiator gave the thioacetate **6**, and finally a hydrolysis reaction afforded the desired thiol **1**. Compound **8** was prepared in two synthetic steps from commercially available materials (Scheme 2.3 B). The first reaction is based on the addition of dihydropyran to HQ to provide the protected di-tetrahydropyrane-hydroquinone **7**, which was purified via recrystallization in hexane after completion of the reaction (monitored with thin layer chromatography (TLC)). Deprotonation of **7** with t-butyllithium (t-BuLi) followed by addition of dibromobutane provided the di-tetrahydropyran-hydroquinone-butylbromide **8**. The purification step was successfully optimized using an unusual solvent mixture of chloroform and dichloromethane that gave better results compared with the previously described hexane-ethyl acetate mixture [19]. Precursor **8** was then used to convert thiol **1** into the desired electroactive HQ derivative **2**. First, thiol **1** was protected with triphenylmethyl chloride, and the subsequent addition of the masked HQ **8**, gave the intermediate **10**, which after treatment with trifluoroacetic acid (TFA) afforded **2**. This second synthetic route may be shortened, since the hydrolysis of the thioacetate **6** to obtain **1**, and subsequent protection with triphenylmethyl chloride to obtain **9**, can be carried out in a one-pot sequence. For experimental details see Section 7.1.1.

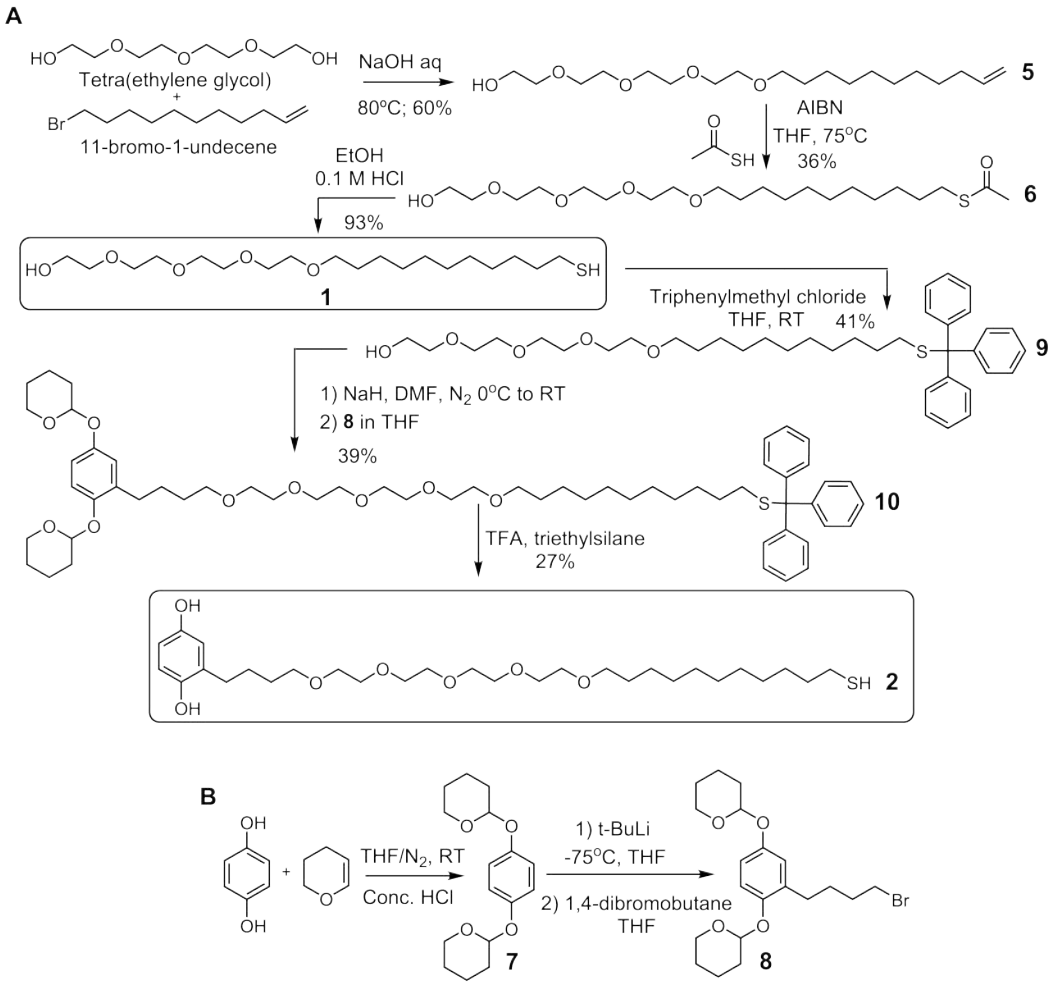


**Scheme 2.3:** (A) Synthesis of thiol **1** and the HQ derivative **2** and (B) synthesis of **8** from HQ and dyhydro-2H-pyran.

## 2.3.2 Synthesis of Fluorescent Probes

The fluorescent molecules **3** and **4** were prepared from the common precursor **14** which were synthesized in a two-step procedure starting from commercially available 5(6)-carboxyfluorescein (CF), see Scheme 2.4. CF was activated as the succinimidyl ester and reacted with 1-(tert-butoxycarbonylamino)-4,7,10-trioxa-13-tridecanamine to prepare compound **13** (see Secion 7.1.1). Removal of the Boc protecting group afforded derivative **14**. The cyclopentadienyl derivative **12** was prepared in a three-step synthesis starting from sodium cyclopentadienylide (NaCp). First, NaCp was alkylated with methyl bromoacetate and the resulting methyl ester was hydrolyzed to obtain **11**, which was then converted to the corresponding activated succinimidyl ester **12** (Cp-COOSu). The coupling between **12** and **14** afforded the desired carboxyfluorescein derivative **3**. On the other hand, 3-(tritylthio)-propanoic acid was converted to the corresponding succinimidyl ester and reacted with **14** to obtain the thiol-protected derivative **15**. Finally, the trityl protecting group was removed to obtain the desired compound **4** (Scheme 2.4). For more details concerning the synthesis see Section 7.1.1.

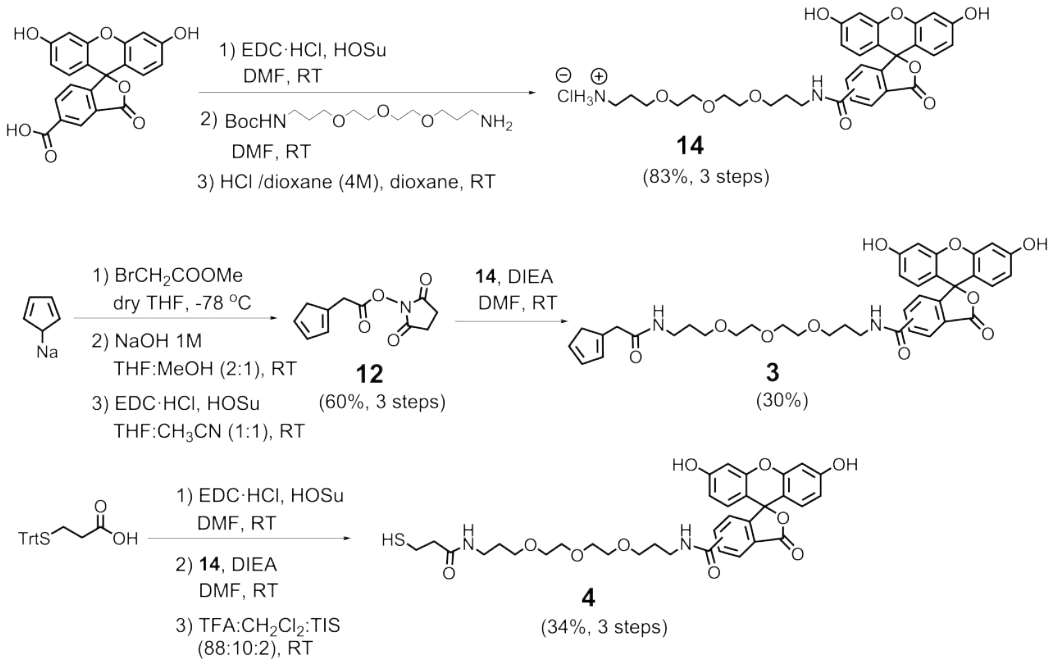


**Scheme 2.4:** Synthesis of the fluorescein-containing molecules **3** (with Cp) and **4** (with thiol).

### 2.3.3 Model Molecules for the Interfacial Reaction Comparison

The simplest molecules used to perform the comparative study of the DA and the MA interfacial reactions consisted of an hexyl chain connected to a Cp or thiol unit: 1-hexyl-1,3-cyclopentadiene (Cp-hexyl, molecule **9**), which was synthesized, and 1-hexanethiol (molecule **10**), which was purchased (Sigma Aldrich). These were used to follow the interfacial reactions by using CV and XPS.

For the synthesis of the Cp-hexyl, sodium-cyclopentadiene was added slowly to a cooled solution of 1-bromohexane to afford the desired product after purification (Scheme 2.5).

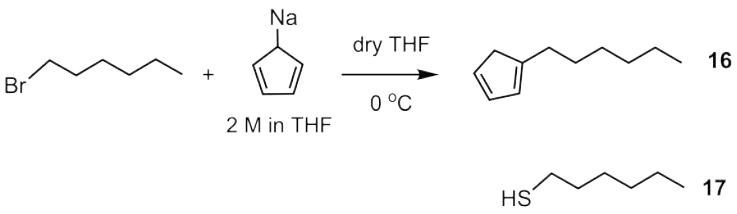


**Scheme 2.5:** Synthetic route of 1-hexyl-1,3-cyclopentadiene (**16**) and purchased 1-hexanethiol (**17**).

## 2.4 HQ/BQ Mixed SAM Preparation and Characterization

The SAM strategy offered us the possibility to precisely control the density of electroactive ligands on the surface by mixing two different pegylated alkanethiol

molecules, the electroactive HQ (**2**) and the hydroxyl-terminated analogue (**1**) in a 1:1 molar ratio. Different ratios will be used, depending on the application or characterization technique. The use of both molecules form a mixed SAM, enabling the proper exposure of the HQ head groups on the surface and thus avoiding the possibility of steric hindrance.

Briefly, after proper cleansing of the substrates, these were immersed in an ethanolic solution of molecules **1** and **2**, with a final concentration of 1 mM, and were left under an inert atmosphere overnight. Details of the experimental procedure can be found in Section 7.1.2.

A multi-technique approach was used for the surface characterization, which included XPS, CV, and CA measurements for both the reduced **S1** and oxidized **S2** SAMs (Figure 2.10). SAM **S2** was obtained by electrochemical oxidation of SAM **S1** using a 3-electrode setup.

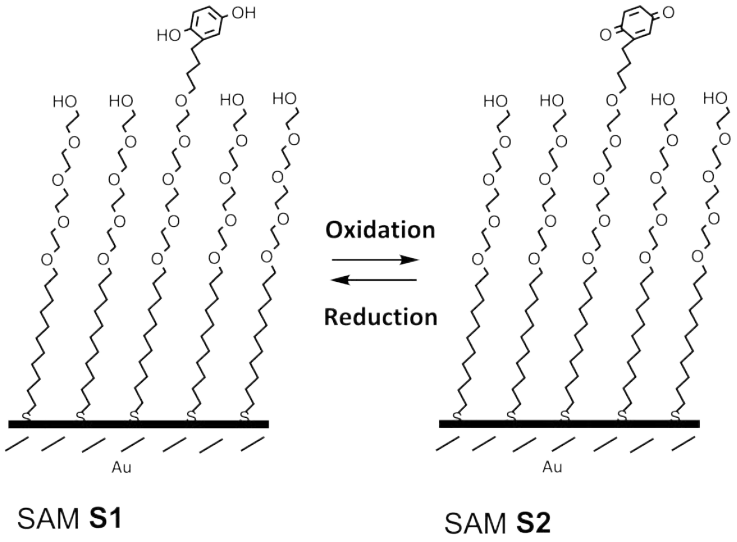


**Figure 2.10:** HQ-terminated SAM **S1** redox process, converted through oxidation into BQ-terminated SAM **S2** and reduced back to SAM **S1**.

## 2.4.1 Cyclic Voltammetry

For CV measurements we used a 3-electrode setup consisting in the SAM formed on a gold surface as the WE, a Pt wire as the CE and a Ag/AgCl the RE with a 1 M $HlO_4$ aqueous solution as electrolyte. Cyclic voltammograms using the prepared SAM **S1** as the WE at different scan rates are depicted in Figure 2.11. Details concerning the experimental procedure can be found in Section 7.1.3. Current peaks found were 0.43-0.47 V for the oxidation peak to SAM **S2** and 0.33-0.26 V (vs. Ag/AgCl) for the reduction peak, back to SAM **S1**, which correspond to what has been previously reported in the literature [79]. A linear relationship between the current intensity and the scan rate (linear regression gave $R^2 = 1$ and $R^2 = 0.996$ for anodic and cathodic peaks, respectively) was obtained, as seen in the Figure 2.11 inset. This fact confirms that the molecules are surface confined [26]. The surface coverage was estimated by integrating the oxidation peak area observed from the CV in 1 M $HClO_4$, taking a $2e^-$, $2H^+$ reaction mechanism, and applying the Equation 1.1 (see

Section 1.6.2). By integrating the area under the oxidative wave, Q was obtained and a density of $\Gamma = 6.21 \times 10^{-12} \frac{moles}{cm^2}$ was found. This is approximately half of the value of what has been previously reported for the full coverage, since we are working with SAMs with only 50% of electroactive molecule **2** [42, 80].

Thus, applying a potential higher than 0.65 V it is possible to pass from SAM **S1** to **S2** and if a potential lower than -0.5 V is applied, SAM **S2** is reduced to **S1**.

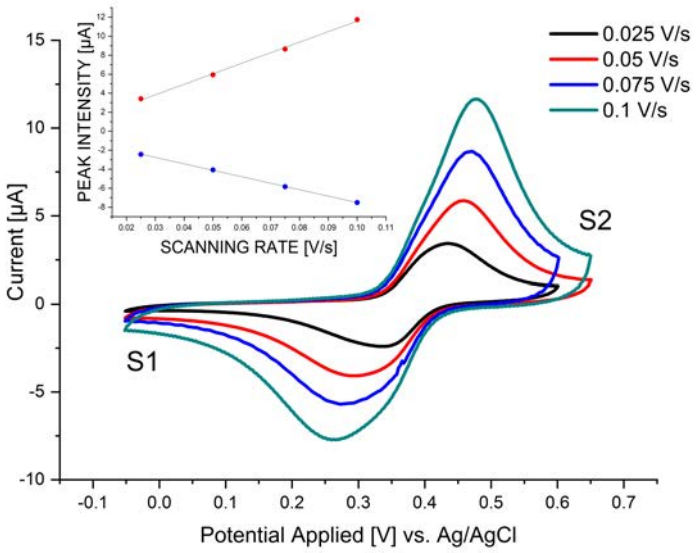


**Figure 2.11:** Cyclic voltammograms of the mixed SAM **S1** with a 1:1 molar ratio between **1** and **2**. For these measurements a 3-electrode setup was used, SAM **S1** as WE, a Pt wire as CE and a Ag/AgCl RE. The electrolyte used was 1 M $HClO_4$. Inset: relation between scanning rate and the reduction and oxidation peak intensity (current) of the SAMs.

## 2.4.2 Contact Angle

In order to characterize the change in the wettability of the surface due to oxidation of the terminal groups of the SAMs, CA measurements were performed for bare gold, for SAM **S1** and SAM **S2**, obtained from the oxidation of SAM **S1**. The values obtained were 66.1±0.4°, 56.1±0.5° and 80.8±2.8°, respectively (Figure 2.12).

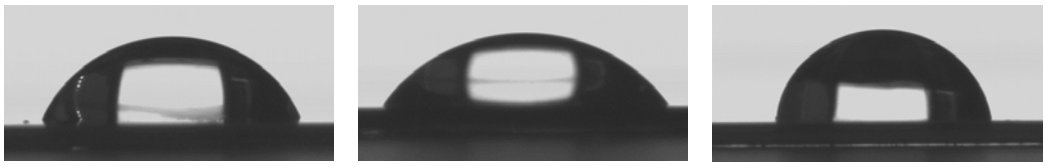


**Figure 2.12:** Contact angle images of (A) bare gold, (B) SAM **S1** and (C) SAM **S2**.

As seen in Figure 2.12, the bare gold surface showed a larger contact angle than SAM **S1** due to the hydrophilicity provided by the hydroxyl groups on the surface of SAM **S1**. On the other hand, SAM **S2** presented the highest contact angle, being the most hydrophobic surface, due to the presence of the carbonyl groups [55].

The capability of fine-tuning the surface tension, switching from a hydrophobic to hydrophilic surface due to the change in the chemical nature of the functional group is an interesting phenomena and can be used for different applications as previously reported [55, 100–102]. Hence, this switchability could be exploited in settings were wettability control is required, using the application of a potential as external stimulus and going from SAM **S1** (56.1 °) to SAM **S2** (80.8 °).

## 2.5 Comparison of Stimulus Activated DA vs. MA Reactions on HQ/BQ SAMs

After performing the characterization of the electroactive SAM **S1** and **S2** system, we proceeded with the analysis of the DA and MA interfacial reactions as a strategy for spatial and temporal control of surface functionalization (Figure 2.13).

Firstly, a voltage was applied in order to oxidize SAM **S1** to **S2** by performing a chronoamperommetry, basically consisting in holding a determined potential constant over time. In the oxidized state (SAM **S2**) BQ moieties could react with specific ligands, via the DA or MA interfacial reaction.

This was followed using CV and XPS by using very simple molecules as specific ligands, namely Cp-hexyl (**16**) and hexanethiol (**17**) (Scheme 2.5). Fluorescence microscopy was also used; in this case, the two synthesized fluorescein derivative molecules, one with a Cp (**3**) and another with a thiol (**4**) termination were used as the specific ligands.

The general process is illustrated in Figure 2.13, SAM **S1** is oxidized to **S2** and in presence of the specific ligands either the DA or the MA reaction takes place, giving place to different types of functionalizations: **S3-hexyl** or **S3-FC** for the DA reaction and **S4-hexyl** or **S4-FC** for the MA reaction, as later described in detail.

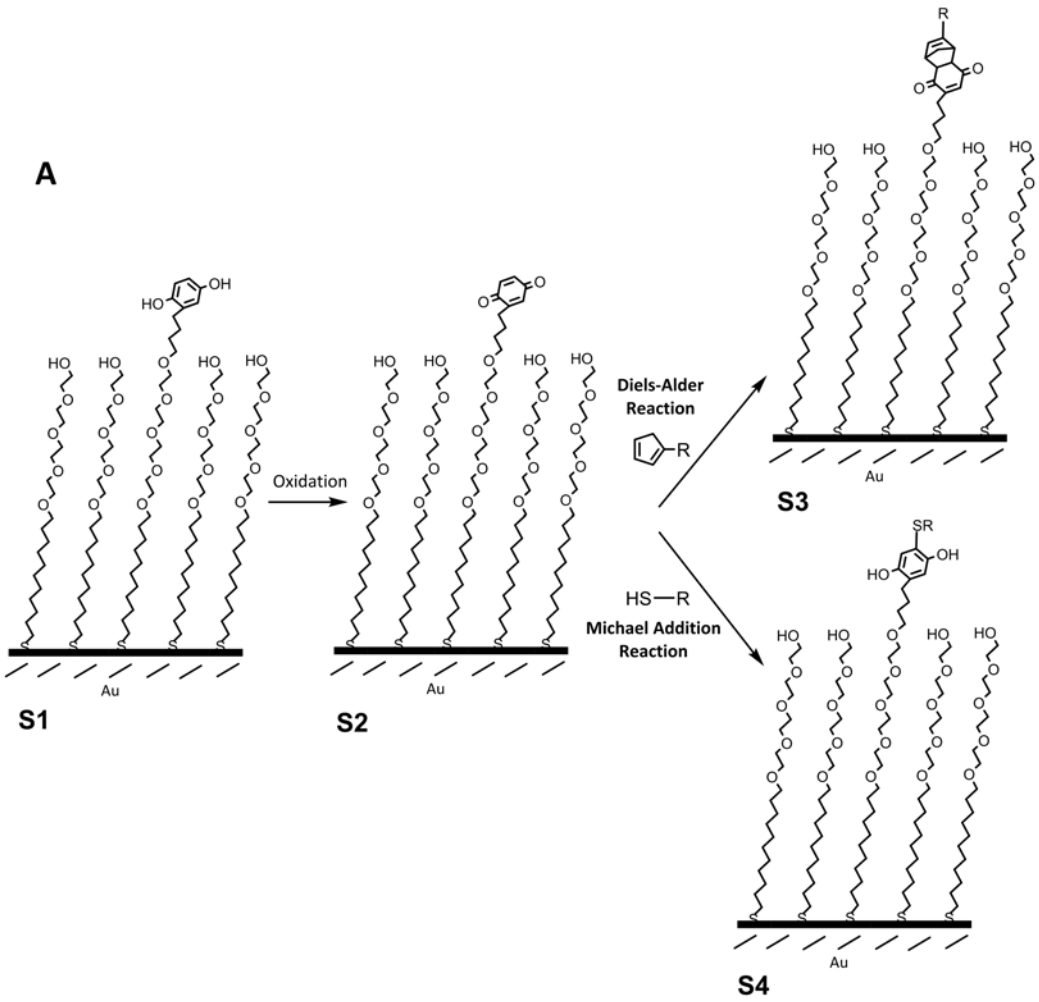


B

| R Type | Rx | Adduct | Nomenclature | R Type | Rx | Adduct | Nomenclature |
|---|---|---|---|---|---|---|---|
| Hexyl | DA | 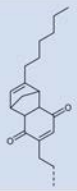 | **S3-hexyl** | Fluorescein (FC) | DA | 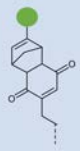 | **S3-FC** |
| | MA | 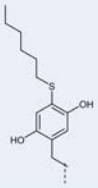 | **S4-hexyl** | | MA | 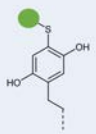 | **S4-FC** |

**Figure 2.13:** (A) DA and MA interfacial reactions using 1 M $HClO_4$ as an electrolyte for the SAM **S1** to SAM **S2** oxidation. (B) Molecules Cp-hexyl (**9**) and hexanethiol (**10**) were used for the DA and MA interfacial reaction, giving place to **S3-hexyl** and **S4-hexyl**, for CV and XPS studies and Cp-fluorescein (**3**) and thiol-fluorescein (**4**) were used for the experiment involving the spatial arrangement of the molecules on surface, giving place to **S3-FC** and **S4-FC**.

### 2.5.1 Cyclic Voltammetry for Interfacial Reaction Optimization

SAM **S1** with a 1:1 molar ratio of molecule **1** and **2** was prepared as described in Section 7.1.2, and the activation of this SAM toward the DA and MA interfacial reactions was studied by CV to optimize the oxidation time needed for a complete conversion from SAM **S1** to **S2**. For this purpose, synthesized Cp-hexyl (**9**) and commercially available hexanethiol (**10**) were used as simple target ligands to react with the electroactivated surface SAM **S2**. To perform these experiments a 3-electrode configuration was used, with a Pt wire as CE, an Ag/AgCl RE and the SAM as WE (for details see Section 7.1.3).

More specifically, substrates were oxidized, SAM **S1** to **S2**, by applying a potential of 650 mV in an electrolyte solution of 1 M $HClO_4$. Ligand solutions were prepared in tetrahydrofuran and phosphate buffer saline, THF:PBS (1:1), in a concentration of 15 mM. In order to evauluate the duration of the application of the potential needed for a complete oxidation of SAM **S1** to **S2**, the potential was applied for 20 seconds three consecutive times. After every 20 seconds of oxidation, SAM **S2** was immersed in the target ligand solution for 30 minutes, to obtain **S3-hexyl** and **S4-hexyl**. After every oxidation and immersion (reaction) step, a CV was performed in order to check the evolution of the DA or MA interfacial reactions. As seen in Figure 2.14, the redox peak during the DA reaction with the Cp-hexyl target ligand disappears after a total of 60 seconds of oxidation, as expected, since the cycloadduct formed is not electroactive anymore. On the contrary, the redox peaks of the MA reaction with the hexanethiol were only slightly decreased and shifted, since, in this case, the product of the reaction is still electroactive and, thus, the redox signal is not lost [80].

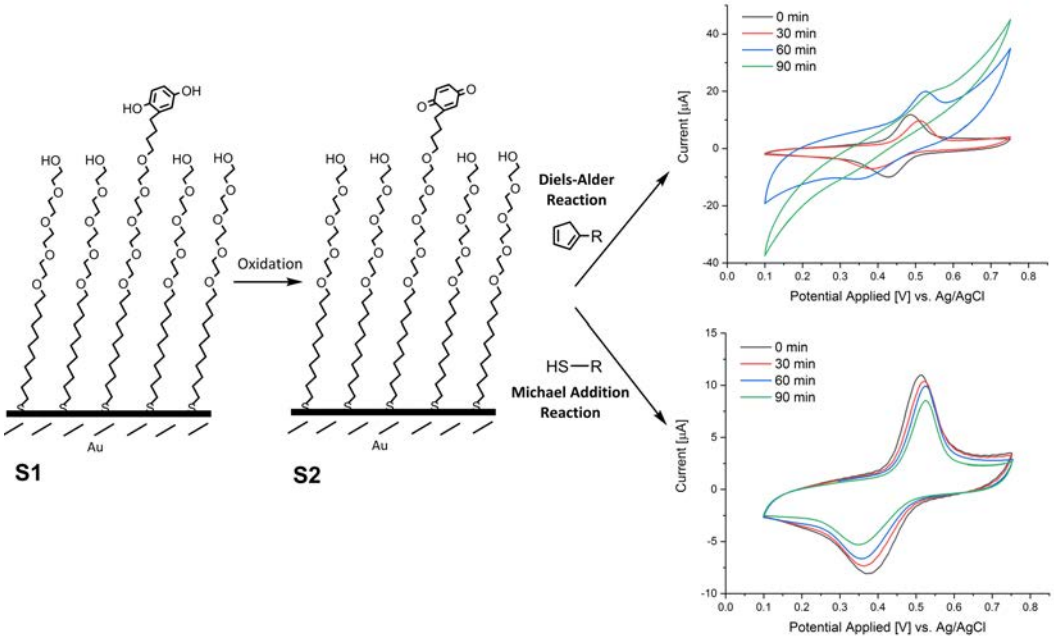


**Figure 2.14:** DA and MA interfacial reactions using 1 M $HClO_4$ as the electrolyte for the SAM **S1** to SAM **S2** oxidation and ligand solutions (Cp-hexyl (**9**) and hexanethiol (**10**)) of 15 mM in THF:PBS (1:1) for the interfacial reactions, giving place to **S3-hexyl** and **S4-hexyl**. Cyclic voltammograms monitoring the three oxidation steps of 20 seconds followed by a 30 minutes immersion in the ligand solution.

### 2.5.2 X-Ray Photoelectron Spectroscopy

To further characterize the surface confined reaction and the adducts obtained with the DA reaction and the MA reaction, XPS was performed for carbon species (Figure 2.15). Sulphur (Figure 2.16) was also analyzed to ensure correct substrate functionalization. SAM **S1** was prepared as previously described and SAM **S2** was achieved by oxidation of SAM **S1** in 1 M $HClO_4$ by applying a potential of 650 mV during 20 seconds. SAM **S3-hexyl** was achieved by immersing SAM **S2** in a Cp-hexyl solution (15 mM in THF:PBS 1:1) during 30 minutes. SAM **S4-hexyl** was achieved by immersing SAM **S2** in an hexanethiol solution (15 mM in THF:PBS 1:1) during 30 minutes.

The C1s spectra of SAM **S1** (Figure 2.15) presents two peaks, one at 285.0 eV that corresponds to the bond energy of aliphatic carbons and another one at 286.7 eV, corresponding to the C-O bond. The C1s peaks of the oxidized SAM **S2** are found at 285.0 eV, corresponding to the bond energy of the aliphatic carbon, at 286.7 eV for the C-O bond, and a new peak is observed at 289.2 eV which is assigned to the oxidized C=O of the BQ moiety. After the DA reaction with Cp-hexyl, yielding SAM **S3-hexyl**, there is a clear increase of the intensity of the peak associated to the aliphatic carbon due to the DA covalent reaction with the Cp, which confirms the covalent anchoring of Cp-hexyl onto the surface. After the MA reaction with hexanethiol, yielding SAM **S4-hexyl**, an increase in the C aliphatic peak is also observed and also the peak attributed to C=O disappears, confirming that the reaction takes place.

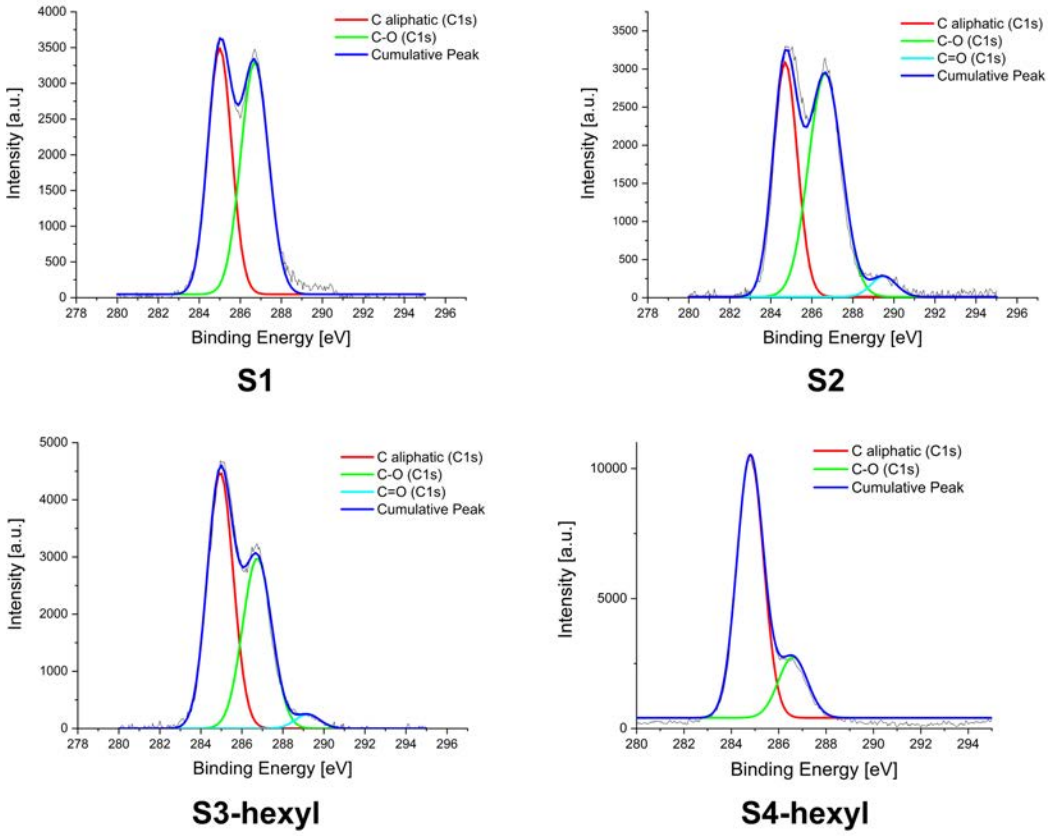


**Figure 2.15:** XPS deconvolutions for C1s spectra of all SAMs, **S1**, **S2**, **S3-hexyl** and **S4-hexyl**.

All SAMs exhibit the S2p doublet structure, $S2p_{3/2}$ with peaks ranging 162.9-163 eV and $S2p_{1/2}$ with peaks ranging 163.15-163.5 eV, which is characteristic of the thiolate bound to a gold surface. Moreover, SAM **S1** presents another peak at 169.3 eV, which corresponds to oxidative sulphur species [103] (Figure 2.16). This might appear due to the fact that substrates were stored for some days before XPS analysis was performed. Peak intensity values with their corresponding element are listed in Table 2.1.

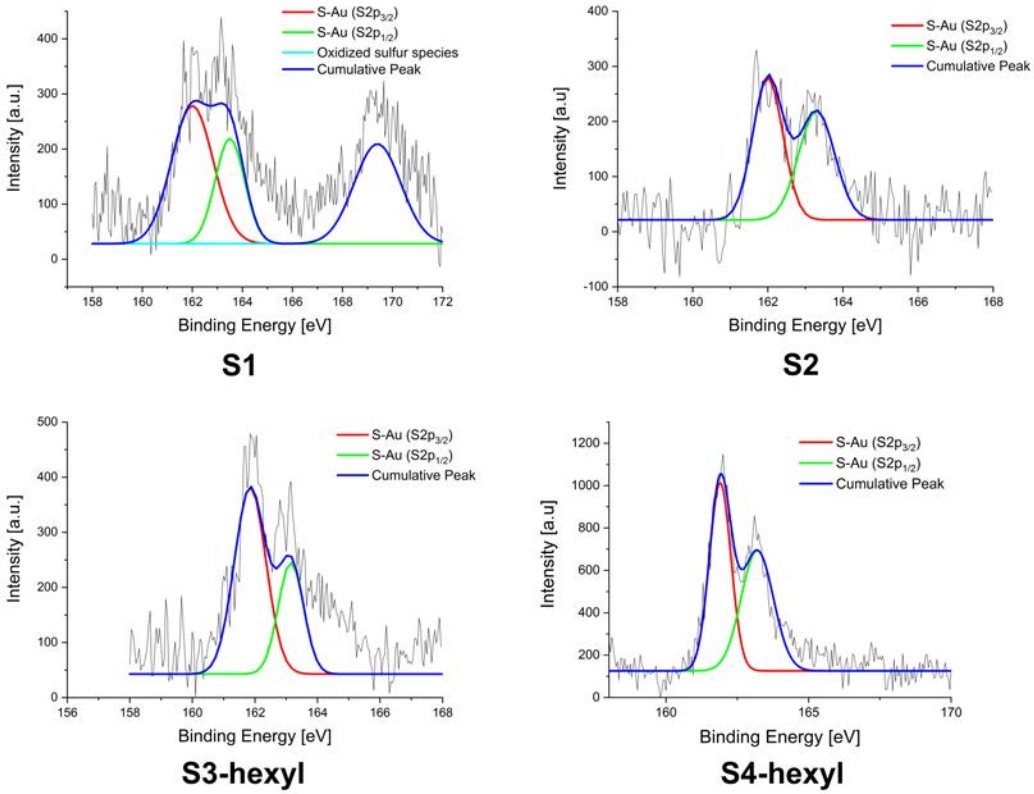


**Figure 2.16:** XPS deconvolutions for S spectra of all SAMs, **S1**, **S2**, **S3-hexyl** and **S4-hexyl**.

Table 2.1: XPS spectra values for SAMs **S1**, **S2**, **S3-hexyl** and **S4-hexyl** for carbon and sulphur.

| SAM | Binding Energy [eV] | Element | Type of Bond |
|---|---|---|---|
| **S1** | 285 | C1s | C aliphatic C-C |
| | 286.7 | C1s | C-O |
| **S2** | 285 | C1s | C aliphatic C-C |
| | 286 | C1s | C-O |
| | 289.2 | C1s | C=O |
| **S3-hexyl** | 285 | C1s | C aliphatic C-C |
| | 286 | C1s | C-O |
| | 289.2 | C1s | C=O |
| **S4-hexyl** | 284.8 | C1s | C aliphatic C-C |
| | 286.6 | C1s | C-O |
| **S1** | 162 | $S2p_{3/2}$ | S-Au |
| | 163.5 | $S2p_{1/2}$ | S-Au |
| | 169.4 | S | Oxidized sulphur species |
| **S2** | 162 | $S2p_{3/2}$ | S-Au |
| | 163.3 | $S2p_{1/2}$ | S-Au |
| **S3-hexyl** | 161.85 | $S2p_{3/2}$ | S-Au |
| | 163.15 | $S2p_{1/2}$ | S-Au |
| **S4-hexyl** | 161.9 | $S2p_{3/2}$ | S-Au |
| | 163.15 | $S2p_{1/2}$ | S-Au |

### 2.5.3 Spatial Control of the Interfacial Reactions

In order to include not only a temporal control but also a selective spatial functionalization upon a certain external stimulus (i.e. applied potential), the μCP technique (see Figure 1.5 in Section 1.4.1) was used to anchor the electroactive molecule **2** only on specific areas of the surface, in our case, forming stripes which are 20 μm wide. Basically, the PDMS stamp was inked with octadecanethiol and the pattern was transferred on the surface by placing the stamp in contact with the substrate. Thereafter, the non-functionalized areas were backfilled with the mixed SAM **S1** by immersing the substrate in a solution containing molecules **1** and **2** in a ratio of 1:1.

To compare the differences between the DA and MA surface confined reactions, fluorescence microscopy images were taken after immersion of the oxidated SAM **S2** in a 20 mM solution of fluorescent ligands **3** and **4** for 30 minutes, giving place to **S3-FC** and **S4-FC**. Oxidation of SAM **S1** was performed by applying a voltage of 650 mV for 60 seconds to ensure the presence of BQ groups on the surface as previously optimized, yielding SAM **S2**. For the DA interfacial reaction, a ligand solution of **3** in THF:water 1:1 was used, whereas for the MA interfacial reaction a ligand solution of molecule **4** in EtOH:water 9:1 was employed. The luminescent micropattern obtained after the surface confined reactions is shown in Figure 2.17.

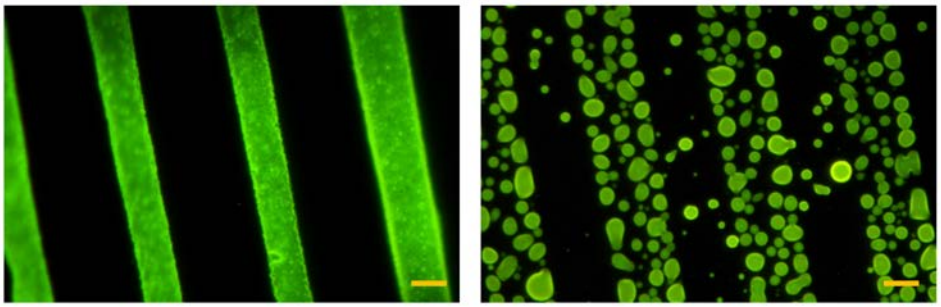


Figure 2.17: Fluorescence images of molecules **3** and (20 mM) covalently attached (after 30 minutes of immersion time) on micropatterns consisting of 20 μm wide stripes of electroactivated HQ surface. The oxidized SAM **S2** reacts through a (A) DA reaction (**S3-FC**) or a (B) MA reaction (**S4-FC**), respectively. The stripe width of the pattern in the left image is narrower than the 20 μm of the PDMS stripes, which can be attributed the excess in pressure exerted when contact printing octadecanethiol, due to the fact that this process is very pressure dependent. The scale bar corresponds to 10 μm.

In spite of the different experimental conditions explored, the MA reaction did not give place to a homogeneous functionalization, but to patchy areas compared to the fully covered surfaces obtained through the DA reaction. The DA reaction has been described to show a rate enhancement in polar solvents and in ethylene glycol environments due to the stabilization of its transition state [104]. On the other hand, the MA reaction, in spite of being considered a powerful click reaction [91], needs mild catalysis (i.e., amounts of a base or a nucleophile in the media) to increase its reaction kinetics and yield, which explains the formation of patchy areas in its absence. Under the present conditions, as we compared the two reactions under similar conditions, we did not add any catalyst. Given the considerable variability of the catalytic reaction, which depends on the pKa of the used thiol (ranging from 7 to 11), the strength and concentration of the catalyst as well as the steric hindrance between the reactants [91], an optimization of the reaction conditions should be considered for each system.

Since the synthesis of the Cp derivatives is more complex and the compounds obtained are less stable than the thiol analogues, we can conclude that there is not a clearly advantageous reaction over the other and therefore their use should be decided according to the singularities of each system, such as the difficulty of synthesizing specific Cp-derivatives, the need for fully coated surfaces, or the possibility of adding a catalyst.

## 2.6 Summary and Perspectives

In this study mixed SAMs have been prepared with electroactive pegylated HQ terminated thiols. Up to now, the main drawback in using this platform has been attributed to synthetic difficulties [26] to achieve the desired molecules. Therefore, in the present study an effort has been put into the optimization of the synthesis and thus, a thorough and complete description of the synthetic routes are provided. To produce spatially and temporally switchable surfaces using these molecules, we

prepared patterned SAMs of HQ that were used as a dynamic interface to immobilize different functional molecules to compare the DA versus MA reactions upon the application of a low electrical potential. Cp-fluorescein (molecule **3**) and thiol-fluorescein (molecule **2**) were used as fluorescent probes to be able to characterize and compare the proper immobilization using fluorescence microscopy for the first time. Even if apparently the DA reaction provides a more homogeneous surface functionalization, the use of Cp functionalized molecules is not easy and these are less stable than their thiol analogues.

Moreover, a multi-technique approach based on XPS, CV and CA measurements of the electroactive SAM was performed, adding characterization information of the system, which to our knowledge, had not been yet reported.

The platform reported within this Chapter has an enormous potential and broad usage scope in different disciplines, ranging from sensing to biomedicine through data storage or cleanup. It could be used, for example, to induce a change in wettability by anchoring different hydrophilic/hydrophobic groups for applications in microfluidics or, alternatively, it could also be used for biomaterial modification to trigger a specific cellular response in tissue engineering applications which require a temporal and spatial control.

# References


[14] A. Pulsipher and M. N. Yousaf. „Self-Assembled Monolayers as Dynamic Model Substrates for Cell Biology“. In: *Advanced Polymer Science* 240 (2010), pp. 103–134 (cit. on pp. 3–6, 9, 27).

[16] W.-S. Yeo, M. N. Yousaf, and M. Mrksich. „Dynamic Interfaces between Cells and Surfaces: Electroactive Substrates that Sequentially Release and Attach Cells“. In: *Journal of the American Chemical Society* 125.49 (2003), pp. 14994–14995 (cit. on pp. 3, 25).

[19] W. S. Dillmore, M. N. Yousaf, and M. Mrksich. „A Photochemical Method for Patterning the Immobilization of Ligands and Cells to Self-Assembled Monolayers“. In: *Langmuir* 20.17 (2004), pp. 7223–7231 (cit. on pp. 3, 9, 31, 36).

[26] J. C. Love, L. A. Estroff, J. K. Kriebel, N. Ralph G., and G. M. Whitesides. „Self-Assembled Monolayers of Thiolates on Metals as a Form of Nanotechnology“. In: *Chem. Rev.* 105 (2005), pp. 1103–1169 (cit. on pp. 6, 7, 12, 27, 28, 31, 35, 39, 48).

[27] J. Robertus, W. R. Browne, and B. L. Feringa. „Dynamic control over cell adhesive properties using molecular-based surface engineering strategies“. In: *Chemical Society reviews* 39.1 (2010), pp. 354–78 (cit. on pp. 6, 26, 30).

[36] E. W. L. Chan, S. Park, and M. N. Yousaf. „An electroactive catalytic dynamic substrate that immobilizes and releases patterned ligands, proteins, and cells“. In: *Angewandte Chemie* 47.33 (2008), pp. 6267–6271 (cit. on pp. 9, 30, 66).

[42] H.-G. Hong and W. Park. „Electrochemical characteristics of hydroquinone-terminated self-assembled monolayers on gold“. In: *Langmuir* 17.8 (2001), pp. 2485–2492 (cit. on pp. 12, 29, 30, 35, 40).

[53] W.-S. Yeo and M. Mrksich. „Electroactive Self-Assembled Monolayers that Permit Orthogonal Control over the Adhesion of Cells to Patterned Substrates“. In: *Langmuir* 22.25 (2006), pp. 10816–10820 (cit. on p. 25).

[54] I. Choi, Y.-. Kim, D.-H. Min, S. Lee, and W.-S. Yeo. „On-Demand Electrochemical Activation of the Click Reaction on Self-Assembled Monolayers on Gold Presenting Masked Acetylene Groups“. In: *Journal of the American Chemical Society* 133.42 (2011), pp. 16718–16721 (cit. on pp. 25, 27).

[55] M. S. Maglione, S. Casalini, S. Georgakopoulos, et al. „Fluid Mixing for Low-Power 'Digital Microfluidics' Using Electroactive Molecular Monolayers“. In: *Small* 14.10 (2018), p. 1703344 (cit. on pp. 25, 40, 41).

[56] W. Ma and Y.-T. Long. „Quinone/hydroquinone-functionalized biointerfaces for biological applications from the macro- to nano-scale“. In: *Chem. Soc. Rev.* 43.1 (2014), pp. 30–41 (cit. on pp. 25, 30).

[57] E. Marchante, N. Crivillers, M. Buhl, J. Veciana, and M. Mas-Torrent. „An Electrically Driven and Readable Molecular Monolayer Switch Based on a Solid Electrolyte“. In: *Angewandte Chemie International Edition* 55.1 (2016), pp. 368–372 (cit. on p. 25).

[58] M. Fibbioli, O. Enger, F. Diederich, et al. „Redox-active self-assembled monolayers as novel solid contacts for ion-selective electrodes“. In: *Chemical Communications* 0.5 (2000), pp. 339–340 (cit. on p. 25).

[59] M. Jurow, A. E. Schuckman, J. D. Batteas, and C. M. Drain. „Porphyrins as Molecular Electronic Components of Functional Devices.“ In: *Coordination Chemistry Reviews* 254.19-20 (2010), pp. 2297–2310 (cit. on p. 25).

[60] S. A. Trammell, M. Moore, D. Lowy, and N. Lebedev. „Surface Reactivity of the Quinone/Hydroquinone Redox Center Tethered to Gold: Comparison of Delocalized and Saturated Bridges“. In: *Journal of the American Chemical Society* 130.16 (2008), pp. 5579–5585 (cit. on pp. 25, 30, 32).

[61] C. Simão, M. Mas-Torrent, J. Casado-Montenegro, et al. „A Three-State Surface-Confined Molecular Switch with Multiple Channel Outputs“. In: *Journal of the American Chemical Society* 133.34 (2011), pp. 13256–13259 (cit. on p. 25).

[62] I. Choi and W.-S. S. Yeo. „Self-Assembled Monolayers with Dynamicity Stemming from (Bio)Chemical Conversions: From Construction to Application“. In: *ChemPhysChem* 14.1 (2013), pp. 55–69 (cit. on p. 25).

[63] E. W. L. Chan and N. M. Yousaf. „Immobilization of Ligands with Precise Control of Density to Electroactive Surfaces“. In: *Journal of the American Chemical Society* 128.48 (2006), pp. 15542–15546 (cit. on pp. 25, 72).

[64] Q. D. Zhang, G. March, V. Noel, et al. „Label-free and reagentless electrochemical detection of PCR fragments using self-assembled quinone derivative monolayer: Application to Mycobacterium tuberculosis“. In: *Biosensors and Bioelectronics* 32.1 (2012), pp. 163–168 (cit. on p. 25).

[65] M. Curreli, C. Li, Y. Sun, et al. „Selective functionalization of InO3 nanowire mat devices for biosensing applications“. In: *Journal of the American Chemical Society* 127.19 (2005), pp. 6922–6923 (cit. on pp. 25, 30, 32).

[66] S. Park, N. P. Westcott, W. Luo, D. Dutta, and M. N. Yousaf. „General chemoselective and redox-responsive ligation and release strategy.“ In: *Bioconjugate chemistry* 25.3 (2014), pp. 543–51 (cit. on p. 27).

[67] P. M. Mendes, K. L. Christman, P. Parthasarathy, et al. „Electrochemically Controllable Conjugation of Proteins on Surfaces“. In: *Bioconjugate Chemistry* 18.6 (2007), pp. 1919–1923 (cit. on p. 27).

[68] J. Li, C.-L. Sun, R. Shen, et al. „An Electrochemically Switched Smart Surface for Peptide Immobilization and Conformation Control“. In: *Journal of the American Chemical Society* 136.31 (2014), pp. 11050–11056 (cit. on pp. 27, 28).

[69] A. Napolitano, L. Panzella, L. Leone, and M. D'ischia. „Red Hair Benzothiazines and Benzothiazoles: Mutation-Inspired Chemistry in the Quest for Functionality". In: *Accounts of Chemical Research* 46.2 (2012), pp. 519–528 (cit. on p. 27).

[70] R. Inaba, A. Khademhosseini, H. Suzuki, and J. Fukuda. „Electrochemical desorption of self-assembled monolayers for engineering cellular tissues". In: *Biomaterials* 30.21 (2009), pp. 3573–3579 (cit. on pp. 27, 28).

[71] B. Wildt, D. Wirtz, and P. C. Searson. „Triggering cell detachment from patterned electrode arrays by programmed subcellular release". In: *Nature protocols* 5.7 (2010), pp. 1273–1280 (cit. on pp. 28, 29, 211, 212).

[72] T. Kawaguchi, H. Yasuda, K. Shimazu, and M. D. Porter. „Electrochemical Quartz Crystal Microbalance Investigation of the Reductive Desorption of Self-Assembled Monolayers of Alkanethiols and Mercaptoalkanoic Acids on Au". In: *Langmuir* (2000) (cit. on p. 28).

[73] K. Sun, B. Jiang, and X. Jiang. „Electrochemical desorption of self-assembled monolayers and its applications in surface chemistry and cell biology". In: *Journal of Electroanalytical Chemistry* 656.1 (2011), pp. 223–230 (cit. on p. 28).

[74] J. Enomoto, N. Mochizuki, K. Ebisawa, et al. „Engineering thick cell sheets by electrochemical desorption of oligopeptides on membrane substrates". In: *Regenerative Therapy* 3 (2016), pp. 24–31 (cit. on pp. 28, 212, 213).

[75] Y. Seto, R. Inaba, T. Okuyama, et al. „Engineering of capillary-like structures in tissue constructs by electrochemical detachment of cells". In: *Biomaterials* 31.8 (2010), pp. 2209–2215 (cit. on pp. 29, 213).

[76] S.-H. Yoon, J. Chang, L. Lin, and M. R. K. Mofrad. „A biological breadboard platform for cell adhesion and detachment studies". In: *Lab on a Chip* 11.3555 (2011) (cit. on pp. 29, 212).

[77] P. Petrangolini, A. Alessandrini, L. Berti, and P. Facci. „An Electrochemical Scanning Tunneling Microscopy Study of 2-(6-Mercaptoalkyl) hydroquinone Molecules on Au(111)". In: *Journal of the American Chemical Society* 132 (2010), pp. 7445–7453 (cit. on p. 30).

[78] W. Luo, N. P. Westcott, A. Pulsipher, and M. N. Yousaf. „Renewable and optically transparent electroactive indium tin oxide surfaces for chemoselective ligand immobilization and biospecific cell adhesion." In: *Langmuir* 24.22 (2008), pp. 13096–101 (cit. on p. 30).

[79] E-j. Lee, W. Luo, E. W. L. Chan, and M. N. Yousaf. „A molecular smart surface for spatio-temporal studies of cell mobility." In: *PLoS ONE* 10.6 (2015), pp. 1–25 (cit. on pp. 30, 32, 39).

[80] M. Shamsipur, S. H. Kazemi, A. Alizadeh, M. F. Mousavi, and M. S. Workentin. „Self-assembled monolayers of a hydroquinone-terminated alkanethiol onto gold surface. Interfacial electrochemistry and Michael-addition reaction with glutathione“. In: *Journal of Electroanalytical Chemistry* 610.2 (2007), pp. 218–226 (cit. on pp. 30, 32, 40, 43).

[81] J. Li, Ch.-L. Sun, L. Tan, Y.-L. Xie, and H.-L. Zhang. „Investigation of an Electrochemically Switched Heterocyclization Reaction on Gold Surface“. In: *Langmuir* 29.17 (2013), pp. 5199–5206 (cit. on pp. 30, 32).

[82] E. W. L. Chan, M. N. Yousaf, and M. Mrksich. „Understanding the Role of Adsoportion in the Reaction of Cyclopentadiene with an Immobilized Dienophile“. In: *Journal of Physical Chemistry A* 104 (2000), pp. 9315–9320 (cit. on pp. 30, 31, 35).

[83] M. N. Yousaf, B. T. Houseman, and M. Mrksich. „Using electroactive substrates to pattern the attachment of two different cell populations“. In: *Proceedings of the National Academy of Sciences* 98.11 (2001), pp. 5992–5996 (cit. on p. 30).

[84] C. Nicosia and J. Huskens. „Reactive self-assembled monolayers: from surface functionalization to gradient formation“. In: *Materials Horizons* 1.1 (2014), p. 32 (cit. on pp. 30, 31).

[85] N. P. Westcott and M. N. Yousaf. „Chemoselective ligand patterning of electroactive surfaces using microfluidics“. In: *Electrophoresis* 30.19 (2009), pp. 3381–5 (cit. on p. 30).

[86] J. H. Collier and M. Mrksich. „Engineering a biospecific communication pathway between cells and electrodes.“ In: *Proceedings of the National Academy of Sciences of the United States of America* 103.7 (2006), pp. 2021–5 (cit. on p. 30).

[87] X.-P. He, X.-W. Wang, X.-P. Jin, et al. „Epimeric Monosaccharide-Quinone Hybrids on Gold Electrodes toward the Electrochemical Probing of Specific Carbohydrate-Protein Recognitions“. In: *Journal of the American Chemical Society* 133.10 (2011), pp. 3649–3657 (cit. on p. 30).

[88] C.-X. Cui, Z.-P. Zhang, L. Zhu, et al. „Reactivity and regioselectivity in Diels–Alder reactions of anion encapsulated fullerenes“. In: *Physical Chemistry Chemical Physics* 19.45 (2017), pp. 30393–30401 (cit. on p. 31).

[89] M. N. Yousaf and M. Mrksich. „Diels-Alder Reaction for the Selective Immobilization of Protein to Electroactive Self-Assembled Monolayers“. In: *American Chemical Society* 121 (1998), pp. 4286–4287 (cit. on p. 31).

[90] B. D. Mather, K. M. Miller, and T. E. Long. „Novel Michael Addition Networks Containing Poly(propylene glycol) Telechelic Oligomers“. In: *Macromolecular Chemistry and Physics* 207.15 (2006), pp. 1324–1333 (cit. on p. 32).

[91] D. P. Nair, M. Podgórski, S. Chatani, et al. „The Thiol-Michael Addition Click Reaction: A Powerful and Widely Used Tool in Materials Chemistry“. In: *Chemistry of Materials* 26.1 (2014), pp. 724–744 (cit. on pp. 32, 48).

[92] S. C. Rizzi and J. A. Hubbell. „Recombinant Protein-co-PEG Networks as Cell-Adhesive and Proteolytically Degradable Hydrogel Matrixes. Part I: Development and Physicochemical Characteristics“. In: *Biomacromolecules* 6 (2005), pp. 1226–1238 (cit. on p. 32).

[93] A. R. Kyvik, C. Luque-Corredera, D. Pulido, et al. „Stimuli-Responsive Functionalization Strategies to Spatially and Temporally Control Surface Properties: Michael vs Diels–Alder Type Additions“. In: *The Journal of Physical Chemistry B* 122.16 (2018), pp. 4481–4490 (cit. on pp. 34, 122).

[94] Y. Qi, I. Ratera, J. Y. Park, et al. „Mechanical and Charge Transport Properties of Alkanethiol Self-Assembled Monolayers on a Au(111) Surface: The Role of Molecular Tilt“. In: *Langmuir* 24 (2008), pp. 2219–2223 (cit. on p. 35).

[95] Y. Qi, X. Liu, B. L. M. Hendriksen, et al. „Influence of Molecular Ordering on Electrical and Friction Properties of $\omega$-( trans-4-Stilbene)Alkylthiol Self-Assembled Monolayers on Au (111)“. In: *Langmuir* 26.21 (2010), pp. 16522–16528 (cit. on p. 35).

[96] L. Fang, J. Y. Park, H. Ma, Y. Jen, and M. Salmeron. „Atomic Force Microscopy Study of the Mechanical and Electrical Properties of Monolayer Films of Molecules with Aromatic End Groups“. In: (2007) (cit. on p. 35).

[97] N. A. Alcantar, E. S. Aydil, and J. N. Israelachvili. „Polyethylene glycol-coated biocompatible surfaces“. In: *Journal of Biomedical Materials Research* 51.3 (2000), pp. 343–351 (cit. on p. 35).

[98] J. Blümmel, N. Perschmann, D. Aydin, et al. „Protein repellent properties of covalently attached PEG coatings on nanostructured SiO2-based interfaces“. In: *Biomaterials* 28.32 (2007), pp. 4739–4747 (cit. on p. 35).

[99] J.-I. Kim, W.-C. Park, and H.-G. Hong. „The Effect of Steric Hindrance on Rate Constant of a Diels-Alder Reaction on the Hydroquinone-Terminated Self-Assembled Monolayer“. eng. In: *Bulletin of the Korean Chemical Society* 25.7 (2004), pp. 1081–1084 (cit. on p. 35).

[100] S. Casalini, M. Berto, C. A. Bortolotti, et al. „Electrowetting of Nitro-Functionalized Oligoarylene Thiols Self-Assembled on Polycrystalline Gold“. In: *ACS Applied Materials & Interfaces* 7.7 (2015), pp. 3902–3909 (cit. on p. 41).

[101] S. M. Morgenthaler, S. Lee, and N. D. Spencer. „Submicrometer Structure of Surface-Chemical Gradients Prepared by a Two-Step Immersion Method“. In: *Langmuir* 22 (2006), pp. 2706–2711 (cit. on p. 41).

[102] N. Ballav, A. Shaporenko, A. Terfort, and M. Zharnikov. „A Flexible Approach to the Fabrication of Chemical Gradients“. In: *Advanced Materials* 19.7 (2007), pp. 998–1000 (cit. on p. 41).

[103] D. G. Castner, K. Hinds, and D. W. Grainger. „X-ray Photoelectron Spectroscopy Sulfur 2p Study of Organic Thiol and Disulfide Binding Interactions with Gold Surfaces“. In: *Langmuir* 12 (1996), pp. 5083–5086 (cit. on p. 45).

[104] V. Beniwal and A. Kumar. „Thermodynamic and molecular origin of interfacial rate enhancements and endo-selectivities of a Diels–Alder reaction“. In: *Physical Chemistry Chemical Physics* 19.6 (2017), pp. 4297–4306 (cit. on p. 48).

# 3 Electroactive SAMs for the Control of Cell Behavior: Adhesion and Vascularization

> *Everything you will ever need to know is within you, the secrets of the universe are imprinted in the cells of your body.*
>
> **— Dan Millman**

## 3.1 Introduction

### 3.1.1 Cell Adhesion

The maintenance and development of biological tissues highly depend and rely on cell adhesion; in fact, cell adhesion plays a fundamental role in cellular and physiological functions, such as in cell regulation and cell communication [105–107]. Cell adhesion, thus, drives stimulating signals which are related to cell cycle, cell survival and cell migration processes [108]. As a consequence, many diseases are related to cell adhesion malfunction, among them cancer [108–110], osteoporosis [111] and arthritis [112]. For example, in cancer cell adhesion is reduced, this leading to the ability of cancer cells to migrate and destroy healthy tissues, which is one of the features which characterize malignant tumors [109].

It is therefore fundamental to achieve a complete understanding of cell adhesion onto different materials, since this is of paramount importance for integrating materials in tissues and minimizing scar tissue formation. In tissue engineering, new strategies to design and tune biointerfaces which match more closely the anatomy and physiology of host tissues are being developed. Moreover, the biochemical and biophysical requirements for specific cell types should also be incorporated into biomimetic materials [107]. To be able to meet these requirements, a control of the topographical, chemical and mechanical surface properties should be achieved at length scales which match with the size of cells [113].

All in all, surfaces which possess cell adhesion and protein binding properties are of high importance in applications within the field of biotechnology [7], for example for the use in biomaterials for medical implants [114], *in vivo* biosensors [115], drug-delivery carriers [116], tissue engineering platforms [117], microbial biofuel cells [118] and whole-cell biochips [119], to mention some.

#### Surface Chemistry for Cell Adhesion Control

One approach to manufacture substrates that allow the control of cell adhesion consists in coating substrates with specifically designed thin organic films which

present functional groups to the growth medium and subsequently to cells as well. These can be designed to have the ability to inhibit unspecific protein adsorption but promote cell adhesion [7]. They are normally deposited onto the substrate by spin-coating [120], plasma deposition [121], polymerization from surface-bound starters, initiators, or catalysts [122]. Another strategy used is the spontaneous formation of molecular monolayers, namely the use of SAMs, which has become very popular since the gold-thiol affinity was discovered [11]. Systems based on SAMs have several advantages even though polymeric films tend to be more stable, specially under cell-culture conditions. As previously mentioned, SAM systems are easily formed with a thermodynamic control: monolayer structure is determined by the structure of the organic molecules adsorbed and the substrate surface material. On the contrary, polymeric films are typically kinetically controlled: processing conditions then have an important effect on the layer formation, which include distribution of the chain length and other structural features [7]. Furthermore, SAMs are readily characterized by several structure-sensitive techniques, which are not equally useful for the characterization of polymeric films.

### 3.1.2 Integrins and Focal Adhesions

#### Integrins

Integrins are transmembrane proteins that form adhesion sites which allow cells to be connected to other cells or to the ECM. Through these sites, cells are also capable of transmitting intra or extracellular forces [105]. These transmembrane proteins, together with other adhesion molecules, attach the cell membrane to the cell cytoskeleton. The composition of the cell cytoskeleton includes predominantly actin fibers, which connect to integrins through the denominated focal adhesion complex, which is basically a highly organized structure composed by a variety of different molecules. Integrins share common structural features between each other [123]; they are linked through non-covalent interactions and are dimeric molecules which contain an $\alpha$ and a $\beta$ subunit (Figure 3.1). These subunits are transmembrane proteins of type I: characteristic of these is their large extracellular domain, which coordinates the assembly of the cytoskeleton and signaling cues, together with its shorter cytoplasmic domain, which normally interacts with macromolecules found in the ECM or with receptors on adjacent cell membranes [124].

As mentioned before, these transmembrane glycoproteins not only aid the structuring of the cytoskeleton, but also work as receptors which are involved in adhesion to ECM components such as fibronectin, laminin, collagens and vitronectin. In addition, they can also participate in certain cell-cell contact, binding to cell adhesion molecules (CAMs), such as the vascular-cell adhesion molecule (VCAM) and the intercellular adhesion molecule (ICAM) [112, 125].

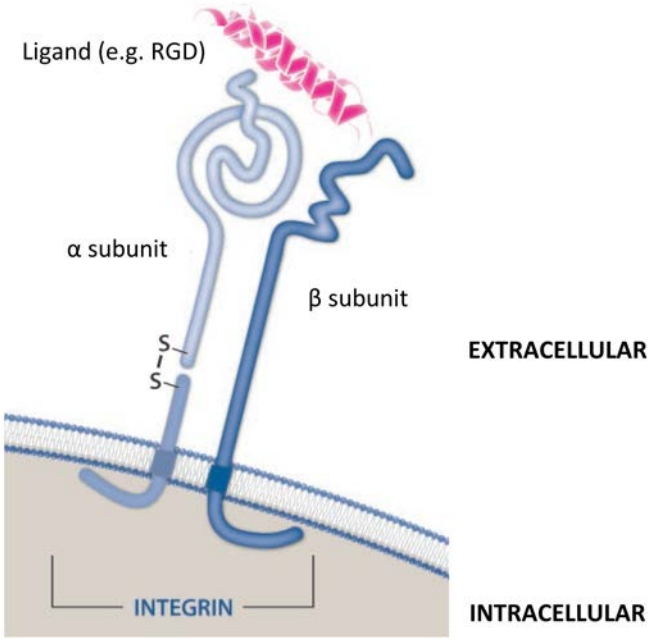


**Figure 3.1:** Schematic representation of the structure of an integrin, in which the $\alpha$ and $\beta$ units are portrayed. Reproduced and modified from [126].

### Focal Adhesions (FAs)

Adhesion to the ECM is mediated by molecular bundles on the plasma membrane denominated focal adhesions (FAs) [125] (Figure 3.2). FAs were firstly observed in the 1970s, initially as dark areas when using interference reflection microscopy, and were attributed to the zones where the cell surface was in close contact with the substratum. These darker regions, when using electron microscopy, exhibited an increased electron density: they were viewed as local dense plaques with associated microfilaments, localized on the inner face of the plasma membrane [127, 128].

In fact, FAs are formed in the regions where the surface of the cell comes closest to the substrate, and where the cytosolic face of the plasma membrane concentrates stress fibers and large bundles of microfilaments [129]. Hence, FAs form normally at the end of the actin stress fibers and in the protrusive parts of cells, such as filopodia and lamellipodia: these structures also have the necessary elements required to form integrin-dependent adhesions [125, 130].

More specifically, in FAs, agglomerations of actin filaments anchor to integrins on the transmembrane through a multi-molecular complex formed by multiple junction plaque proteins (Figure 3.2). These have different functions, some support the structural link between the actin cytoskeleton and membrane receptors while others participate as signaling molecules [125]. Although these complexes are mostly analyzed on 2D surfaces, FA formation also occurs within the 3D network of the ECM [130].

For visualizing FAs with fluorescence microscopy normally either paxillin or vinculin are stained with specific antibodies. Paxillin is a focal adhesion-associated, phosphotyrosine-containing protein that plays a role in several signaling pathways

[131] and vinculin localises to integrin-mediated cell–matrix adhesions and cadherin-mediated cell-cell junctions [132].

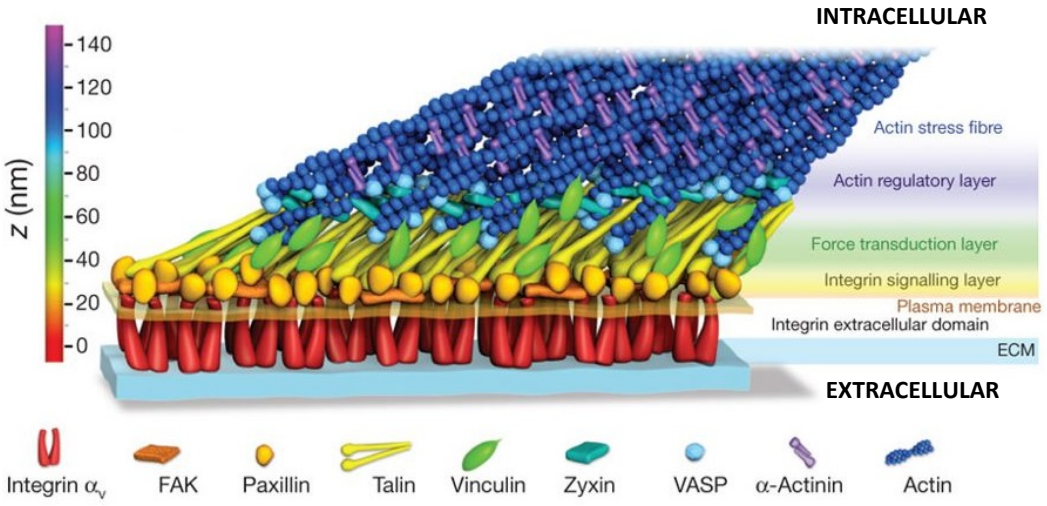


**Figure 3.2:** Schematic representation of the FA complex with all the components involved in its formation: integrins, paxillin, talin, vinculin, zyxin, VASP (Vasodilator-Stimulated Phosphoprotein), actinin and actin. Reproduced with permission from [133].

### 3.1.3 RGD: A Model Ligand for Cell Adhesion

A lot of effort has been put into defining integrin recognition sites on different ligands and counter-receptors, the first one being the amino acid sequence Arg-Gly-Asp, the denominated RGD sequence. RGD is present in fibronectin, vitronectin and other adhesive proteins, and is one of the most relevant sequences responsible for mediating cell attachment through integrins. Herein, the crucial importance of this tripeptide for mediating cell-substratum and cell-cell interactions. Integrins recognizing RGD are the five $\alpha$V integrins, together with both $\beta$1 integrins ($\alpha$5 and $\alpha$8) and $\alpha$IIb$\beta$3 [123, 124, 134]. Therefore, RGD analogues and peptides present an important tool in providing more information regarding the fundamental mechanisms of how cell adhesion works, and moreover, are potential therapeutic agents for different diseases such as thromobosis and some sorts of cancer [123].

RGD interacts with the integrins through the interface between their $\alpha$ and $\beta$ subunits: the R amino acid fits into a cleft in the $\beta$-propeller module found in the $\alpha$ subunit. The D amino acid coordinates a cation bound in a von Willebrand factor localized in the factor A-domain in the $\beta$ subunit. Actually, studies have shown that the crystal structures of $\alpha$V$\beta$3 and $\alpha$IIb$\beta$3 complexed with RGD ligands are, at the atomic level, identical [135, 136].

The RGD-binding integrins are among the most undiscriminating in the family, this being the case in particular for $\beta$3 integrins, since they bind to a large number of ECM and soluble vascular ligands. However, the ligand affinity does vary, and the ranking order of this is dependent on the precision of the fit between the tripeptide RGD and the specific active sites localized in the $\alpha$-$\beta$ subunits [124].

### 3.1.4 Micro and Nano-patterning of Cell Adhesion Motifs

Several properties are relevant when working with materials functionalized with cell binding ligands: it is known that (i) the surface density of the ligand, (ii) the spatial distribution of these and (iii) their conformation, provide important surface cues [137]. In fact, surfaces with a controlled microstructure can maintain better cell morphology, differentiation and functionality over longer periods of time. Accordingly, not only the composition but also the spatial organization of the ECM environment is important in regulating cell-ECM interactions [138].

#### Micropatterning

In 1998 Ingeber et al. [31] used soft lithography to pattern ECM in micrometer-scale size patterns to explore how this spatial distribution could affect cell position and shape. It was seen that cells would adopt the shape of the pattern, when these did not exceed the size of the maximum spreading area of the cell. Also, bridging capabilities of cells between ECM patterns over non-adhesive regions were observed when the spacing was below 10 and 20 μm depending on the cell type, and was found to be independent from the size of the ECM island. In a following study [139], it was found that the FA area of cells increased with cell spreading, even though the total amount of patterned ECM was held constant.

In a more recent study, carried out by Lehnert et al. [140] the technique of μCP was used to create micro-patterns of fibronectin; it was found that cell spread is directly correlated to the total coverage of the surface with ECM proteins, independent from the geometrical shape of the patterned ECM. Specifically, the ability of cells to spread and migrate on dots of around 1 $\mu m^2$ was confirmed, this being inhibited when the dot separation was larger than 30 μm, similar to what had been already reported [31].

#### Nanopatterning

The group of Spatz has focused on the creation of platforms to investigate cell adhesion at the molecular level. This has been done by creating substrates with a controlled spacing of gold nanodots which are then functionalized with RGD-thiol molecules. In such a way, each nanodot presenting RGD is additionally small enough to represent a single binding site for an individual integrin (which have a size of approximately 8-12 nm) [138].

Wang et al. [141] have taken a step further by creating a platform with micro/nano patterns on a non-fouling background in order to study cell-material interactions at the molecular and cell level. By doing this, they were able to decouple the effect of the distance between RGDs (nanopatterns) and cell spreading size (obtained by micropatterns). They found that RGD nanospacing, even with little cell spreading, provides stronger cell tension and hence, plays a role in cell differentiation.

### 3.1.5 Dynamic Surfaces for Cell Adhesion Control

The ability to turn off or on the cell adhesive properties of surfaces is very interesting in a broad spectrum of applications in material sciences, in the interface between cell biology, chemistry and technology. This property can be used, for example, in microfluidic chips integrated into lab-on-chip devices, for the formation of cell sheets or the study of cell-material interfaces [2, 142]. Since it allows real time monitoring of how cells interact with biological ligands, inducing specific cellular responses, it facilitates the study of these processes with more accuracy [9], i.e. having a temporal control. In fact, the ability to control the cellular microenvironment is relevant for several scientific fields, comprising tissue engineering, cell biology and medicine [2, 142].

Ng et al. [17] have reported a surface which is switchable from cell-repulsive to cell-adhesive and back again. This was done by using SAMs composed of molecules which are able to conceal or expose RGD peptides depending on the polarity. SAMs composed of RGD and an EG molecule with a charge were fabricated: the charged EG molecules would flip to conceal or expose the neighboring peptides, by the application of a negative or positive potential [17].

Another strategy using a photochemical external stimulus has been reported by Liu et al., consisting of a mixed SAM of a pegylated alkanethiol and an azobenzene functionalized with a peptide which promotes cell adhesion. The reversible photochemical switchability from E to Z conformation of azobenzene allows the surface to switch from a cell-adhesive to a cell-repelling state (Figure 3.3) [143].

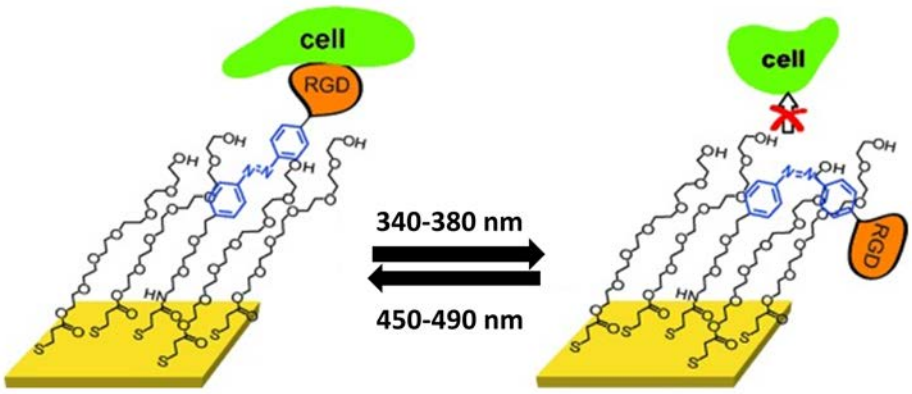


**Figure 3.3:** The azobenzene moiety is converted photochemically between the E and Z configurations, presenting or masking the RGD ligand and consequently modulating cell adhesion. Reproduced from [143].

Yousaf's group has developed a platform which is capable of immobilizing oxyamine ligands on a HQ terminated SAM, using an external electrochemical stilumus. This strategy also allows for the release of the ligands, by electrochemical reduction, in this way achieving a control of cell adhesion with another type of external stimulus [36].

### 3.1.6 Vascularization in Tissue Engineering

In the field of tissue engineering, vascularization, for sufficient diffusion of nutrients, oxygen and waste products in tissues, is essential when working with tissues larger than 100-200 μm, in agreement with the diffusion limit of oxygen [144]. Also, strategies which increase angiogenesis, thus promoting vascularization, are potential treatments for ischemic tissues [145, 146]. Actually, one of the big challenges when it comes to the formation of viable scaffolds for tissue engineering applications, is the successful formation of vascular networks within these: this explains the very few examples of *in vitro* tissues, since the creation of engineered blood vessels is still under research [146, 147]. Hence, creating a functional vasculature is still one of the most demanding goals in the field of tissue engineering [148] and as such, much scientific research has been focused in finding new approaches and strategies in order to overcome this major challenge.

Three processes are attributed to new vessel formation *in vivo*: (i) *de novo* formation, denominated vasculogenesis, (ii) sprouting of pre-existing vessels, called angiogenesis [146, 148] and (iii) arteriogenensis, which consists in the remodeling of existing vasculature to form functional arteries [149]. Angiogenesis and arteriogenesis take place normally in adult tissues, and vasculogenesis is the responsible for shaping the circulatory system in the early stages of development [149]. *In vivo*, the ECM plays a regulative role in the process of vascularization, by presenting biochemical cues such as growth factors, together with a 3D physical support at the nano- and macroscale [147].

A large amount of approaches based on the formation of biomaterial based structs have been using the vascular endothelial growth factor (VEGF), which induces vascular endothelial cells to initiate angiogenesis when binding to transmembrane VEGF receptors (VEGFR) [148]. VEGF is a potent angiogenic factor and a critical regulator, which works at a narrow concentration range, and thus, its dose must be regulated in a quantitative way, both spatially and temporally. Above its ideal concentration, capillary formation is not well controlled, and thus leaky and defective structures are formed, similar to those in tumoral tissues and consequently leading to vascular disaster [148, 150, 151].

### 3.1.7 The VEGF Receptor

Such as integrins bind to RGD, VEGF also has cell receptors through which it mediates the activation of intracellular signaling cascades that direct cellular behavior. In humans, these are VEGFR-1 (referred to as Flt-1), VEGFR-2 (referred to as Flk-1 or KDR), and VEGFR-3 [152]. VEGFRs are typical tyrosine kinase receptors (TKRs) [153] composed by an extracellular domain, which binds to the ligand, a transmembrane domain and a cytoplasmic domain which includes a tyrosine kinase domain [154].

The most important regulators of endothelial cell proliferation, survival, migration and vascular permeability in adult tissues are the VEGFR-2 and VEGF-A. VEGF-A is responsible for receptor dimerization, phosphorylation, and subsequent signal trans-

duction. Therefore, a big interest exists in being able to regulate its concentration and it is actually an interesting target for therapies inducing pro or anti-angiogenic effects, together with the control of VEGFR-2 dimerization or activation [155].

### 3.1.8 Qk-peptide: A Tubulogenesis Promoting Motif

Most of the strategies looking for alternative, non-invasive and biomaterial-based ways to achieve a controlled delivery of pro-angiogenic factors, with a spatial and temporal control, have primarily concentrated on the delivery of specific proteins. In most of the cases VEGF has been used, but recently, attention has been put on peptide sequences which mimic the biochemical function of growth factors [149, 156]. The fact is that these short peptidic sequences are easier and cheaper to synthesize and are more stable in biological fluids even upon chemical modifications [157], which is important for any real application where scale-up in production is a must. Also, the immugenicity properties and the narrow concentration window make VEGF difficult to work with [151].

The Qk-peptide is a VEGF mimicking peptide, which imitates the helical structures of the binding sites of VEGF, specifically the native $\alpha$-helical receptor-binding domain of VEGF, and has a high affinity for the VEGFR [158]: it possesses the same biological activity as the full length VEGF protein with the advantages abovementioned of being a short peptidic sequence [147, 151].

D'Andrea et al. were the first ones to synthesize the Qk-peptide. Based on the X-ray structure of VEGF bound to the receptor, they mimicked the sequence of the VEGF binding interfaces, reproducing the VEGF17–25 helix region. At first they discovered that the unstructured VEGF15 peptide did not display bioactivity. They also found that the presence of the helical core region of the peptide is critical for the binding with VEGFR, which led to the introduction of amino acid alterations in the peptidic sequences to ensure the preservation of the structure [158] and, as a consequence, of the bioactivity as well.

### 3.1.9 Strategies using Qk-peptide

Since the proof of bioactivity of the Qk-peptide sequence, many different approaches have been exploiting the benefits of using this VEGF mimicking peptide. Leslie-Barbick et al. integrated an acetylated Qk into PEG hydrogels covalently, and showed that *in vitro* and *in vivo* a pro-angiogenic effect was obtained when seeding endothelial cells in these functionalized hydrogels matrices [159]. Another strategy has involved the use of silk fibroin hydrogels incorporating cleavable peptide sequences, among these Qk-pepides, in order to attract endothelial cells, make them infiltrate the hydrogel and promote the creation of blood vessels. In the *in vitro* studies, proliferation was augmented, and *in vivo* studies were also performed. The subcutaneous implantation of the hydrogels in rats showed that endothelial cells not only could infiltrate into the hydrogels but they also promoted new tissue formation in replacement of the fibroin hydrogels [160].

In another study, reported by Zhou et al., electrospun membranes modified with Qk-peptides were shown to enhance proliferation of vascular endothelial cells more

in comparison with those modified with REDV peptides (REDV peptide mediates adsorption and migration of vascular endothelial cells) [151].

For drug delivery purposes, Young et al. created hydrogel nanoparticles which were designed to be able to release in a sustained way the Qk-peptide, through a diffusion mechanism. The efficacy of the system and the biological activity of the pro-angiogenic peptide was characterized using circular dichroism spectroscopy, to ensure the preservation of the secondary structure of the peptide, and a tubulogenesis assay, in which the presence of the loaded nanoparticles were found to enhance tubulogenesis [157].

Studies reporting approaches using Qk covalently attached to substrates are very few to our knowledge, the only one found is the interesting study conducted by Koepsel et al. comparing soluble Qk and surface bound Qk. SAM arrays presenting different densities of covalently immobilized Qk and a cell adhesion promoting peptide were used to probe for changes in human umbilical vein endothelial cell (HUVEC) attachment, proliferation and tubulogenesis (Figure 3.4). For covalently immobilized Qk, results showed that this form inhibited several pro-angiogenic cell behaviors (attachment and proliferation), but on the other hand, promoted tubulogenesis. This was not the case for soluble Qk, which promoted attachment and proliferation, but did not induce tubule formation, in accordance to older studies performed with VEGF in polyacrylamide gels [161]. In presence of both, it seems that the immobilized form inhibited the soluble form. This indicates the strong influence of the context in which ligands are presented to the cell surface [155].

Hence, different studies in literature have reported all or some pro-angiogenic outcomes in cell behavior in presence of VEGF and Qk, enhancement of (i) cell attachment, (ii) proliferation or (iii) tubulogenesis. In fact, studies show that Qk exhibits pro-angiogenic properties when delivered in different formats; as a soluble molecule, when reversibly associated with a biomaterial, when conjugated within a biomaterial via a flexible polymer linker or when immobilized on a surface. However, the pro-angiogenic effects are not always enhanced at the same time, or even act as inhibitors in some cases. Therefore, it is important to realize that many parameters play a role and it is not easy to separate these to understand how each of these effect cell behavior. Furthermore, especially when working with artificial materials, it is necessary to be aware that not only the chemical cues these present decide cell fate and behavior, but that the mechanical properties of the materials used also play a crucial role [161].

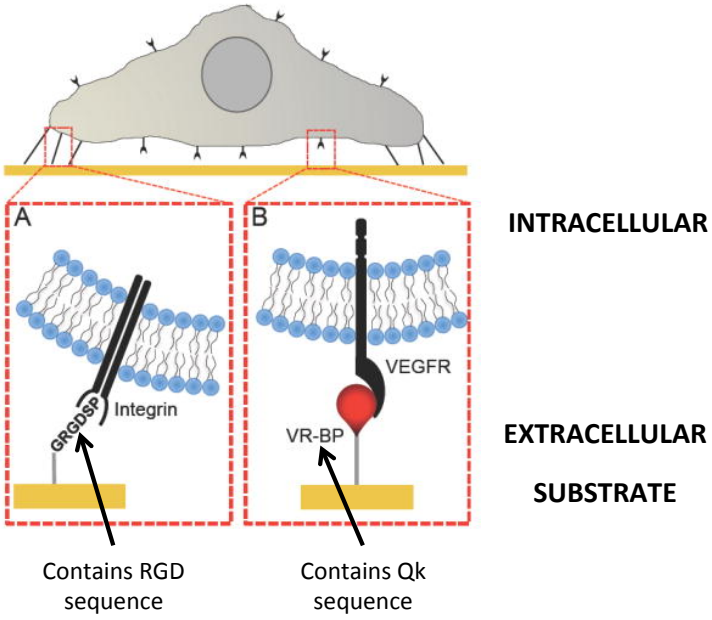


**Figure 3.4:** SAM arrays presenting (A) the cell adhesion ligand interacting with the integrin and (B) Qk-peptide interacting with the VEGFR. Reproduced from [155].

## 3.2 Objectives and Strategy

In this Chapter we will explore the use of stimulus driven interfaces for the control of cell adhesion. More specifically, for the first time, a comparison of the interfacial reactions of DA and MA by using Cp and thiol modified RGD peptides to decorate gold coated surfaces will be reported. Cell adhesion will be evaluated by looking at cell density, cell spreading and FA area in substrates coated with RGD, prepared using both interfacial reactions.

In order to study the effect of immobilized Qk on surface for cell differentiation towards tubule formation, a novel study will be conducted using thiol functionalized Qk. With the aim of discovering any synergistic or inhibitory effect in presence of RGD, this will be done also by combining it with immobilized RGD. For this, a tubulogenesis assay using Matrigel coated surfaces to support cell tube formation and a cell viability assay will be conducted.

In order to be able to carry out this work, we will focus on the following specific tasks:

- Comparison of the DA and MA interfacial reaction for the immobilization of functionalized RGD peptides. In order to do this, (i) the synthesis of RGD tagged molecules with a Cp and thiol termination[1] is carried out and (ii) SAMs are prepared with HQ-terminated alkanethiols, as described in Chapter 2. Finally, (iii) interfacial reactions are performed: firstly a low voltage is applied, inducing the oxidation of surface tethered HQ molecules and in a second step, RGD peptides are immobilized via the DA and the MA interfacial reactions.

[1]This work was carried out by the Combinatorial Chemistry Unit (Technology Platform of the Barcelona Science Park) in a collaborative framework.

- Study of the efficient immobilization of RGD ligands on surface. This is done by (i) seeding cells onto the peptide decorated surfaces (prepared by the use of the DA and MA interfacial reaction) and (ii) studying and quantifying cell density, cell spreading and FA area (Figure 3.5) and subsequently, performing a deep statistical analysis. For this, fixation and immunostaining of cells is carried out, followed by observing the samples using confocal microscopy.

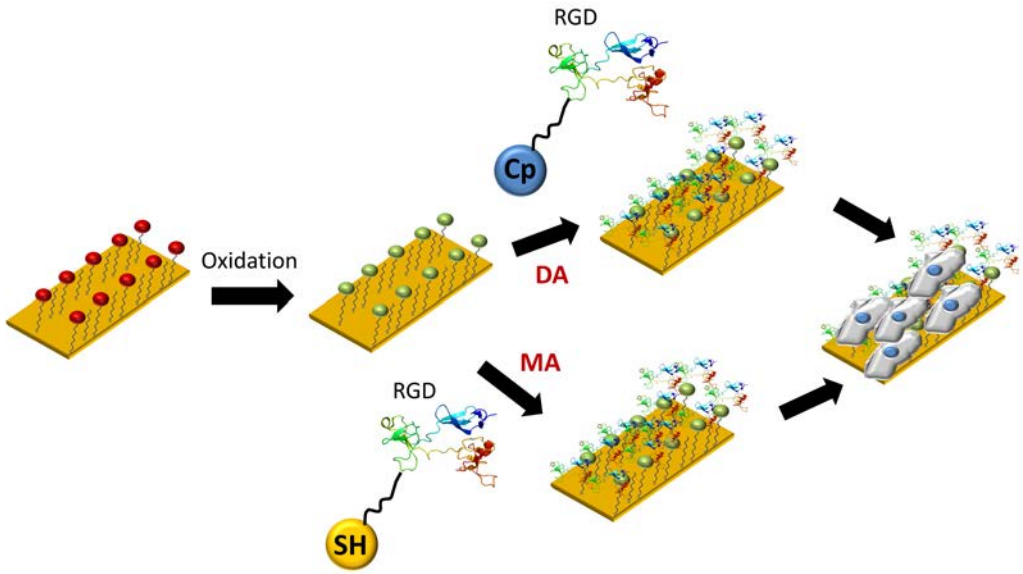


**Figure 3.5:** Scheme illustrating the experimental procedure of the work described in this Chapter for the comparative study of DA and MA using RGD functionalized peptides.

- Study the enhancement of tubule network formation with immobilized Qk. For this, a tubulogenesis assay using substrates with immobilized Qk and RGD peptides in different ratios together with control samples is conducted (Figure 3.6).

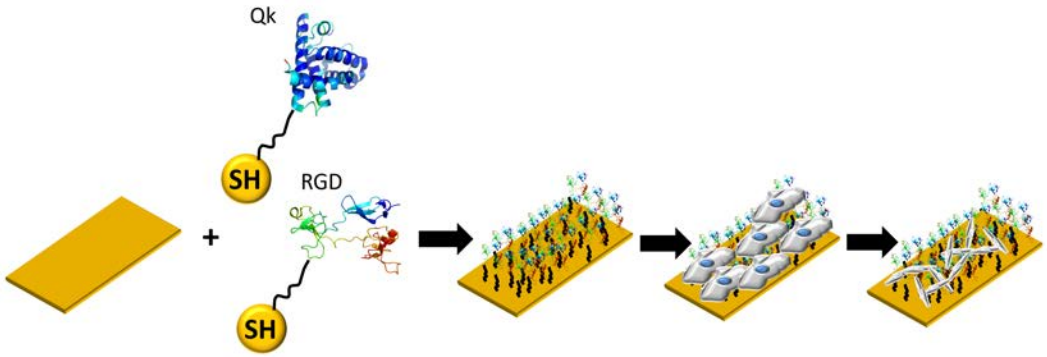


**Figure 3.6:** Scheme illustrating the experimental procedure of the work described in this Chapter concerning the tubulogenesis assay on Qk and RGD functionalized substrates.

## 3.3 Interfacial Reactions to Control Cell Adhesion

Firstly, cell adhesion was studied on functionalized surfaces using the DA or the MA interfacial reactions to immobilize Cp and thiol tagged RGD peptides. Cell density, cell spreading and FA area was studied in order to be able to assess the efficiency of the decorated surfaces to enhance cell adhesion.

### 3.3.1 MA vs. DA Interfacial Reactions with RGD-functionalized Molecules

To our knowledge, few groups have used the DA for immobilizing RGD peptides [162], but no study has been focused on comparing this strategy with the use of the MA interfacial reaction. This is an attractive approach, since thiol moieties are easily attached to biomolecules, and in fact, many biomolecules bear these naturally. In addition, the use of Cp for solid phase peptide synthesis is not really feasible since Cp actually decomposes under cleavage conditions [63]. This really supports the relevance in studying the efficiency of immobilizing RGD via the MA reaction and studying cell behavior on these modified surfaces. In fact, it might be a better way to conduct studies with real time monitoring of how cells interact with biological ligands which induce specific cellular responses.

Therefore, in this study, the interfacial reactions of DA and MA were studied using RGD molecules functionalized with a Cp and a thiol moiety, molecule **Cp-RGD** and **SH-RGD**, respectively (Figure 3.7). Cell density, cell spreading and FA quantification were used to be able to compare the effect of these two interfacial reactions related to their cell adhesive properties in response to an electrochemical stimulus.

Molecules **Cp-RGD** and **SH-RGD** were synthesized using standard protocols of solid phase peptide synthesis, details are given in Section 7.2.2.

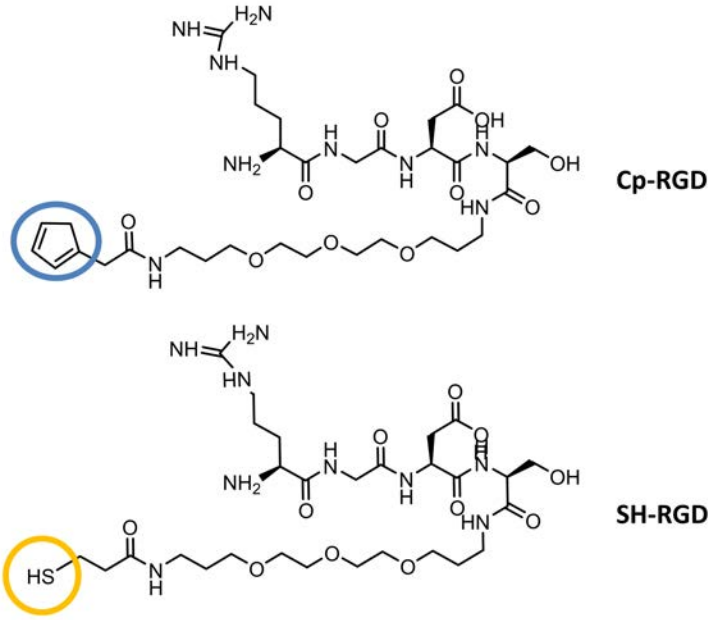


**Figure 3.7:** Molecular structures of RGD molecules used for the comparative study of the interfacial reactions. Molecule **Cp-RGD** corresponds to the cyclopentadiene-RGD (Cp circled in blue) and **SH-RGD** to the thiol-RGD (thiol circled in yellow).

### 3.3.2 Sample Preparation

In order to be able to compare the two interfacial reactions, samples were prepared by following different steps, these listed in Table 3.1.

Summarizing, in Step 1, mixed SAMs composed of alkanethiols terminated in HQ and pegylated alkanethiols, molecules **2** and **1** (Figure 2.7) (SAM **S1**, in a 1:99 ratio) were prepared as described in Section 7.2.1. For the preparation of samples with immobilized peptides, in Step 2, a low voltage was applied to oxidize the HQ on surface and thereafter in order to obtain SAM **S2**, in Step 3, they were incubated in a solution (15 mM in PBS) containing the respective RGD molecule (molecule **Cp-RGD** or **SH-RGD**), depending on the interfacial reaction to take place (DA or MA), and thus obtaining **S3-RGD** or **S4-RGD** (Figure 3.9). For minimizing the use of molecules which are expensive and hard to synthesize, a humid chamber was used for SAM biofunctionalization. Specifically, incubation of the substrates was done using a plastic petri dish with a piece of parafilm onto which a droplet of the molecule solution was disposed. Thereafter, substrates were carefully put face down onto the molecule solution, as shown in Figure 3.8. These were then rinsed and stored in PBS before proceeding to cell seeding. As a control, samples with no electrochemical activation were also incubated in ligand solutions (samples $\mathbf{t_0}$, one for the Cp solution and one for the thiol solution), providing information about cell behavior on functionalized substrates in absence of the external stimulus. For the positive control sample, instead of functionalization with a SAM, substrates were coated with fibronectin and no voltage was applied. As already mentioned, fibronectin contains among other cell-adhesive proteins, also RGD motifs.

In Step 4, osteoblastoma sarcoma cells (U2-OS) were seeded onto all the substrates and these were left in the incubator overnight. Before proceeding to cell fixation (Step 5), substrates were observed using an optical microscope to ensure cell seeding had been performed properly. After approximately 24 hours, in Step 6, cells were fixed using paraformaldehyde (PFA) and in order to visualize cells using fluorescence microscopy, nuclei of the cells were stained with Hoechst (blue), and paxillin was stained using a primary and a secondary antibody (green), providing information on FA localization and size. Details of the experimental methodologies related to sample preparation and immunostaining are described in Sections 7.2.2 and 7.2.3.

For these experiments U2-OS cells were used since they present RGD cell membrane receptors but are not as adhesive as other cell lines (i.e. fibroblasts), and therefore are more discriminating when exposed to more or less efficient binding sites. This cell line has also been used for probing cell adhesion in previous studies [133, 163].

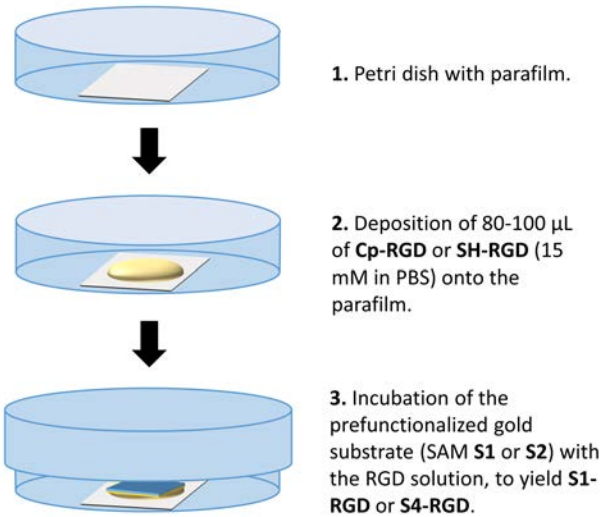


**Figure 3.8:** Schematic illustration depicting the methodology developed for the incubation of prefunctionalized substrates with RGD peptides in a humid chamber. To ensure that the solution would not dry up, a wet piece of paper was inserted carefully onto the border of the petri dish and the chamber was sealed with parafilm.

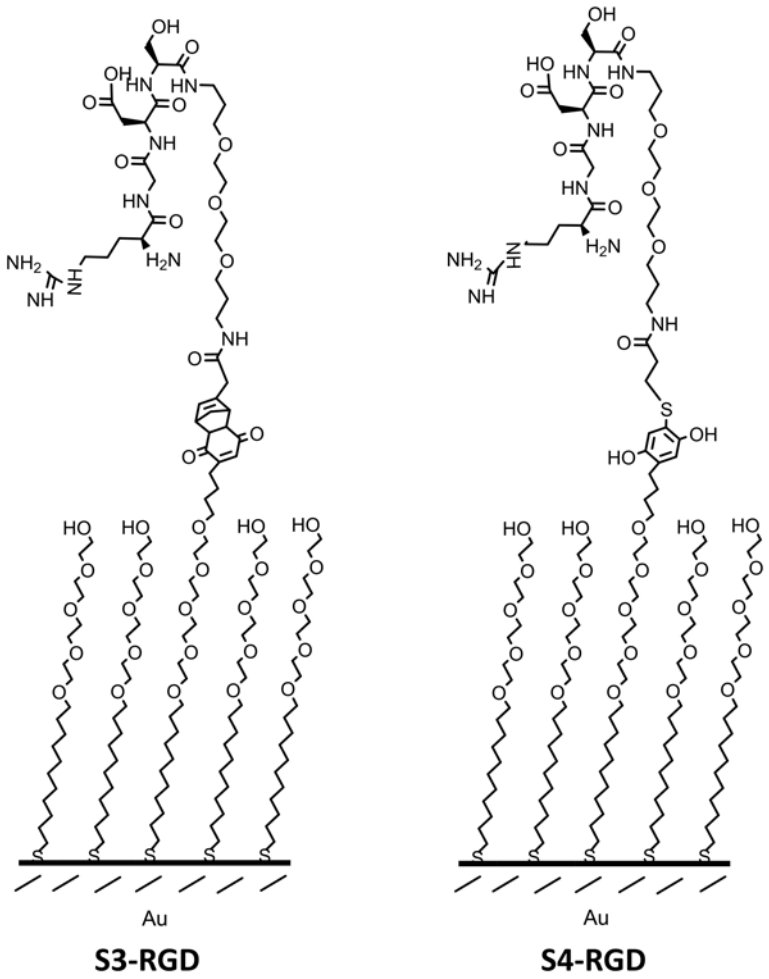


**Figure 3.9:** Sketch depicting the molecular structures of biofunctionalized SAMs, SAM **S3-RGD** obtained with the DA interfacial reaction and SAM **S4-RGD** obtained with the DA interfacial reaction with molecules **Cp-RGD** and **SH-RGD**, respectively.

**Table 3.1:** Different samples prepared and steps followed for the comparative study of the use of DA and MA interfacial reactions to anchor RGD functionalized molecules. 1:99 refers to the ratio between molecule **1** and **2** (Figure 2.7).

| **Substrate Type** | **Positive Control** | **$t_0$ Control DA** | **$t_0$ Control MA** | **SAM S3-RGD** | **SAM S4-RGD** |
|---|---|---|---|---|---|
| **Step 1** | Glass coverslip | SAM **S1** on gold coated glass coverslip 1:99 | SAM **S1** on gold coated glass coverslip 1:99 | SAM **S1** on gold coated glass coverslip 1:99 | SAM **S1** on gold coated glass coverslip 1:99 |
| **Step 2** | Coat with fibronectin using a standard protocol [164] | - | - | Oxidized during 20 s with 0.8 V to yield SAM **S2** | Oxidized during 20 s with 0.8 V to yield SAM **S2** |
| **Step 3** | - | Immersion in 15 mM Cp-RGD | Immersion in 15 mM SH-RGD | Immersion in 15 mM Cp-RGD | Immersion in 15 mM SH-RGD |
| **Step 4** | Cell seeding | Cell seeding | Cell seeding | Cell seeding | Cell seeding |
| **Step 5** | Optical microscope observation | Optical microscope observation | Optical microscope observation | Optical microscope observation | Optical microscope observation |
| **Step 6** | Cell fixation and staining | Cell fixation and staining | Cell fixation and staining | Cell fixation and staining | Cell fixation and staining |
| **Step 7** | Confocal microscope observation | Confocal microscope observation | Confocal microscope observation | Confocal microscope observation | Confocal microscope observation |
| **Expected results** | Cell adhesion | No cell adhesion, similar to 100% PEG | No cell adhesion, similar to 100% PEG | Cell adhesion | Cellular adhesion |

### 3.3.3 Cell Density Analysis

In order to perform the cell density analysis, after staining the cells and mounting the substrates onto glass slides, optical and confocal imaging of these followed. Different captures of each sample for three independent set of experiments were taken. The Image J cell count plugin was used to quantify the number of healthy cells by counting the nuclei.

In Figure 3.10 a representative image of each sample taken in bright field mode before cell fixation is shown and in Figure 3.11 representative fluorescence images are portrayed. Results corresponding to cell quantification are collected in Figure 3.12.

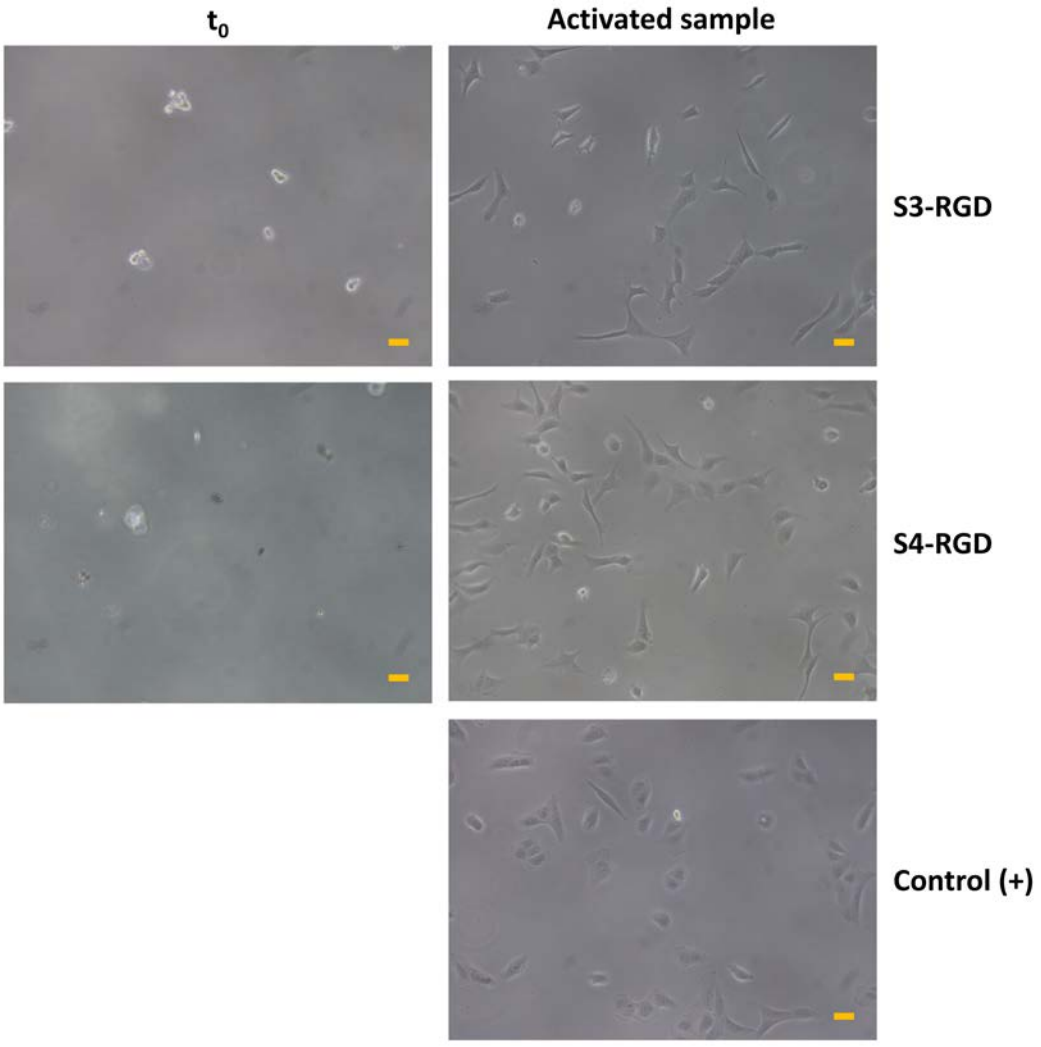


**Figure 3.10:** Representative bright field image for each sample before cell fixation: the **S3-RGD** sample, the **S4-RGD** sample, the $\mathbf{t_0}$ samples and the positive control, using fibronectin coated substrates. Scale bars correspond to 100 μm.

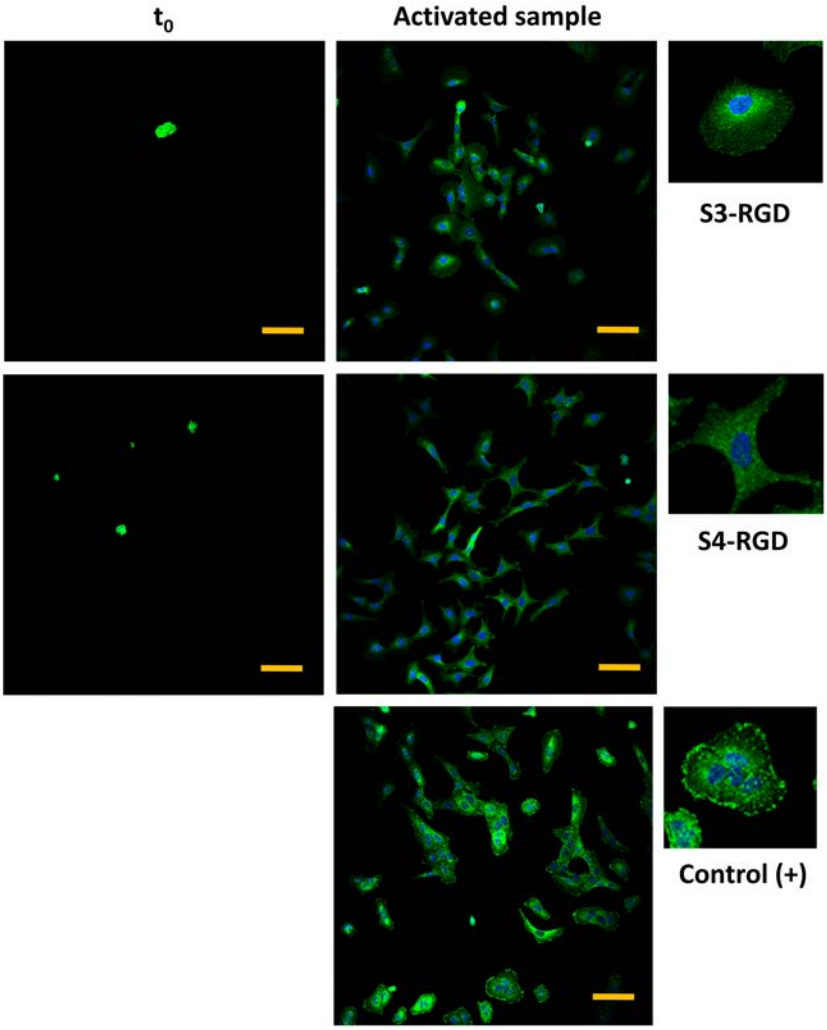


Figure 3.11: Representative fluorescence image for each sample: the **S3-RGD** sample, the **S4-RGD** sample, the $\mathbf{t_0}$ samples and the positive control, using fibronectin coated substrates. Scale bars correspond to 100 μm.

Figures 3.10 and 3.11 confirm that cells are properly fixed and that the stained samples portray the same morphology of cells before fixation. Immunostaining was successfully achieved: the blue signal is appreciated were the nuclei is found and the green signal comes from the stained paxillin, a protein that is part of the FA complex. The interfacial reactions DA and MA successfully provided surfaces (**S3-RGD** and **S4-RGD**) onto which more cells adhered, similar to the control samples. Importantly, a big difference is seen in $\mathbf{t_0}$ samples: if samples are not exposed to the electrochemical stimulus, and thus instead of BQ, HQ groups are exposed on the surfaces (SAM **S1**), no reaction takes place and thus, no RGD is immobilized. This is confirmed by the fact that almost no cells were found on these samples. Quantified results regarding cell density are found in Figure 3.12.

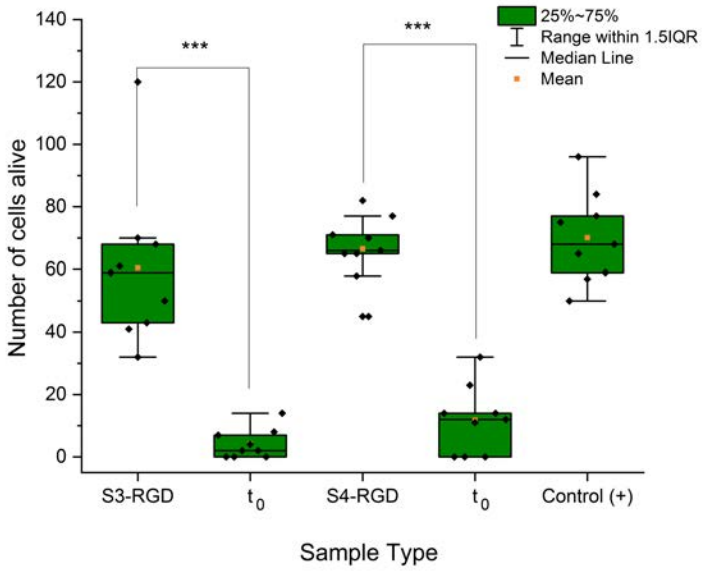


**Figure 3.12:** Results related to cell density in cell adhesion experiments using electroactive SAMs after incubation with RGD molecules, giving place to **S3-RGD** with the DA reaction and **S4-RGD** with the MA reaction. Respective $\mathbf{t_0}$ samples and the positive control using fibronectin coated surfaces (Control (+)) are also shown. See Table 3.1. Data is extracted from 3 captures of each sample for 3 independent sets of experiments. Analysis of cell density was performed using the Image J software. The asterisks in the graphs show the statistical differences with a significance level of 0.001 (***) using the non-parametric Kruskal-Walis ANOVA test, performed with Origin.

As seen in Figure 3.12, functionalized surfaces using the DA and MA interfacial reactions (**S3-RGD** and **S4-RGD**) yield cell densities similar to those provided by the positive control, fibronectin coated surfaces. **S3-RGD** and **S4-RGD** samples presented cell densities significantly higher than their respective $\mathbf{t_0}$ samples and between the **S3-RGD** and **S4-RGD** samples the difference was not significant. This indicates, regarding cell density results, that both interfacial reactions provide a good strategy for the enhancement of cell adhesive properties. Furthermore, this strategy allows the temporal control of surface functionalization by using an electrochemical external stimulus, clearly indicated by the low cell density found in $\mathbf{t_0}$ samples. This allows studies with temporal control of surface biofunctionalization, clearly relevant in fundamental biological studies for the study of cell behavior in environments which replicate more closely the *in vivo* conditions.

### 3.3.4 Cell Spreading Quantification Analysis

Cell spreading was also quantified by using the Image J software: cell contour was manually delimited using the free shape ROI tool provided by the software (see Section 7.2.5 for an example). Cell area was properly displayed since cytoplasmic paxillin was stained and consequently, cell contour could be easily delimited. Cell spreading was quantified for 20 cells for each sample, for 3 independent experiments.

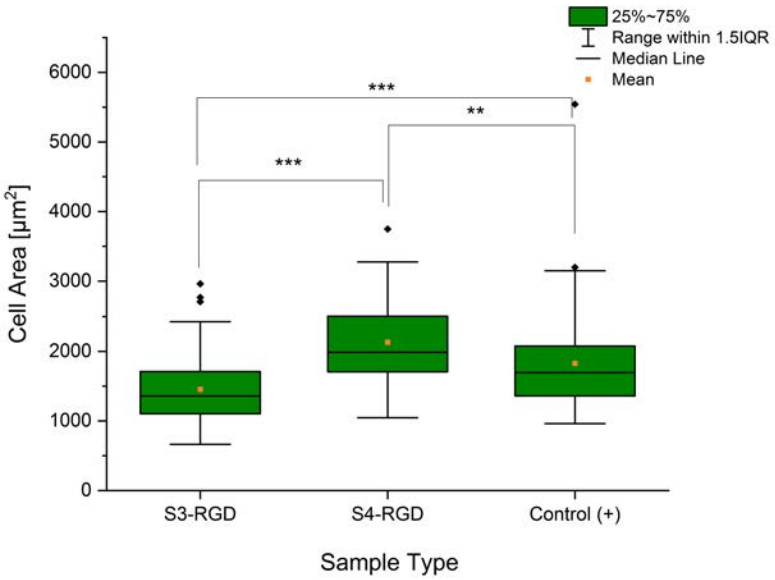


**Figure 3.13:** Results related to cell spreading quantification using electroactive SAMs after incubation with RGD molecules, giving place to **S3-RGD** with the DA reaction and **S4-RGD** with the MA reaction. The positive control using fibronectin coated surfaces (Control (+)) is also shown. Data is extracted from 20 cells in each sample for 3 independent sets of experiments. Analysis of cell spreading was performed using the Image J software. The asterisks in the graphs shows the statistical differences with a significance level of 0.001 (***) and 0.01 (**) using the non-parametric Kruskal-Walis ANOVA test, performed with Origin.

Analysis of cell spreading (Figure 3.13) revealed that cells spread more in **S4-RGD** samples. A possible explanation to this could be that the spatial arrangement of the ligands on surface in **S4-RGD** samples, consisting of patches, have a positive effect on cell spreading. This was observed in a previous study described in Section 2.5.3. Therefore, the difference in cell area can be attributed to the presence of several micron sized patches, in contrast with the more homogeneous RGD distribution in **S3-RGD** and fibronectin surfaces. This potential effect seems to be able to overcome the stronger adhesion capacity of fibronectin over RGD, since fibronectin normally promotes good cell adhesion due to the numerous binding sites it has and the roughness it displays once deposited on a substrate.

It is known that cells adhere and then try to reach and adapt to ECM patterns since FA assembly is modulated by the tensional forces transmitted across integrin receptors [165]. In fact, as reported previously, cells are able to bridge non-adhesive regions as large as 25 µm during cellular spreading [140], and in fact, geometry of the ECM pattern appears not to be relevant [139].

Moreover, as reported by Lehnert et al. [140], a concentration of 15% or higher of ECM is needed for maximum cell spreading to occur. If this is taken as true, more ECM coverage (expected to have in **S3-RGD** samples), does not necessarily lead to higher cell area.

### 3.3.5 FAs Quantification Analysis

After cell spreading analysis, to complement the cell adhesion comparative study, FA area quantification was also conducted. In order to do this, images were captured to visualize FAs more precisely. For the quantification, single cells were imaged and analyzed separately: 20 cells in each sample for 3 independent sets of experiments were analyzed.

#### Image Processing

After image acquisition had been performed (representative images of these are shown in Figure 3.14) a macro script was generated in order to quantify FA area using the Image J software. This protocol was developed based on previous studies which used similar image processing methodologies [166, 167]. Basically it consisted in saturating the image, subtracting the background and thresholding it to finally select the FAs, always confirming proper selection with the original image. Finally, the area selected was quantified for each cell and a statistical study was performed. For specifications of the image analysis protocol refer to Section 7.2.5.

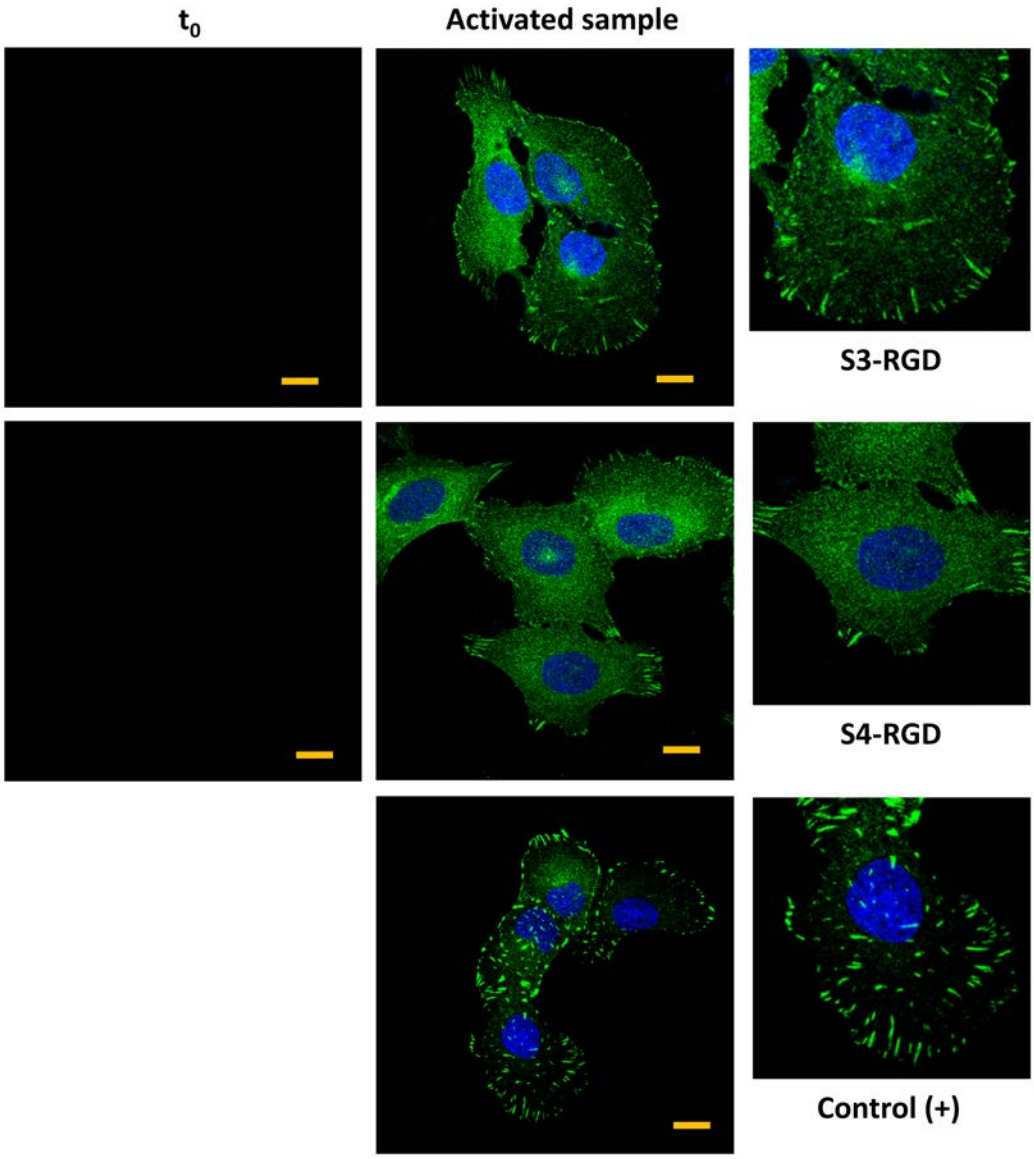


**Figure 3.14:** Representative fluorescence image for the **S3-RGD** sample, the **S4-RGD** sample, $\mathbf{t_0}$ samples and the positive control observed using a 63X magnification (1.7 zoom) in order to obtain captures for FA quantification. Scale bars correspond to 15 μm.

Values obtained after image processing concerning FA area are portrayed in the graph shown in Figure 3.15.

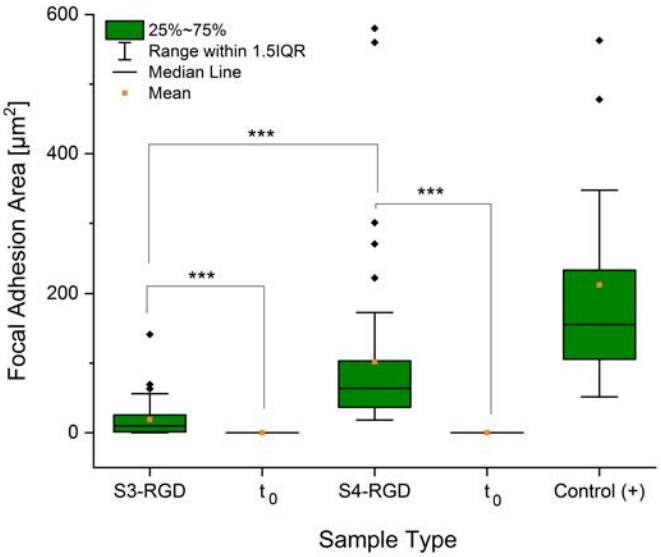


**Figure 3.15:** Results related to FA quantification in the cell adhesion experiments using electroactive SAMs after incubation with RGD molecules, giving place to **S3-RGD** with the DA reaction and **S4-RGD** with the MA reaction. Respective $\mathbf{t_0}$ samples and the positive control using fibronectin coated surfaces (Control (+)) are also shown. Data is extracted from 20 cells in each sample for 3 independent sets of experiments. Analysis of FA area was performed using the Image J software. The asterisks in the graphs show the statistical differences with a significance level of 0.001 (***) using the non-parametric Kruskal-Walis ANOVA test, performed with Origin.

When it comes to FA analysis, as seen in Figure 3.14, results show that when using the MA reaction (**S4-RGD**) a significantly larger area of FAs is obtained, when compared to the DA reaction (**S3-RGD**). In $\mathbf{t_0}$ samples, cells that appear unspecifically adsorbed onto the substrates did not present the formation of FAs.

It is known that modulation in FA arrangement and formation, depending on the spatial arrangement of the RGD ligands on the surface [139, 168], occurs and if cell area appears larger, it has been reported that FA area is increased [139]. According to this, **S4-RGD** samples therefore present higher FA area, compared to **S3-RGD** samples. However, a more recent study has indicated that the average size of FAs is influenced by both adhesion and spreading area, but the total area of FAs is determined mainly by the available cell adhesion area, so the amount of ECM, rather than the cell spreading area [166].

This could explain the larger FA area found in fibronectin coated surfaces (Control(+)), which has a higher roughness and therefore a larger surface to accommodate binding sites, those from RGD, in addition to those which are not RGD.

Summarizing, the MA reaction provides a useful and promising temporally controlled biofunctionalization strategy, compatible with biological environments.

## 3.4 Vascularization Studies

Promising results were obtained in previous experiments for the immobilization of RGD-peptides functionalized with thiol groups in response to an external stimulus through an interfacial reaction. On that account and moving forward, we decide to explore how this platform would work when not only controlling the adhesion but the subsequent differentiation of cells when immobilizing a tubulogenesis promoting peptide, namely Qk-peptide. Towards this aim, a novel experiment is designed using a new QK-peptide functionalized with a thiol group. Firstly, the peptide is synthesized and thereafter immobilized directly on gold surfaces as SAMs to test their ability to enhance the formation of tubular networks when placed in a semi-3D environment using a thin coating of Matrigel. Moreover, synergy between the presence of RGD adhesion promoters and Qk is studied.

### 3.4.1 Synthesis of Thiol-Qk

Thiolated Qk-peptide (**SH-Qk**) was synthesized using standard procedures for solid phase peptide synthesis. For the experimental details concerning the synthesis see Section 7.2.6. Circular RGD (**SH-cRGD**) was provided by ?? and thiol-PEG (**SH-PEG**) was bought from a commercial provider.

### 3.4.2 Sample Preparation: Thiol-cRGD and Thiol-Qk SAMs

SAMs consisting of **SH-cRGD**, **SH-Qk** and **SH-PEG** (Figure 3.16) were prepared, either with only one of the peptides or with both, in an equitative way. A control sample was prepared with fibronectin.

The specific SAM composition (ratio values are given) of the prepared samples were: **S-RGD** (SAMs 1:9 **SH-PEG**:**SH-cRGD**), **S-Qk** (SAMs 1:9 **SH-PEG**:**SH-Qk**, **S-RGD-Qk** (SAMs 1:4.5:4.5 **SH-PEG**:**SH-cRGD**:**SH-Qk**) and **S-Fibro** (fibronectin coated coverslips).

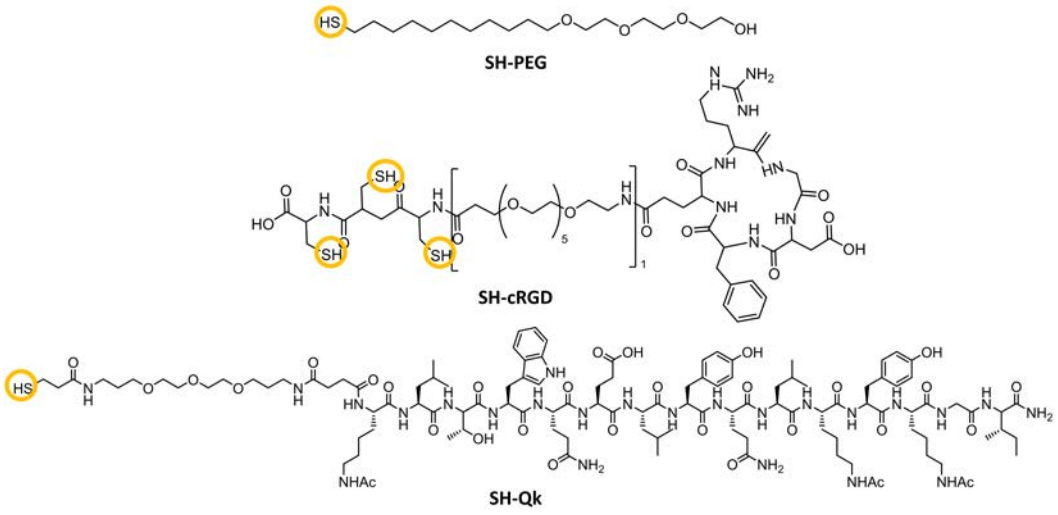


**Figure 3.16:** Molecular structures of molecules used for the functionalization of substrates for vascularization studies: **SH-PEG**, **SH-cRGD** and **SH-Qk**. Thiol anchoring moieties are circled in yellow.

For the preparation of the SAMs, glass coverslips coated with gold were incubated with the peptide solution (0.5 mM in MQ-water) during 1 hour and thereafter these were rinsed and stored in PBS until cell seeding. Details of the experimental protocol followed is given in Section 7.2.6.

### 3.4.3 Tubulogenesis Assay

Firstly, functionalized and sterile substrates were seeded with HUVEC cells and left in the incubator overnight. Images were captured after overnight incubation and then these were deposited onto a thin layer of Matrigel, following the procedure illustrated in Figure 3.17. Pictures were taken just after substrate deposition onto Matrigel, after 5 hours and after 18 hours (Figure 3.18). Details of the experimental procedure followed is described in Section 7.2.6.

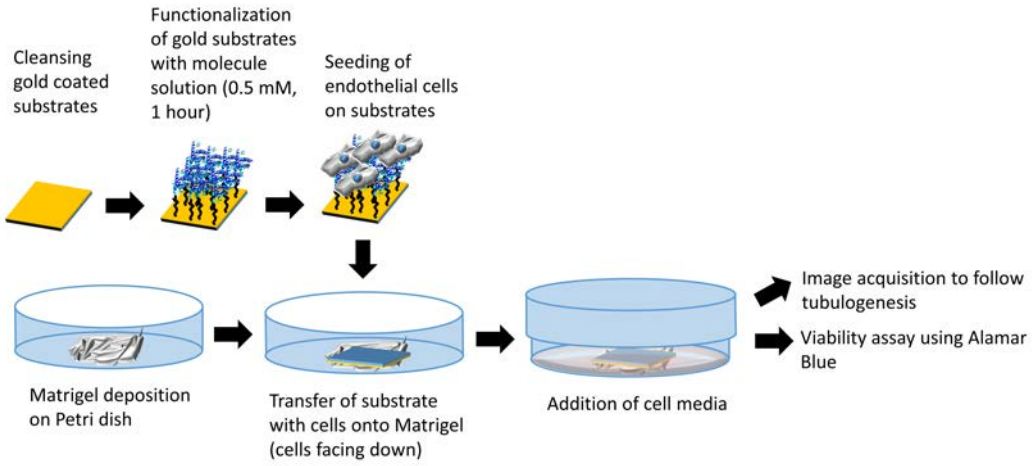


**Figure 3.17:** Experimental setup describing the mounting of cell seeded substrates onto a Matrigel coating.

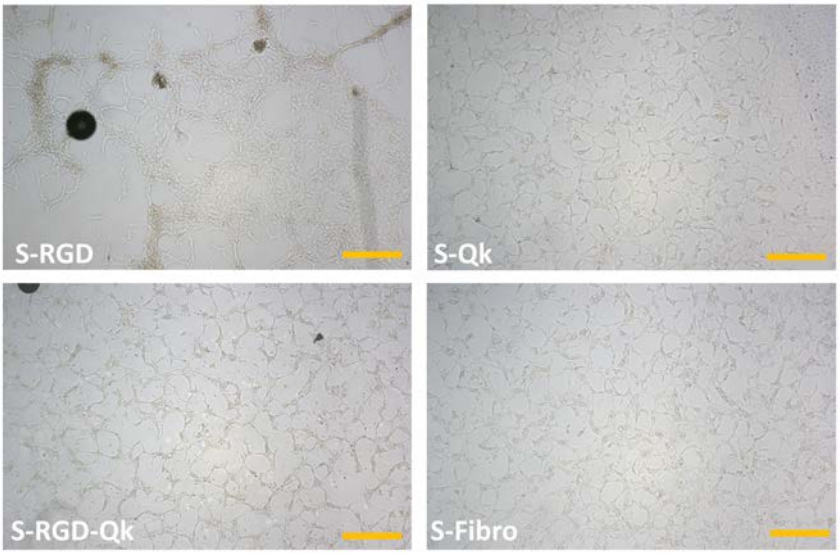


**Figure 3.18:** Representative image of each sample: **S-RGD**, **S-Qk**, **S-RGD-Qk**, **S-Fibro**. These were taken after 18 hours of exposure of seeded HUVEC cells to Matrigel films. Scale bars correspond to 500 μm.

Images in Figure 3.18 show less tubular network formation in **S-RGD** samples than in the rest of the samples, due to the absence of Qk-peptide. Moreover, more captures should be taken to be able to make a statistical study of the tubulogenesis by processing and studying the images. Several studies have reported a image processing protocol for the study of tubule formation [155, 159, 169, 170].

### 3.4.4 Cell Viability Assay

To assess cell viability a test using Alamar Blue (AB) was performed. AB is a resazurin-based solution which works by indicating cell health through the reducing power of cells, since resazurin is a non-toxic and cell permeable compound with blue color. It is non-fluorescent but when it enters into living cells it becomes reduced to resorufin, a compound which is red and highly fluorescent. This change in color and fluorescence indicates cell viability upon measurement with an absorbance or fluorescence plate reader [171].

The assay (Figure 3.19) was performed with duplicates, in both batches it is clear that cell viability is increased with the presence of Qk-peptide (**S-Qk** and **S-RGD-Qk**), even more so than when using fibronectin samples (**S-Fibro**). On the other hand, the two batches show different cell viability for **S-Qk** and **S-RGD-Qk** and thus no clear conclusion could be extracted concerning the synergistic effect between Qk and RGD.

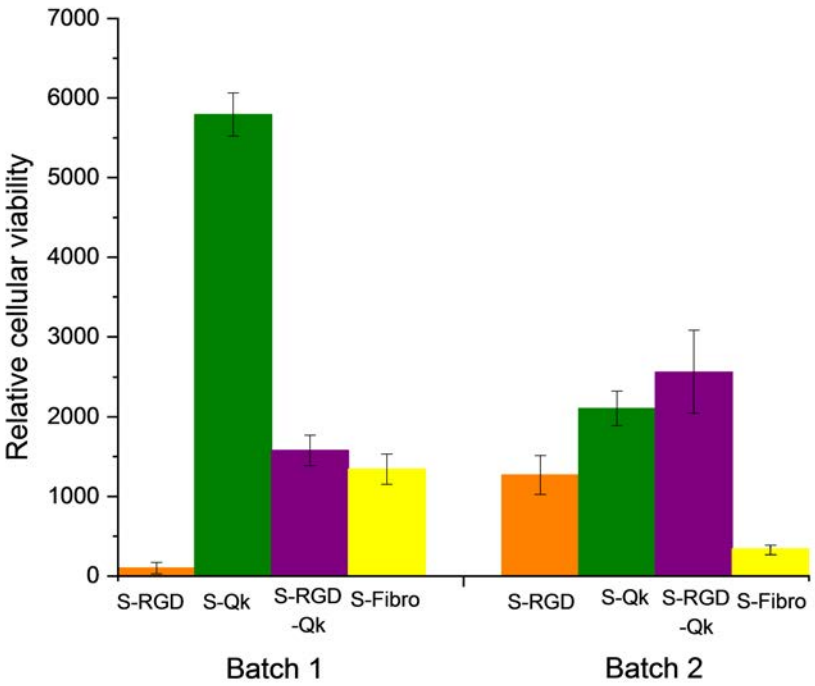


**Figure 3.19:** Values obtained for the viability test using an AB assay. Error bars indicate the standard deviation of absorbance measurements.

### 3.4.5 Cell Fixation and Immunostaining

After 18 hours, cell fixation was performed using PFA at 4% and cell nuclei was stained with Hoescht and actin with phalloidin 647. Details of these procedures can

be found in Sections 7.2.10 and 7.2.11. Representative images taken with confocal microscopy are shown in Figure 3.20.

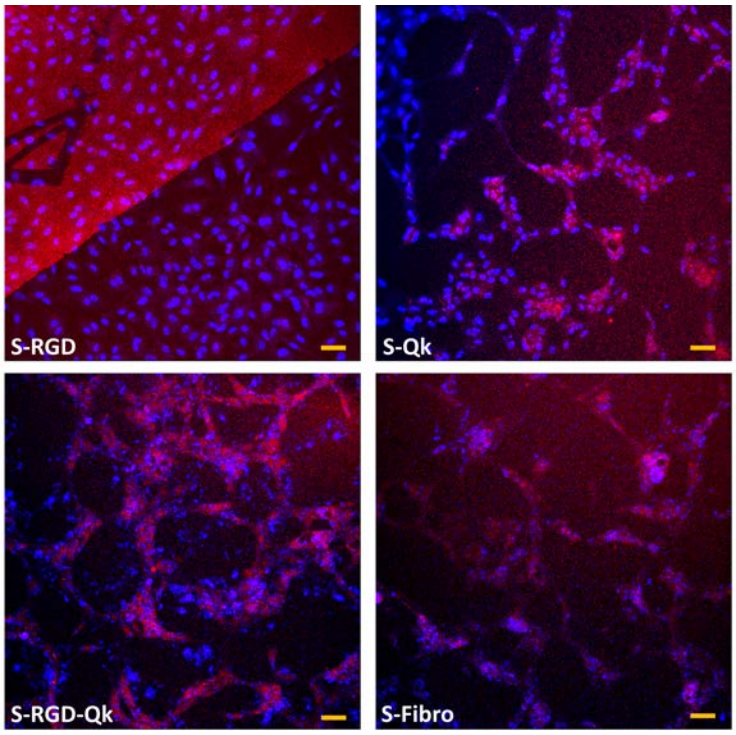


**Figure 3.20:** Representative image taken by confocal microscopy for each sample: **S-RGD**, **S-Qk**, **S-RGD-Qk**, **S-Fibro**. Scale bars correspond 50 μm.

As seen in Figure 3.20, stained cells portray nuclei in blue and actin filaments in red, confirming what had been seen in Figure 3.18, that samples with Qk-peptide display a clearer tubular network formation than those without.

Studies have reported VEGF binding sites in fibronectin [172, 173] and therefore, fibronectin coated surfaces also promote tubulogenesis, but in fact, these first results demonstrate that Qk enhances it even more. In regard to these findings, Qk immobilization provides a promising platform for biomedical device coating where vascular growth is necessary and difficult to promote otherwise.

## 3.5 Summary and Perspectives

Cell adhesion is an important and complex biological process and its control is very important to understand fundamental aspects of cell behavior (e.g. cell migration, adhesion, differentiation...). We have exploited the interfacial reactions DA and MA to immobilize pegylated RGD functionalized peptides containing Cp or thiol groups which allow the control of cell attachment with an electrochemical stimulus. Moreover, a quantitative analysis of cell attachment, by looking at cell density, cell spreading and FA area has been performed to compare the DA and MA platforms. Samples biofunctionalized through the MA reaction showed better cell adhesive properties, concerning cell spreading and FA area. The creation of RGD patches using the MA interfacial reaction has a positive effect, promoting better cell attachment, compared to biofunctionalization via de DA reaction and fibronectin

samples, although the FA area was higher in the latter. This could be attributed to the availability of other cell adhesion promoting molecules presented by fibronectin. The versatility of this biocompatible platform opens up for new possible innovative applications where temporal control is needed within the biomedical field. In this context also an electrochemical cell for *in situ* studies has been designed (see Annex 7.4.7).

Moving a step forward we proposed the use of the platform not only for the control of cell adhesion, but for the subsequent differentiation into blood vessels. To do this in a first study, new thiolated Qk molecules have been synthesized and tethered onto surfaces through their thiol group and tubulogenesis on substrates with Qk-peptide alone and in presence of RGD was studied together with the cellular viability. Cell viability and tube formation was enhanced when Qk was present, demonstrating thus, the real potential of this peptide to be used to functionalize materials for biological applications where a vascular network is a must.

# References


[2] E. Wischerhoff, N. Badi, J. F. Lutz, and A. Laschewsky. „Smart bioactive surfaces“. In: *Soft Matter* 6.4 (2010), pp. 705–713 (cit. on pp. 1, 66).

[7] F. Meiners, I. Plettenberg, J. Witt, et al. „Local control of protein binding and cell adhesion by patterned organic thin films“. In: *Analytical and Bioanalytical Chemistry* 405.11 (2013), pp. 3673–3691 (cit. on pp. 2, 61, 62).

[9] A. Pulsipher and M. N. Yousaf. „Surface chemistry and cell biological tools for the analysis of cell adhesion and migration“. In: *ChemBioChem* 11.6 (2010), pp. 745–753 (cit. on pp. 2, 4, 66).

[11] C. D. Bain, J. Evall, and G. M. Whitesides. „Formation of Monolayers by the Coadsorption of Thiols on Gold: Variation in the Head Group, Tail Group, and Solvent“. In: *Journal of the American Chemical Society* 43.2 (1989), pp. 51–45 (cit. on pp. 2, 62).

[17] C. Chi Albert Ng, A. Magenau, S. H. Ngalim, et al. „Using an Electrical Potential to Reversibly Switch Surfaces between Two States for Dynamically Controlling Cell Adhesion“. In: *Angewandte Chemie* 51.31 (2012), pp. 7706–10 (cit. on pp. 3, 66).

[31] C. S. Chen, M. Mrksich, S. Huang, G. M. Whitesides, and D. E. Ingber. „Micropatterned Surfaces for Control of Cell Shape, Position, and Function“. In: *Biotechnology Progress* 14.3 (1998), pp. 356–363 (cit. on pp. 7, 65).

[36] E. W. L. Chan, S. Park, and M. N. Yousaf. „An electroactive catalytic dynamic substrate that immobilizes and releases patterned ligands, proteins, and cells“. In: *Angewandte Chemie* 47.33 (2008), pp. 6267–6271 (cit. on pp. 9, 30, 66).

[63] E. W. L. Chan and N. M. Yousaf. „Immobilization of Ligands with Precise Control of Density to Electroactive Surfaces“. In: *Journal of the American Chemical Society* 128.48 (2006), pp. 15542–15546 (cit. on pp. 25, 72).

[105] A. A. Khalili and M. R. Ahmad. „A Review of Cell Adhesion Studies for Biomedical and Biological Applications.“ In: *International journal of molecular sciences* 16.8 (2015), pp. 18149–84 (cit. on pp. 61, 62).

[106] B. M. Gumbiner. „Cell Adhesion: Review The Molecular Basis of Tissue Architecture and Morphogenesis“. In: *Cell* 84 (1996), pp. 345–357 (cit. on p. 61).

[107] K. Anselme, L. Ploux, and A. Ponche. „Cell/Material Interfaces: Influence of Surface Chemistry and Surface Topography on Cell Adhesion“. In: *Journal of Adhesion Science and Technology* 24.24 (2010), pp. 831–852 (cit. on p. 61).

[108] S. Huang and D. E. Ingber. „The structural and mechanical complexity of cell-growth control“. In: *Nature Cell Biology* 1.5 (1999), E131–E138 (cit. on p. 61).

[109] T. Okegawa, R.-C. Pong, Y. Li, and J.-T. Hsieh. „The role of cell adhesion molecule in cancer progression and its application in cancer therapy“. In: *Acta Biochimica Polonica* 51.2 (2004) (cit. on p. 61).

[110] S. Hirohashi and Y. Kanai. „Cell adhesion system and human cancer morphogenesis.“ In: *Cancer Science* 94.7 (2003), pp. 575–81 (cit. on p. 61).

[111] H. Perinpanayagam, R. Zaharias, C. Stanford, et al. „Early cell adhesion events differ between osteoporotic and non-osteoporotic osteoblasts“. In: *Journal of Orthopaedic Research* 19.6 (2001), pp. 993–1000 (cit. on p. 61).

[112] Z. Szekanecz and A. E. Koch. „Cell-cell interactions in synovitis endothelial cells and immune cell migration“. In: *Arthritis Res.* 2 (2000), pp. 368–373 (cit. on pp. 61, 62).

[113] A. W. Feinberg, W. R. Wilkerson, C. A. Seegert, et al. „Systematic variation of microtopography, surface chemistry and elastic modulus and the state dependent effect on endothelial cell alignment“. In: *Journal of Biomedical Materials Research Part A* 86A.2 (2008), pp. 522–534 (cit. on p. 61).

[114] M. Tirrell, E. Kokkoli, and M. Biesalski. „The role of surface science in bioengineered materials“. In: *Surface Science* 500 (2002), pp. 61–83 (cit. on p. 61).

[115] P. Dungel, N. Long, B. Yu, Y. Moussy, and F. Moussy. „Study of the effects of tissue reactions on the function of implanted glucose sensors“. In: *Journal of Biomedical Materials Research - Part A* 85.3 (2008), pp. 699–706 (cit. on p. 61).

[116] M. Lee, D. Yao, and W. Hsu. „An Implantable Drug-delivery System on a Chip“. In: *Current Topics in Medicinal Chemistry* 15.15 (2015), pp. 1516–1524 (cit. on p. 61).

[117] N. Sadr, M. Zhu, T. Osaki, et al. „SAM-based cell transfer to photopatterned hydrogels for microengineering vascular-like structures“. In: *Biomaterials* 32.30 (2011), pp. 7479–7490 (cit. on p. 61).

[118] M. Hakamada, M. Takahashi, and M. Mabuchi. „Enzyme electrodes stabilized by monolayer-modified nanoporous Au for biofuel cells“. In: *Gold Bull* 45 (2012), pp. 9–15 (cit. on p. 61).

[119] A. Kira, K. Okano, Y. Hosokawa, et al. „Micropatterning of perfluoroalkyl self-assembled monolayers for arraying proteins and cells on chips“. In: *Applied Surface Science* 255 (2009), pp. 7647–7651 (cit. on p. 61).

[120] M. E. Nash, W. M. Carroll, P. J. Foley, et al. „Ultra-thin spin coated crosslinkable hydrogels for use in cell sheet recovery-synthesis, characterisation to application“. In: *Soft Matter* 8.14 (2012), p. 3889 (cit. on p. 62).

[121] G. Balasundaram, D. M. Storey, and T. J. Webster. „Molecular plasma deposition: biologically inspired nanohydroxyapatite coatings on anodized nanotubular titanium for improving osteoblast density.“ In: *International journal of nanomedicine* 10 (2015), pp. 527–35 (cit. on p. 62).

[122] R. Barbey, L. Lavanant, D. Paripovic, et al. „Polymer Brushes via Surface-Initiated Controlled Radical Polymerization: Synthesis, Characterization, Properties, and Applications“. In: *Chemical Reviews* 109.11 (2009), pp. 5437–5527 (cit. on p. 62).

[123] S. E. D'Souza, M. H. Ginsberg, and E. F. Plow. „Arginyl-Glycyl-Aspartic acid (RGD): a cell adhesion motif“. In: *TIBS* 16 (1991), pp. 246–250 (cit. on pp. 62, 64).

[124] J. D. Humphries. „Integrin ligands at a glance“. In: *Journal of Cell Science* 119.19 (2006), pp. 3901–3903 (cit. on pp. 62, 64).

[125] V. Petit and J.-P. Thiery. „Focal adhesions: structure and dynamics“. In: *Biology of the Cell* 97 (2000), pp. 477–494 (cit. on pp. 62, 63).

[126] R&D Systems. *Intergrin Subunit Interactions* (cit. on p. 63).

[127] M. Abercrombie, J. E. M. Heaysman, and S. M. Pegrum. „The Locomotion of Fibroblasts in Culture IV. Electron Microscopy of the Leading Lamella“. In: *Experimental Cell Research* 67 (1971), pp. 359–367 (cit. on p. 63).

[128] J. R. Couchman and D. A. Rees. „The behaviour of fibroblasts migrating from chick heart explants: changes in adhesion, locomotion and growth, and in the distribution of actomyosin and fibronectin“. In: *J. Cell Sci.* 39 (1979), pp. 149–165 (cit. on p. 63).

[129] K. Burridge, K. Fath, T. Kelly, G. Nuckolls, and C. Turner. „Focal Adhesions: Transmembrane Junctions Between the Extracellular Matrix and the Cytoskeleton“. In: *Annual Review of Cell Biology* 4.1 (1988), pp. 487–525 (cit. on p. 63).

[130] B. Wehrle-Haller. „Structure and function of focal adhesions“. In: *Current Opinion in Cell Biology* 24 (2012), pp. 116–124 (cit. on p. 63).

[131] A. Carisey and C. Ballestrem. „Vinculin, an adapter protein in control of cell adhesion signalling“. In: *European Journal of Cell Biology* 90.2 (2011). Invadosomes, pp. 157 –163 (cit. on p. 64).

[132] M. D. Schaller. „Paxillin: a focal adhesion-associated adaptor protein“. In: *Oncogene* 20 (Oct. 2001), p. 6459 (cit. on p. 64).

[133] P. Kanchanawong, G. Shtengel, A. M. Pasapera, et al. „Nanoscale architecture of integrin-based cell adhesions“. In: *Nature* 468.7323 (2010), pp. 580–584 (cit. on pp. 64, 74).

[134] R. O. Hynes. „Integrins: Versatility, modulation, and signaling in cell adhesion“. In: *Cell* 69.1 (1992), pp. 11–25 (cit. on p. 64).

[135] J.-P. Xiong, T. Stehle, R. Zhang, et al. „Crystal Structure of the Extracellular Segment of Integrin $\alpha V\beta 3$ in Complex with an Arg-Gly-Asp Ligand“. In: *Science* 296.5565 (2002), pp. 151–5 (cit. on p. 64).

[136] T. Xiao, J. Takagi, B. S. Coller, J.-H. Wang, and T. A. Springer. „Structural basis for allostery in integrins and binding to fibrinogen-mimetic therapeutics“. In: *Nature* 432.7013 (2004), pp. 59–67 (cit. on p. 64).

[137] C. Chollet, S. Lazare, F. Guillemot, and M. C. Durrieu. „Impact of RGD micro-patterns on cell adhesion“. In: *Colloids and Surfaces B: Biointerfaces* 75 (2010), pp. 107–114 (cit. on p. 65).

[138] E. A. Cavalcanti-Adam, A. Micoulet, J. Blümmel, et al. „Lateral spacing of integrin ligands influences cell spreading and focal adhesion assembly“. In: *European Journal of Cell Biology* 85.3-4 (2006), pp. 219–224 (cit. on p. 65).

[139] C. S. Chen, J. L. Alonso, E. Ostuni, G. M. Whitesides, and D. E. Ingber. „Cell shape provides global control of focal adhesion assembly“. In: *Biochemical and Biophysical Research Communications* 307.2 (2003), pp. 355–361 (cit. on pp. 65, 80, 83).

[140] D. Lehnert, B. Wehrle-Haller, C. David, et al. „Cell behaviour on micropatterned substrata: limits of extracellular matrix geometry for spreading and adhesion“. In: *Journal of cell science* 117.1 (2004), pp. 41–52 (cit. on pp. 65, 80).

[141] X. Wang, S. Li, C. Yan, P. Liu, and J. Ding. „Fabrication of RGD Micro/Nanopattern and Corresponding Study of Stem Cell Differentiation“. In: *Nano Letters* 17 (2015), pp. 1457–1467 (cit. on p. 65).

[142] P. M. Mendes. „Stimuli-responsive surfaces for bio-applications“. In: *Chemical Society Reviews* 37.11 (2008), pp. 2512–2529 (cit. on p. 66).

[143] D. Liu, Y. Xie, H. Shao, and X. Jiang. „Using Azobenzene-Embedded Self-Assembled Monolayers To Photochemically Control Cell Adhesion Reversibly“. In: *Angewandte Chemie* 121.24 (2009), pp. 4470–4472 (cit. on p. 66).

[144] M. Lovett, K. Lee, A. Edwards, and David L. Kaplan. „Vascularization strategies for tissue engineering“. In: *Tissue engineering. Part B, Reviews* 15.3 (2009), pp. 353–70 (cit. on p. 67).

[145] A. H. Van Hove, E. Antonienko, K. Burke, E. Brown, and D. S. W. Benoit. „Temporally Tunable, Enzymatically Responsive Delivery of Proangiogenic Peptides from Poly(ethylene glycol) Hydrogels“. In: *Advanced Healthcare Materials* 4.13 (2015), pp. 2002–2011 (cit. on p. 67).

[146] E. C. Novosel, C. Kleinhans, and P. J. Kluger. „Vascularization is the key challenge in tissue engineering“. In: *Advanced Drug Delivery Reviews* 63 (2011), pp. 300–311 (cit. on p. 67).

[147] L. Wang, M. Zhao, S. Li, et al. „Click immobilization of a VEGF-mimetic peptide on decellularized endothelial extracellular matrix to enhance angiogenesis“. In: *ACS Applied Materials and Interfaces* 6.11 (2014), pp. 8401–8406 (cit. on pp. 67, 68).

[148] E. S. Place, N. D. Evans, and M. M. Stevens. „Complexity in biomaterials for tissue engineering“. In: *Nature Materials* 8.6 (2009), pp. 457–470 (cit. on p. 67).

[149] A. H. Van Hove and D. S. W. Benoit. „Depot-Based Delivery Systems for Pro-Angiogenic Peptides: A Review“. In: *Frontiers in Bioengineering and Biotechnology* 3 (2015), p. 102 (cit. on pp. 67, 68).

[150] G. D. Yancopoulos, S. Davis, N. W. Gale, et al. „Vascular-specific growth factors and blood vessel formation“. In: *Nature* 407 (2000), p. 242 (cit. on p. 67).

[151] F. Zhou, X. Jia, Y. Yang, et al. „Peptide-modified PELCL electrospun membranes for regulation of vascular endothelial cells“. In: *Materials Science and Engineering C* 68 (2016), pp. 623–631 (cit. on pp. 67–69).

[152] M. J. Cross, J. Dixelius, T. Matsumoto, and L. Claesson-Welsh. „VEGF-receptor signal transduction“. In: *Trends in Biochemical Sciences* 28.9 (2003), pp. 488–494 (cit. on p. 67).

[153] N. Ferrara, H.-P. Gerber, and J. LeCouter. „The biology of VEGF and its receptors“. In: *Nature Medicine* 9.6 (2003), pp. 669–676 (cit. on p. 67).

[154] M. Shibuya. „Vascular Endothelial Growth Factor (VEGF) and Its Receptor (VEGFR) Signaling in Angiogenesis: A Crucial Target for Anti- and Pro-Angiogenic Therapies.“ In: *Genes & cancer* 2.12 (2011), pp. 1097–105 (cit. on p. 67).

[155] J. T. Koepsel, E. H. Nguyen, and W. L. Murphy. „Differential effects of a soluble or immobilized VEGFR-binding peptide“. In: *Integrative biology* 4.8 (2012), pp. 914–24 (cit. on pp. 68–70, 86).

[156] X. Lin, K. Takahashi, S. Campion, et al. „Synthetic peptide F2A4-K-NS mimics fibroblast growth factor-2 in vitro and is angiogenic *in vivo*“. In: *International Journal of Molecular Medicine* 17.5 (2006), pp. 833–839 (cit. on p. 68).

[157] D. A. Young, M. B. Pimentel, L. D. Lima, et al. „Design and characterization of hydrogel nanoparticles with tunable network characteristics for sustained release of a VEGF-mimetic peptide“. In: *Biomaterials Science* 5.10 (2017), pp. 2079–2092 (cit. on pp. 68, 69).

[158] L. D. D'Andrea, G. Iaccarino, R. Fattorusso, et al. „Targeting angiogenesis: Structural characterization and biological properties of a *de novo* engineered VEGF mimicking peptide“. In: *Proceedings of the National Academy of Sciences of the United States of America* 102.40 (2005), pp. 14215–20 (cit. on p. 68).

[159] J. E. Leslie-Barbick, J. E. Saik, D. J. Gould, M. E. Dickinson, and J. L. West. „The promotion of microvasculature formation in poly(ethylene glycol) diacrylate hydrogels by an immobilized VEGF-mimetic peptide“. In: *Biomaterials* 32.25 (2011), pp. 5782–5789 (cit. on pp. 68, 86).

[160] Y. Kambe, A. Murakoshi, H. Urakawa, Y. Kimura, and T. Yamaoka. „Vascular induction and cell infiltration into peptide-modified bioactive silk fibroin hydrogels“. In: *J. Mater. Chem. B* 5.36 (2017), pp. 7557–7571 (cit. on p. 68).

[161] R. L. Saunders and D. A. Hammer. „Assembly of Human Umbilical Vein Endothelial Cells on Compliant Hydrogels“. In: *Cell Mol. Bioeng.* 3 (2010), pp. 60–67 (cit. on p. 69).

[162] M. N. Yousaf, B. T. Houseman, and M. Mrksich. „Turning on cell migration with electroactive substrates“. In: *Angewandte Chemie - International Edition* 40.6 (2001), pp. 1093–1096 (cit. on p. 72).

[163] J. Guasch, B. Conings, S. Neubauer, et al. „Segregation Versus Colocalization: Orthogonally Functionalized Binary Micropatterned Substrates Regulate the Molecular Distribution in Focal Adhesions“. In: *Advanced Materials* 27.25 (2015), pp. 3737–3747 (cit. on p. 74).

[164] Advanced Bioimaging Facility. *Fibronectin coating coverslips Plating Cells for microscopy*. 2014 (cit. on p. 76).

[165] D. Riveline, E. Zamir, N. Q. Balaban, et al. „Focal Contacts as Mechanosensors: Externally Applied Local Mechanical Force Induces Growth of Focal Contacts by an mDia1-dependent and ROCK-independent Mechanism“. In: *The Journal of Cell Biology* 153.6 (2001), pp. 1175–1185 (cit. on p. 80).

[166] X. Wang, X. Hu, I. Dulińska-Molak, et al. „Discriminating the Independent Influence of Cell Adhesion and Spreading Area on Stem Cell Fate Determination Using Micropatterned Surfaces“. In: *Scientific Reports* 6.28708 (2016), pp. 1–13 (cit. on pp. 81, 83).

[167] J. A. Broussard, N. L. Diggins, S. Hummel, et al. „Automated Analysis of Cell-Matrix Adhesions in 2D and 3D Environments“. In: *Scientific Reports* 5.1 (2015), p. 8124 (cit. on p. 81).

[168] C. H. Thomas, C. D. McFarland, M. L. Jenkins, et al. „The role of vitronectin in the attachment and spatial distribution of bone-derived cells on materials with patterned surface chemistry“. In: *Journal of Biomedical Materials Research* 37.1 (1997), pp. 81–93 (cit. on p. 83).

[169] K. L. DeCicco-Skinner, G. H. Henry, C. Cataisson, et al. „Endothelial cell tube formation assay for the *in vitro* study of angiogenesis“. In: *Journal of visualized experiments: JoVE* 91 (2014), e51312 (cit. on p. 86).

[170] C. P. Khoo, K. Micklem, and S. M. Watt. „A comparison of methods for quantifying angiogenesis in the Matrigel assay *in vitro*“. In: *Tissue engineering. Part C, Methods* 17.21517696 (Sept. 2011), pp. 895–906 (cit. on p. 86).

[171] Thermo Fischer. *alamarBlue™ Cell Viability Reagent*. 2018 (cit. on p. 86).

[172] M. Mitsi, Z. Hong, C. E. Costello, and M. A. Nugent. „Heparin-Mediated Conformational Changes in Fibronectin Expose Vascular Endothelial Growth Factor Binding Sites“. In: *Biochemistry* 45.34 (2006). PMID: 16922507, pp. 10319–10328 (cit. on p. 87).

[173] S. Wijelath Errol, R. Salman, N. Mayumi, et al. „Heparin-II Domain of Fibronectin Is a Vascular Endothelial Growth Factor-Binding Domain“. In: *Circulation Research* 99.8 (Dec. 2018), pp. 853–860 (cit. on p. 87).

# 4 Electroactive SAMs for Bilayer Diffusion Control: Using Lipid Bilayers as Cell Membrane Models

> *To develop drugs for people, we basically dismantle the system. In the lab, we look at things the size of a cell or two. We dismantle life into very small models.*
>
> — **Aaron Ciechanover**

## 4.1 Introduction

### 4.1.1 Lipid Bilayers as Cell Membrane Models

Membranes present in biological systems are of paramount importance since they are crucial for many biological processes. These include, when it comes to cell membranes, (i) protection of subcellular structures, (ii) compartmentalization of these, (iii) signal transductions processes and (iv) selective permeability, allowing only specific molecules to be transported into and from the cell. In addition, cell membranes take part in other relevant processes including molecular recognition, cellular adhesion, enzymatic catalysis and membrane fusion, to mention some [174]. Hence, biological membranes, whilst controlling the transfer of ions and molecules between the inside and outside of the cell and taking part of various extra and intracellular processes, are a central structural and regulatory feature of living cells and thus, play a key role in the cell's life [175, 176].

These membranes are essentially lipid membranes, consisting of dynamic and complex assemblies of lipids, proteins and carbohydrates. The lipid molecules are mainly phospholipids (referred to also as glycerophospholipids), sphingolipids and sterols. Phospholipids are amphipathic molecules, meaning that they are composed of two basic parts: a polar head, which contains a phosphate group and two non-polar fatty acid tails. Basically, membranes consist of a bilayer of phospholipids and sphingolipids arranged in two different layers, with the molecules arranged with their polar heads to the outside, and their hydrophobic tails to the inside, held together by hydrophobic interactions. In this structure, of around a few nanometers of thickness, the hydrophilic heads are exposed to the cytosol and the hydrophobic tails are sheltered [174, 175]. Also, proteins embedded in the lipid bilayer are responsible for providing channels within the bilayer which serve as transporters for hydrophilic molecules and ions.

Actually, membrane proteins embedded or transiently associated with the lipid bilayers, such as the denominated transmembrane or peripheral membrane proteins, are key components in several cell metabolism processes such as biocatalysis and other pathways such as signal transduction, cell-cell interactions and transport of ions and nutrients [177].

As mentioned earlier, membranes are key components which allow living cells to maintain and organize their function, and proteins incorporated in them, have such vital functions that they present a perfect target choice for pharmaceuticals. Therefore, understanding and unlocking the secrets of biological membranes is a great challenge which many want to tackle. However, due to the complexity of cell membranes system, which comprise intra- and extracellular networks, the direct study of these and particularly of membrane protein function *in situ* remains very challenging [177].

With the aim of addressing this problem, much research has been focused on developing artificial membranes which are able to mimic the structure of the cell membrane and in which the proteins are able to retain their structural integrity and their function. These models try to provide a system in which the intrinsic 2D fluidity of the cell membrane is preserved, allowing the investigation of membrane related processes by closely replicating native cell membranes [178].

A variety of models have been developed, such as solid supported membranes [179, 180], polymer cushioned membranes [181], hybrid bilayer lipid membranes [182], suspended or free-standing lipid bilayers [183] and tethered lipid bilayers [177, 178].

### 4.1.2 Supported and Tethered Lipid Bilayers

Lipid monolayers, lipid vesicles and supported lipid bilayers (SLBs) have been among the most commonly used models of native membrane systems. Great attention has been put into SLBs (Figure 4.1), since they provide a sound platform to be used as cell membrane models. These are composed of a single lipid bilayer on a solid substrate, normally glass, silica or mica. They can be formed either via vesicle fusion, through which unilamellar vesicles spontaneously adhere, rupture and fuse onto the substrate, or using the Langmuir deposition, in which individual monolayer leaflets are created and added to each other [184].

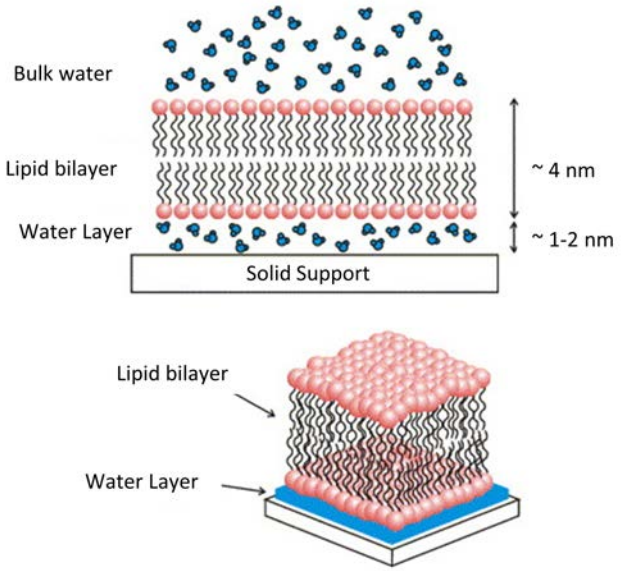


**Figure 4.1:** Schematic illustration of a solid supported lipid bilayer. A hydration layer is formed between the solid support and the bilayer. Reproduced from [180].

In the SLB setup one side of the lipid leaflet faces the solid support, from which it is separated by a thin hydration film. Its hydrophobic acyl chains interact with the second lipid leaflet and its hydrophilic head groups face the bulk solution. It is a stable system with the ability to enable lateral lipid diffusivity, imitating in this way the dynamic nature of native cell membranes [185]. Normally, SLBs are in close proximity to the surface, restricting the incorporation of proteins or their mobility and, as a consequence, the stability of transmembrane proteins [178]. With the aim of overcoming this constrain, tethered bilayer lipid membranes (tLBMs) have been developed (Figure 4.2). In these platforms, the lipid bilayer is covalently coupled to the solid support via a flexible spacer giving to this system the mechanical and chemical stability and robustness that is needed [186]. The spacer group serves in principle as a cushion that lifts the bilayer off the surface, compensates for surface roughness effects and can act as an ion reservoir underneath the membrane [187].

The functional task of lipid molecules that act as anchor groups is to immobilize the bilayer through a (partial) covalent attachment of the membrane to the substrate, and in this way prevent the bilayer from being washed away upon mechanical or chemical (osmotic) stress during manipulation. They also aid in preventing the lipid bilayer from interacting too strongly with the solid support. By achieving this, the dynamic properties of the bilayer are not compromised as much (i.e. lateral diffusion) [186].

The challenge in the construction of these functional platforms is finding the right balance between the grafting density, the chemistry and length of the spacer group together with the appropriate anchor chemistry. Furthermore, the lipid membranes can be assembled using different approaches, normally the lipid monolayer is formed using either self-assembly or through Langmuir deposition [187].

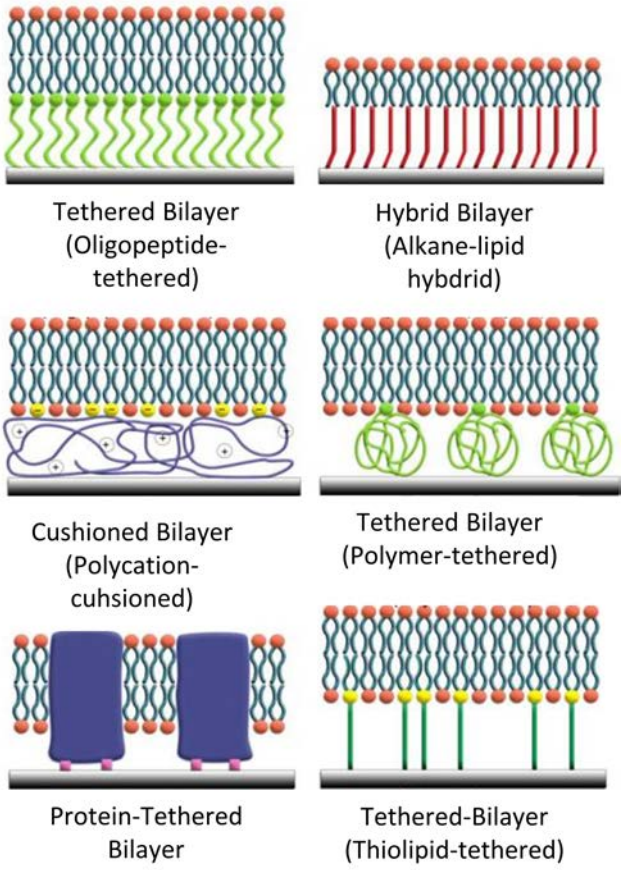


**Figure 4.2:** Schematic illustration of different ways of forming tBLMs. Different tethering units can be used: oligopeptides, SAMs, polycations, polymers, proteins or thiolipids. Reproduced from [188].

### 4.1.3 Giant Unilamellar Vesicles (GUVs)

Giant unilamellar vesicles (GUVs) are vesicles made out of lipids, and these are used extensively as membrane model systems since they are easily observable using optical microscopy. Compared to other unilamellar vesicles, such as small unilamellar vesicles (SUVs), and large unilamellar vesicles (LUVs), GUVs have a size range up to 100 μm, so they can be tuned to have the size of cells, their mean size being around 25 μm [189–191].

GUV membranes can thus be observed with light microscopy, but also, if fluorescent probes are included in GUV formation, confocal or fluorescence microscopy can be used as well [192, 193]. Furthermore, thanks to these characterization techniques, together with the size of GUVs and their curvature, the observation of specific membrane structural details of single vesicles can be carried out. This is not possible with, for example, smaller constructs such as SUVs. Moreover, the study of membrane components is not possible with other techniques such as differential scanning calorimetry, fluorescence spectroscopy or X-ray diffraction, among others, in which solutions of lipids are used to extract information, and the single vesicle cannot be characterized [192].

The molecular composition of GUVs can be finely tuned and thanks to this flexibility, GUVs have been used in several applications in which the composition, tension

and geometry of the membrane is manipulated and controlled by using several microscopy techniques [194]. Also, the lipid composition of the vesicles has been varied using natural or synthetic lipids and incorporating proteins [195, 196] or components from native cell membranes [197].

### Electroformation of GUVs

Different techniques have been developed for the production of GUVs, such as those based on dialysis or dilution methods, those using chaotropic salts, or vesicle fusion by freezing and thawing [198]. However, the most used one in the beginning was the swelling method, also denominated hydration method [199], described by Faucon et al. [200]. This was an adaptation of the previously reported method from Reeves et al. [201], widely used since it was easily performed and could be adapted to different environments, including physiological relevant ones [189].

However, this strategy presented some important drawbacks, since for the formation of GUVs in physiological conditions, a high proportion of negatively charged lipids had to be used [202], limiting the options to design the lipid composition of the GUV at will. Moreover, the long time required for GUV formation, in the range of days, hindered its use with lipids which degrade fast, as in the case of unsaturated lipids [189]. This, in addition to the low efficacy in GUV production [198], have made other strategies more popular.

Electroformation of GUVs was firstly reported in 1986 by Angelova et al. [203] as an alternative to the spontaneous swelling method. This strategy allowed the formation of GUVs in hours, typically between 1 and 3 hours [198], and as a consequence of the time reduction, allowed to work with lipids which were not that stable over time. Since the underlying principle of GUV formation using this method is still not clearly understood many different protocols have been described in the literature [190]. However, the common traits consist in (i) dissolving the lipids in an organic solvent and depositing these onto an electrode surface, (ii) drying the surface under vacuum to obtain a dry lipid film on the electrode, (iii) immersing the surface in a buffer and lastly, (iv) applying an alternate current (AC) field (Figure 4.9 and 4.9). The most common procedure consists in the application of a 1.2 V AC field and a frequency of 10 Hz during 2 hours [204]. Nevertheless, parameters including time, frequency, voltage, lipid concentration and type of electrode are some of those that have been varied in different reported studies [190].

As explained in [205] there are several mechanisms which induce lipid swelling and vesicle formation in presence of an electric field [203, 206–208]. These are the following: (i) electrostatic interaction between the electrode and the bilayers; (ii) mechanical stresses induced electroosmotically; (iii) redistribution of the double layer of counter-ions between bilayers; (iv) decreased surface, membrane and line tension; (v) electrochemical reactions; (vi) injection of charges from electrodes and (vii) reorientation and lateral redistribution of lipid molecules. Nevertheless, the exact mechanism of electroformation is not entirely understood, and the level of speculation increases from (i) to (vii).

In fact, as reported by Sens et al. [209], the electric field has a very specific impact on lipid membranes: it creates an unbalanced electric stress by inducing an ionic current across a non-perfectly flat membrane, giving rise to a destabilizing surface energy and provoking an enhancement of undulations. This is due to the distinctive dynamics and peculiarities of fluid membranes, which have specific bending and stretching energies.

As abovementioned, the most common protocol used is the denominated 10 Hz "electroformation protocol", and the most important underlying mechanism is the electroosmotic movement of the water in contact with the electrode. These vibrations, generated onto the electrode, provoke the pulling off and swelling of the lipid film from the electrode surface. Actually, these vibrations are similar to mechanical ones, formed when sonicating, but they present some advantages: they are more gentle and they can be tuned and controlled by varying the parameters of the electric field [209].

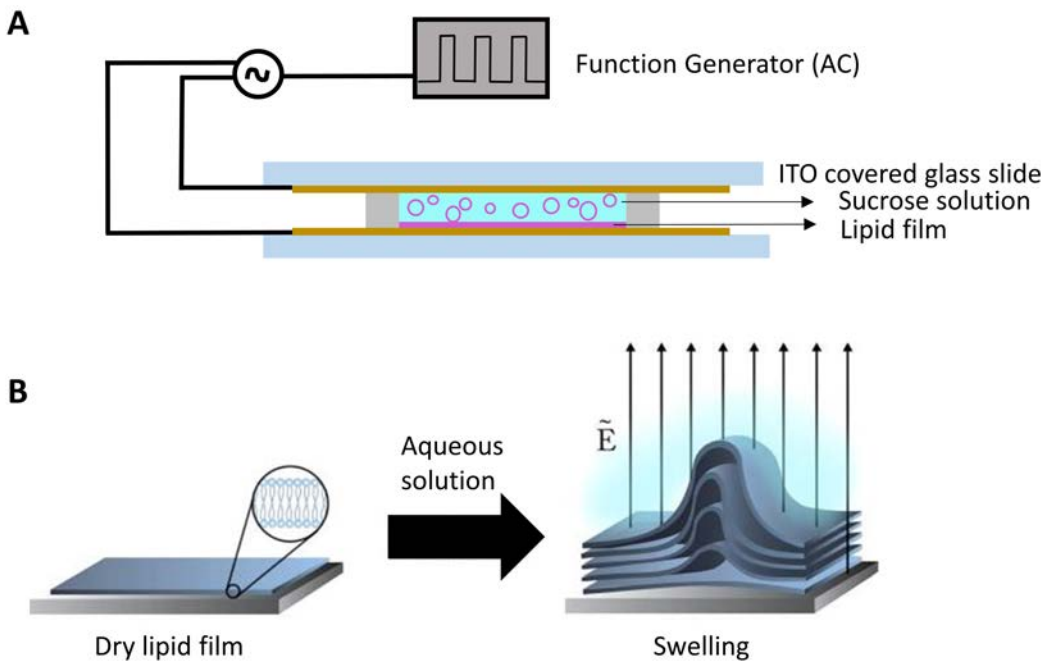


**Figure 4.3:** (A) Typical electroformation setup consisting in a lipid film on an ITO electrode, covered with an analogous one to form a solution reservoir and connected to a function generator. (B) Illustration of the swelling phenomena attributed to the formation of GUVs using an AC electric field. Reproduced from [210].

### Bilayer Formation

Plenty of theoretical and experimental studies have been carried out in order to better understand the underlying forces involved in vesicle rupture from solution onto solid supports. In fact, it has been found that different parameters such as the size of the vesicles, the osmotic pressure of these, the surfaces properties of the solid support and the inter-vesicle interactions, play a role [211]. Bilayer film formation by vesicle fusion in a spontaneous way was firstly observed by Tamm and

McConnell using glass surfaces. Bilayers were formed on a hydrating water layer of the thickness of 1 nm, providing a weak bound onto the surface and a certain degree of mobility to the lipid molecules [212].

Normally, vesicles in solution adsorb spontaneously forming lipid bilayers on hydrophilic surfaces since the lipid head and hydrophilic surfaces interact in a way that favors bilayer formation [213]. Even though the driving force for vesicle adsorption is this attraction, the hydrophobicity of the lipid tail is crucial for the final outcome of vesicle rupture on the support. Furthermore, the chemical and physical features of lipids, which provide certain characteristics to the vesicles they form, also influence SLB formation [211]. In addition, in some cases, supported vesicular layers (SVLs) can be formed, such as in the case of oxidized gold [214]. On hydrophobic surfaces, lipid monolayers are formed [182, 215].

The procedure for bilayer formation consists in mainly the following steps: (i) vesicle adsorption onto the surface, (ii) vesicle fusion to form larger ones and finally (iii) rupture of these with consequent bilayer formation (Figure 4.4). The specific principles which actually control this mechanism of vesicle rupture are still under investigation, some of these being i.e. the intrinsic stability of the vesicle, the presence of other vesicles or the edges of already formed bilayers on surface [175].

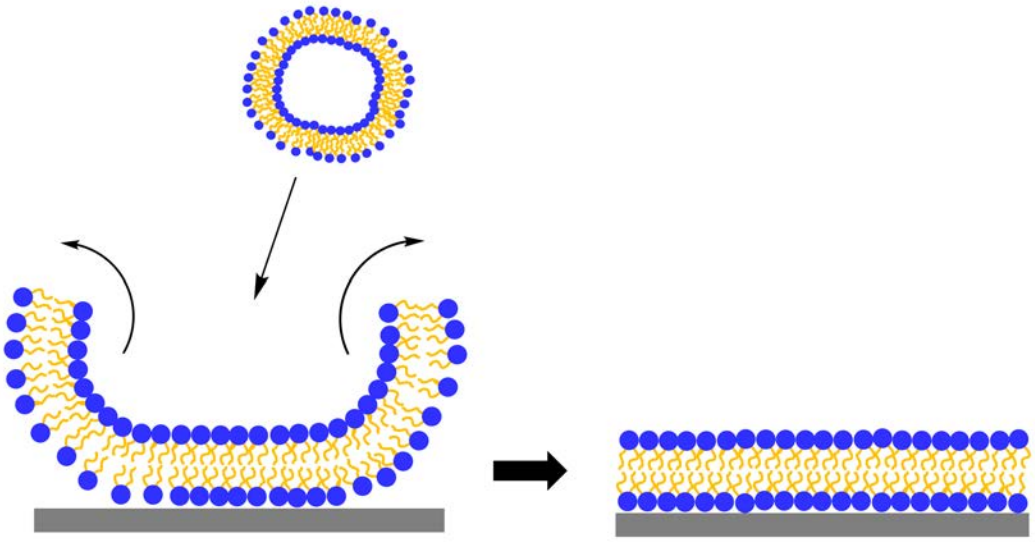

**Figure 4.4:** Schematic representation of bilayer formation due to vesicle rupture on a solid support.

### 4.1.4 Protein or Peptide Tethered Lipid Bilayers

During the last years, many groups have developed new surfaces or nanostructures which mimic more accurately the physiological properties of cell membranes by incorporating transmembrane proteins into these artificial systems [174]. Membrane proteins have a relevant role in living cells, from playing key roles in cell metabolism and in fundamental biochemical reactions such as respiration and photosynthesis [216]. Because of this, they are also a common target for pharmaceuticals: 60% of

the drugs in the market target proteins which are located on the cell surface [217, 218].

The ability to create artificial cell membrane models which incorporate membrane proteins has shed light into understanding more about how proteins integrated onto solid supports behave when changing different parameters. In fact, temperature, pH, ionic strength, adsorption behavior, conformational reorientation and surface density of bilayer membranes affect how proteins are incorporated onto solid surfaces [174].

In these systems it is important to keep the dynamic structure of native cell membranes: bilayers should be immobilized while preserving the dynamics of the lateral diffusion of the molecules and at the same time possess sufficient mechanical stability [218]. Not only that, but for applications involving proteins, they should be able to incorporate integral membrane proteins in their correctly folded conformation [219], since the function of a protein is directly dependent on its conformation [220].

This nature of lipid bilayers as a 2D fluid, however, poses technical challenges when using some characterization tools. Membrane proteins are notoriously difficult to image by AFM due to their diffusion, a couple orders of magnitude faster than the scanning speed of a standard AFM [221]. That is why AFM imaging of membrane proteins requires the formation of 2D protein crystals on substrates, which pins down the proteins and enables high-resolution imaging, but might also alter their conformation [221]. In electrophysiological characterization of ion channels and pore-forming peptides, black lipid membranes (BLMs) are used [222]. In these systems lipids dissolved in an organic solvent are painted over an aperture (d= 10-200 mm) in a Teflon membrane under an aqueous solution. Diffusion of channels in BLMs also causes difficulty in tracking the same single channel over time, because the proteins that diffuse out of the central bilayer region and touch the annulus of the BLMs, where the organic solvent is accumulated, tend to alter their structure and lose their function. Therefore, an approach to control the diffusion of lipids and membrane proteins would be beneficial when using these characterization tools. Moreover, this would allow characterization of proteins in an environment which mimics more accurately their actual cellular environment.

Several groups have reported strategies for developing lipid bilayers incorporating tethered or embedded proteins (Figure 4.5). In some cases, the thiol groups in the cysteines of the proteins have been used to immobilize these on gold surfaces, being able to monitor the process using SPR spectroscopy [223] or AFM [224]. Sinner et al. [225] have reported an optimized peptide-tethered lipid bilayer in which integrins were incorporated into a membrane model, in order to study integrin-ligand interactions using surface plasmon-enhanced fluorescence spectroscopy (SPFS).

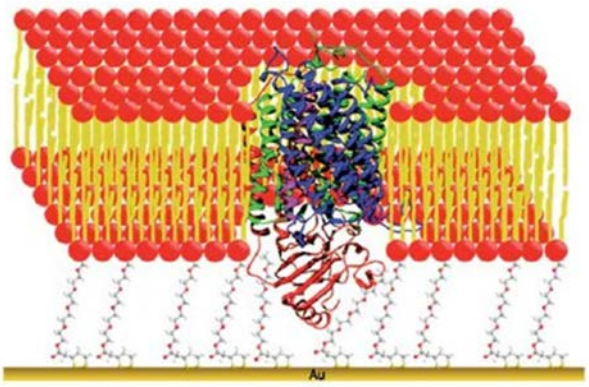


**Figure 4.5:** Schematic representation of a transmembrane protein integrated into a SLB. Reproduced from [226].

Becucci et al. published a strategy in which they incorporate channel forming peptides in a mercury SBL consisting in a tethered thiolipid monolayer with a self-assembled dioleoylphosphatidylcholine monolayer on top of it [227]. The thiolipid consists of a hexapeptide chain terminating in a thiol group which anchors onto the metal. The chain bears two triethyleneoxy side chains that provide hydrophilicity which intend to keep the anchored thiolpeptide chains sufficiently apart, in order to accommodate water molecules and inorganic ions and create a suitable environment for the incorporation of integral proteins.

The group of Sinner et al. has also developed a novel strategy for inserting complex membrane proteins into an artificial membrane system, through an *in vitro* expression and immediate post-translation membrane insertion of these molecules [228].

The interaction between substrates and lipids dominantly affect the diffusion properties of SLBs, where anchoring lipids to the underlying surface typically slows down the diffusion and decreases the mobile fraction. For example, tBLMs (D = 0.8-1.3 $\mu m^2/s$) [229, 230], negatively-charged bilayers on cationic polyelectrolytes (D = 0.02-0.08 $\mu m^2$) [231, 232], phospholipid monolayers formed on alkyl thiol SAMs on gold (D = 1-4 $\mu m^2/s$) [233], all vary their diffusion behaviors in comparison to the bilayers on glass (4 $\mu m^2/s$) [229, 230, 234]. These methods enable the reduction of lipid and protein diffusion, however, all the approaches provide a fixed molecular diffusion in the system, where there is no possibility to alter it over time. This is not ideal, because membrane proteins and bilayer-targeted signaling proteins require membrane fluidity to collide between each other for initiating the signaling complex formation, redox and enzymatic reactions [235]. For example, pore-forming peptides such as the toxin from *Staphylococcus aureus* ($\alpha$-hemolysin) and human immune peptide (LL-37) [236] typically adsorb onto lipid bilayers from solution as a monomer, diffuse inside the membranes for finding each other, and form oligomers to present the desired function (i.e. formation of ion channels). For such pore-forming peptides, the fluidity of bilayers is necessary at the initial phase for the oligomerization, after which lowering their diffusion is desirable for protein characterization using for example AFM imaging. Therefore, the current critical

missing technology is a method to control the diffusion of lipids and membrane proteins in a temporal manner, where the membranes initially retain reasonable diffusion yet can be tethered at a certain moment in time. Temperature-induced lipid phase transition has been used for a similar purpose [237], yet the control of the temperature in the range of 15 °C - 45 °C during AFM imaging imposes technical challenges (e.g. the thermal drift of the signals) and possible damages in proteins.

### 4.1.5 Measuring Diffusion of Lipid Bilayers using FRAP

Fluorescence recovery after photobleaching (FRAP) is a quantitative fluorescence technique that can be used to measure the dynamics of molecular mobility in 2D by taking advantage of the fact that most fluorophores are irreversibly bleached by incident light of very high intensity [238]. FRAP is applicable to a wide range of biological phenomena utilizing physiologically relevant concentration of fluorophores [239]. Basically, it consists in photobleaching a delimited area of the fluorescent sample and thereafter monitoring the fluorescence recovery over time, as shown schematically in Figure 4.6.

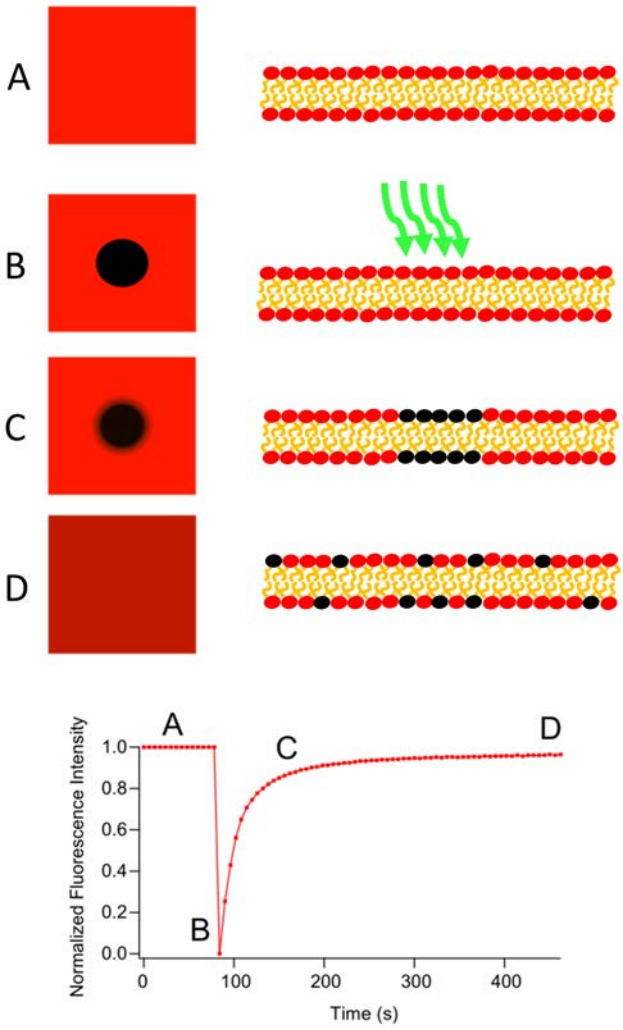


**Figure 4.6:** Basic principle underlying the FRAP technique. (A) Bilayer before bleaching, (B) irradiation of high intensity light for photobleaching, (C) photobleached area visible right after irradiation and (D) diffusion of molecules give place to the recovered bilayer, and the bleached spot disappears. Fluorescence recovery is graphically represented by plotting the normalized fluorescence vs. time.

### Data Fitting

For the extraction of information obtained by FRAP plots, treatment of the data has to be carried out. In this work data fitting was performed using the Soumpasis Diffusion equation (Equation 4.1) used for diffusion-limited FRAP recovery curves [240].

$$f(t) = Aexp(-2\tau/t)[I_0(2\tau/t) + I_1(2\tau/t)] \tag{4.1}$$

In which $I_0$ is the modified Bessel function of the first kind of order 0 and $I_1$ is the modified Bessel functions of the first kind of first order to find only parameters A and $\tau$. A is the mobile fraction and the diffusion coefficient ($D$) is calculated using the Equation 4.2.

$$D = w^2/\tau \tag{4.2}$$

Where $w$ is the radius of the circular FRAP region of interest (ROI). Equations 4.1 and 4.2 are taken from the paper Sprague et al. 2004 [241].

## 4.2 Objectives and Strategy

The objective of this work will be to design and develop a platform for tethering lipid bilayers with a temporal control using an external stimulus, in this case an electrochemical one. This allows the control of lipid diffusion at a certain time point, presenting a platform in which transmembrane proteins can be characterized in an environment which resembles more the actual cell membrane one.

Hence, we will report a strategy involving a tethered lipid bilayer, which actually becomes tethered upon the application of a low voltage. We will use the electroactive interfaces described in Chapter 2 and an interfacial reaction to anchor covalently the lower leaflet of a lipid membrane on a prefunctionalized surface.

Specifically, the MA interfacial reaction will be used to anchor onto prefunctionalized gold surfaces lipid membranes containing thiol-phospholipids, using the HQ SAM redox activity controlled through a voltage application (Figure 4.7). The control of diffusion in lipid membranes will be assessed using the FRAP technique.

To achieve this objective, the following tasks will be performed[1]:

- Formation of bifunctional GUVs using an electroformation protocol.
- SAM formation using molecule **1** and **2** (Figure 2.7) with different ratios on gold coated substrates.
- Lipid bilayer formation by GUV rupture on prefunctionalized gold surfaces.
- Study of the immobilization effect of lipid bilayers using thiolated GUVs and the interfacial MA reaction: (i) study of the change in diffusion coefficient when using HQ terminated SAMs **S1** versus electroactivated BQ terminated SAMs **S2** and (ii) study the effect of the change in concentration of the electroactive anchoring moiety on surface. Study of the diffusion coefficient using the FRAP technique.

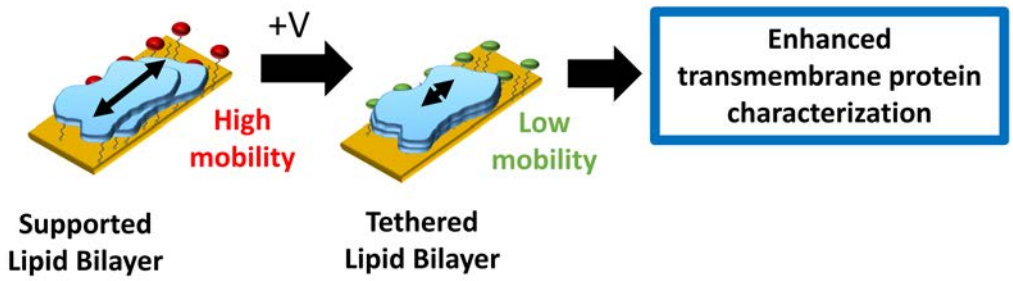


**Figure 4.7:** Sketch of the immobilization strategy of lipid bilayers on electroactivated reactive SAMs towards enhanced transmembrane protein characterization.

[1]This has been done in collaboration with Sugihara's Lab, at the University of Geneva, during a research stay funded by a COST Action (Arbre Mobieu) and a mobility scholarship from CIBER-BBN.

## 4.3 Lipid Bilayer on Electroactive SAMs

### 4.3.1 GUV Formation

Bilayers were formed by the fusion of formed bifunctional GUVs on prefunctionalized surfaces. GUVs were prepared using the electroformation protocol illustrated in Figure 4.9. Concretely, a solution containing 89% phosphatidylcholine (POPC), 10% 1,2-Dipalmitoyl-sn-Glycero-3-Phosphothioethanol (DPTTE) and 1% POPC-Rhodamine (Figure 4.8) was prepared in chloroform from stock solutions. POPC was used since it is a standard lipid molecule widely used for vesicle formation, DPTTE was used since it incorporates a thiol group, enabling the MA interfacial reaction to take place and POPC-Rho, which incorporates rhodamine, enables the visualization of the formed vesicles with fluorescence microscopy since rhodamine is a fluorophore. Not only that, but the presence of the fluorophore also permits the use of FRAP to study membrane dynamics.

The electroformation protocol (Figure 4.9 A) consisted in firstly preparing the lipid solution in chloroform. Thereafter, a small volume (2 μL) of this solution was disposed, in the form of tiny droplets, onto ITO covered glass slides and these were dried under vacuum during 2 hours. Thereafter, a well using white clay was used to create a chamber with an analogous ITO substrate on top. The created chamber was filled with a sucrose solution (315 mM) and sealed to avoid leakage. Using copper tape contacts both ITO substrates were connected to a function generator. A sinusoidal wave was applied during 2 hours (10 Hz) and successful GUV formation was confirmed using optical microscopy (bright field or fluorescence) (Figure 4.9 B). For further details concerning the experimental procedure, refer to Section 7.3.2.

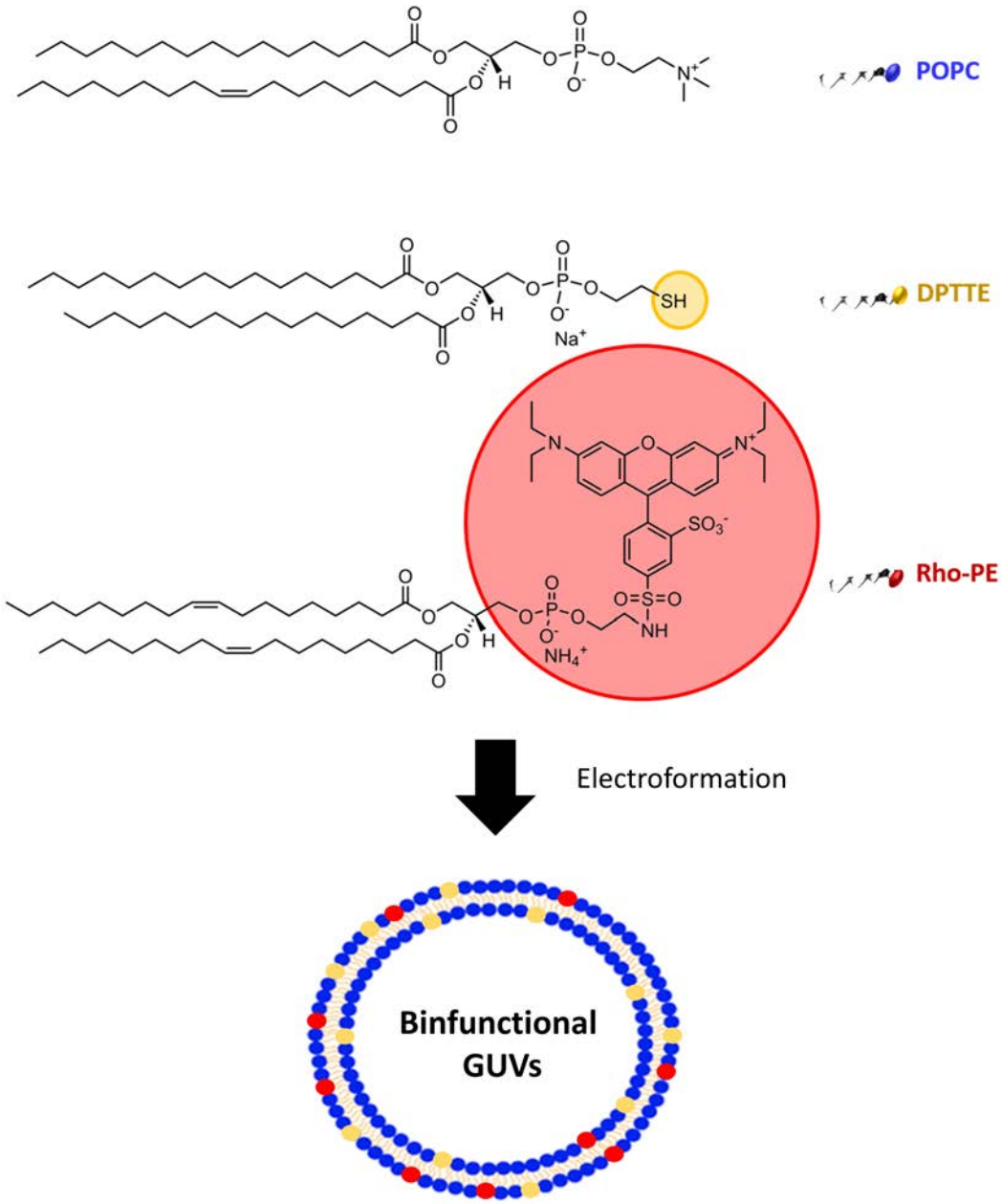


Figure 4.8: Molecular structure of POPC, DPTTE and Rho-POPC molecules. The red circle indicates the rhodamine, and the yellow one the thiol anchoring group. These are the components of the electroformed bifunctional GUVs.

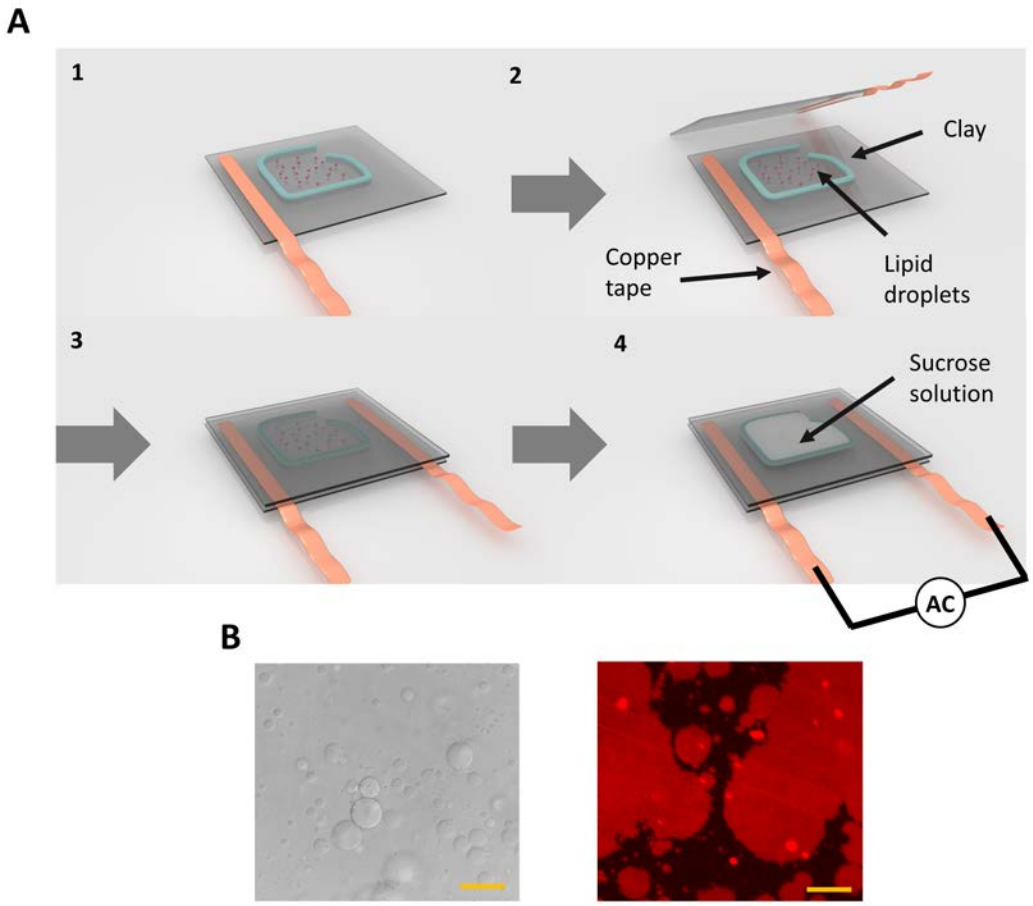


**Figure 4.9:** (A) Illustration of the electroformation protocol performed for the obtention of bifunctional GUVs for the formation of lipid bilayers on gold surfaces. (B) Bright field and fluorescent images of electroformed bifunctional GUVs. Scale bars corresponds to 200 μm.

### 4.3.2 Electroactivated Interfacial Reaction with Lipid Bilayers

As a preliminary study, bifunctional GUVs were ruptured on glass coverslips, presenting diffusion coefficients reported in literature for bilayers on glass. Thereafter, we proceeded to study the formation of bilayers on oxidized gold substrates, however, as previously observed, formation of patches was hardly seen, GUVs were not rupturing and remained intact in the solution and on the surface interface [214].

Following, studies including functionalized gold substrates were used, specifically surfaces with a mixed SAM **S1** formed with molecule **1** and **2** (Figure 2.7) in different ratios, specified later.

Importantly, in this system (i) tethering of the lipid bilayer can be achieved via the MA interfacial reaction, (ii) thanks to the use of the pegylated alkanethiol molecules the bilayer is distanced from the surface, offering numerous advantages. This spacer linker provides flexibility and stability to the bilayer and the possibility of a hydration layer to be formed between the bilayer and the surface. Additionally, if proteins are incorporated to the bilayer, it helps shield the protein from the substrate and avoid compromising the dynamic properties of the bilayer [180].

Due to the complexity of the setup required for *in situ* studies of lipid diffusion, lipid bilayers either on reduced SAMs **S1** or oxidized SAMs **S2** were investigated separately, a seen in Figure 4.10 A, so obtaining sample **S1-LB** when rupturing GUVs on SAMs **S1** and **S4-tLB**, when rupturing them on SAMs **S2**.

On these, which should not be given for granted since on oxidized gold surfaces GUVs would not rupture, GUVs ruptured to form lipid bilayers big enough to be able to perform FRAP measurements, as seen in Figure 4.10 B.

After confirming the feasibility of having patches large enough to measure their diffusion coefficient, we proceeded to investigate if the increase of electroactive moiety HQ/BQ on surface would decrease even more the diffusion of the lipid bilayers, since the anchoring points would also increase. For this purpose, SAMs **S1** with different HQ concentrations were prepared: 1% (**S1-1**), 5% (**S1-5**), 15% (**S1-15**), 25% (**S1-25**) and 50% (**S1-50**). The oxidized samples were prepared by oxidizing SAMs **S1** to **S2**, yielding **S2-1**, **S2-5**, **S2-15**, **S2-25** and **S2-50**.

When lipid bilayers were formed by spontaneous rupture of bifunctional GUVs on these, we obtained **S1-LB-1**, **S1-LB-5**, **S1-LB-15**, **S1-LB-25** and **S1-LB-50** for reduced SAMs, and **S4-tLB-1**, **S4-tLB-5**, **S4-tLB-15**, **S4-tLB-25** and **S4-tLB-50**, for oxidized samples. On these, the MA interfacial reaction takes place between the thiol group in DPTTE molecules and the BQ groups exposed on the surface.

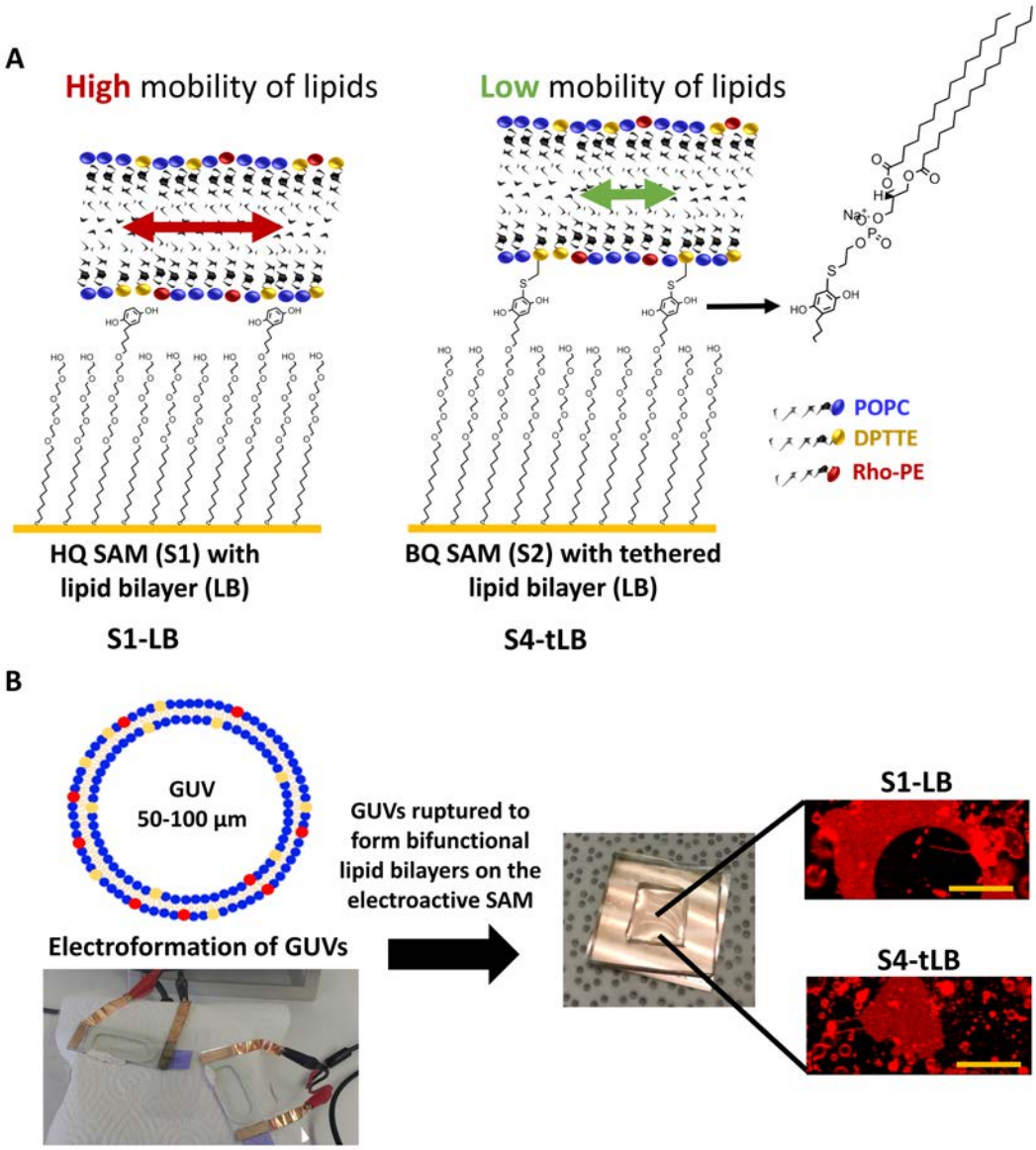


**Figure 4.10:** (A) Schematic representation of the MA interfacial reaction for partial covalent attachment of the lower leaflet of the lipid bilayer. (B) Sketch of bifunctional GUVs (with thiol and rhodamine containing lipids) formed by the electroformation protocol using ITO coated glass slides as electrodes, picture of the PDMS pool and fluorescence microscopy images as confirmation of correct bilayer formation. Scale bar= 20 µm.

## 4.4 Diffusion Coefficient Analysis

### Sample Preparation for FRAP Measurements

For the preparation of the lipid bilayers on SAMs a PDMS well was used to confine a pool of solution consisting of HEPES buffer (see picture in Figure 4.10 B), in which a small volume of GUV solution was inserted in order to form lipid bilayers via GUV rupture. These GUVs were incubated protected from light for at least 1 hour to allow the interfacial reaction to take place. The experimental setup was optimized in order to get reliable and consistent results, lower incubation times led to a large disparity in results, and this was attributed to too little time for the interfacial reaction to

take place. Before proceeding to FRAP measurements the PDMS pool was rinsed thoroughly to eliminate the non-ruptured GUVs.

### FRAP Measurements

To analyze and compare the diffusion of the lipid membranes on the dynamic surfaces, FRAP was used to extract values corresponding to diffusion coefficient and mobile fraction. Using the laser of the confocal microscope, a ROI was irradiated to photobleach the fluorophores and images were acquired to follow the recovery of fluorescence in this region over time. Concretely, substrates containing the PDMS pool were mounted onto the microscope and were visualized with a 60X water objective, and thereafter, bilayer patches were focused and a large enough patch was found to be able to perform FRAP. This is important since in order to obtain reliable values for diffusion coefficients using the FRAP technique, it is important to photobleach an area which consists of a small fraction of the total one: this allows lipids to diffuse into the photobleached area as if there were an infinite reservoir of lipids surrounding the photobleached area [242]. The fluorescence intensity of the region was quantified, normalized and the data was plotted over time. The obtained curve was then fitted to the Soumpasis Diffusion equation (Equation 4.2). At least three different measurements in three different patches were performed on each of the samples analyzed.

FRAP results obtained for samples **S1-LB-1**, **S1-LB-15**, **S4-tLB-1** and **S4-tLB-15** can be visualized in Figure 4.11. In this Figure, screenshots of the images obtained during FRAP measurements are shown together with the time (**t**) corresponding to it. To visualize the photobleached area and the recovery of fluorescence, screenshots before photobleaching ($\mathbf{t_1}$) and right after photobleaching ($\mathbf{t_3}$ and $\mathbf{t_4}$) are shown, together with the last one ($\mathbf{t_5}$).

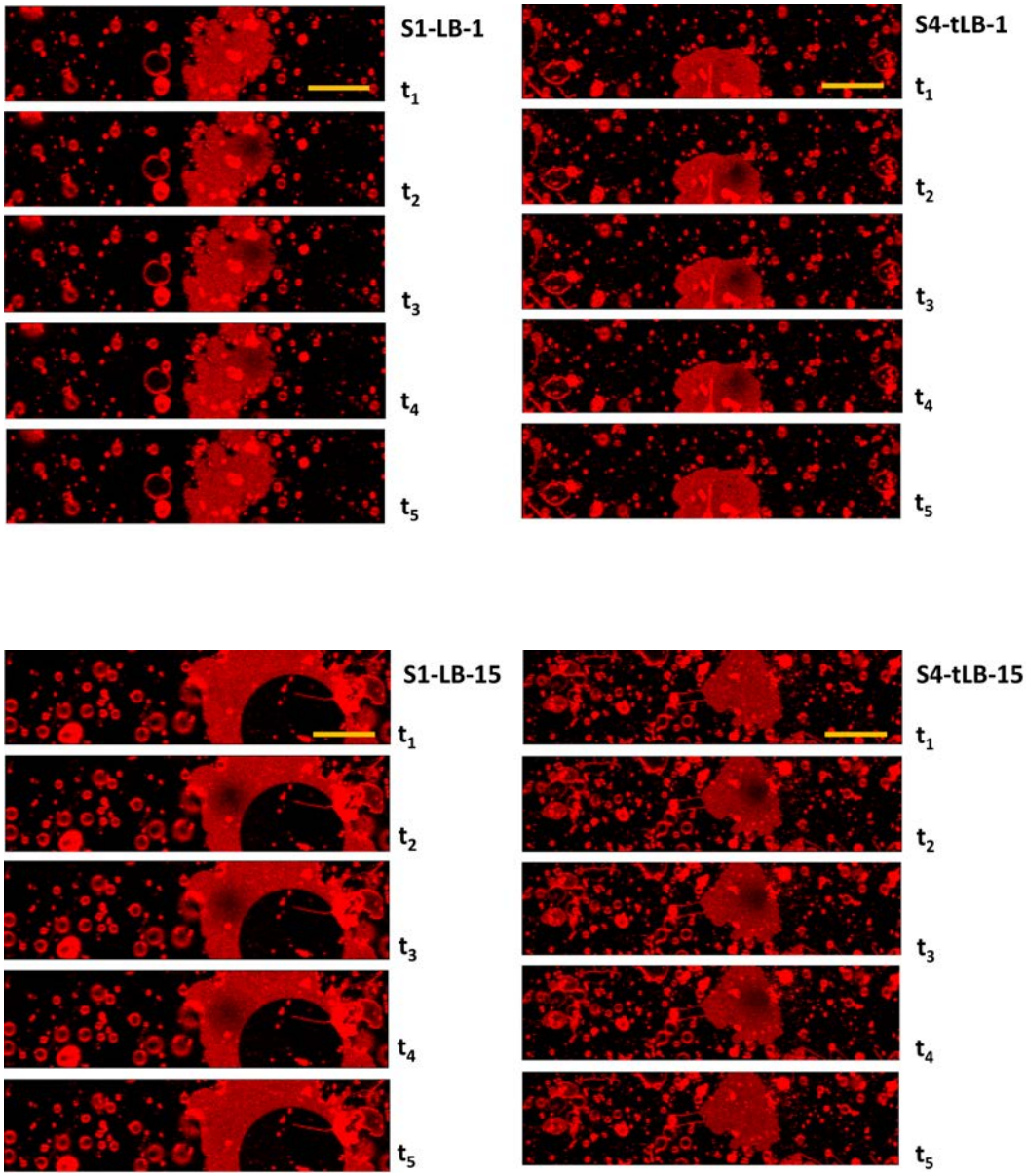


**Figure 4.11:** Screenshots of microscopy images taken from FRAP experiments consisting of the photobleaching of bilayers in **S1-LB-1**, **S1-LB-15**, **S4-tLB-1** and **S4-tLB-15** samples. Frames shown for each sample correspond to frame number 1 (prebleach, $\mathbf{t_1}$), frame number 4 (first image captured postbleach, $\mathbf{t_2}$), frame number 5 (second image captured postbleach, $\mathbf{t_3}$), frame number 6 (third image captured postbleach, $\mathbf{t_4}$) and frame 400 (last image captured, $\mathbf{t_5}$). Scale bar= 20 μm.

Fluorescence recovery plots obtained in FRAP experiments for samples **S1-LB-1**, **S1-LB-15**, **S4-tLB-1** and **S4-tLB-4** are displayed in Figure 4.12. The data was fitted to Equation 4.2 to obtain values for the diffusion coefficient and mobile fraction (shown in Table 4.1).

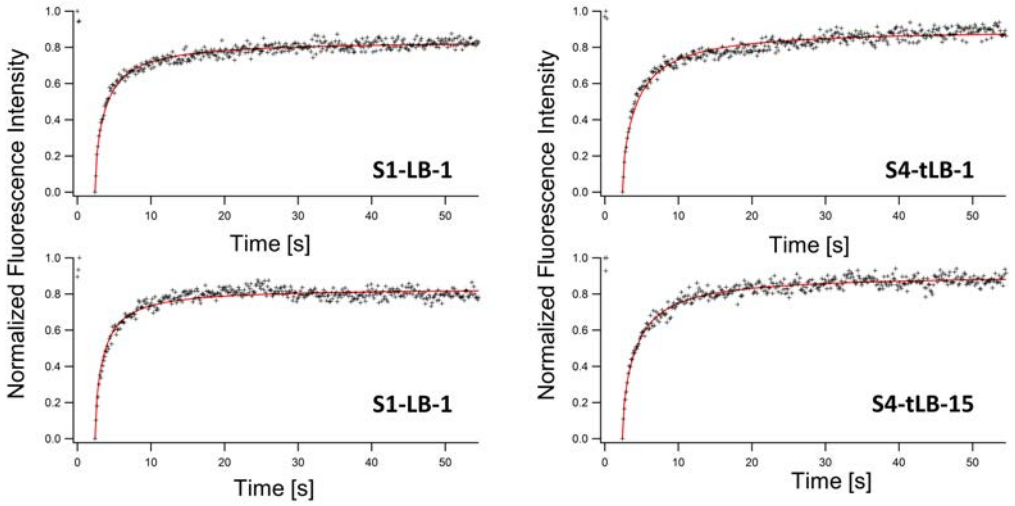


**Figure 4.12:** Plot of the data obtained for samples found in Figure 4.11 and fitting of the data using the Soumpasis Diffusion Equation.

**Table 4.1:** Mobile fraction and diffusion coefficient average values for **S1-LB-1**, **S4-tLB-1**, **S1-LB-15**, **S4-tLB-15**.

| | **S1-LB-1** | **S4-tLB-1** | **S1-LB-15** | **S4-tLB-15** |
|---|---|---|---|---|
| **Mobile Fraction** | $0.88 \pm 0.22$ | $0.97 \pm 0.13$ | $0.86 \pm 0.02$ | $0.84 \pm 0.05$ |
| **Diffusion coefficient [$\mu m^2/s$]** | $4.56 \pm 0.43$ | $3.63 \pm 2.36$ | $6.04 \pm 0.69$ | $4.29 \pm 0.59$ |

In a second experiment, samples **S1-LB-25**, **S1-LB-25**, **S1-LB-50** and **S4-tLB-50** were analyzed, values for diffusion and mobile fraction are collected in Table 4.2.

**Table 4.2:** Mobile fraction and diffusion coefficient average values for **S1-LB-25**, **S4-tLB-25**, **S1-LB-50**, **S4-tLB-50**.

| | **S1-LB-25** | **S1-LB-25** | **S1-LB-50** | **S4-tLB-50** |
|---|---|---|---|---|
| **Mobile Fraction** | $0.86 \pm 0.08$ | $1.11 \pm 0.10$ | $0.84 \pm 0.07$ | $0.82 \pm 0.06$ |
| **Diffusion coefficient [$\mu m^2/s$]** | $1.87 \pm 0.50$ | $0.54 \pm 0.24$ | $2.40 \pm 1.54$ | $2.68 \pm 0.46$ |

Results shown in Table 4.1 and 4.2 are graphically portrayed in Figure 4.13 and 4.14.

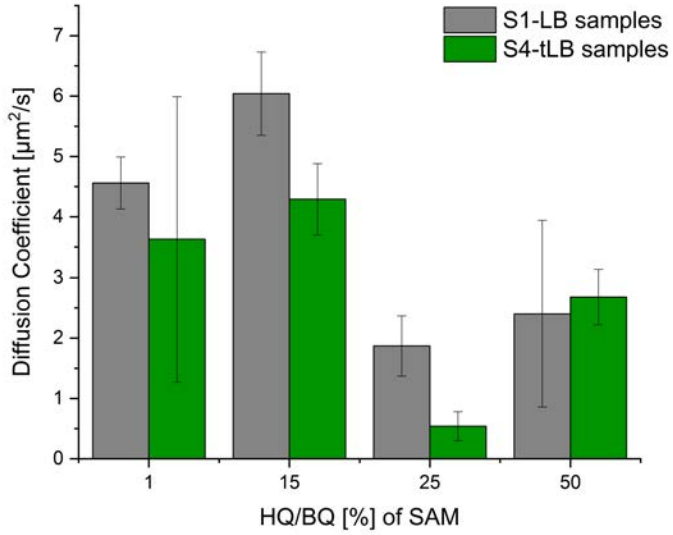


**Figure 4.13:** Plot showing the different diffusion coefficients obtained for all samples: **S1-LB-1**, **S4-tLB-1**, **S1-LB-15**, **S4-tLB-15**, **S1-LB-25**, **S4-tLB-25**, **S1-LB-50** and **S4-tLB-50**.

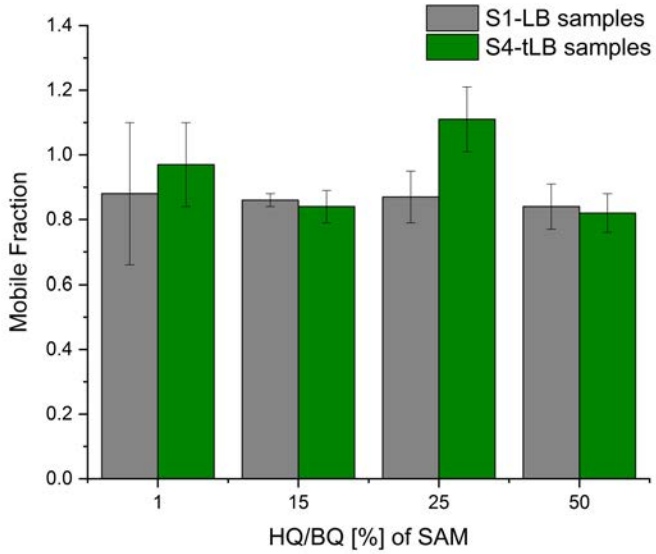


**Figure 4.14:** Plot showing the different mobile fractions obtained for all samples: **S1-LB-1**, **S4-tLB-1**, **S1-LB-15**, **S4-tLB-15**, **S1-LB-25**, **S4-tLB-25**, **S1-LB-50** and **S4-tLB-50**.

A decrease of the diffusion coefficient was obtained when using oxidized SAMs **S2**, compared to the reduced form, SAMs **S1**, due to the tethering of the lower leaflet of the lipid bilayer through the MA interfacial reaction, except in sample **S4-tLB-50** (Figure 4.14).

In fact, the difference is larger between **S1-LB-15** and **S4-tLB-15** than between **S1-LB-1** and **S4-tLB-1**, values being 1.75 versus 0.93. This is expected since the

number of anchoring points is increased (from 1 to 15%) when the HQ percentage on surface is increased, leading to a more restrictive mobility of the bilayer and hence decreasing the diffusion coefficient.

As mentioned before, surprisingly, the diffusion coefficient of **S4-tLB-50** did not diminish, as we would have expected it to. In fact, at this concentration there is a big variation in results as portrayed by the large error bar. This could be attributed to steric hindrance between the BQ groups, leading to decreased efficiency of the interfacial reaction.

We also observed that when increasing so much the concentration of BQ on surface, vesicles did not rupture as much, as compared to when working with lower concentrations, and patches found were normally smaller. This can be explained partly by the hydrophobicity of the surface, since as previously reported, the contact angle for SAMs with 50% of BQ groups on surface is 80.8 °[93], this leading normally to the formation of monolayers instead of bilayers [182, 215].

Just by varying the HQ% in **S1-LB** samples a difference in diffusion coefficient is already obtained, this could be attributed to different phenomena, as discussed and reviewed in [243]. As stated by Chantia et al. [244] low diffusion can be associated to the presence of unruptured vesicles or fluorophore aggregates on the surface of the bilayer.

Also important to take into account is, again, the effect of the wettability of the solid support, the more hydrophobic the surface, affecting the hydration layer, leads to the lowering of diffusion coefficient [245]. An increase in hydrophobicity in oxidized samples when increasing the BQ% is expected, hence, we cannot explicitly attribute the lowering of the diffusion to solely the interfacial reaction taking place, but the change in wettability of the surface might be also playing a role.

All in all, values obtained show that in fact we achieve a decrease of the diffusion coefficient when using SAMs as supporting lipid bilayers, and by applying a potential, and making the SLB a tethered-SLB we even get a larger reduction of the diffusion.

Clearly, in our setup, when we vary the percentage of HQ/BQ on SAMs, different parameters influence the resulting diffusion coefficient of the lipid bilayers. The effects mentioned have been: (i) the number of anchoring points for tethering the lipid bilayer, (ii) the effect of steric hindrance and (iii) the change in the wettability of the surface.

In regard to the mobile fraction no trend is observed, however, recovery is not 100%, but limited to around 80% in all samples. This can be due to the tricky experimental setup used; the presence of fluorescent artifacts was minimized by several rinsings but could not be entirely eliminated.

Nonetheless, the 25% sample seems a promising platform for investigating further, since it allows the formation of lipid bilayers (not achieved at the concentration of 50%) and also lowers the diffusion coefficient in respect to values obtained for glass SLBs [229, 230, 234]. Furthermore, the establishment of a rigorous experimental methodology, proper rinsing and removal of artifacts, is essential for avoiding distortion of results.

## 4.5 Summary and Perspectives

Nowadays there is a big interest in finding new ways to study proteins in their real environment. Specifically, the study of membrane active proteins is of paramount importance for the design of peptide therapeutics against bacteria (antimicrobial activity) and cancers. A critical aspect in the structure-function relationship of membrane active proteins is their specific activity relative to the lipid membrane composition of the cell target. In fact, proteins specificity significantly depends on the lipid compositions of different cell membranes and thus it is very important not only to study the proteins alone but also immersed in the membrane to characterize them and evaluate their real activity. The study of membrane protein activity using single-molecule techniques, which enable strong correlations of peptide biological activity and peptide structure and physicochemical properties is very difficult due to the diffusion character of cell membranes. This is thus an important drawback for the study of structure-function relationship which gives insight into how these peptides function at the membrane interface. Actually, membrane proteins are notoriously difficult to characterize for example by AFM because they diffuse faster than the scanning speed of conventional AFMs.

To overcome this drawback, we have used an electrochemically controlled dynamic interface which allows controlling the diffusion of lipid bilayers in a spatio-temporal manner. Specifically, we have developed a new strategy that enables the control of diffusion by anchoring lipid bilayers to the surface upon application of an external stimulus. Towards this aim, we have designed, synthesized and characterized HQ terminated molecules to get electroactive SAMs which are compatible with biological environments. Such a dynamic interface, in a second step, permits the immobilization of thiol terminated molecules via a MA reaction upon the application of a low potential. FRAP is a quantitative fluorescence technique that can be used to measure the dynamics of molecular mobility in 2D by taking advantage of the fact that most fluorophores are irreversibly bleached by high intensity incident light. Since FRAP is applicable to a wide range of biological phenomena utilizing physiologically relevant concentration of fluorophores we have used this technique to analyze the diffusion in our system.

In this study we successfully achieved a control in the diffusion coefficient of lipid bilayers with an electrochemical external input (temporal control), which is relevant for the study of membrane proteins. This temporal control enables the tethering of the bilayer at a determined time and thus minimizing the time in which the lipid bilayer is artificially anchored onto the substrate, making this a promising platform for studies pursuing characterization of transmembrane proteins. Following experiments would include the incorporation of transmembrane proteins (e.g. $\alpha$-hemolysin) and their characterization in the developed temporally controlled tethered lipid bilayers.

# References


[93] A. R. Kyvik, C. Luque-Corredera, D. Pulido, et al. „Stimuli-Responsive Functionalization Strategies to Spatially and Temporally Control Surface Properties: Michael vs Diels–Alder Type Additions“. In: *The Journal of Physical Chemistry B* 122.16 (2018), pp. 4481–4490 (cit. on pp. 34, 122).

[174] M. Shuja Khan, N. S. Dosoky, and J. D. Williams. „Engineering Lipid Bilayer Membranes for Protein Studies“. In: *Int. J. Mol. Sci* 14 (2013), p. 14 (cit. on pp. 101, 107, 108).

[175] R. P. Richter, R. Bérat, and A. R. Brisson. „Formation of Solid-Supported Lipid Bilayers: An Integrated View“. In: *Langmuir* 22.8 (2006), pp. 3497–3505 (cit. on pp. 101, 107).

[176] L. Kam and S. G. Boxer. „Spatially Selective Manipulation of Supported Lipid Bilayers by Laminar Flow: Steps Toward Biomembrane Microfluidics“. In: *Langmuir* 19 (2003), pp. 1624–1631 (cit. on p. 101).

[177] S. Rebaud, O. Maniti, and A. P. Girard-Egrot. „Mini-review Tethered bilayer lipid membranes (tBLMs): Interest and applications for biological membrane investigations“. In: *Biochimie* 107 (2014), pp. 135–142 (cit. on p. 102).

[178] H. Basit, A. der Heyden, C. Gondran, et al. „Tethered Bilayer Lipid Membranes on Mixed Self-Assembled Monolayers of a Novel Anchoring Thiol: Impact of the Anchoring Thiol Density on Bilayer Formation“. In: *Langmuir* 27.23 (2011), pp. 14317–14328 (cit. on pp. 102, 103).

[179] T. J. Crites, M. Maddox, K. Padhan, et al. „Supported Lipid Bilayer Technology for the Study of Cellular Interfaces“. In: *Curr Protoc Cell Biol* 68 (2015) (cit. on p. 102).

[180] E. T. Castellana and P. S. Cremer. „Solid supported lipid bilayers: From biophysical studies to sensor design“. In: *Surface Science Reports* 61 (2006), pp. 429–444 (cit. on pp. 102, 103, 115).

[181] E. Sackmann and M. Tanaka. „Supported membranes on soft polymer cushions: fabrication, characterization and applications“. In: *Tibitech February* 18 (2000) (cit. on p. 102).

[182] A. L. Plant. „Supported Hybrid Bilayer Membranes as Rugged Cell Membrane Mimics“. In: *Langmuir* 15.6 (1999), pp. 5128–5135 (cit. on pp. 102, 107, 122).

[183] D.-W. Jeong, H. Jang, S. Q. Choi, and M. C. Choi. „Enhanced stability of freestanding lipid bilayer and its stability criteria“. In: *Scientific Reports* 6 (2016), pp. 1–7 (cit. on p. 102).

[184] E. Kalb, S. Frey, and L. K. Tamm. „Formation of supported planar bilayers by fusion of vesicles to supported phospholipid monolayers“. In: *Biochimica et Biophysica Acta* 1103 (1992), pp. 307–316 (cit. on p. 102).

[185] G. J. Hardy, R. Nayak, and S. Zauscher. „Model cell membranes: Techniques to form complex biomimetic supported lipid bilayers via vesicle fusion“. In: *Current Opinion in Colloid & Interface Science* 18.5 (2013), pp. 448–458 (cit. on p. 103).

[186] W. Knoll, I. Köper, R. Naumann, and E.-K. Sinner. „Tethered bimolecular lipid membranes-A novel model membrane platform“. In: *Electrochimica Acta* 53.23 (2008), pp. 6680–6689 (cit. on p. 103).

[187] I. Kö and I. Koper. „Insulating tethered bilayer lipid membranes to study membrane proteins“. In: *Mol. BioSyst.* 3.10 (2007), pp. 651–657 (cit. on p. 103).

[188] J. A. Jackman, W. Knoll, and N.-J. Cho. „Biotechnology Applications of Tethered Lipid Bilayer Membranes“. In: *Materials* 5 (2012), pp. 2637–2657 (cit. on p. 104).

[189] P. Méléard, L. A. Bagatolli, and T. Pott. „Chapter 9 - Giant Unilamellar Vesicle Electroformation: From Lipid Mixtures to Native Membranes Under Physiological Conditions“. In: *Methods in Enzymology* 465 (2009), pp. 161–176 (cit. on pp. 104, 105).

[190] D. Drabik, J. Doskocz, and M. Przybyło. „Effects of electroformation protocol parameters on quality of homogeneous GUV populations“. In: *Chemistry and Physics of Lipids* 212 (2018), pp. 88–95 (cit. on pp. 104, 105).

[191] O. Wesołowska, K. Michalak, J. Maniewska, and A. B. Hendrich. „Giant unilamellar vesicles-a perfect tool to visualize phase separation and lipid rafts in model systems“. In: *Acta Biochimica Polonica* 56 (2009), pp. 33–39 (cit. on p. 104).

[192] M. Fidorra, A. Garcia, J. H. Ipsen, S. Härtel, and L. A. Bagatolli. „Lipid domains in giant unilamellar vesicles and their correspondence with equilibrium thermodynamic phases: A quantitative fluorescence microscopy imaging approach“. In: *Biochimica et Biophysica Acta* 1788 (2009), pp. 2142–2149 (cit. on p. 104).

[193] J. Zupanc, B. Drašler, S. Boljte, et al. „Lipid Vesicle Shape Analysis from Populations Using Light Video Microscopy and Computer Vision“. In: *PLoS ONE* 9.11 (2014). Ed. by Xiao-Feng Yang, pp. 1–14 (cit. on p. 104).

[194] T. Bhatia, P. Husen, J. Brewer, et al. „Preparing giant unilamellar vesicles (GUVs) of complex lipid mixtures on demand: Mixing small unilamellar vesicles of compositionally heterogeneous mixtures“. In: *BBA - Biomembranes* 1848 (2015), pp. 3175–3180 (cit. on p. 105).

[195] P. Girard, J. Pé, G. Lenoir, et al. „A New Method for the Reconstitution of Membrane Proteins into Giant Unilamellar Vesicles“. In: *Biophysical Journal* 87 (2004), pp. 419–429 (cit. on p. 105).

[196] J.-L. Rigaud, B. Pitard, and D. Levy. „Reconstitution of membrane proteins into liposomes: application to energy-transducing membrane proteins“. In: *Biochimica et Biophysica Acta* 1231 (1995), pp. 223–246 (cit. on p. 105).

[197] L.-R. Montes, A. Alonso, F. M. Goñi, and L. A. Bagatolli. „Giant Unilamellar Vesicles Electroformed from Native Membranes and Organic Lipid Mixtures under Physiological Conditions“. In: *Biophysical Journal* 93 (2007), pp. 3548–3554 (cit. on p. 105).

[198] M. I. Angelova, S. Soléau, P. Méléard, F. Faucon, and P. Bothorel. „Preparation of giant vesicles by external AC electric fields. Kinetics and applications“. In: *Trends in Colloid and Interface Science VI* 131.899 (1992), pp. 127–131 (cit. on p. 105).

[199] N. F. Morales-Penningston, J. Wu, E. R. Farkas, et al. „GUV preparation and imaging: Minimizing artifacts“. In: *Biochimica et Biophysica Acta* 1798 (2010), pp. 1324–1332 (cit. on p. 105).

[200] J. F. Faucon, M. D. Mitov, P. Méléard, I. Bivas, and P. Bothorel. „Bending elasticity and thermal fluctua-tions of lipid membranes. Theoretical and experimental requirements“. In: *Journal de Physique* 50.17 (1989) (cit. on p. 105).

[201] J. P. Reeves and R. M. Dowben. „Formation and properties of thin-waled phospholipid vesicles“. In: *J. Cell. Physio.* 73.1 (1969), pp. 49–60 (cit. on p. 105).

[202] K.-I. Akashi, H. Miyata, H. Itoh, and K. Kinosita. „Preparation of Giant Liposomes in Physiological Conditions and Their Characterization under an Optical Microscope“. In: *Biophysical Journal* 71 (1996), pp. 3242–3250 (cit. on p. 105).

[203] M. I. Angelova and D. S. Dimitrov. „Liposome Electroformation“. In: *Faraday Discuss. Chem. Soc.* 81 (1986), pp. 303–311 (cit. on p. 105).

[204] C. Herold, G. Chwastek, P. Schwille, and E. P. Petrov. „Efficient Electroformation of Supergiant Unilamellar Vesicles Containing Cationic Lipids on ITO-Coated Electrodes“. In: *Langmuir* 28 (2012), pp. 5518–5521 (cit. on p. 105).

[205] N. Puff and M. I. Angelova. „Chapter 7: Lipid Vesicles-Development and Applications for Studding Membrane Heterogeneity and Interactions“. In: *Advances in Planar Lipid Bilayers and Liposomes* 5.0 (2006), pp. 173–228 (cit. on p. 105).

[206] M. I. Angelova and D. S. Dimitrov. „Swelling of Charged Lipids and Formation of Liposomes on Electrode Surfaces“. In: *Molecular Crystals and Liquid Crystals Incorporating Nonlinear Optics* 152 (1987), pp. 89–104 (cit. on p. 105).

[207] D. S. Dimitrov and M. I. Angelova. „Lipid swelling and liposome formation on solid surfaces in external electric fields“. In: *New Trends in Colloid Science*. Darmstadt: Steinkopff, 1987, pp. 48–56 (cit. on p. 105).

[208] M. Angelova and D. S. Dimitrov. „A mechanism of liposome electroformation“. In: *Trends in Colloid and Interface Science II*. Darmstadt: Steinkopff, 1988, pp. 59–67 (cit. on p. 105).

[209] P. Sens and H. Isambert. „Undulation Instability of Lipid Membranes under an Electric Field“. In: *Physical Review Letters* 88.12 (2002), pp. 1–4 (cit. on p. 106).

[210] Valerio Pereno, Dario Carugo, L. Bau, et al. „Electroformation of Giant Unilamellar Vesicles on Stainless Steel Electrodes“. In: (2017) (cit. on p. 106).

[211] H.-L. Wu, P.-Y. Chen, C.-L. Chi, H.-K. Tsao, and Y.-J. Sheng. „Vesicle deposition on hydrophilic solid surfaces Soft Matter“. In: *Soft Matter* 9 (2012), pp. 1908–1919 (cit. on pp. 106, 107).

[212] L. K. Tamm and H. M. Mcconnell. „Supported Phospholipid Bilayers“. In: *Biophysical Journal* 47 (1985), pp. 105–113 (cit. on p. 107).

[213] E. Reimhult, M. Zäch, F. Höök, and B. Kasemo. „A Multitechnique Study of Liposome Adsorption on Au and Lipid Bilayer Formation on SiO2“. In: *Langmuir* 22 (2006), pp. 3313–3319 (cit. on p. 107).

[214] C. A. Keller and B. Kasemo. „Surface Specific Kinetics of Lipid Vesicle Adsorption Measured with a Quartz Crystal Microbalance“. In: *Biophysical Journal* 75 (1998), pp. 1397–1402 (cit. on pp. 107, 115).

[215] J.-W. Park and G. U. Lee. „Properties of Mixed Lipid Monolayers Assembled on Hydrophobic Surfaces through Vesicle Adsorption“. In: *Langmuir* 22 (2006), pp. 5057–5063 (cit. on pp. 107, 122).

[216] F. Giess, M. G. Friedrich, J. Heberle, R. L. Naumann, and W. Knoll. „The Protein-Tethered Lipid Bilayer: A Novel Mimic of the Biological Membrane“. In: *Biophysical Journal* 87 (2004), pp. 3213–3220 (cit. on p. 107).

[217] J. P. Overington, B. Al-Lazikani, and A. L. Hopkins. „How many drug targets are there?“ In: *Nature Reviews Drug Discovery* 5.12 (2006), pp. 993–996 (cit. on p. 107).

[218] M. Chadli, O. Maniti, C. Marquette, et al. „A new functional membrane protein microarray based on tethered phospholipid bilayers“. In: *Analyst* 143 (2018), p. 2165 (cit. on pp. 107, 108).

[219] Y. Fang, A. G. Frutos, and J. Lahiri. „G-Protein-Coupled Receptor Microarrays“. In: *ChemBioChem* 3.10 (2002), pp. 987–991 (cit. on p. 108).

[220] J. M. Berg, J. L. Tymoczko, and L. Stryer. *Biochemistry*. Freeman, W. H., 2002 (cit. on p. 108).

[221] D. J. Müller and A. Engel. „Atomic force microscopy and spectroscopy of native membrane proteins“. In: *Nature Protocols* 2.9 (2007), pp. 2191–2197 (cit. on p. 108).

[222] P. Mueller, D. O. Rudin, H. Ti Tien, and W. C. Westcott. „Reconstitution of Cell Membrane Structure in vitro and its Transformation into an Excitable System“. In: *Nature* 194 (1962), pp. 979–980 (cit. on p. 108).

[223] B. Wiltschi, W. Knoll, and E.-K. Sinner. „Binding assays with artificial tethered membranes using surface plasmon resonance“. In: *Methods* 39.2 (2006), pp. 134–146 (cit. on p. 108).

[224] T. Baumgart, M. Kreiter, H. Lauer, et al. „Fusion of small unilamellar vesicles onto laterally mixed self-assembled monolayers of thiolipopeptides“. In: *Journal of Colloid and Interface Science* 258.2 (2003), pp. 298–309 (cit. on p. 108).

[225] E.-K. Sinner, U. Reuning, F. N. Kök, et al. „Incorporation of integrins into artificial planar lipid membranes: characterization by plasmon-enhanced fluorescence spectroscopy“. In: *Analytical Biochemistry* 333.2 (2004), pp. 216–224 (cit. on p. 108).

[226] R. L. C. Naumann, C. Nowak, and W. Knoll. „Proteins in biomimetic membranes: promises and facts“. In: *Soft Matter* 7 (20 2011), pp. 9535–9548 (cit. on p. 109).

[227] L. Becucci, R. Guidelli, C. Peggion, . Toniolo, and M. R. Moncelli. „Incorporation of channel-forming peptides in a Hg-supported lipid bilayer“. In: *Journal of Electroanalytical Chemistry* 576.1 (2005), pp. 121–128 (cit. on p. 109).

[228] R. Robelek, E. S. Lemker, B. Wiltschi, et al. „Incorporation of In Vitro Synthesized GPCR into a Tethered Artificial Lipid Membrane System“. In: *Angewandte Chemie International Edition* 46 (2007), pp. 605–608 (cit. on p. 109).

[229] D. Beyer, G. Elender, W. Knoll, et al. „Influence of Anchor Lipids on the Homogeneity and Mobility of Lipid Bilayers on Thin Polymer Films“. In: *Angewandte Chemie International Edition in English* 35.15 (1996), pp. 1682–1685 (cit. on pp. 109, 122).

[230] M. L. Wagner and L. K. Tamm. „Tethered Polymer-Supported Planar Lipid Bilayers for Reconstitution of Integral Membrane Proteins: Silane-Polyethyleneglycol-Lipid as a Cushion and Covalent Linker“. In: *Biophysical Journal* 79.3 (2000), pp. 1400–1414 (cit. on pp. 109, 122).

[231] K. Sugihara, J. Vörös, and T. Zambelli. „A Gigaseal Obtained with a Self-Assembled Long-Lifetime Lipid Bilayer on a Single Polyelectrolyte Multilayer-Filled Nanopore“. In: *ACS Nano* 4.9 (2010), pp. 5047–5054 (cit. on p. 109).

[232] T. Cassier, A. Sinner, A. Offenhauser, and H. Mohwald. „Colloids and surfaces. B, Biointerfaces.“ In: *Colloids and Surfaces B: Biointerfaces*. Vol. 3-4. 15. Elsevier Science, 1999, pp. 215 –225 (cit. on p. 109).

[233] S. M. Schiller, R. Naumann, K. Lovejoy, H. Kunz, and W. Knoll. „Archaea Analogue Thiolipids for Tethered Bilayer Lipid Membranes on Ultrasmooth Gold Surfaces“. In: *Angewandte Chemie International Edition* 42.2 (2003), pp. 208–211 (cit. on p. 109).

[234] K. Sugihara, B. Jang, M. Schneider, J. Vörös, and T. Zambelli. „A universal method for planar lipid bilayer formation by freeze and thaw“. In: *Soft Matter* 8.20 (2012), p. 5525 (cit. on pp. 109, 122).

[235] B. P. Ziemba and J. J. Falke. „Lateral diffusion of peripheral membrane proteins on supported lipid bilayers is controlled by the additive frictional drags of (1) bound lipids and (2) protein domains penetrating into the bilayer hydrocarbon core“. In: *Chemistry and Physics of Lipids* 172-173 (2013), pp. 67–77 (cit. on p. 109).

[236] U. H. N. Dürr, U. S. Sudheendra, and A. Ramamoorthy. „LL-37, the only human member of the cathelicidin family of antimicrobial peptides“. In: *Biochimica et Biophysica Acta (BBA)* 1758 (2006), pp. 1408–1425 (cit. on p. 109).

[237] C. Leung, N. V. Dudkina, N. Lukoyanova, et al. „Stepwise visualization of membrane pore formation by suilysin, a bacterial cholesterol-dependent cytolysin“. In: *eLife* 3 (2014), pp. 1–17 (cit. on p. 110).

[238] S. R. Swift and L. Trinkle-Mulcahy. „Basic principles of FRAP , FLIM and FRET“. In: *Proceedings of the Royal Microscopical Society* (2004) (cit. on p. 110).

[239] C. De Los Santos, C.-W. Chang, M.-A. Mycek, and R. A. Cardullo. „FRAP, FLIM, and FRET: Detection and analysis of cellular dynamics on a molecular scale using fluorescence microscopy.“ In: *Molecular reproduction and development* 82.7-8 (2015), pp. 587–604 (cit. on p. 110).

[240] D. M. Soumpasis. „Theoretical Analysis of Fluorescence Photobleaching Recovery Experiments“. In: () (cit. on p. 111).

[241] B. L. Sprague and J. G. McNally. „FRAP analysis of binding: proper and fitting“. In: *Trends in Cell Biology* 15.2 (2005), pp. 84–91 (cit. on p. 112).

[242] C. Hamai, P. S. Cremer, and S. M. Musser. „Single Giant Vesicle Rupture Events Reveal Multiple Mechanisms of Glass-Supported Bilayer Formation“. In: *Biophysical Journal* 92.6 (2007), pp. 1988–1999 (cit. on p. 118).

[243] R. Macháň and M. Hof. „Lipid diffusion in planar membranes investigated by fluorescence correlation spectroscopy“. In: *Biochimica et Biophysica Acta (BBA) - Biomembranes* 1798.7 (2010), pp. 1377–1391 (cit. on p. 122).

[244] S. Chiantia, J. Ries, N. Kahya, and P. Schwille. „Combined AFM and Two-Focus SFCS Study of Raft-Exhibiting Model Membranes“. In: *ChemPhysChem* 7.11 (2006), pp. 2409–2418 (cit. on p. 122).

[245] L. Renner, T. Osaki, S. Chiantia, et al. „Supported Lipid Bilayers on Spacious and pH-Responsive Polymer Cushions with Varied Hydrophilicity“. In: *Journal of Physical Chemistry B* 112 (2008), pp. 6373–6378 (cit. on p. 122).

# 5 Surface Immobilization of a Novel Antimicrobial Protein using SAMs: a Multi-Characterization Study

> *The more we look at drug resistance, the more concerned we are. It basically shows us that the end of the road isn't very far away for antibiotics.*
>
> — **Tom Frieden**

## 5.1 Introduction

### 5.1.1 Antimicrobial Activity

Antibiotic resistance of bacteria has become a global health concern. According to the World Health Organization, "antibiotic resistance happens when bacteria change and become resistant to the antibiotic used to the infections they cause" [246]. New resistance mechanisms are emerging and consequently, a growing list of infections, such as pneumonia, tuberculosis, blood poisoning, gonorrhoea and foodborne diseases, are becoming harder, if not impossible, to treat while antibiotics are losing they effectiveness [247]. One of the reasons behind the acceleration of the loss of antibiotic efficacy is the misuse of existing drugs: more than 40 million antibiotic prescriptions during 2011 were unnecessary and, currently, the 60% and 30% of antibiotic prescriptions for adults and children, respectively, are not needed [246]. Another two relevant causes of this problem are the fact that no new major antibiotic has been developed in the last 30 years [248], and that there is an overuse of these drugs in livestock and fish farming, while it is known that resistant bacteria can be transmitted to humans via food intake [249].

Therefore, preventive measures are gaining more and more attention since these present cheaper, more efficient and practical ways to help solve the antibiotic crisis [250]. Nanotechnology provides a sound platform for adjusting the physicochemical properties of numerous materials [251], for example, for the development of antimicrobial materials for settings with high risk of bacterial contamination, e.g. in hospitals and food packaging, thus avoiding the much higher cost of post-infection treatment [252]. Bacterial colonization of medical devices, such as catheters, orthoprostheses and fracture fixation devices lead to infections that can result in serious disabilities, involving implant failure and implant removal, all leading to patient suffering, prolonged hospitalization and, in the worst case, even death [252].

Furthermore, infections occurring due to bacterial adhesion, growth and proliferation on indwelling or implanted devices in the form of biofilm formation are a big concern. This is the case for many medical devices such as urinary or venous

catheters, contact lenses and orthopedic stents, to mention some [253]. Therefore, the development of biomaterials with inherent properties, which are capable of not only preventing bacterial adhesion and colonization but also have the capability of killing microorganisms are of paramount importance [254]. For the development of these antimicrobial materials, it is necessary to prevent microbial adhesion onto surfaces and the subsequent formation of biofilms [255]. There have been many approaches explored to find solutions for biofilm prevention: antibiotics have been widely used to treat infections over the past decades, however, antibiotic resistance, as mentioned earlier, is a major clinical concern in the present [256]. For that reason, different approaches have been developed to create new antibacterial agents, such as polymers, quaternary ammonium salts, silver nanoparticles and titanium compounds [253, 257, 258]. These provide an effective treatment, but they come with some drawbacks: they possess side effects which include cytotoxicity, short-term bacterial protection and hypersensitivity [259].

### 5.1.2 Antimicrobial Surfaces

The approaches used to prepare antimicrobial surfaces can be classified into different types, namely (i) repelling surfaces, which include those that are self-polishing and those that are exempt of binding sites and (ii) killing surfaces, including surfaces which release biocides and contact killing surfaces [260]. These are illustrated in Figure 5.1.

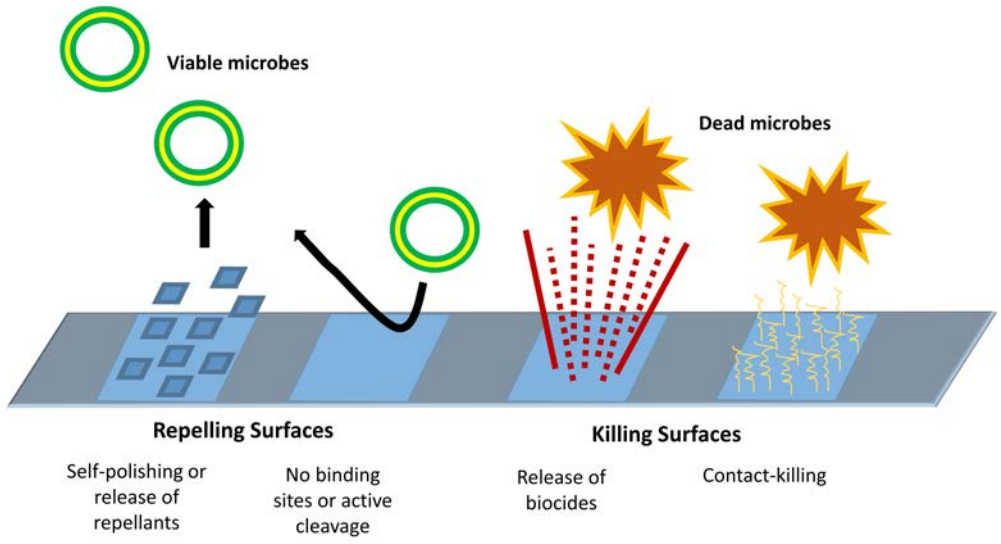


**Figure 5.1:** Illustration depicting the general classes of antimicrobial surfaces: repelling surfaces and killing surfaces. Modified and reproduced with permission from [260].

The latter two types (killing surfaces) are the most interesting ones and currently the contact-killing surfaces are in the spotlight due to their non-leaching nature, which biocide-releasing surfaces do not possess. The non-leaching nature prevents the contamination of the environment with the release of bioactive molecules. Generally, contact-killing surfaces have positive charges provided by quaternary

ammonium groups [261], which are believed to attract negative charges from the outer cell membranes of both Gram-positive and Gram-negative bacteria [262].

In the literature there are several successful studies reporting effective antimicrobial surfaces. For example, Shang et al. designed a nanostructured titanium surface with an antimicrobial peptide anchored that showed a powerful antimicrobial and biofilm resistance capability against two types of *Staphylococcus* [263]. Moreover, the immobilization of lactoferrin and lactoferricin on a glass surface [264] has been reported by Chen et al. Also, the antibacterial effect against *Staphylococcus epidermis* of Tet-24 peptides attached electrostatically on a polyethylenimine film has been reported [265]. In addition, the immobilization of antimicrobial peptides and proteins via click chemistry has showed satisfactory enzymolysis performances and an improved stability against several bacteria [266]. Liposomes loaded with an antibacterial drug and subsequently anchored to a solid surface by thiol groups have displayed resistance against some bacteria [267].

While the structure-activity relationship is the key factor for the development of a potent biofunctionalized surface, the simplicity of the fabrication is also an essential factor for real applications. An example of simplicity and broad applicability is the biocompatible surface of $Ti/TiO_2$ developed by Schilardi et al., which incorporated two different antimicrobial mechanisms that performed against Gram-positive bacteria and, additionally, was synthetized through a two-step process [268].

### 5.1.3 Antimicrobial Peptides and Proteins (AMPs)

Unfortunately, many of the reported antimicrobial surfaces can only act against certain types of bacteria and cannot effectively prevent all types of bacterial adhesion. This is where antimicrobial peptides and proteins (AMPs) become relevant, since they are natural products of the innate immune system and provide a unspecific defense against bacteria, fungi, virus, tumors, etc. [269]. They are promising candidates as antimicrobial agents on surface thanks to their broad spectrum of activity, low toxicity, high activity and long-term stability [270].

Lately, a large focus has been put on the development of AMPs since these offer an alternative to traditional antibiotics: they possess desirable properties including a broad spectrum of activity, high structural stability, low toxicity for mammalian cells and low susceptibility to bacterial resistance [253, 271, 272].

AMPs also play an important role in the innate and adaptive immune system, thus presenting an attractive alternative to conventional antibiotics since they don't evoke an immune response [254]. Hence, due to their unique structural and chemical properties they are promising for novel antimicrobial coatings for a large range of applications [253]. AMPs are found innately in our bodies, they can be found in most of the human body sites which are normally exposed to microbes, such as the skin, intestinal mucosa, oral mucosa, lungs, eyes and reproductive tract [273]. However, these can also be synthesized using recombinant technology [274].

These peptides and proteins have already been used for the creation of antimicrobial surfaces, such as the case of the AMP cecropin P1, which was immobilized onto a maleimide-terminated SAM and a mixed maleimide and hydroxyl-terminated

SAM. Although the orientation varied from one SAM to another, in both cases similar bactericidal activities were achieved [275].

### 5.1.4 Nickel(III)-chelated Nitriloacetic Acid (Ni-NTA) Strategy

Protein binding can be carried out through several types of interactions such as electrostatic, covalent and supramolecular interactions. The advantages of supramolecular interactions are that protein attachment, reversibility and orientation can be controlled thanks to the immobilization of the protein via specific binding sites [276].

An example of supramolecular interaction is the binding of nickel(II)-chelated nitrilotriacetic acid (Ni-NTA) with six-histidine-tagged proteins ($His_6$), a strategy that is widely used in metal affinity chromatography for purifying proteins labeled with a short histidine sequence [277]. A molecular dynamic simulation study of adsorption of a His-tagged peptide in water with different metallic surfaces showed a stronger affinity of the peptide to a Ni surface, while a weaker affinity on copper and gold surfaces [278]. In the same study, the adsorption energy of lysine (Lys), His and glycine (Gly) was tested and it was confirmed that the His amino acid is the one that contributes primarily to the peptide-metal binding interaction. Since $Ni^{2+}$ has a coordination number of six, the tetradentate NTA can occupy four coordination positions and, in this way, leave two positions available for tight but reverse attachment of imidazole groups of the His-tag of the protein [279] (see Figure 5.2). When His is in equilibrium the imidazole rings are located parallel to the substrate with the lowest adsorption energy in the metal surface [280].

Generally, most immobilization techniques that use chemically modified proteins may lead to the denaturalization and hence, loss of activity. These methods normally also lack control over the orientation of the protein after immobilization, due to the presence of multiple sites on the protein which can be modified [281]. Two well-known strategies presenting these disadvantages are the (i) biotin-streptavidin interaction, that permits the immobilization of biotin-labelled proteins, but in turn reduces their activity due to the chemical modification [282], and (ii) the use of the covalent attachment of lysine residues to carboxyl-terminated SAMs through an amide bond [283], because whilst it is very stable, it results in immobilized proteins with a range of different orientations depending on the location and number of lysine residues [284].

However, in the case of Ni-NTA, the small and flexible $His_6$-tag allows the function of the protein to be conserved and, whilst not requiring a modification of the protein, solely the addition of a short sequence of His, the orientation of the immobilization can be controlled because of the site specific binding [285–288]. Also, it provides (i) a very specific binding of the protein with a dissociation constant of $k_D = 10^{-13}$ [289–291], which is a sub pM constant, surpassing the affinity of most antibody-antigen and protein-biomolecule interactions, and (ii) a reverse binding of the protein, since the dissociation can be induced either by using ethylenediaminetetraacetic acid (EDTA), by which the chelate complex is released via the reprotonation of the His

with a low pH, or by using imidazole or His, which act as competitive agents of the His-tagged protein [281, 285, 292–303].

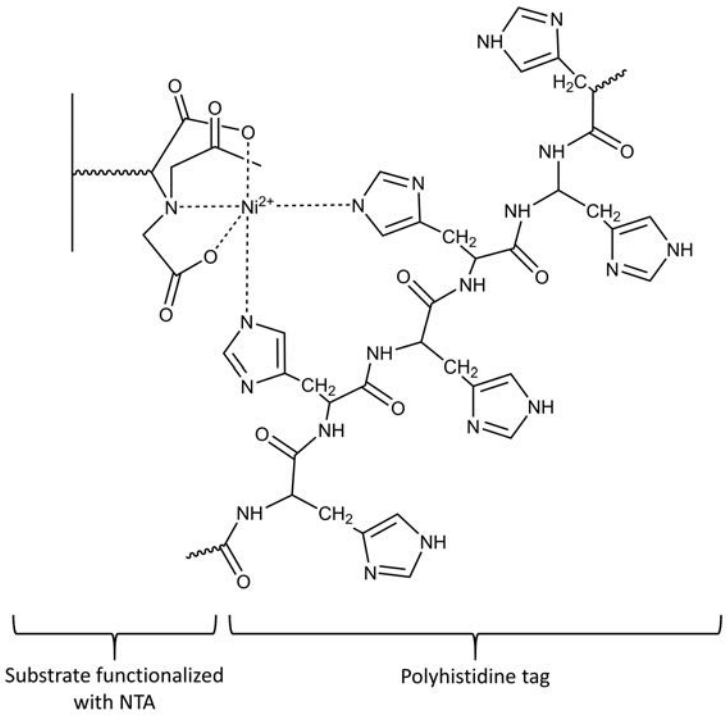


**Figure 5.2:** Representation of the interaction of two imidazole groups of the His-tag with the chelated Ni by the NTA group.

In view of the numerous advantages that this immobilization strategy provides, many research groups have already proposed some systems using it: the immobilization of His-tagged protein on SAMs introducing the one-point attachment idea was first published by the groups of Vogel and Whitesides in several publications [281, 300, 302, 303] using a mixture of alkanethiols to prepare the SAMs. Piehler and Tampe also studied the high affinity of multivalent chelator headgroups (MCH) made of two, three [301] and even four NTA moieties and they applied it to design switchable adaptors for His-tagged proteins [296] and to enable selective labeling of proteins, for example in cell lysates, by using different dyes conjugated to the NTA moieties [297].

### Spatial Control using Lithographic Techniques

This versatile strategy has also been employed to control the spatial arrangement of proteins on surfaces. Tampe et al. introduced a new development to the NTA-His tag approach by employing μCP to control the spatial distribution of the mixed thiol SAM [285, 304], and went as far as to fabricate a biochip of metal chelators by piezo dispensing bis-NTA thiol on a patterned SAM, aimed for the dissection of multiprotein complex formation [305]. So far, all the studies aforementioned that used the μCP technique, employed it to print surface tethered molecules. However, a method in which the $Ni^{2+}$ ions, instead of the SAM molecules, were the ones being stamped on a NTA SAM has been described, obtaining the immobilization

of His-tagged biomolecules at a micrometer and submicrometer scale. They also reached the same results by dip-pen nanolithography (DPN) [295].

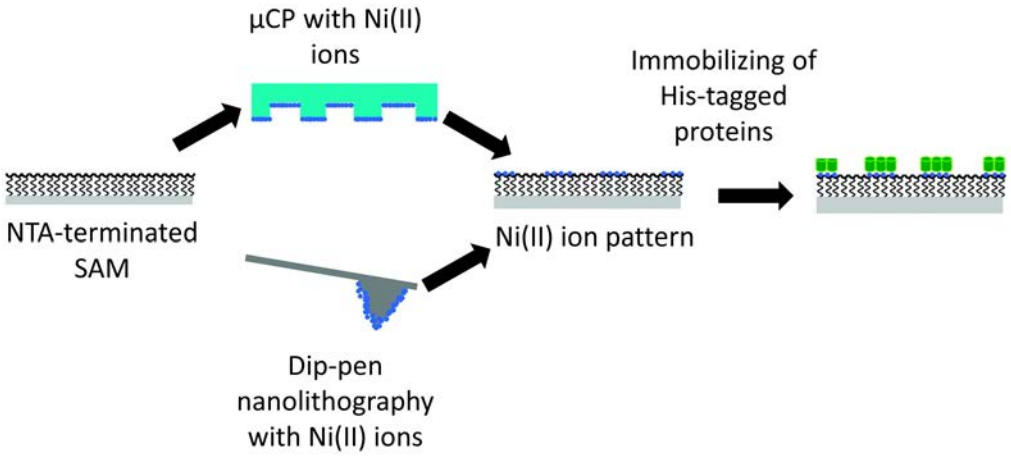


**Figure 5.3:** Strategy used for the fabrication of $Ni^{2+}$ patterns onto NTA-terminated SAM with μCP and dip-pen nanolithography (DPN) to immobilize His-tagged biomolecules. Reproduced with permission from [295].

Another approach which used nanolithography consisted in the preparation of patterned NTA SAMs using a poly(methyl methacrylate) (PMMA) resist patterned by nanoimprint lithography (NIL) as a template, followed by a NTA backfilling of the uncovered areas using a covalent multistep process [294]. An alternative way to form Ni-NTA SAMs, in which these are synthetized *in situ* on a pre-prepared homogeneous carboxyl terminated SAM has also been described [306]. Although it does not make use of μCP, with this method, denominated the "post NTA-modification", the amount of NTA conjugated is controllable and consequently the amount of His-tag protein being immobilized can be tuned.

Furthermore, the feasibility of the Ni-NTA SAMs strategy to bind His-tagged proteins has been demonstrated by a cell-based assay using neural stem cells (NSCs) [307]. In this study, a microarray that displayed recombinant epidermal growth factor (EGF) having a His-tag (EGF-His) was prepared and then the behavior of NSCs could be assessed since EGF is known to be a potent mitogen for the expansion of NSCs. Therefore, this study is also a proof-of-concept that His-tagged immobilized proteins still preserve their activity.

### 5.1.5 Antimicrobial Assays

In order to assess the antimicrobial properties of functionalized surfaces with antimicrobial peptides and proteins there has been different approaches reported in the literature.

In a study using antimicrobial surfaces different techniques were used to test for their antimicrobial activity. Bacterial cell viability, live-dead cell analysis with staining followed by observation with confocal, field emission electron scanning microscopy and, in addition, an enzymolysis test was performed [266]. In another

study [254], AMPs were grafted onto titanium surfaces and a bacterial killing assay was performed by measuring the fluorescence of propidium iodide (which intercalates into the DNA of dead cells) using a microtiter plate reader. Also reported [253] is the antimicrobial activity of peptides and proteins immobilized on substrates using silane SAMs, tested with a live-dead assay combined with the observation of propidium iodide with fluorescence microscopy. It has been reported also in another study [308] that antibacterial activity of functionalized substrates was assessed by observing substrates with phase contrast and also staining with fluorescein isothiocyanate (FITC) to detect cells with compromised cell membranes. Actually, the achievement of antimicrobial activity of surface tethered peptides and proteins requires the optimization of several parameters, such as the length of the spacer and the concentration of the accessible peptide on surface [259]. However, it has been reported in the same study that the immobilization does not influence the activity pattern at the biological level, so the membrane-permeabilizing effect is preserved.

## 5.2 Objectives and Strategy

To fight against antibiotic resistance, in this Chapter we report on the formation of an antimicrobial surface through the immobilization of a novel antimicrobial protein using a SAM on gold. Specifically we will use the interaction of the protein terminal His-tag with the Ni-NTA complex found at the surface of the SAM. With this aim, four specific objectives are proposed.[1]

- Design and production of a novel AMP by means of DNA recombinant technology in a soluble and an insoluble (inclusion body, IB) format.[2]
- Design and preparation of the pre-functionalized patterned and non-patterned SAMs Ni-NTA SAMs.
- Optimization of the μCP procedure to achieve spatial control of the distribution of the **SH-NTA** and **SH-PEG** molecules (Figure 5.4) in the patterned SAM formation. A His-tagged green fluorescent protein (GFP), enabling an easily visualized control in the same substrate. CV will be used for protein coverage evaluation.

[1] This work has been performed in collaboration with the Institute of Agrifood Research and Technology (IRTA).
[2] This work has been performed by Ramon Roca at the IRTA.

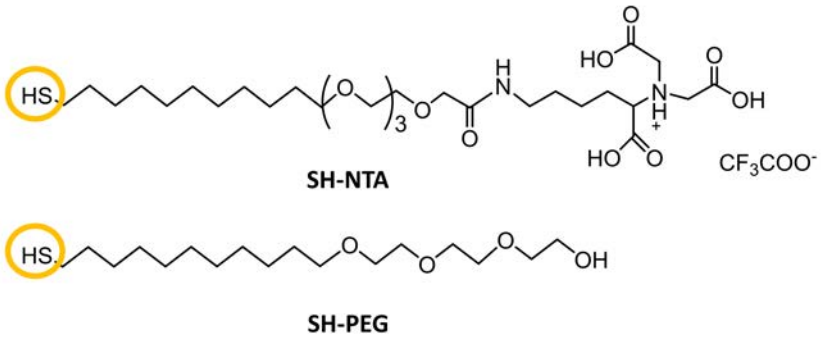


**Figure 5.4:** Molecular structure of the molecules used for NTA SAM formation. The NTA terminated thiol (**SH-NTA**) and (b) the commercial pegylated alkanethiol (**SH-PEG**).

- Immobilization of the novel antimicrobial protein in its soluble form and in IB form on gold coated substrates and characterization of these using a multi-technique approach in order to (i) verify the successful realization of each SAM formation step, (ii) the specific immobilization of the protein and (iii) compare the differences when immobilizing the soluble versus the IB form.[3]
- Performance of a biofilm assay to evaluate the actual antimicrobial effect of the surfaces modified with the novel antimicrobial protein in its soluble and IB form.

A schematic representation of the work flow is depicted in Figure 5.5.

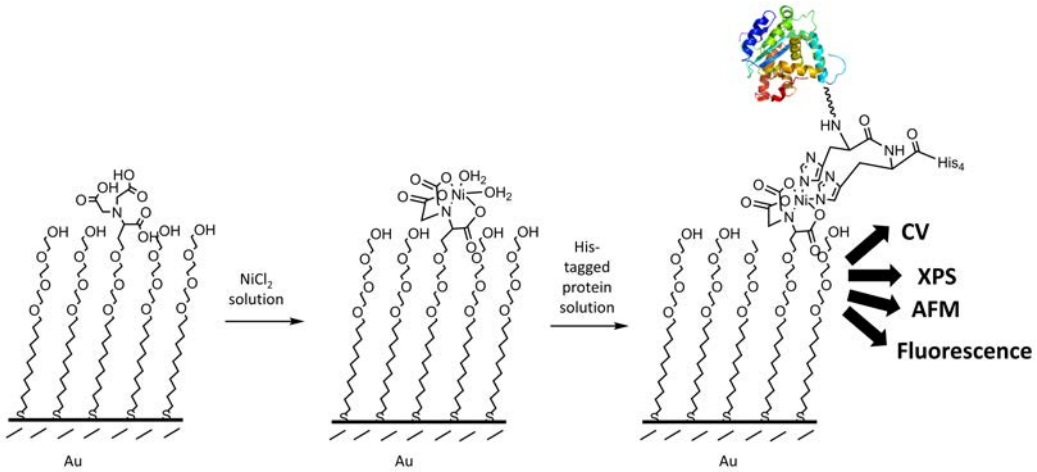


**Figure 5.5:** Sketch of the immobilization of His-tagged proteins using the Ni-NTA strategy: NTA SAM formation, immersion in a $NiCl_2$ solution, followed by the incubation with the His-tagged protein. Finally a multi-technique approach is used for its characterization.

[3]This has been performed with the help of Marta Martos, in the framework of her Bachelor thesis.

## 5.3 Optimization of His-tagged GFP Ni-NTA SAMs

GFP with a C-terminal His-tag was used to assess if the prepared Ni-NTA SAM would correctly immobilize His-tagged proteins, before proceeding to use the novel antimicrobial protein. GFP was chosen because, on one hand, it is a very studied protein, often used as a model protein to test new methods [293–295, 299, 306, 307, 309] with a well-known structure. On the other hand, it has fluorescence properties and, therefore, the visualization is very straightforward using fluorescence microscopy, without the need of additional immunostaining techniques. GFP is made of 238 amino acids residues [310] and, regarding its optical properties, it has two excitation peaks, the main one at 295 nm (long wave UV) and the smaller one at 475 nm (blue), and an emission peak at 509 nm (green) [311]. Hence, the use of GFP was ideal to test the correct spatial arrangement of the molecules by using the μCP technique. Briefly, a PDMS stamp inked with a **SH-PEG** ethanolic solution (1 mM) was put in contact with the clean gold surface, peeled off carefully and thereafter incubated with a **SH-NTA** ethanolic solution (1 mM) for subsequent backfilling of the non-patterned areas. Negative control samples were prepared by treatment with EDTA. EDTA acts as a competitive chelator for NTA, cleaving the chelated Ni from NTA to form a Ni-EDTA complex.

For the experimental details see Section 7.4.1.

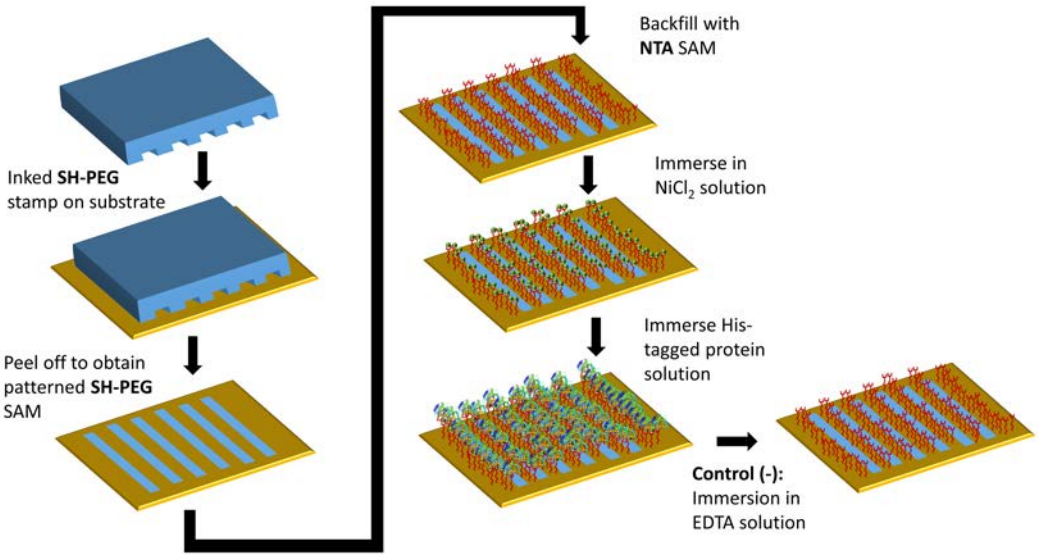


**Figure 5.6:** Schematic representation of the experimental procedure to prepare patterned Ni-NTA SAMs, using the μCP technique, for subsequent protein immobilization via their His-tag termination. Negative controls were prepared by immersing the substrates in a solution of EDTA (10 or 100 mM).

### 5.3.1 Characterization of His-tagged GFP Ni-NTA SAMs

#### Fluorescence Microscopy

The fluorescent striped pattern obtained from following the procedure depicted in Figure 5.6 can be observed very clearly, presenting a quite homogeneous coverage of the stripes, as seen in Figure 5.7. This demonstrates that the His-tagged GFP is

correctly immobilized on the Ni-NTA SAM. Therefore, these results show that we have successfully optimized the spatial control of the SAM formation via the μCP technique and that the His-tag shows a high affinity for the Ni-NTA complex.

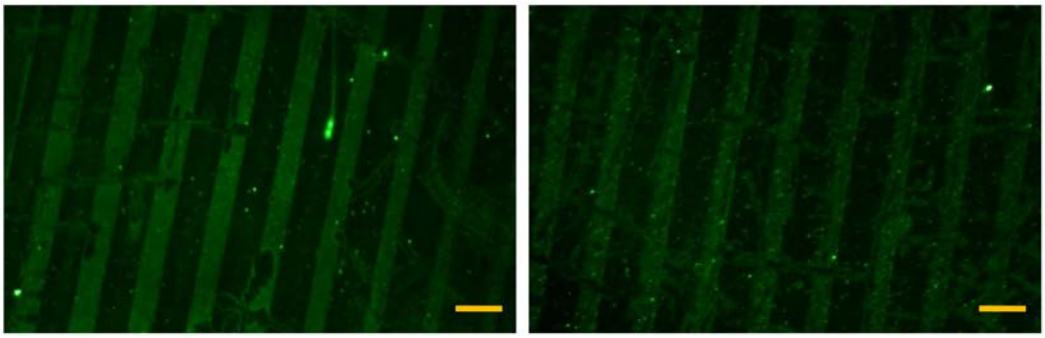

**Figure 5.7:** Fluorescence microscopy images of patterned His-tagged GFP using the Ni-NTA SAM strategy. Micropatterns observed were created using the μCP technique with a PDMS stamp with a pattern of 20 μm. Images acquired using a Scale bar correspond to 30 μm.

### Cyclic Voltammetry

CV was used to examine the barrier properties and integrity of the SAM modified surfaces. Since the Ni-NTA SAMs on gold substrates do not have redox groups, like in the previously studied case of HQ (Chapter 2), it was necessary to use a redox probe in order to study the electron transfer reactions between the redox probe and the gold surface. There are several redox probes that can be used, but it has been reported that hexaammineruthenium(III) chloride ($[Ru(NH_3)_6)]^{3+}$) can detect even the smallest defects in SAMs, which are invisible for other markers [40, 312] such as ferrocyanide. The greater sensitivity of $[Ru(NH_3)_6)]^{3+}$ probe can be explained by the location of its excess charge, located on the metal core in the ion center, whereas, for example, in the case of hexacyano metal complexes, it is located on the terminal nitrogen atoms of cyano ligands [313].

As a consequence, $[Ru(NH_3)_6)]^{3+}$ species can penetrate further into SAMs and diffuse along the SAM chains, in the presence or even absence of probable collapsed sites, and thus, even if the SAM is very compacted, current signal can still appear in the recorded voltammogram. Several studies have confirmed that the longer the molecule chains, the thicker the SAM and higher the blocking properties [313, 314], as shown in Figure 5.8.

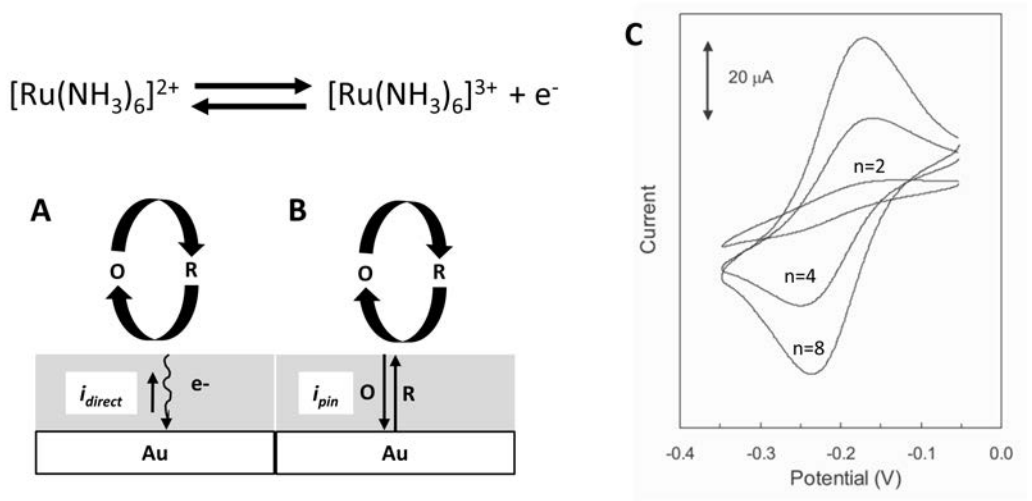


**Figure 5.8:** Schematic representation of the electron transfer between a gold surface and $[Ru(NH_3)_6)]^{3+/2+}$ in (A) a packed and well-ordered SAM (ideal conditions) and in (B) a SAM presenting defects. Reproduced and modified from [314]. (C) CV of SAMs (with varying number of methylene groups, n=2, 4, 8) on gold electrodes. The peak current decreases as the methylene number increases. Reproduced from [313].

When performing CV experiments with His-GFP functionalized substrates (for these experiments non-patterned surfaces were used) the current decreases when the NTA SAM is formed on the gold surface, and decreases even more when the His-GFP is immobilized (Figure 5.9). This indicates, as desired, that more molecules are covering the gold surface, and thus there is a higher blocking effect which hinders electrons to travel from the redox probe to the gold surface and vice versa. The presence of GFP on surface hinders even more the access of electrons to the gold surface, not only because they imply a larger separation distance between the gold and $[Ru(NH_3)_6)]^{3+}$, acting like a new layer of impedance for the electrons to overcome, but because their bigger size and volume in comparison to the SAM molecules makes the electron transfer even harder. Therefore, a relevant decrease of both the oxidation and reduction peaks can be observed. In view of these results, we can conclude qualitatively that a seemingly densely packed NTA SAM has been assembled and that the His-GFP is correctly immobilized.

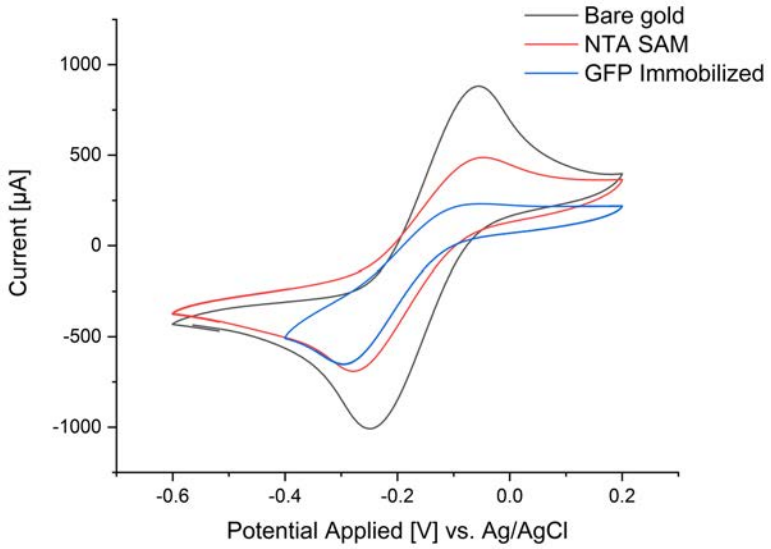


**Figure 5.9:** Cyclic voltammograms of bare gold, NTA-terminated SAM and immobilized GFP on NTA-terminated SAM. The electrolyte used was aqueous KCl solution (50 mM) with the redox probe $[Ru(NH_3)_6)]^{3+/2+}$ (5 mM). Scan rate used was 0.1 V/s.

## 5.4 Preparation of Antimicrobial Protein Surfaces

### 5.4.1 Antimicrobial Protein Preparation[4]

The novel antimicrobial protein is a recombinant construct produced by bacteria containing the recombinant plasmid that in turn carries the designed protein gene. More specifically, for the synthesis of these proteins, genetic constructs were designed to code for the protein of interest adding also an expression vector (i.e. plasmid), which allows the production of the protein in *Esterichia choli* in presence of an inductor in the cell medium (Isopropyl $\beta$-D-1-thiogalactopyranoside, IPTG , an analogue of lactose). Bacteria is hence used as a cellular factory for the production of proteins, which are afterwards purified by affinity chromatography.

These proteins are relevant since the combination of different active domains give place to modular constructs which are novel, since these are synthetic and there are no bacteria that have developed resistance towards these, at least not yet. Furthermore, the design of the protein has been thought and optimized to grant an optimum antimicrobial effect, with a wide spectra to ensure a killing effect towards different types of bacteria. The modular expression allows also the formation of larger proteins composed of smaller peptides which are hard to express but have a valuable function.

The designed protein contains three active domains: the first one (D1) is an antimicrobial peptide sequence that at the same time is a host defense peptide; it has a role in the innate immune response and is found naturally in all organisms.

[4]The construct was designed and synthesized Ramon Roca at the Department of Ruminant Production at IRTA.

It provides antimicrobial activity against both Gram negative and Gram positive bacteria by disrupting their cell membrane. The second one (D2) is an enzymatic domain from the sPLA2 family, which also helps breaking both Gram negative and Gram positive bacteria by degrading fatty acids present in their cell wall. The third one (D3) consist of a binding domain that interacts with a component of the cell wall and that allows the attachment of the antimicrobial protein to the bacterial cell wall. The protein is obtained in two forms (Figure 5.10), soluble and insoluble (in the form of IB), depending on the presence or not of two additional small aggregation-seeding domains (AD1 and AD2).[5] Both forms of the protein present the $His_6$-tag at the C-terminus which on one side allows protein purification by affinity chromatography, and, on the other side, enables its immobilization on surface via the His-tag-Ni-NTA interaction.

[5]Names are not revealed since this work has not been published.

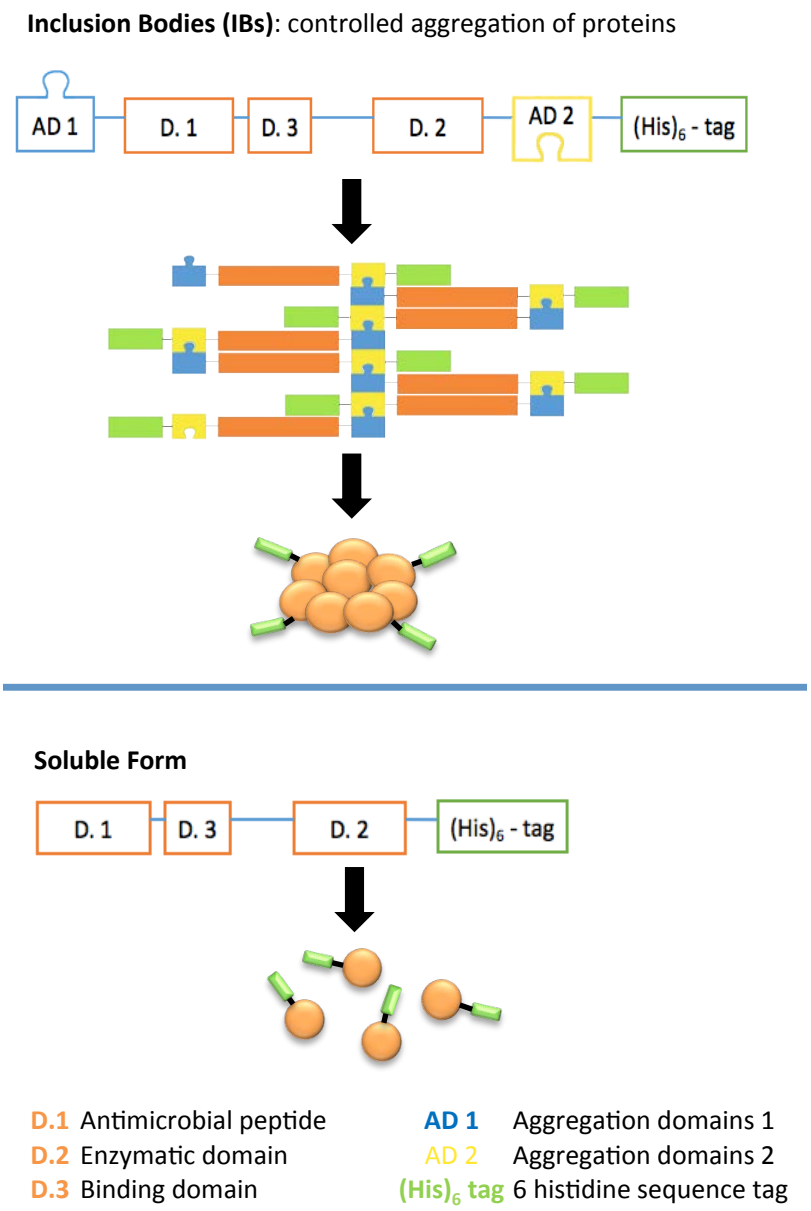


**Figure 5.10:** Schematic representation of the antimicrobial protein construct for the IB and the soluble form.

It is interesting to study both soluble and IB forms of the protein since aggregated antimicrobial peptides and proteins can present not only membrane perturbations, but also bactericidal intracellular activity. This intracellular mechanism is based on the internalization of the aggregated antimicrobial protein by bacteria, which disrupts the bacterial protein homeostasis [315] and this likely leads to the aggregation of toxic protein within the bacterial cell. It has been demonstrated that the internalization of these peptides and proteins can occur without severe disruption of the cell wall [316], which means that this bactericidal approach can take place independently of the effectiveness of the membrane perturbation activity.

### 5.4.2 Multi-Characterization Study of His-tagged Antimicrobial Protein Ni-NTA SAMs

In order to characterize the SAM formation and the subsequent antimicrobial protein immobilization a multi-technique approach was carried out, based on XPS, AFM, CV analysis and fluorescence microscopy. Furthermore, a biofilm assay was performed to obtain a first insight on the bactericidal effect of the biofunctionalized surfaces.

### 5.4.3 Fluorescence Microscopy

Patterned NTA SAMs were prepared as described previously (Section 5.3). However, since in this case proteins are depleted of a GFP, to able to see the pattern, immunostaining had to be performed using a primary and secondary antibody. The experimental details can be found in Section 7.4.2 and 7.4.2.

Following the procedure described in Figure 5.6 a homogeneous functionalization of the antimicrobial protein onto patterned Ni-NTA SAM was achieved, both with the soluble and IB form of the protein (Figure 5.11). The fluorescent stripes appear well delimited, and a uniform coverage of the protein is found along the pattern. The absence of fluorescent pattern in the negative controls, prepared by immersing the substrates in EDTA (10 mM), as shown in Figure 5.11 (C) and (D), indicate the reversibility of the union and, hence, the possibility of reusing the substrates. In other words, it demonstrates that Ni is kidnapped from the NTA and chelated by EDTA, inducing the removal of the His-tag and, therefore, of the protein from the surface. Moreover, the dark images obtained from the generic negative control (Figure 5.11 (E)) which consisted in the immunostaining of a patterned NTA SAM, is a proof that the immunostaining technique worked correctly and that the fluorescence is specific for the immunostained proteins.

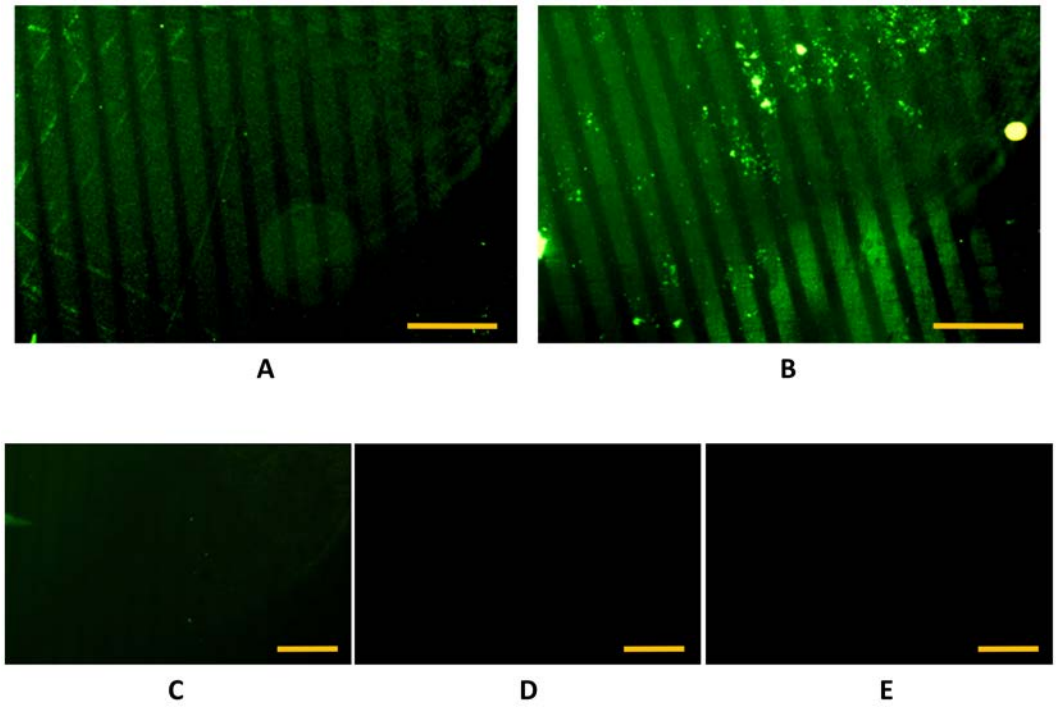


**Figure 5.11:** Fluorescence images of a 20 μm striped pattern of (A) His-tagged soluble antimicrobial protein and (B) His-tagged antimicrobial IBs immobilized on Ni-NTA SAMs prefunctionalized surfaces. The scale bar corresponds to 100 μm. Fluorescence images of the negative controls (by immersion in EDTA (10 mM)) of a 20 μm striped pattern of (C) His-tagged soluble antimicrobial protein and (D) His-tagged antimicrobial IBs. (E) A generic negative control of the immunostaining technique, which consisted in patterned NTA/PEG-SAM. The scale bars correspond to 100 μm.

In addition, the fluorescence intensity profiles displayed in Figure 5.12 (A), for the immobilized antimicrobial soluble protein, and in Figure 5.12 (B), for the immobilized antimicrobial IBs, show peaks with practically the same intensity in both cases, indicating a homogeneous coverage of the protein on the desired areas. A periodicity in the intensity peaks is observed: there is low or no fluorescence intensity between peaks, implying that there are no luminescent antibodies and therefore, no antimicrobial protein. Hence, the antimicrobial His-tagged protein is specifically attached only onto the Ni-NTA groups, and the PEG molecules form a protein repelling surface, as desired. These results also confirm that μCP allows a correct spatial control of the protein immobilization.

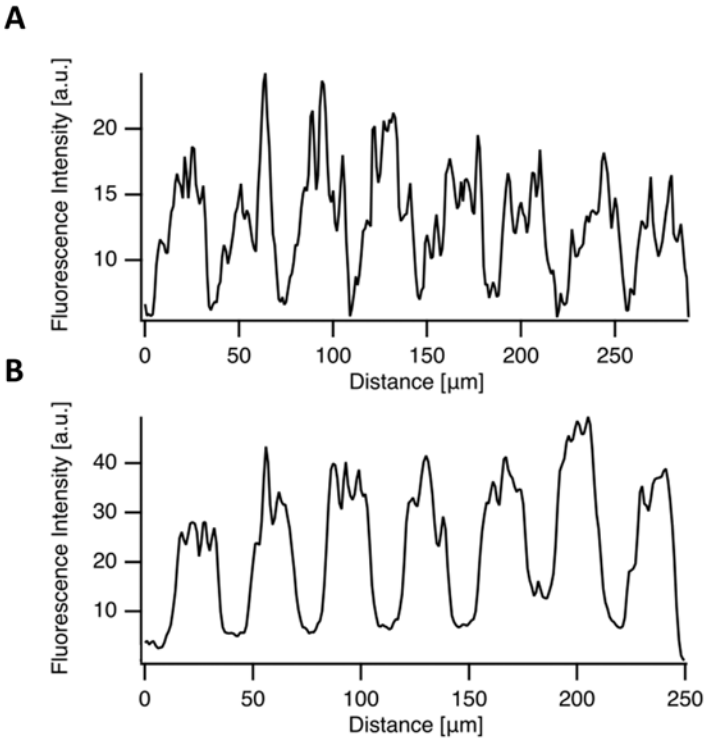


**Figure 5.12:** Fluorescence profiles extracted from fluorescence images of immobilized (A) soluble protein and (B) IB. Specifically, these profiles correspond to the images portrayed in Figure 5.11, (A) and (B).

### 5.4.4 Cyclic Voltammetry

As explained in Section 5.9, we have used CV to study the correct formation of the NTA SAM, with a model GFP-His molecule and in this Section, we go on to study the immobilization of the antimicrobial proteins.

When analyzing the results of the CV experiments, obtained when using SAM modified substrates as WE (Figure 5.13), a decrease in current is observed after NTA SAM formation, as expected. Protein immobilization decreases the current, but only slightly, for the oxidation peak. This means that this protein has a higher blocking effect on the electrons when these go from the redox probe $[Ru(NH_3)_6)]^{3+/2+}$ to the gold substrate ($[Ru(NH_3)_6)]^{2+} \rightarrow [Ru(NH_3)_6)]^{3+} + e^-$), in other words, the proteins on surface hinder more the access of electrons when they have to penetrate the SAM, than when they come from the gold substrate to reduce $[Ru(NH_3)_6)]^{3+}$, which is to say, when they are leaving the SAM.

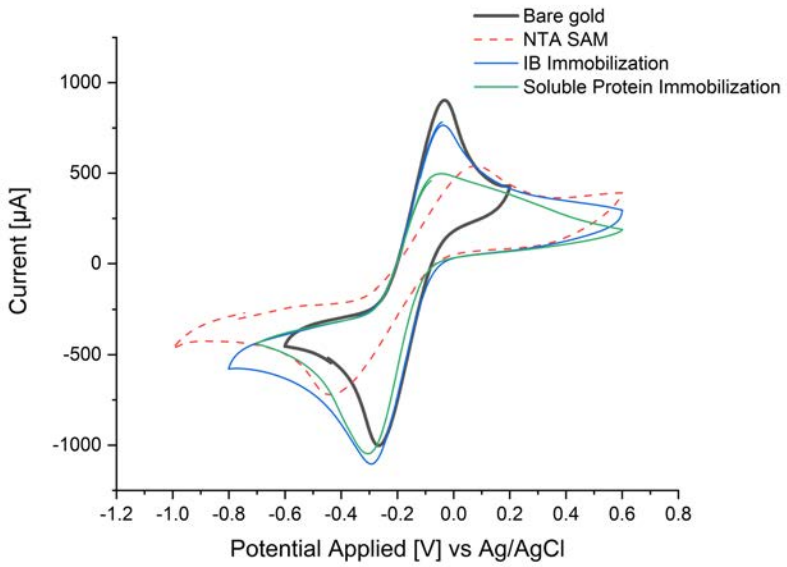


**Figure 5.13:** Cyclic voltammograms of bare gold, NTA-terminated SAM, immobilized antimicrobial protein on NTA SAMs, in soluble and IB form. The electrolyte used was aqueous KCl solution (50 mM) with the redox probe $[Ru(NH_3)_6)]^{3+/2+}$ (5 Mm). Scan rate used was 0.1 V/s.

Additionally, it is observed that the reduction of current is not as large as in the case of His-GFP (Figure 5.9). The reason may be that GFP is much smaller than the antimicrobial protein: GFP has 238 amino acids, while the novel antimicrobial protein has 487 amino acids, more than double. Therefore, the attachment of the GFP to Ni-NTA is easier and with a stochiometric relation of protein:**SH-NTA** more equal than in the case of the larger antimicrobial protein. Also, due to its size, steric hindrance may play a role, making it more difficult to occupy all the Ni-NTA units with a His-tag belonging to the protein. Hence, the coverage of the NTA SAM with the soluble antimicrobial protein, even if efficiently performed, as seen in Section 5.4.3, is not as homogeneous as with the smaller GFP: it presents more defects, including probably small holes.

Regarding the voltammogram obtained after immobilization of the IB an increase of current with respect to the NTA SAM was observed. From other characterization techniques we already know that IBs are successfully immobilized by Ni-NTA SAMs (Section 5.4.3), but the voltammogram did not show a clear decrease in current peaks, as we would have expected. The cause may reside in the structure of the IB, since they are formed by the aggregation of soluble proteins into an insoluble body. Therefore, the number of His-tags exposed on the outer face of the IBs is not predictable and controllable, and thus, it can be very low. Consequently, the percentage of immobilized IBs would be even lower than for immobilized soluble protein.

### 5.4.5 Atomic Force Microscopy

The 2 µm wide stripped pattern expected to be obtained after following the procedure described in Figure 5.6, for both soluble and IB form of the antimicrobial protein,

can be observed on both topographical (Figure 5.14 (A) and Figure 5.15 (A)) and phase shift images (Figure 5.14 (B) and Figure 5.15 (B)), confirming the correct functionalization of the surface by the protein.

Measurements were conducted in dry conditions. It is worth mentioning that these are biological samples, proteins immobilized, as mentioned earlier, are obtained by bacterial cells. As such, these samples are not always homogeneous, and therefore, big aggregates can be observed even though multiple rinsings were performed.

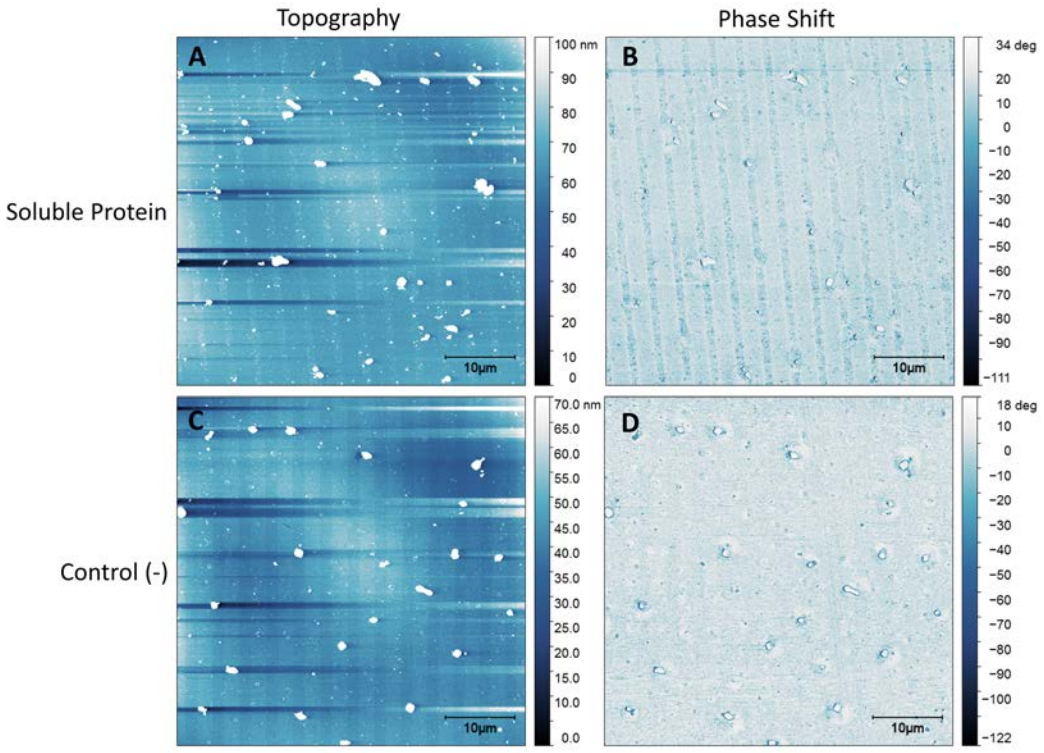


**Figure 5.14:** (A)(C) Topographical and (B)(D) phase shift AFM images of the 2 µm wide striped pattern of immobilized His-tagged antimicrobial soluble protein on a Ni-NTA SAM formed on a gold surface and (C)(D) their negative controls treated with EDTA (100 mM).

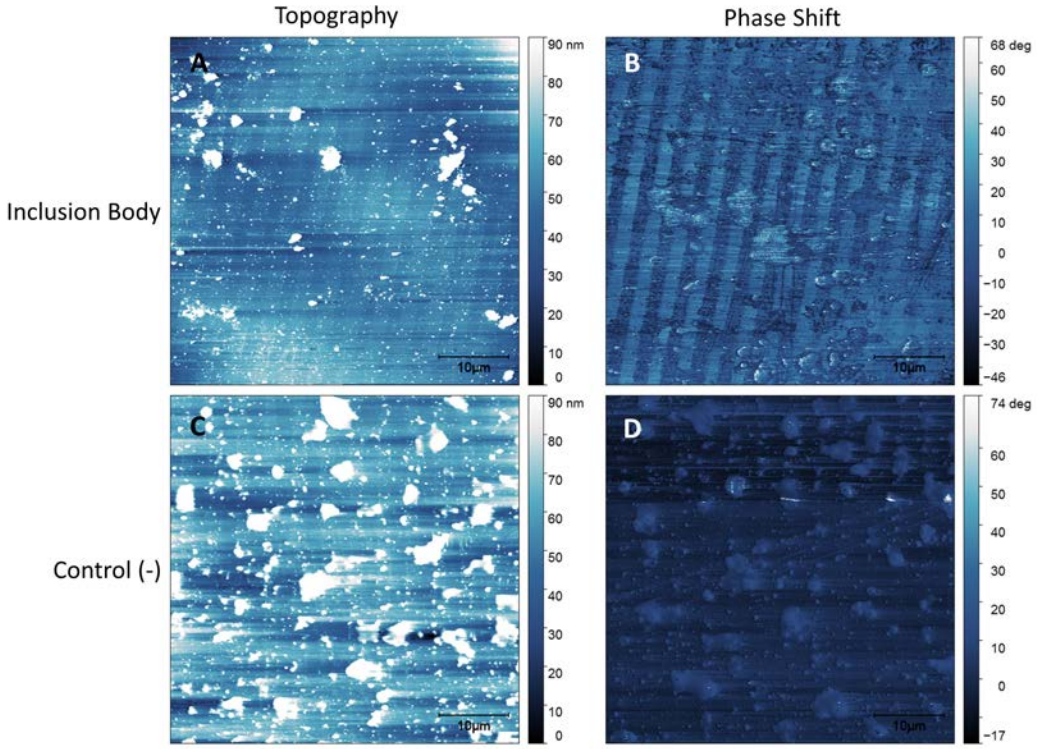


**Figure 5.15:** (A)(C) Topographical and (B)(D) phase shift AFM images of the 2 µm wide striped pattern of immobilized His-tagged antimicrobial IB on Ni-NTA SAM on gold and (C)(D) their negative controls treated with EDTA (100 mM).

When looking at topography, patterns with immobilized protein clearly display the expected pattern, as seen in Figure 5.14 A and Figure 5.15 A, as expected. Nonetheless, the pattern in the negative control samples can also be detected, as seen in Figure 5.14 C and Figure 5.15 C. This can be attributed to the fact that the negative control is basically a patterned SAM of **SH-NTA** and **SH-PEG** molecules, in which the NTA group is bigger than the alcohol group at the end of the pegylated alkanethiol. In addition, both thiol chains have three ethylene glycols ($EG_3$), but the **SH-NTA** has 11 aliphatic carbons while the PEG thiol has only 8. The **SH-NTA** is thus expected to surpass the height of the **SH-PEG** and, therefore, a topographic pattern is observed.

From the topographic profiles of each sample (Figure 5.16), obtained by drawing a perpendicular line to the stripes of each topographical image, we observed that the stripes of the soluble protein are better delimited than the ones of the IBs pattern, and in addition, the stripes of the IBs pattern are wider than the ones of the soluble protein pattern.

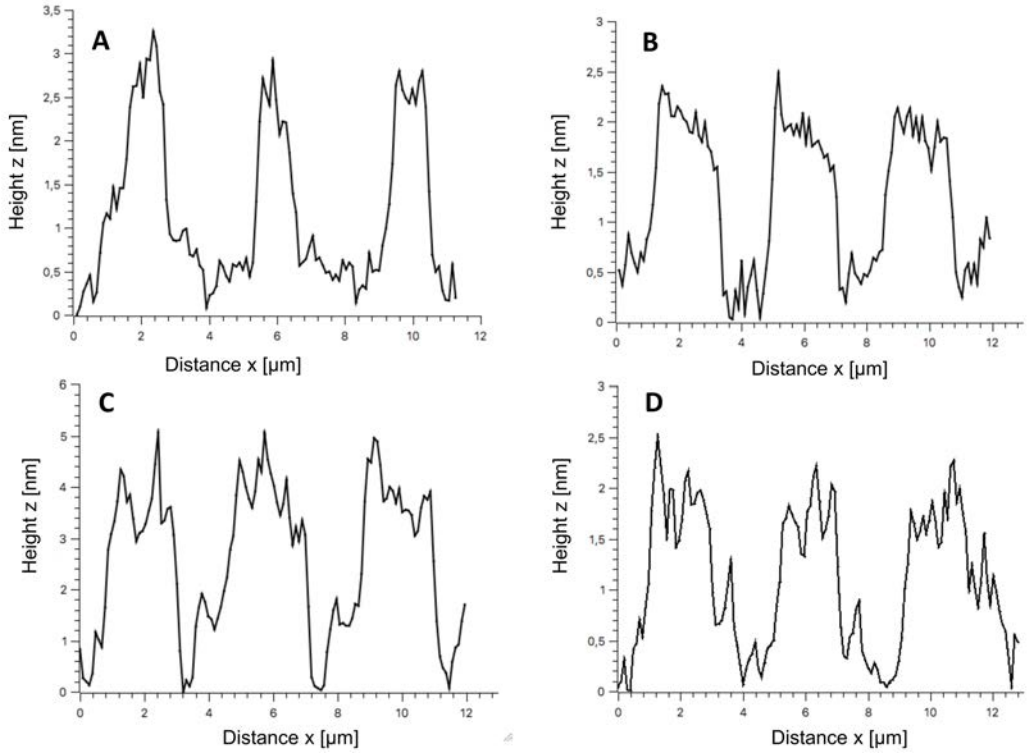


**Figure 5.16:** Topographic profiles of (A) immobilized soluble antimicrobial protein, (B) negative control ofimmobilized soluble antimicrobial protein, (C) immobilized antimicrobial IBs and (D) negative control of immobilized antimicrobial IBs.

For analysis purposes, the average measurements of the height and the width of three topography peaks displayed in Figure 5.16 for each sample is recorded in Table 5.1.

**Table 5.1:** Values corresponding to the average peak width= and height extracted from the AFM images.

| | Sample | | | |
|---|---|---|---|---|
| | **Soluble Protein** | **Control (-)** | **IB** | **Control (-)** |
| Mean peak width [µm] | 1.40 | 2.15 | 2.20 | 2.05 |
| Mean height [nm] | 2.56 | 1.64 | 4.08 | 1.74 |

The difference in height from the negative controls (Figure 5.16 C and D), which consist in a patterned NTA-PEG SAM, and the ones with bound protein (Figure 5.16 A and B), is in fact, the height of the immobilized antimicrobial protein. It is important to note that, measurements were conducted in dry conditions and thus the protein is dehydrated. By analyzing the results portrayed in Table 5.1, this height is around 1 nm for the soluble protein and around 2.3 nm for the IBs. We have to take into account the dry conditions of the experiment, because protein hydration is very important for their 3D structure, dynamics and activity [317]. Regarding the protein size, the aqueous media around the protein can affect $\sim$ 15 Å from the protein surface, as hydration layer [318]. In view of this implication, the removal of water from our substrates may have provoked the reduction of proteins size and

even the loss of their 3D structure. Therefore, the measured value of their height is not comparable with other tabulated protein sizes, because those reported normally are measured in aqueous conditions. Nonetheless, these measurements give an insight about the protein mass immobilized on the surface, since when comparing the height of the soluble protein and the IBs, the height of the IBs is greater than the one from soluble protein. IBs are composed of more amino acids than the soluble form, and also these are organized differently, hence, results obtained indicate the successful immobilization of both soluble and IB proteins. The width differences observed between peaks, may be due, again, to the nature of the IB, which forms aggregates, and if immobilized on the edge of the patterned NTA, can surpass in extension the pattern, resulting in wider peaks compared to those obtained with the soluble protein.

Phase imaging provides a map of stiffness variations on the sample surface: a stiffer region has a more positive phase shift than a less stiff region and, hence, appears brighter in a phase image [319]. In soft materials, the phase shift is highly dependent on the viscoelasticity of the material, aside from the stiffness [320]. The antimicrobial protein in both forms can be detected in the negative phase shift regions, appearing darker, because **SH-PEG** and **SH-NTA** form a compact SAM with intermolecular forces between the thiolated chains. Therefore, the areas functionalized with **SH-PEG** appear stiffer than the areas with immobilized protein, which are only attached to the SAM by the His-tag, and, therefore, are more likely to deform.

For negative controls, the pattern is not detected in the phase shift images, as seen in Figure 5.14 D (soluble protein) and Figure 5.15 D (IBs), because both **SH-NTA** and **SH-PEG** form together a compact SAM, where their aliphatic chains are interacting between each other. As a result, both types of thiols are subjected to practically the same interactions, forces, restrictions and the same degrees of freedom. Therefore, their stiffness and viscoelastic properties are likely to be very similar and, thus, the phase shift scan does not make a distinction between the two of them and no pattern can be appreciated.

### 5.4.6 X-Ray Photoelectron Spectroscopy

In order to get more chemical information about the proper binding of the proteins onto the Ni-NTA SAMs, XPS measurements were performed for 6 different samples: (A) immobilized antimicrobial soluble protein, (B) negative control of soluble protein (treatment with EDTA 10 mM), (C) immobilized antimicrobial IBs, (D) negative control of IBs (treatment with EDTA 100 mM), (E) Ni-NTA SAM, and (F) NTA SAM. Nitrogen, sulfur, nickel, oxygen and carbon were analyzed and deconvoluted. Information extracted from carbon and oxygen spectra is tricky, since carbon and oxygen species are abundant and not highly specific for our samples and thus, nitrogen, sulfur and nickel spectra provided more valuable information. For this reason, only those spectra with information are shown and commented.

Firstly, for the N 1s spectra (Figure 5.17), the peak at around 400-401 eV corresponds to the N-C bond found in the NTA, in amino acids, and also attributed

to 'pyrrole-like nitrogen'. Positive samples (A and C) present the His-tag, which in turn has imidazole groups that contain 'pyrrole-like' nitrogen (Figure 5.18), and the amino acid tryptophan, which also has 'pyrrole-like' nitrogen (binding energy corresponding to 401 eV), whereas negative controls do not have 'pyrrole-like' nitrogen. This could explain that both negative controls (B and D) have this peak slightly shifted to a higher binding energy, closer to 401 eV, with respect to the other samples.

The other peak, absent in sample B and appearing with lower intensity in D, is found at 402 eV. Energies of about 402-403.5 eV have been typically assigned to various oxidized nitrogen configurations, pyridine-N-oxide being the most frequently suggested one [321–323]. 'Pyridine-like' nitrogen (Figure 5.18) is present in the His-tag and, therefore, in the positive samples containing protein (A and C) in which the 402-403 eV peak appears. Also, energies of 401-402 eV are attributed to positively charged amines [324, 325], which are present in amino acids of proteins.

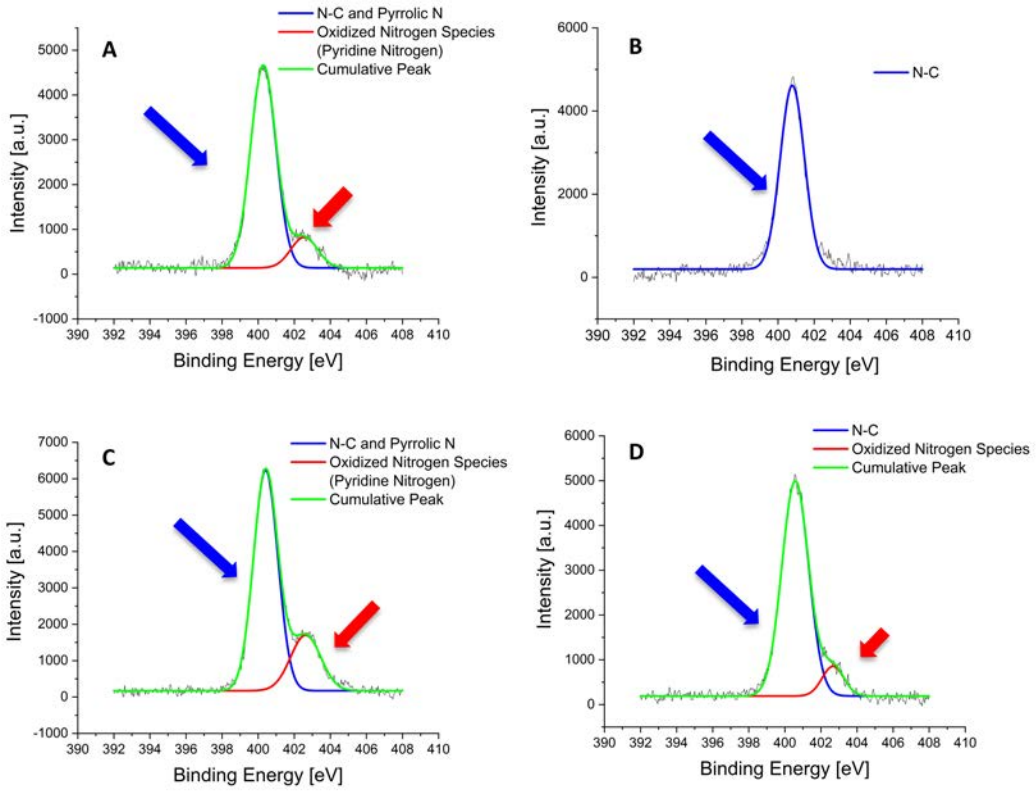


**Figure 5.17:** XPS deconvolutions of N 1s spectra for (A) immobilized antimicrobial soluble protein, (B) negative control of soluble protein (treatment with EDTA 10 mM), (C) immobilized antimicrobial IBs, and (D) negative control of IBs (treatment with EDTA 100 mM). Green aroow indicates the contribution of 'pyridine-like' nitrogen and red arrow of 'pyrrole-like' nitrogen.

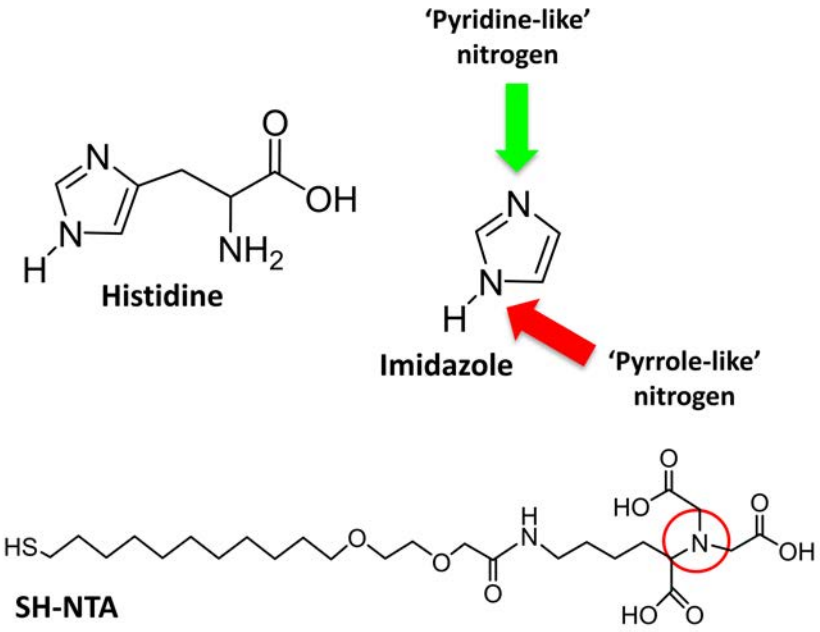


**Figure 5.18:** Representation of the different attributions to the nitrogen spectra: 'pyrrole-like' nitrogen, 'pyridine-like' and N-C.

For the analysis of sulfur (Figure 5.19), the S 2p spectra presented four peaks. From the analysis of the deconvoluted peaks, the peak at 161.9 eV and the peak at around 162.8-163.4 eV are attributed to the split of the orbital 2p into the doublet $2p_{3/2}$ and $2p_{1/2}$, respectively. These peaks come from the thiol bond (S-Au) of the thiolated NTA chains to the gold surface, which is present in all samples.

On the other hand, there are two more peaks, one at around 168.5 eV and the other at 169.7-171.8 eV, both correspond to oxidized sulfur species, which can come from the thiol groups in the alkanethiols or from cysteine amino acids present in the antimicrobial proteins. For this reason, these peaks appear in protein sample A. Since the negative control does not have protein immobilized (B), these peaks are less intense in its spectrum.

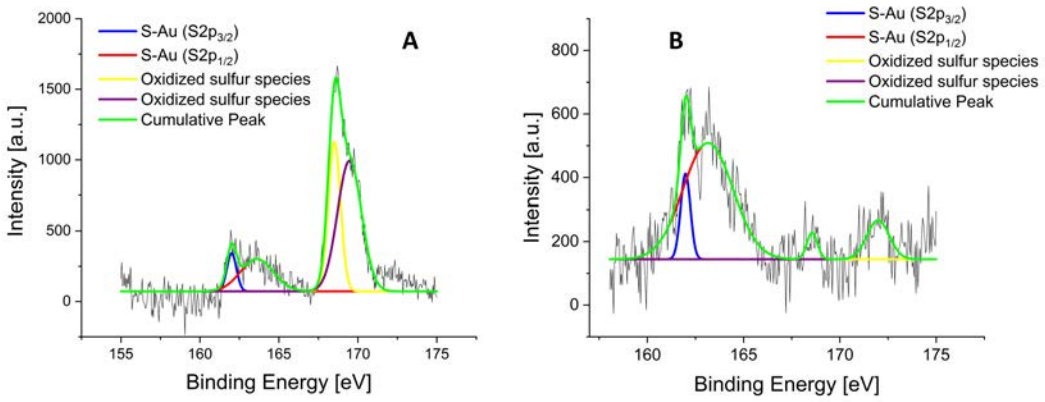


**Figure 5.19:** XPS deconvolutions of S 2p spectra for (A) immobilized antimicrobial soluble protein and (B) negative control of soluble protein (treatment with EDTA 10 mM).

The Ni 2p spectra from Figure 5.20 showed a lot of noise, which made peak detection difficult. This may be due to the low Ni concentration and high background in these regions, as reported previously by Schartner et al. [326] and Kang E. et al. [309]; where they could not detect any characteristic Ni signal when Ni was chelated.

From the analysis of the deconvoluted peaks, the peak at around 856 eV and the peak at around 873 eV correspond to the split of the orbital 2p into the doublet $2p_{3/2}$ and $2p_{1/2}$, respectively. In addition to these peaks, there is another peak wich appears at 862 eV, interpreted as the satellite peak of the main peak, which is to say, the $2p_{3/2}$ satellite peak. The presence of these peaks is assigned to oxidized Ni, confirming the success of metal ion chelation [292, 293].

However, in the negative control (sample D), the two main peaks, $2p_{1/2}$ and $2p_{3/2}$ also appear. This indicates the presence of a small amount of undesired and unspecifically adsorbed Ni on the surface, which is in agreement with the results obtained by O. Du Roure et al. [327]. In accordance to their reported results, after sample treatment with high concentrations of EDTA (100 mM) or imidazole (200 mM) Ni peaks were still detected. Since this technique does not study the displacement of the anchored protein with EDTA treatment but it studies only the effect of this competitive chelator on the surface concentration of Ni, the study concluded that the complex between the His-tagged protein and the Ni is more fragile than the complex between Ni and the NTA group [327]. Hence, the presence of Ni 2p peaks in the negative control of the protein (D) come from the incomplete removal of the $Ni^{2+}$ ions from the surface.

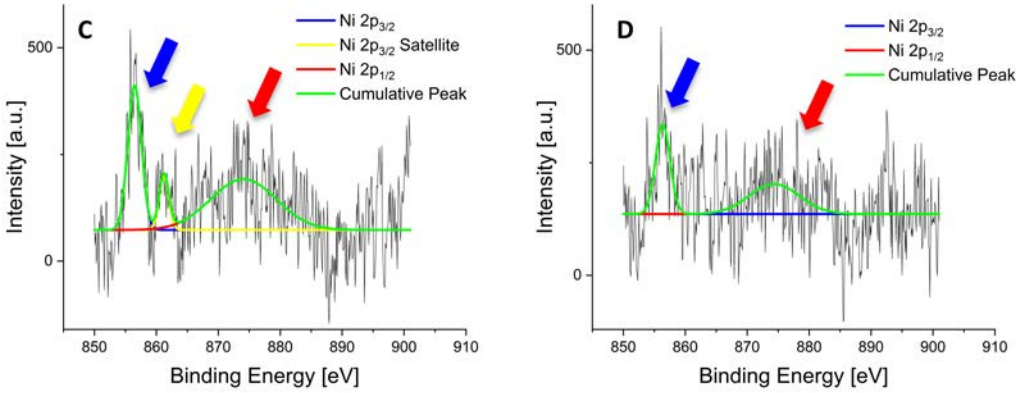


**Figure 5.20:** XPS deconvolutions of Ni 2p spectra for (C) immobilized antimicrobial IBs and (D) negative control of IBs (treatment with EDTA 100 mM).

In the O 1s spectra (Figure 5.21) samples present two common peaks. The peak at around 532 eV corresponds to the C-O bond and the one at around 532.7-532.9 eV corresponds to the C=O bond. Besides, except for the negative control B, the other samples also show a peak at around 537 eV. From literature, the latter peak is attributed to either adsorbed water [328], acetate species [329] or oxygen species interacting with Ni [330]. Therefore, it can be associated to the presence of –COOH groups in the amino acids or it can be associated to the interaction of oxygen and

Ni in the chelating complexes. Either way, both cases demonstrate the presence of His-tag and soluble protein/IBs, as there is no peak in the negative control of the soluble protein (B). The peak present in the negative control of IBs (D), can be attributed to undesired oxidation due to their aging (the sample was analyzed three days after preparation). The ratio difference between the C–O and C=O peaks in samples A and C may be due to the differences between the soluble protein and IBs.

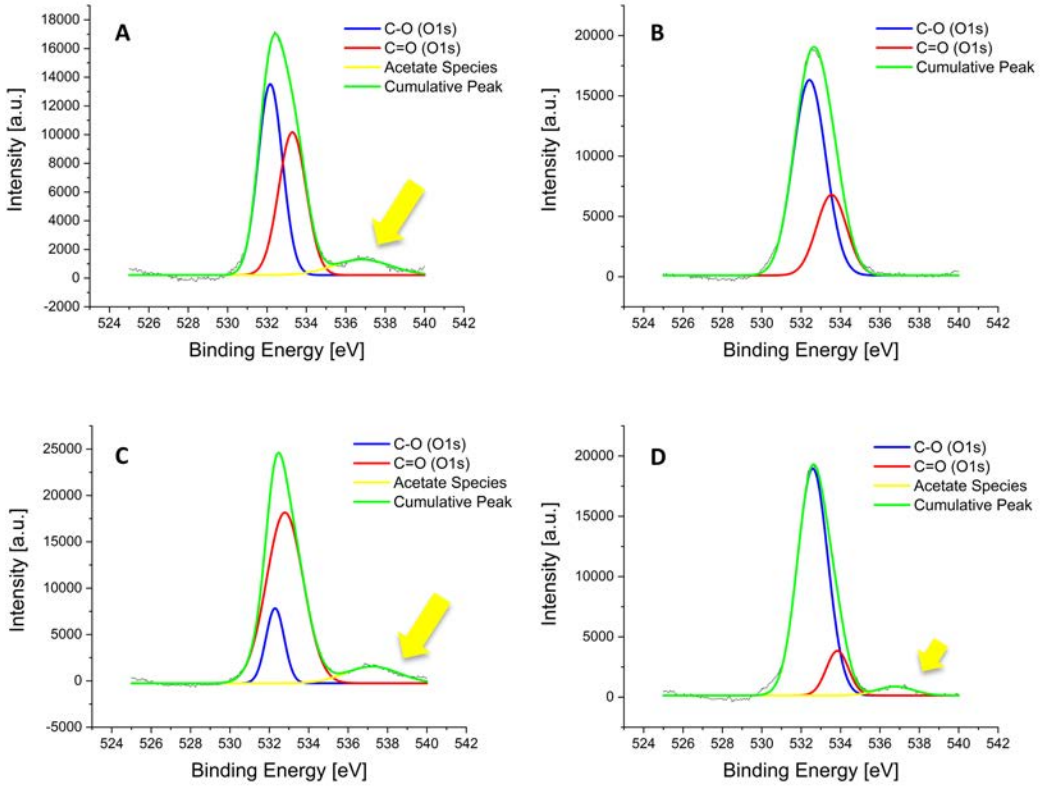


**Figure 5.21:** XPS deconvolutions of O 1s spectra for (A) immobilized antimicrobial soluble protein, (B) negative control of soluble protein (treatment with EDTA 10 mM), (C) immobilized antimicrobial IBs and (D) negative control of IBs (treatment with EDTA 100 mM).

Due to contamination sources of carbon, this spectra did not provide useful information and is therefore not displayed.

### 5.4.7 Antimicrobial Assay

In order to evaluate the antimicrobial properties of biofunctionalized surfaces an antimicrobial assay was carried out. Concretely, the capacity of inhibiting biofilm formation was studied. Following and adapting a protocol involving staining with crystal violet [331, 332] the assay consisted in preparing protein decorated surfaces and exposing them to a *Escherichia coli* DH5$\alpha$ culture overnight. These were then rinsed and cells were stained with crystal violet. Cells were detached using acetic acid and the quantity of cells was determined using a microplate reader to measure absorbance at 595 nm. Experimental details can be found in Section 7.4.7. For the assay, samples were incubated with two different concentrations of soluble protein, 20 μM and 0.5 μM. Also, control samples were prepared: a positive control consisting

of the cell medium with cells and a negative control consisting of only the medium. In addition, a SAM control consisted in a Ni-NTA SAM, without immobilization of protein. Results obtained from are show in Figure 5.22.

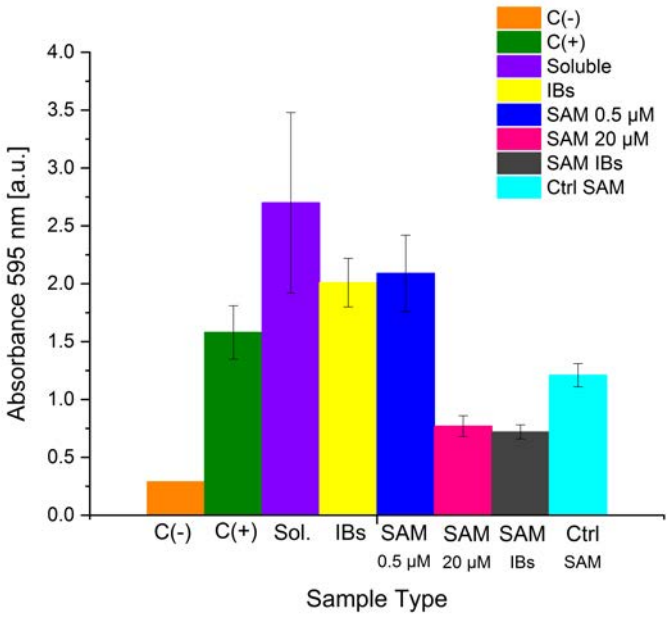


**Figure 5.22:** Graph displaying the absorbance results obtained from the biofilm formation assay. Error bars show the standard error of the mean (SEM). Absorbance results for samples consisting in: the negative control (C(–)), the positive control (C(+)), soluble protein in solution (Sol.), IBs in solution (IBs), sample with immobilized soluble protein with 0.5 mM solution (SAM 0.5 μM), sample with immobilized soluble protein with 20 μM solution (SAM 20 μM), sample with immobilized IBs (SAM IBs) and the control SAM, without any protein immobilized (Ctrl. SAM).

Figure 5.22 shows that when working in suspension (Sol. and IB) the use of protein aggregates (IBs) already enhance inhibit bacterial biofilm growth. Moreover, when anchoring both protein forms on surface by means of the selected Ni-NTA strategy with a flexible linker, the antimicrobial activity is enhanced even more. More specifically, a positive trend is observed as the concentration of the soluble protein is increased from 0.5 to 20 μM. Finally, it is worth mentioning, that a significant difference was obtained ($p < 0.05$) for SAM IBs and also for SAM 20 μM ($p < 0.1$) when performing a student t test, revealing a real enhancement of the biofilm growth inhibition of IBs anchored on surface.

Differences obtained between the positive control (C(+)) and soluble and IB in solution (Sol. and IBs) is normal due to manual manipulation of samples. Interestingly, the Ni-NTA SAM (Ctrl SAM) also showed a slight enhancement in preventing bacterial cell growth, however this was minor. This could be due to the presence of Ni, actually Ni nanoparticles are being investigated for their antimicrobial properties [333, 334].

In conclusion, as a first biological, results obtained are very promising, since both SAM 20 μM and SAM IBs showed biofilm formation prevention, not observed with the soluble protein and IB in solution. (IBs and Sol.).

## 5.5 Summary and Perspectives

Successful formation of a patterned NTA SAM on a gold surface using the μCP technique has been confirmed through a multi-technique surface characterization approach. A correct functionalization of the NTA SAM with a novel His-tagged antimicrobial protein, both in soluble and insoluble (IB) form and the spatial control of the attachment of the protein on the surface using μCP technique the His-Ni-NTA interaction is reported. The proper pattern formation was verified by fluorescence microscopy of the immunostained immobilized proteins, as well as by topographical and phase shift AFM analysis showing a homogeneous protein coverage in all cases. XPS measurement of N 1s, S 2p, Ni 2p and O 1s, followed by the spectra treatment, showed peaks, shifts and intensity relations that are in agreement with the expected results for each type of sample, demonstrating as well successful protein immobilization. The regeneration of the surface was performed by treatment with EDTA and verified via the aforementioned characterization techniques.

The antimicrobial protein attachment was also analyzed using CV and $[Ru(NH_3)_6)]^{3+}$ as a redox probe. The amount of antimicrobial IBs immobilized was found to be lower than for the soluble protein due to the nature of the IBs, as CV results have portrayed, since they are a partially aggregated proteins yielding less controllable orientations and, therefore, the His-tags exposed can be low. Finally, the biofilm assay confirmed the effectiveness of preventing biofilm formation against *E. coli* DH5$\alpha$ when immobilizing the soluble protein and the IBs, best results given by the latter.

In conclusion, a novel biofunctionalized surface with antimicrobial properties has been developed and characterized in response to the need of new antimicrobial agents to overcome the antibiotic crisis. Looking into the future and after further studies, this platform could be applied to coat surfaces of medical devices or could be incorporated into food packaging materials, among other applications.

# References


[40] P. Krysinski, M. R. Moncelli, and F. Tadini-Buoninsegni. „A voltammetric study of monolayers and bilayers self-assembled on metal electrodes“. In: *Electrochimica Acta* 45.12 (2000), pp. 1885–1892 (cit. on pp. 10, 11, 146).

[246] *antibiotic-resistance @ www.who.int* (cit. on p. 137).

[247] R. Laxminarayan, A. Duse, C. Wattal, et al. „Antibiotic resistance-the need for global solutions“. In: *The Lancet Infectious Diseases* 13.12 (2013), pp. 1057–1098 (cit. on p. 137).

[248] C. L. Ventola. „The antibiotic resistance crisis. Part 1: causes and threats“. In: *Pharmacy and Therapeutics* 40.4 (2015), pp. 277–83 (cit. on p. 137).

[249] Z. Golkar, O. Bagasra, and D. G. Pace. „Bacteriophage therapy: a potential solution for the antibiotic resistance crisis“. In: *Journal of infection in developing countries* 8.2 (2014), pp. 129–36 (cit. on p. 137).

[250] K. Blecher, A. Nasir, and A. Friedman. „The growing role of nanotechnology in combating infectious disease“. In: *Virulence* 2.5 (2011), pp. 395–401 (cit. on p. 137).

[251] N. Beyth, Y. Houri-Haddad, A. Domb, W. Khan, and R. Hazan. „Alternative Antimicrobial Approach: Nano-Antimicrobial Materials“. In: *Evidence-Based Complementary and Alternative Medicine* 2015 (2015), pp. 1–16 (cit. on p. 137).

[252] M. Rauytanapanit, A. Opitakorn, M. Terashima, R. Waditee-Sirisattha, and T. Praneenararat. „Antibacterial cotton fabrics based on hydrophilic amino-containing scaffolds“. In: *Colloids and Surfaces B: Biointerfaces* 164 (2018), pp. 42–49 (cit. on p. 137).

[253] Y. Li, S. Wei, J. Wu, et al. „Effects of Peptide Immobilization Sites on the Structure and Activity of Surface-Tethered Antimicrobial Peptides“. In: *The Journal of Physical Chemistry C* 119.13 (2015), pp. 7146–7155 (cit. on pp. 138, 139, 143).

[254] M. Gabriel, K. Nazmi, E. C. Veerman, A. V. N. Amerongen, and A. Zentner. „Preparation of LL-37-Grafted Titanium Surfaces with Bactericidal Activity“. In: *Bioconjugate Chemistry* 17 (2006), pp. 548–550 (cit. on pp. 138, 139, 142).

[255] I. Armentano, C. R. Arciola, E. Fortunati, et al. „The Interaction of Bacteria with Engineered Nanostructured Polymeric Materials: A Review“. In: *The Scientific World Journal* 2014 (2014), pp. 1–18 (cit. on p. 138).

[256] P. S. Stewart and J. William Costerton. „Antibiotic resistance of bacteria in biofilms“. In: *The Lancet* 358.9276 (2001), pp. 135–138 (cit. on p. 138).

[257] A. E. Mohammed. „Green synthesis, antimicrobial and cytotoxic effects of silver nanoparticles mediated by *Eucalyptus camaldulensis* leaf extract“. In: *Asian Pacific Journal of Tropical Biomedicine* 5.5 (2015), pp. 382–386 (cit. on p. 138).

[258] S. A. Onaizi and S. S. J. Leong. „Tethering antimicrobial peptides: Current status and potential challenges“. In: *Biotechnology Advances* 29.1 (2011), pp. 67–74 (cit. on p. 138).

[259] M. Bagheri, M. Beyermann, and M. Dathe. „Immobilization reduces the activity of surface-bound cationic antimicrobial peptides with no influence upon the activity spectrum.“ In: *Antimicrobial agents and chemotherapy* 53.3 (2009), pp. 1132–41 (cit. on pp. 138, 143).

[260] J. C. Tiller. „Antimicrobial Surfaces“. In: *Bioactive Surfaces. Advances in Polymer Science* 240 (2010), pp. 193–217 (cit. on p. 138).

[261] R. Kaur and S. Liu. „Antibacterial surface design - Contact kill“. In: *Progress in Surface Science* 91.3 (2016), pp. 136–153 (cit. on p. 139).

[262] P. A. Annis. *Understanding and Improving the Durability of Textiles*. Woodhead Publishing Limited, Elsevier, 2012, p. 296 (cit. on p. 139).

[263] C. Zhu, W. wei Zhang, S. yuan Fang, et al. „Antibiotic peptide-modified nanostructured titanium surface for enhancing bactericidal property“. In: *Journal of Materials Science* 53.8 (2018), pp. 5891–5908 (cit. on p. 139).

[264] R. Chen, N. Cole, D. Dutta, N. Kumar, and M. D. P. Willcox. „Antimicrobial activity of immobilized lactoferrin and lactoferricin“. In: *Journal of Biomedical Materials Research Part B: Applied Biomaterials* 105.8 (2017), pp. 2612–2617 (cit. on p. 139).

[265] J. Hernandez-Montelongo, Y. R. Corrales Ureña, D. Machado, et al. „Electrostatic immobilization of antimicrobial peptides on polyethylenimine and their antibacterial effect against *Staphylococcus epidermidis*“. In: *Colloids and Surfaces B: Biointerfaces* 164 (2018), pp. 370–378 (cit. on p. 139).

[266] J. He, J. Chen, G. Hu, et al. „Immobilization of an antimicrobial peptide on silicon surface with stable activity by click chemistry“. In: *Journal of Materials Chemistry B* 6.1 (2017), pp. 68–74 (cit. on pp. 139, 142).

[267] S. Mourtas, G. Diamanti, A. Foka, et al. „Inhibition of bacterial attachment on surfaces by immobilization of tobramycin-loaded liposomes“. In: *Journal of Biomedical Nanotechnology* 11.12 (2015), pp. 2186–2196 (cit. on p. 139).

[268] D. E. Pissinis, G. A. Benítez, and P. L. Schilardi. „Two-step biocompatible surface functionalization for two-pathway antimicrobial action against Gram-positive bacteria“. In: *Colloids and Surfaces B: Biointerfaces* 164 (2018), pp. 262–271 (cit. on p. 139).

[269] K. V. R. Reddy, R. D. Yedery, and C. Aranha. „Antimicrobial peptides: Premises and promises“. In: *International Journal of Antimicrobial Agents* 24.6 (2004), pp. 536–547 (cit. on p. 139).

[270] K. Lim, R. R. Y. Chua, R. Saravanan, et al. „Immobilization studies of an engineered arginine-tryptophan-rich peptide on a silicone surface with antimicrobial and antibiofilm activity“. In: *ACS Applied Materials and Interfaces* 5.13 (2013), pp. 6412–6422 (cit. on p. 139).

[271] R. E. W. Hancock and H.-G. Sahl. „Antimicrobial and host-defense peptides as new anti-infective therapeutic strategies“. In: *Nature Biotechnology* 24.12 (2006), pp. 1551–1557 (cit. on p. 139).

[272] H. Jenssen, P. Hamill, and R. E. W. Hancock. „Peptide antimicrobial agents.“ In: *Clinical microbiology reviews* 19.3 (2006), pp. 491–511 (cit. on p. 139).

[273] L.-j. Zhang and R. L. Gallo. „Antimicrobial peptides“. In: *Current Biology* 26.1 (2016), R14–R19 (cit. on p. 139).

[274] M. F. Mohamed, A. Abdelkhalek, and M. N. Seleem. „Evaluation of short synthetic antimicrobial peptides for treatment of drug-resistant and intracellular *Staphylococcus aureus*“. In: *Scientific Reports* 6 (2016), p. 29707 (cit. on p. 139).

[275] Q. Wang, S. Wei, J. Wu, et al. „Interfacial Behaviors of Antimicrobial Peptide Cecropin P1 Immobilized on Different Self-Assembled Monolayers“. In: *Journal of Physical Chemistry C* 119.39 (2015), pp. 22542–22551 (cit. on p. 140).

[276] D. A. Uhlenheuer. *Supramolecular control over protein assembly*. Tech. rep. 2011, pp. 1–145 (cit. on p. 140).

[277] A. Spriestersbach, J. Kubicek, F. Schäfer, H. Block, and B. Maertens. „Purification of His-Tagged Proteins“. In: 2015, pp. 1–15 (cit. on p. 140).

[278] C. Montemagno and G. Bachand. „Constructing nanomechanical devices powered by biomolecular motors“. In: *Nanotechnology* 10.3 (1999), pp. 225–231 (cit. on p. 140).

[279] A. Thess, S. Hutschenreiter, M. Hofmann, et al. „Specific Orientation and Two-dimensional Crystallization of the Proteasome at Metal-chelating Lipid Interfaces“. In: *Journal of Biological Chemistry* 277.39 (2002), pp. 36321–36328 (cit. on p. 140).

[280] Z. Yang and Y.-P. Zhao. „Adsorption of His-tagged peptide to Ni, Cu and Au (100) surfaces: Molecular dynamics simulation“. In: *Engineering Analysis with Boundary Elements* 31.5 (2007), pp. 402–409 (cit. on p. 140).

[281] G. B. Sigal, C. Bamdad, A. Barberis, J. Strominger, and G. M. Whitesides. „A Self-Assembled Monolayer for the Binding and Study of Histidine-Tagged Proteins by Surface Plasmon Resonance“. In: *Analytical and Bioanalytical Chemistry* 68 (1996), pp. 490–497 (cit. on pp. 140, 141).

[282] V. Verma, C. Kaur, P. Grover, A. Gupta, and V. K. Chaudhary. „Biotin-tagged proteins: Reagents for efficient ELISA-based serodiagnosis and phage display-based affinity selection“. In: *PLoS ONE* 13.1 (2018). Ed. by Heping Cao, e0191315 (cit. on p. 140).

[283] A. S. N. Murthy and J. Sharma. „Glucose oxidase bound to self-assembled monolayers of bis(4-pyridyl) disulfide at a gold electrode: Amperometric determination of glucose“. In: *Analytica Chimica Acta* 363.2-3 (1998), pp. 215–220 (cit. on p. 140).

[284] B. K. Raliski, C. A. Howard, and D. D. Young. „Site-Specific Protein Immobilization Using Unnatural Amino Acids“. In: *Bioconjugate Chemistry* 25.11 (2014), pp. 1916–1920 (cit. on p. 140).

[285] A. Tinazli, J. Tang, R. Valiokas, et al. „High-affinity chelator thiols for switchable and oriented immobilization of histidine-tagged proteins: A generic platform for protein chip technologies“. In: *Chemistry - A European Journal* 11.18 (2005), pp. 5249–5259 (cit. on pp. 140, 141).

[286] S. Hutschenreiter, A. Tinazli, K. Model, and R. Tampé. „Two-substrate association with the 20S proteasome at single-molecule level.“ In: *The EMBO journal* 23.13 (2004), pp. 2488–97 (cit. on p. 140).

[287] N.l Haddour, S. Cosnier, and C. Gondran. „Electrogeneration of a Poly(pyrrole)-NTA Chelator Film for a Reversible Oriented Immobilization of Histidine-Tagged Proteins“. In: *Journal of the American Chemical Society* 127.16 (2005), pp. 5752–5753 (cit. on p. 140).

[288] I. T. Dorn, K. Pawlitschko, S. C. Pettinger, and R. Tampé. „Orientation and Two-Dimensional Organization of Proteins at Chelator Lipid Interfaces“. In: *Biological Chemistry* 379.8-9 (1998) (cit. on p. 140).

[289] E. Hochuli, H. Döbeli, and A. Schacher. „New metal chelate adsorbent selective for proteins and peptides containing neighbouring histidine residues“. In: *Journal of Chromatography A* 411.C (1987), pp. 177–184 (cit. on p. 140).

[290] J. Schmitt, H. Hess, and H. G. Stunnenberg. „Affinity purification of histidine-tagged proteins“. In: *Molecular biology reports* 18.3 (1993), pp. 223–230 (cit. on p. 140).

[291] L. R. Paborsky, K. E. Dunn, C. S. Gibbs, and J. P. Dougherty. „A nickel chelate microtiter plate assay for six histidine-containing proteins“. In: *Analytical Biochemistry* 234.1 (1996), pp. 60–65 (cit. on p. 140).

[292] H. M. Chen, Wei C. Wang, and Sheng H. Chen. „A metal-chelating piezoelectric sensor chip for direct detection and oriented immobilization of polyhis-tagged proteins“. In: *Biotechnology Progress* 20.4 (2004), pp. 1237–1244 (cit. on pp. 140, 161).

[293] J. K. Lee, Y. G. Kim, Y. S. Chi, W. S. Yun, and I. S. Choi. „Grafting nitrilotriacetic groups onto carboxylic acid-terminated self-assembled monolayers on gold surfaces for immobilization of histidine-tagged proteins“. In: *Journal of Physical Chemistry B* 108.23 (2004), pp. 7665–7673 (cit. on pp. 140, 145, 161).

[294] P. Maury, M. Escalante, M. Péter, et al. „Creating nanopatterns of his-tagged proteins on surfaces by nanoimprint lithography using specific Ni NTA-histidine interactions“. In: *Small* 3.9 (2007), pp. 1584–1592 (cit. on pp. 140, 142, 145).

[295] C.-C. Wu, D. N. Reinhoudt, C. Otto, A. H. Velders, and V. Subramaniam. „Protein Immobilization on Ni(II) Ion Patterns Prepared by Microcontact Printing and Dip-Pen Nanolithography“. In: *ACS Nano* 4.2 (2010), pp. 1083–1091 (cit. on pp. 140–142, 145).

[296] S. Lata, A. Reichel, R. Brock, R. Tampé, and J. Piehler. „High-affinity adaptors for switchable recognition of histidine-tagged proteins“. In: *Journal of the American Chemical Society* 127.29 (2005), pp. 10205–10215 (cit. on pp. 140, 141).

[297] S. Lata, M. Gavutis, R. Tampé, and J. Piehler. „Specific and stable fluorescence labeling of histidine-tagged proteins for dissecting multi-protein complex formation“. In: *Journal of the American Chemical Society* 128.7 (2006), pp. 2365–2372 (cit. on pp. 140, 141).

[298] M. J. W. Ludden, A. Mulder, K. Schulze, et al. „Anchoring of histidine-tagged proteins to molecular printboards: Self-assembly, thermodynamic modeling, and patterning“. In: *Chemistry - A European Journal* 14.7 (2008), pp. 2044–2051 (cit. on p. 140).

[299] S. V. Wegner and J. P. Spatz. „Cobalt(III) as a stable and inert mediator ion between NTA and His6-tagged proteins“. In: *Angewandte Chemie - International Edition* 52.29 (2013), pp. 7593–7596 (cit. on pp. 140, 145).

[300] M. Liley, T. A. Keller, C. Duschl, and H. Vogel. „Direct Observation of Self-Assembled Monolayers, Ion Complexation, and Protein Conformation at the Gold/ Water Interface: An FTIR Spectroscopic Approach“. In: *Biopolymers* 12.9 (1997), pp. 4190–4192 (cit. on pp. 140, 141).

[301] S. Lata and J. Piehler. „Stable and functional immobilization of histidine-tagged proteins via multivalent chelator headgroups on a molecular poly(ethylene glycol) brush“. In: *Analytical Chemistry* 77.4 (2005), pp. 1096–1105 (cit. on pp. 140, 141).

[302] T. A. Keller, C. Duschl, D. Kriiger, et al. „Reversible oriented immobilization of histidine- tagged proteins on gold surfaces using a chelator thioalkane“. In: *Supramolecular Science* 2 (1996), pp. 155–160 (cit. on pp. 140, 141).

[303] D. Kröger, M. Liley, W. Schiweck, A. Skerra, and H. Vogel. „Immobilization of histidine-tagged proteins on gold surfaces using chelator thioalkanes“. In: *Biosensors and Bioelectronics* 14.2 (1999), pp. 155–161 (cit. on pp. 140, 141).

[304] R. Valiokas, G. Klenkar, A. Tinazli, et al. „Differential protein assembly on micropatterned surfaces with tailored molecular and surface multivalency“. In: *ChemBioChem* 7.9 (2006), pp. 1325–1329 (cit. on p. 141).

[305] G. Klenkar, R. Valiokas, I. Lundstro, et al. „Piezo Dispensed Microarray of Multivalent Chelating Thiols for Dissecting Complex Protein-Protein Interactions“. In: *Analytical Chemistry* 78.11 (2006), pp. 3643–3650 (cit. on p. 141).

[306] T. T. Le, C. P. Wilde, N. Grossman, and A. E. G. Cass. „A simple method for controlled immobilization of proteins on modified SAMs“. In: *Physical Chemistry Chemical Physics* 13.12 (2011), p. 5271 (cit. on pp. 142, 145).

[307] K. Kato, H. Sato, and H. Iwata. „Immobilization of Histidine-Tagged Recombinant Proteins onto Micropatterned Surfaces for Cell-Based Functional Assays“. In: *Langmuir* 21.4 (2005), pp. 7071–7075 (cit. on pp. 142, 145).

[308] A. R. Statz, J. P. Park, N. P. Chongsiriwatana, A. E. Barron, and P. B. Messersmith. „Surface-immobilised antimicrobial peptoids.“ In: *Biofouling* 24.6 (2008), pp. 439–48 (cit. on p. 143).

[309] E. Kang, J.-W. Park, S. J. Mcclellan, et al. „Specific Adsorption of Histidine-Tagged Proteins on Silica Surfaces Modified with $Ni^{2+}$/NTA-Derivatized Poly(ethylene glycol)“. In: *Langmuir* 23.17 (2007), pp. 6281–6288 (cit. on pp. 145, 161).

[310] O. V. Stepanenko, V. V. Verkhusha, I. M. Kuznetsova, V. N. Uversky, and K. K. Turoverov. „Fluorescent proteins as biomarkers and biosensors: throwing color lights on molecular and cellular processes.“ In: *Current protein & peptide science* 9.4 (2008), pp. 338–69 (cit. on p. 145).

[311] *GFP, Microscopy* (cit. on p. 145).

[312] S. Rondinini, A. Vertova, and L. Pilan. „The Use of Hexaaammineruthenium(III) Redox Marker for the Characterization of SAM-Au Amperometric Sensors“. In: *Electroanalysis* 15.1516 (2003), pp. 1297–1301 (cit. on p. 146).

[313] T. D. Dolidze, S. Rondinini, A. Vertova, M. Longhi, and D. E. Khoshtariya. „Charge-Transfer Patterns for $[Ru(NH_3)_6]^{3+/2+}$ at SAM Modified Gold Electrodes: Impact of the Permeability of a Redox Probe“. In: *The Open Physical Chemistry Journal* 2.1 (2008), pp. 17–21 (cit. on pp. 146, 147).

[314] B. Liu, A. J. Bard, M. V. Mirkin, and S. E. Creager. „Electron Transfer at Self-Assembled Monolayers Measured by Scanning Electrochemical Microscopy“. In: *Journal of the American Chemical Society* 126.5 (2004), pp. 1485–1492 (cit. on pp. 146, 147).

[315] M. Torrent, D. Pulido, M. V. Nogués, and E. Boix. „Exploring new biological functions of amyloids: bacteria cell agglutination mediated by host protein aggregation.“ In: *PLoS pathogens* 8.11 (2012), e1003005 (cit. on p. 150).

[316] N. G. Bednarska, J. van Eldere, R. Gallardo, et al. „Protein aggregation as an antibiotic design strategy“. In: *Molecular Microbiology* 99.5 (2016), pp. 849–865 (cit. on p. 150).

[317] A. R. Bizzarri and S. Cannistraro. „Molecular Dynamics of Water at the Protein-Solvent Interface“. In: *The Journal of Physical Chemistry B* 106.26 (2002), pp. 6617–6633. eprint: https://doi.org/10.1021/jp020100m (cit. on p. 157).

[318] J. W. Bye, S. Meliga, D. Ferachou, et al. „Analysis of the Hydration Water around Bovine Serum Albumin Using Terahertz Coherent Synchrotron Radiation“. In: *The Journal of Physical Chemistry A* 118.1 (2014), pp. 83–88 (cit. on p. 157).

[319] S. N. Magonov, V. Elings, and M.-H. Whangbo. „Phase imaging and stiffness in tapping-mode atomic force microscopy“. In: *Surface Science* 375.2-3 (1997), pp. L385–L391 (cit. on p. 158).

[320] J. Tamayo and R. García. „Deformation, Contact Time, and Phase Contrast in Tapping Mode Scanning Force Microscopy“. In: *Langmuir* 12.18 (1996), pp. 4430–4435 (cit. on p. 158).

[321] S. Point, T. Minea, B. Bouchet-Fabre, A. Granier, and G. Turban. „XPS and NEXAFS characterisation of plasma deposited vertically aligned N-doped MWCNT“. In: *Diamond and Related Materials* 14.3-7 (2005), pp. 891–895 (cit. on p. 159).

[322] J. R. Pels, F. Kapteijn, J. A. Moulijn, Q. Zhu, and K. M. Thomas. „Evolution of nitrogen functionalities in carbonaceous materials during pyrolysis“. In: *Carbon* 33.11 (1995), pp. 1641–1653 (cit. on p. 159).

[323] T. Susi, T. Pichler, and P. Ayala. „X-ray photoelectron spectroscopy of graphitic carbon nanomaterials doped with heteroatoms“. In: *Beilstein Journal of Nanotechnology* 6 (2015), pp. 177–192 (cit. on p. 159).

[324] C. Vasile, M. C. Baican, C. M. Tibirna, et al. „Microwave plasma activation of a polyvinylidene fluoride surface for protein immobilization“. In: *Journal of Physics D: Applied Physics* 44.47 (2011), p. 475303 (cit. on p. 159).

[325] A. F. Raigoza and L. J. Onyirioha K.and Webb. „Controlling noncovalent interactions between a lysine-rich $\alpha$-helical peptide and self-assembled monolayers of alkanethiols on Au through functional group diversity“. In: *Applied Surface Science* 396 (2017), pp. 1831–1839 (cit. on p. 159).

[326] J. Schartner, J. Güldenhaupt, B. Mei, et al. „Universal Method for Protein Immobilization on Chemically Functionalized Germanium Investigated by ATR-FTIR Difference Spectroscopy“. In: *Journal of the American Chemical Society* 135.10 (2013), pp. 4079–4087 (cit. on p. 161).

[327] O. D. Roure, C. Debiemme-Chouvy, J. Malthête, and P. Silberzan. „Functionalizing Surfaces with Nickel Ions for the Grafting of Proteins“. In: (2003) (cit. on p. 161).

[328] F. G. Pacheco, A. A. C. Cotta, H. F. Gorgulho, et al. „Comparative temporal analysis of multiwalled carbon nanotube oxidation reactions: Evaluating chemical modifications on true nanotube surface“. In: *Applied Surface Science* 357 (2015), pp. 1015–1023 (cit. on p. 161).

[329] A. F. Carley, M. K. Rajumon, M. W. Roberts, and P. B. Wells. „XPS and LEED studies of 10,11-dihydrocinchonidine adsorption at Pt(111). Implications for the role of cinchona alkaloids in enantioselective hydrogenation“. In: *Journal of the Chemical Society, Faraday Transactions* 91.14 (1995), p. 2167 (cit. on p. 161).

[330] A. I. Stadnichenko, S. V. Koshcheev, and A. I. Boronin. „An XPS and TPD study of gold oxide films obtained by exposure to RF-activated oxygen“. In: *Journal of Structural Chemistry* 56.3 (2015), pp. 557–565 (cit. on p. 161).

[331] H. Liu, Y. Zhao, D. Zhao, et al. „Antibacterial and anti-biofilm activities of thiazolidione derivatives against clinical *staphylococcus strains*“. In: *Emerging Microbes and Infections* 4 (2015), p. 1 (cit. on p. 162).

[332] B. Mishra and G. Wang. „Individual and Combined Effects of Engineered Peptides and Antibiotics on *Pseudomonas aeruginosa* Biofilms“. In: *Pharmaceuticals* 10 (2017) (cit. on p. 162).

[333] C. Jeyaraj Pandian, R. Palanivel, and S. Dhanasekaran. „Screening Antimicrobial Activity of Nickel Nanoparticles Synthesized Using Ocimum sanctum Leaf Extract“. In: *Journal of Nanoparticles* (2016), pp. 1–13 (cit. on p. 163).

[334] L. Argueta-Figueroa, R. A. Morales-Luckie, R. J. Scougall-Vilchis, and O. F. Olea-Mejía. „Synthesis, characterization and antibacterial activity of copper, nickel and bimetallic Cu–Ni nanoparticles for potential use in dental materials“. In: *Progress in Natural Science: Materials International* 24.4 (2014), pp. 321–328 (cit. on p. 163).

# General Conclusions

# 6

> *Not all those who wander are lost.*
>
> **— J. R. R. Tolkien**

This doctoral dissertation has focused on developing strategies for surface modification to use in three different biological applications. It has consisted in an extremely multidisciplinary work, spanning from organic chemistry, to surface engineering and also biology: it has included the synthesis of the molecules used, the optimization of the protocols for surface modification using, in our case, stimulus-responsive SAMs, and the use of biomolecules and their evaluation with cell cultures. It is worth mentioning, that in order to carry out this work it has been necessary to understand the basics of different fields, and to bridge the knowledge acquired to properly design the experimental work to overcome the proposed challenges.

From the research conducted and presented in this dissertation the following conclusions can be withdrawn:

- By using stimulus activated SAMs to study the DA and MA interfacial reactions, we have concluded that DA provides a more homogeneous coverage than MA using similar experimental conditions.
- Additionally, the stimulus activated DA and MA interfacial reactions were used to immobilize, on surface, cell adhesion promoting peptides, namely RGD. Cell adhesion was studied looking at cell density, cell spreading and FA area, to compare how the DA and MA surface functionalization affected differently cell adhesion. It was found that MA provides better surface modification according to results obtained. This could be explained by the spatial arrangement of the immobilized peptides, providing a topography which facilitates and enhances cell attachment and subsequent, cell spreading.
- Furthermore, findings in a first study involving immobilized Qk-peptides on surfaces showed tubular network formation and enhanced endothelial cell viability in Qk-coated surfaces. In general, it has been shown that controlled peptide immobilization on surfaces provide an essential tool for fundamental cell behavior studies.
- Provided the usefulness of these interfacial reactions for surface modification, the more versatile MA was used to immobilize lipid bilayers on prefunctionalized surfaces, as cell membrane models, which led to the diminishing of the diffusion coefficient. Clearly, this presents an attractive platform to control the tethering of lipid bilayers with an external stimulus for enhancing the

characterization of transmembrane proteins embedded in lipid bilayers, used as cell membrane models.

- Moreover, a supramolecular strategy was used to immobilize on surface a novel multi-domain antimicrobial protein. Findings show that the Ni-NTA SAM provides a good strategy for immobilizing these proteins on surface and that μCP can be used to acquire a controlled spatial distribution of these on surface. A biofilm assay confirmed the bactericidal effect of the surface tethered proteins: this platform provides, hence, a useful antimicrobial coating strategy, which could be adapted to coat different types of material surfaces, such as medical grade polymers or metals.

Based on these conclusions, this works provides insights in different strategies based on the use of SAMs to modify surfaces for biological applications. Moreover, the use of stimulus activated SAMs, opens up for the possibility of designing more studies using this platform for the further investigation of biological challenging problems where the temporal and spatial control of biomolecule immobilization are important.

# Experimental Methodologies

7

> *A scientist in his laboratory is not a mere technician: he is also a child confronting natural phenomena that impress him as though they were fairy tales.*
>
> — **Marie Curie**

## 7.1 Chapter 2

### 7.1.1 Synthesis of Molecules

**General procedures**

Chemicals were used as received without special purification unless stated otherwise. Analytical thin-layer chromatography was performed on $SiO_2$ (Merck silica gel 60 $F_{254}$), and the spots were located using different TLC revealers. THF was dried and freed of oxygen by refluxing over sodium/benzophenone under nitrogen and distilled prior to use when stated anhydrous conditions. Chromatography refers to flash chromatography and was carried out on $SiO_2$ (SDS silica gel 60 ACC, 35-75 μm, 230-240 mesh ASTM) unless otherwise stated. Drying of organic extracts during workup of reactions was performed over anhydrous $MgSO_4$. Evaporation of solvent was accomplished with a rotary evaporator. NMR spectra were recorded in $CDCl_3$ on a Bruker Avance III 400SB or Bruker Avance DRX-250. Chemical shifts of $^1H$ and $^{13}C$ NMR spectra are reported in ppm downfield ($\delta$) from $Me_4Si$.

**Undec-1-en-11-yl-tetra(ethylene glycol) (5)**

Tetra(ethylene glycol) (7 mL, 40.54 mmol) was heated up to 80 °C using an oil bath and 4 mL of saturated aqueous NaOH was slowly added to it. The mixture was left to stir for 30 minutes and 11-bromo-1-undecene (1 mL, 4.56 mmol) was then added dropwise. The mixture was left under stirring overnight. The product was extracted with hexane, dried over $MgSO_4$, filtered and dried under vacuum. This resulted in a yellow oil which was purified by column chromatography on silica gel with ethyl acetate and gave **5** (1.9 g, 60%). Rf 0.34 (EtOAc) using an iodine chamber and TLC plate stained with p-anisaldehyde (dark blue stains). $^1H$ NMR (400 MHz, $CDCl_3$) $\delta$ 5.87 – 5.74 (m, 1H), 5.02-4.87 (m, 2H), 3.75 – 3.53 (m, 16H), 3.44 (t, 2.3 Hz, 2H), 2.95 (s, 1H), 2.07 - 1.98 (m, 2H), 1.61 – 1.52 (m, 2H), 1.40 – 1.21 (m, 12H). See Scheme 7.1 and Figure 7.2.

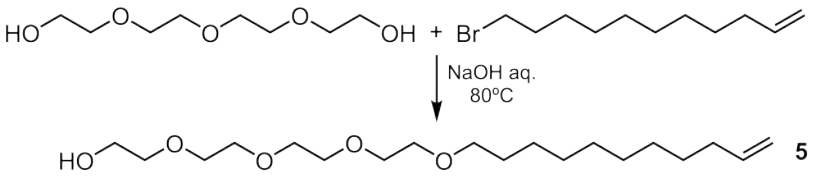


**Scheme 7.1:** Synthetic step to achieve compound **5**.

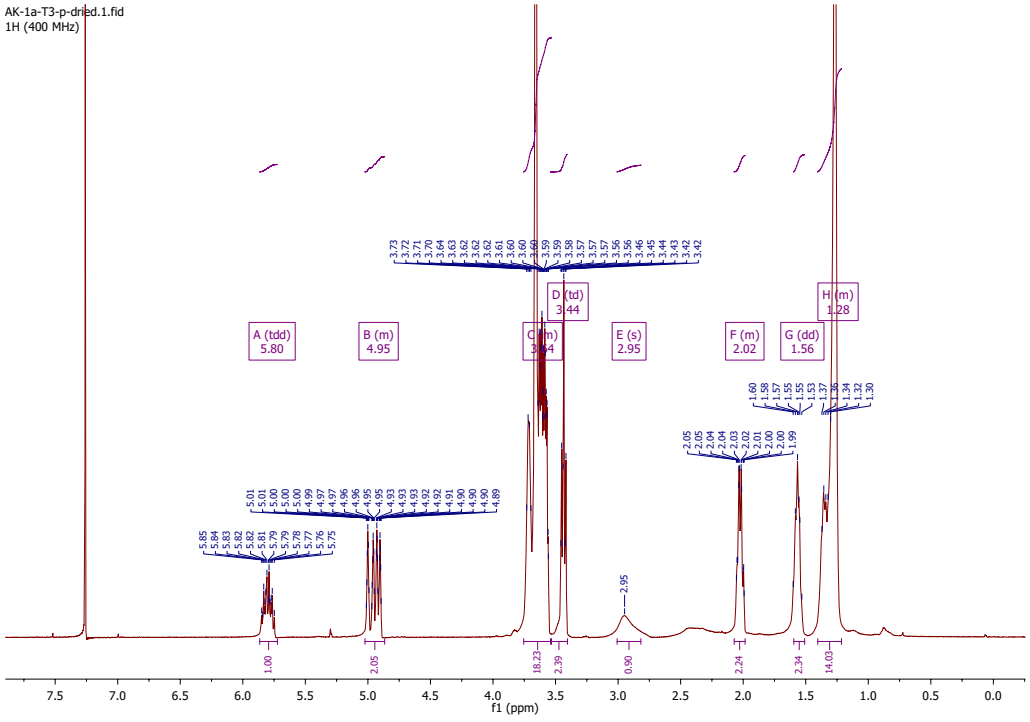


**Figure 7.1:** NMR spectra of compound **5**.

### 1-(Thiolacetyl)undec-11-yl-tetra(ethylene glycol) (6)

A solution of **5** (1 g, 2.89 mmol) in dry THF (15 mL) was refluxed under an atmosphere of nitrogen followed by the addition of AIBN (2,2'-azobisisobutyronitrile, 11.8 mg, added in three separate doses). Thiolacetic acid (0.62 mL, 8.66 mmol) was added dropwise and the reaction mixture was stirred overnight under reflux conditions. Concentration of the reaction mixture was performed with rotary evaporation at reduced pressure and was followed by purification by column chromatography with ethyl acetate, which gave the thioacetate **6** (444 mg, 36%). Rf 0.36 (EtOAc) using a iodine chamber and TLC plate stained with p-anisaldehyde (yellow stains). The product is also visible with UV light. $^{1}$H NMR (400 MHz, $CDCl_3$) $\delta$ 3.72 - 3.53 (m, 16H), 3.43 (dt, J = 6.8, 3.1 Hz, 2H), 2.87 - 2.81 (m, 2H), 2.66 (s, 1H), 2.30 (s, 3H), 1.59 - 1.49 (m, 4H), 1.24 (s, 14H). See Scheme 7.2 and Figure 7.2.

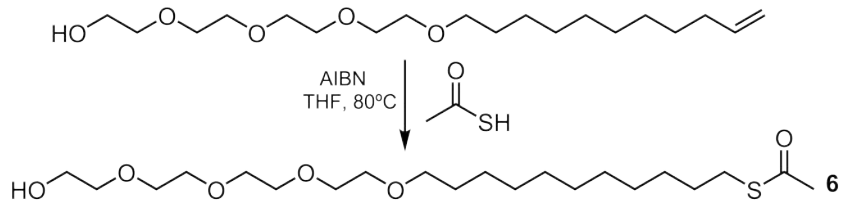


**Scheme 7.2:** Synthetic step to achieve compound **6**.

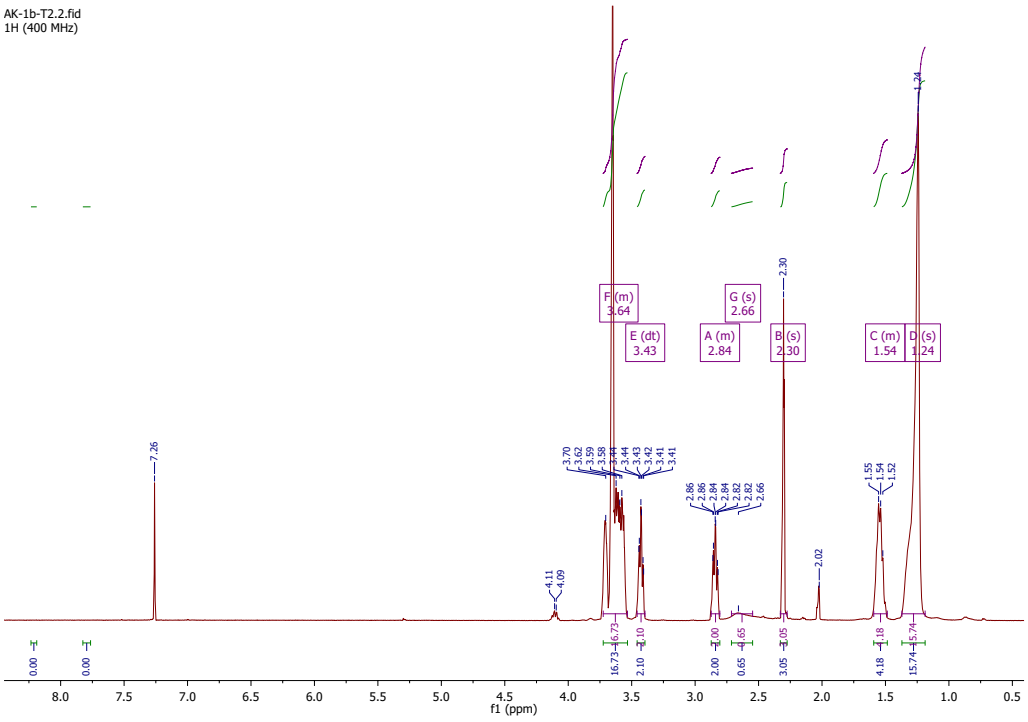


**Figure 7.2:** NMR spectra of compound **6**.

### 1-Mercaptoundec-11-yl-tetra(ethylene glycol) (1) (OH-SH)

A solution of 6 (1.69 mL, 4.25 mmol) in 0.1 M HCl in EtOH (85 mL) was refluxed for 15 hours under inert atmosphere. The mixture was dried by evaporation under reduced pressure and then dissolved in ethyl acetate. For neutralization it was washed with 1 M $NaHCO_3$, then it was also washed with water and brine, concentrated and purified by column chromatography with ethyl acetate to give **4** (OH-SH) (1.5 g, 92%). Rf 0.28 (EtOAc) TLC plate stained with p-anisaldehyde (yellow stains) $^1H$ NMR (250 MHz, CDCl3) $\delta$ 3.78 – 3.54 (m, 16H), 3.44 (t, J = 6.8 Hz, 2H), 2.53 (q, J = 7.4 Hz, 2H), 1.66 – 1.50 (m, 4H), 1.39 – 1.22 (m, 16H). HRMS calcd for $C_{19}H_{41}NO_5S$ (M + H+) 381.5800, found 381.2673. See Scheme 7.3 and Figure 7.3.

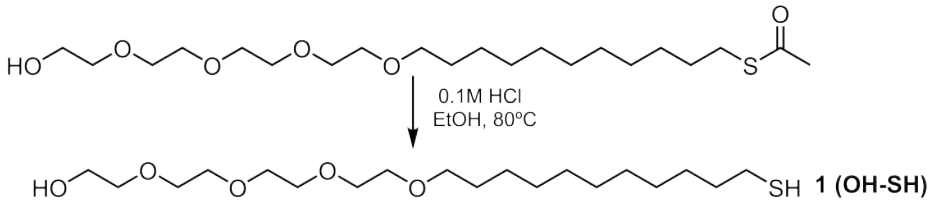


**Scheme 7.3:** Synthetic step to achieve compound **1**.

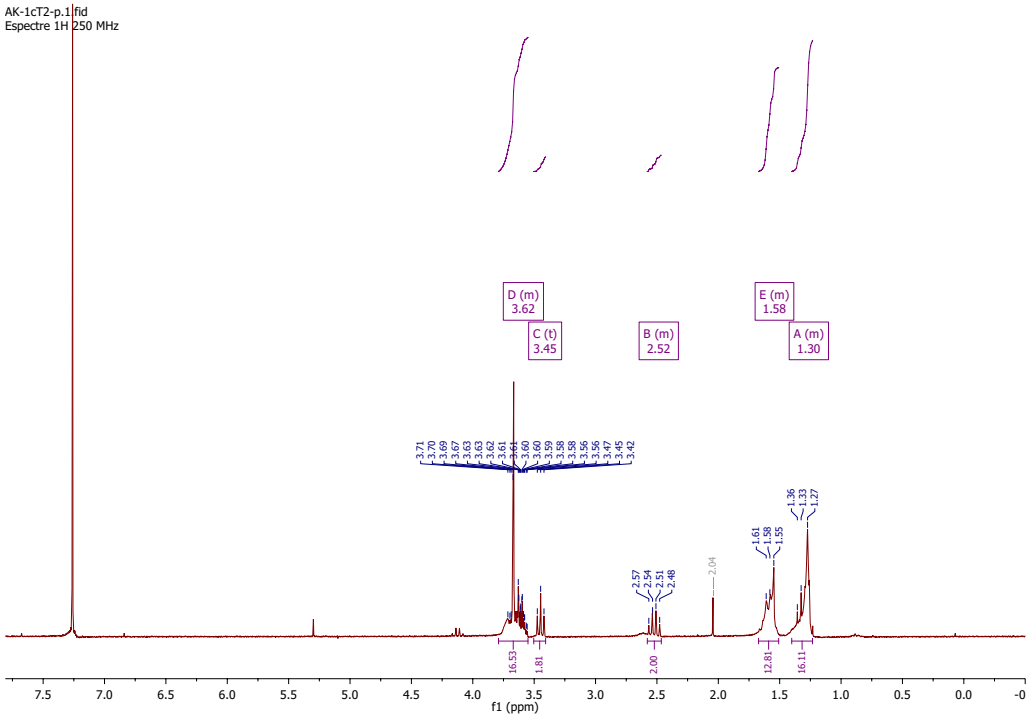


**Figure 7.3:** NMR spectra of compound **1**.

### Di-tetrahydropyran-hydroquinone (7)

Hydroquinone (3.3 g, 30.0 mmol) was dissolved in THF (20 mL) and to this was added 4-dihydro-2H-pyran (21.9 mL, 249 mmol) and 1-2 drops of concentrated HCl. The reaction mixture was stirred overnight at RT, concentrated by rotary evaporation and the resulted crude oil was dissolved in DCM, washed with 1 M $NaHCO_3$ and brine, and the organic layers were dried with $MgSO_4$. Concentration of the solution by rotary evaporation resulted in a white solid which was then purified by recrystallization in hexane to afford pure **7** (3.3 g, 39%). Rf 0.36 (DCM) TLC plate stained with PMA (phosphomolybdic acid or p-anisaldehyde. $^1$H NMR (400 MHz, $CDCl_3$) $\delta$ 6.97 (s, 4H), 5.32 – 5.29 (m, 2H), 3.97 – 3.89 (t, 2H), 3.62 – 3.55 (m, 2H), 2.05 – 1.93 (m, 2H), 1.87 – 1.81 (m, 4H), 1.72 – 1.56 (m, 6H). See Scheme 7.4 and Figure 7.4.

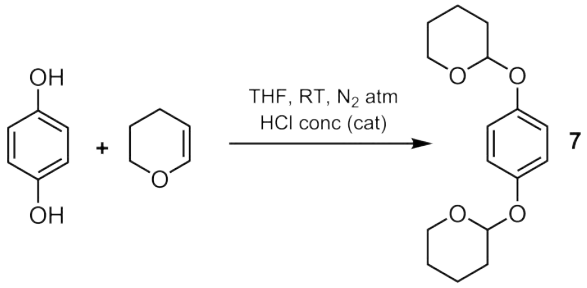


**Scheme 7.4:** Synthetic step to achieve compound **7**.

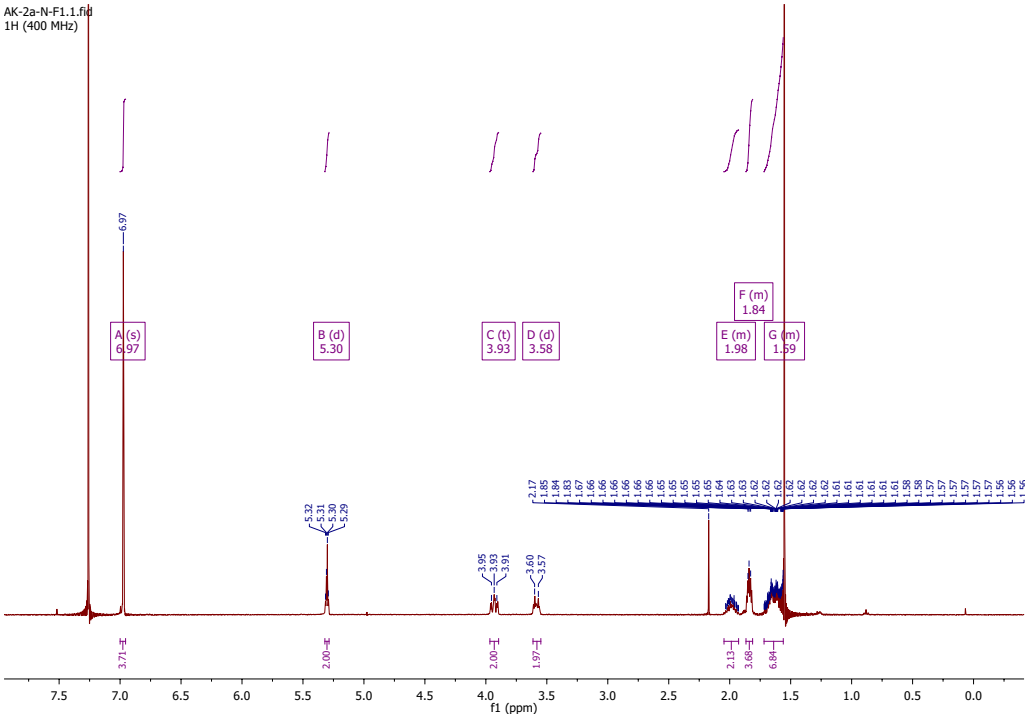


**Figure 7.4:** NMR spectra of compound **7**.

### Di-tetrahydropyran-hydroquinone-butyl bromide (8)

A solution of 7 (1 g, 3.6 mmol) in dry THF (20 mL) was brought to -75 °C and to it tert-butyllithium solution in pentane (1.7 M, 2.64 mL, 4.49 mmol) was added dropwise under an atmosphere of nitrogen. This mixture was stirred for 30 minutes and then brought slowly (over 2 hours) to 0 °C and stirred for an additional 30 minutes to quench any excess of tert-butyllithium. To this solution 1,4-dibromobutane (1.6 mL, 13.3 mmol) in THF was added dropwise over 20 minutes. The mixture was stirred overnight and then diluted with 30 mL of DCM and washed with $NH_4Cl$ three times and thereafter with brine, dried over $MgSO_4$, filtered and concentrated under reduced pressure. Purification of the crude oil with silica gel using DCM as eluent solvent afforded the product **8** (422 mg, 28 %). Rf 0.38 (DCM) TLC plate stained with PMA. $^1$H NMR (400 MHz, $CDCl_3$) $\delta$ 7.03 – 6.99 (m, 1H), 6.86 – 6.82 (m, 2H), 5.30 (m, 2H), 3.98 – 3.87 (m, 2H), 3.64 – 3.56 (m, 2H), 3.43 (t, J = 6.8 Hz, 2H), 2.64 (t, J = 7.5 Hz, 2H), 2.05 – 1.59 (m, 16H). See Scheme 7.5 and Figure 7.5.

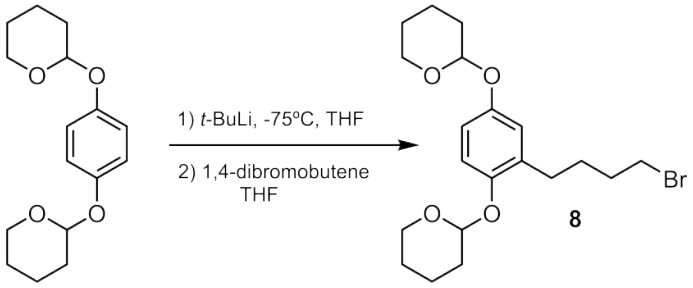


**Scheme 7.5:** Synthetic step to achieve compound **8**.

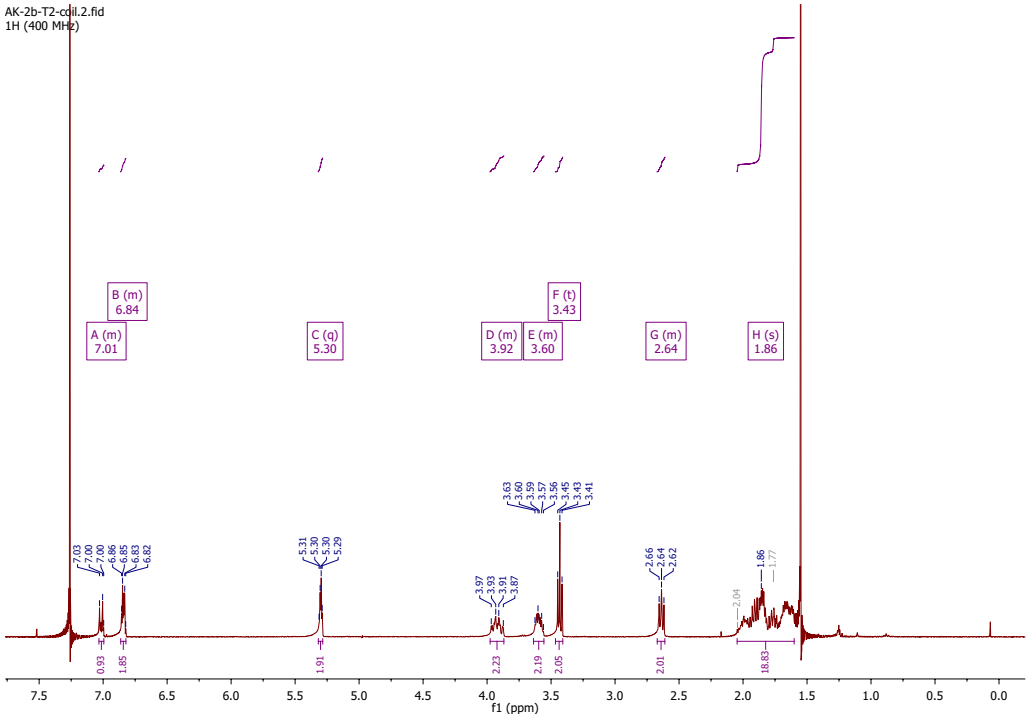


**Figure 7.5:** NMR spectra of compound **8**.

### Tetra(ethylene glycol)undecanethiol-trityl (9)

To a solution of 1-mercaptoundec-11-yl-tetra(ethylene glycol) **1** (OH-SH) (1.5 g, 3.94 mmol) in dry THF (30 mL) was added triphenylmethyl chloride (1.5 g, 5.52 mmol). The reaction mixture was stirred under nitrogen at RT for 20 hours and then concentrated. The purification of the crude by column chromatography using gradient elution from hexane/ethyl acetate (1/1) to 100 % ethyl acetate, afforded the product **9** (1 g, 40 %). Rf 0.375 (EtOAc) using a iodine chamber and also visible in UV. $^{1}$H NMR (400 MHz, $CDCl_3$) $\delta$ 7.42 – 7.38 (m, 6H), 7.30 – 7.24 (m, 6H), 7.22 – 7.17 (m, 3H), 3.74 – 3.56 (m, 16H), 3.44 (t, J = 6.8 Hz, 2H), 2.82 (s, 1H), 2.13 (t, J = 7.3 Hz, 2H), 1.56 (m, J = 7.2 Hz, 2H), 1.42 – 1.10 (m, 16H). See Scheme 7.6 and Figure 7.6.

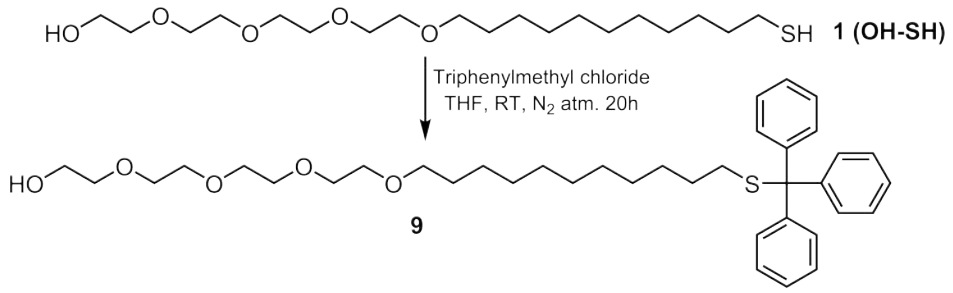


**Scheme 7.6:** Synthetic step to achieve compound **9**.

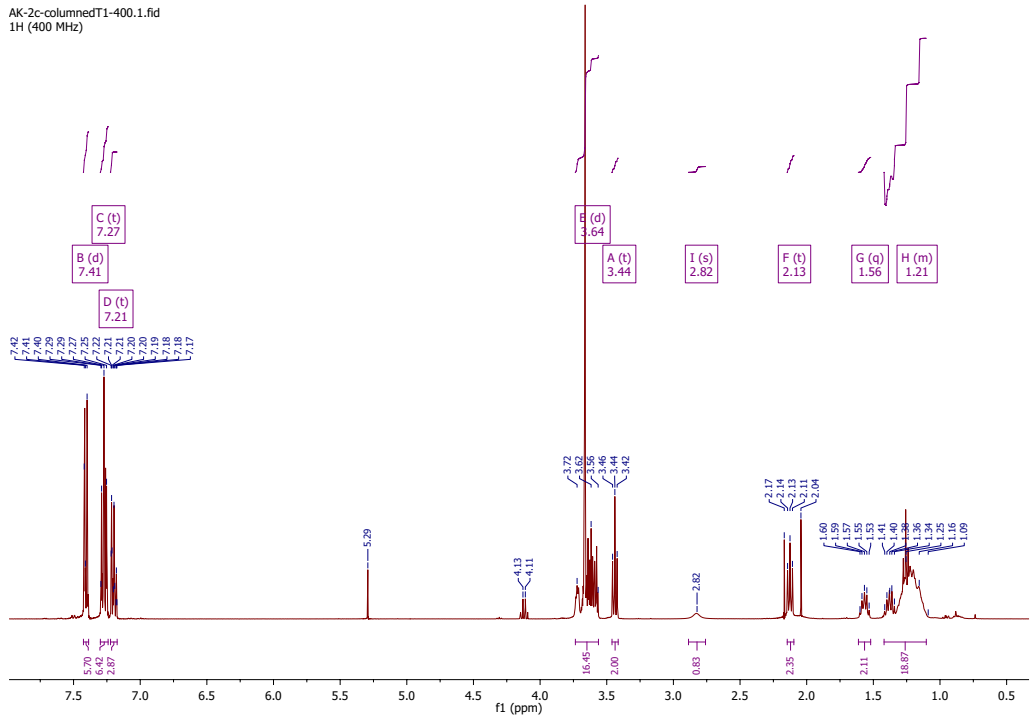


**Figure 7.6:** NMR spectra of compound **9**.

**Di-tetrahydropyran-hydroquinone-tetra(ethylene glycol)alkane-trityl (10)**

To a solution of **9** (265 mg, 0.43 mmol) in DMF (3 mL) at 0 °C was added NaH (480 mg, 20 mmol) slowly. This reaction mixture was stirred at 0 °C for 1 hour and then stirred at RT for 2 hours. During this time bubbles were observed in the reaction mixture. To this solution, **8** dissolved in 5 mL THF (316.5 mg, 0.77 mmol) was added dropwise. The reaction mixture was stirred for another 5 hours at RT, then diluted with 40 mL of ethyl acetate. This reaction mixture was then washed with $NH_4Cl$ and brine, and dried over $MgSO_4$. The resulting yellow oil was purified by column chromatography with hexane/ethyl acetate (1/1) to give the pure **10** as a clear oil (157 mg, 38%). Rf 0.79 (hexane/EtOAc 1/1) TLC plate stained with p-anisaldehyde, PMA or HCl and also visible under UV light. $^1$H NMR (400 MHz, $CDCl_3$) $\delta$ 7.43 – 7.38 (m, 6H), 7.30 – 7.23 (m, 6H), 7.22 – 7.17 (m, 3H), 7.02 – 6.98 (m, 1H), 6.83 (m, 2H), 5.31 – 5.27 (m, 2H), 3.98 – 3.86 (m, 2H), 3.67 – 3.55 (m, 18H), 3.50 – 3.41 (m, 4H), 2.62 (t, J = 7.0 Hz, 2H), 2.13 (t, J = 7.3 Hz, 2H), 2.03 –

1.93 (m, 2H), 1.87 – 1.80 (m, 4H), 1.72 – 1.52 (m, 8H), 1.43 – 1.08 (m, 20H). See Scheme 7.7 and Figure 7.7.

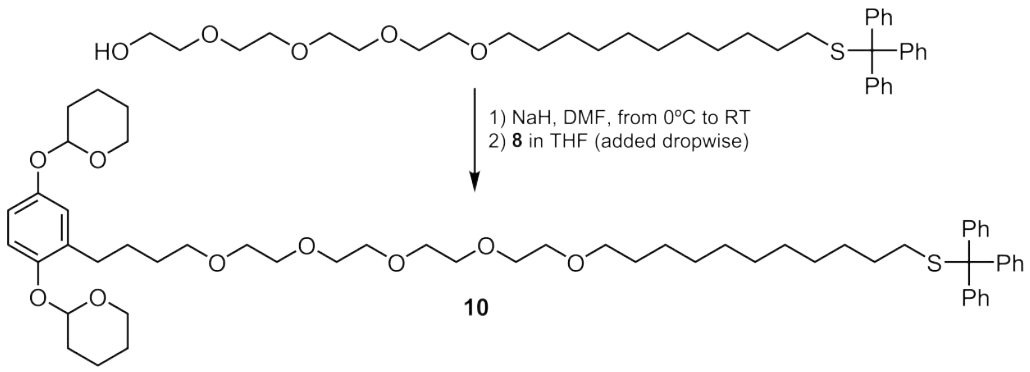


**Scheme 7.7:** Synthetic step to achieve compound **10**.

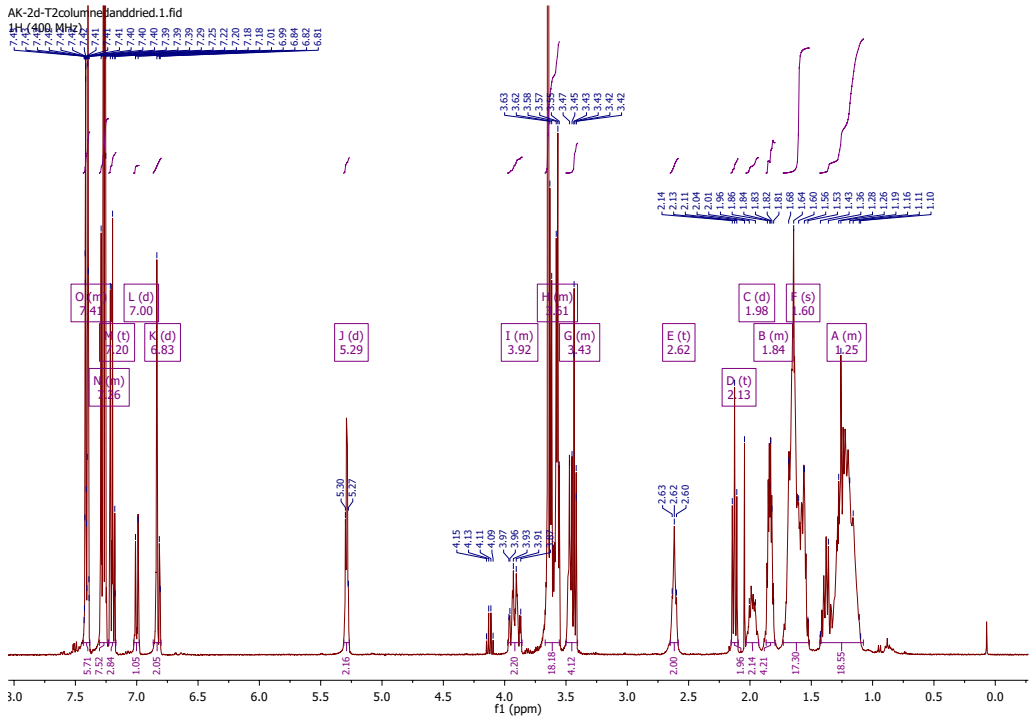


**Figure 7.7:** NMR spectra of compound **10**.

### Hydroquinone-tetra(ethylene glycol)alkanethiol (2) (HQ-SH)

To a solution of **10** (188 mg, 1.25 mmol) in 5 mL of trifluoroacetic acid (0.1 mL, 5% solution in $CH_2Cl_2$) triethylsilane (0.2 mL, 2.5 mmol) was added. This reaction mixture was stirred at RT for 2 hours (when **10** was not observed in TLC) and then concentrated under pressure to give a pale yellow oil. Silica gel chromatography with hexane/ethyl acetate (1/1) afforded the final product **2** (HQ-SH) as a clear oil (27%). Rf 0.58 (hexane/EtOAc 1/1) TLC plate stained with p-anisaldehyde or PMA. $^1$H NMR (400 MHz, CDCl3) $\delta$ 6.67 – 6.61 (m, 2H), 6.56 – 6.52 (m, 1H), 3.68 – 3.56 (m, 16H), 3.53 (t, J = 5.9 Hz, 2H), 3.44 (t, J = 6.9 Hz, 2H), 2.61 (t, J = 7.3 Hz, 2H), 2.55 – 2.48 (m, 2H), 1.72 (p, J = 6.9 Hz, 3H), 1.58 (d, J = 42.4 Hz, 4H), 1.34

(d, J = 69.2 Hz, 32H). HRMS calcd for $C_{19}H_{41}NO_5S$ (M + H+) 381.5800, found 381.2673. See Scheme 7.8 and Figure 7.5.

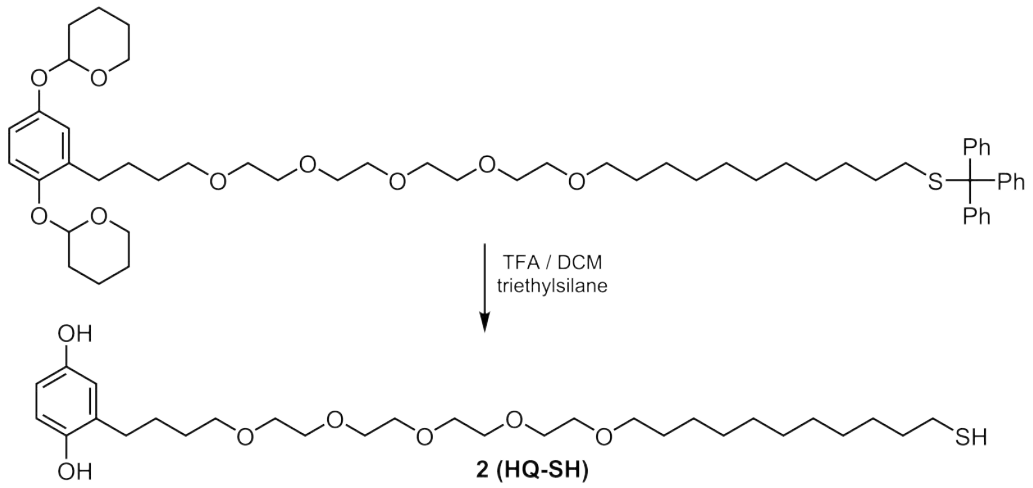


**Scheme 7.8:** Synthetic step to achieve compound **2**.

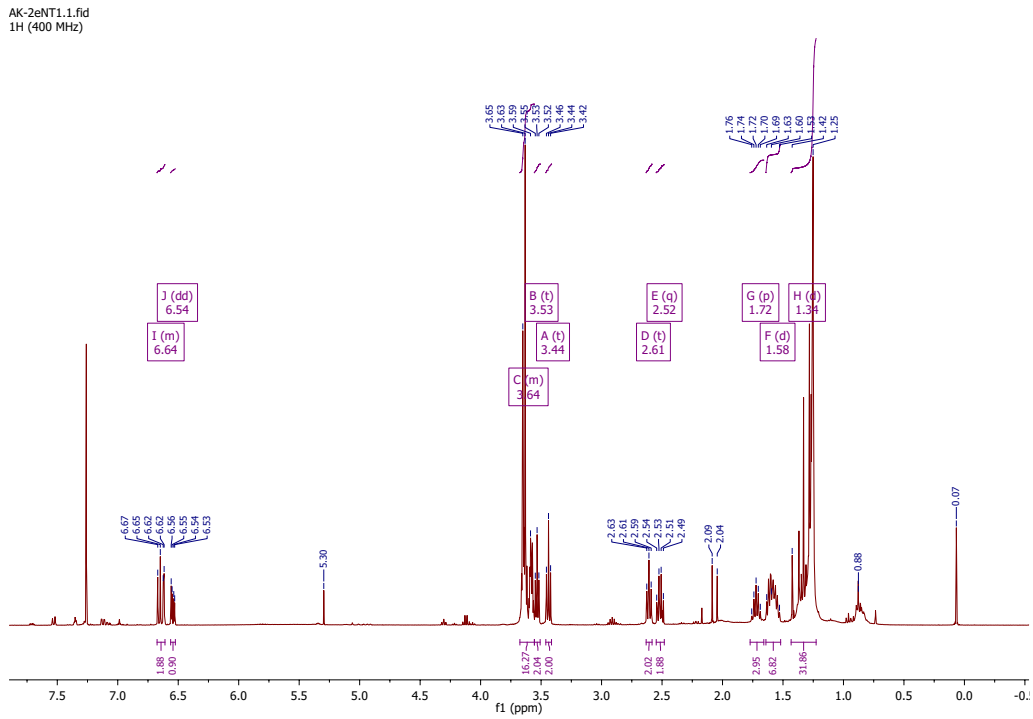


**Figure 7.8:** NMR spectra of compound **2**.

**2-(cyclopenta-1,3-dien-1-yl)acetic acid and 2-(cyclopenta-1,4-dien-1-yl)acetic acid (11)**

To a solution of methyl bromoacetate (1.2 mL, 12.9 mmol) in dry THF (10 mL) at -78 °C was added a solution of sodium cyclopentadienylide (2 M in THF, 6.5 mL, 13.0 mmol) dropwise over 20 min. The reaction mixture was stirred for 3 h at -78 °C, and then, $CH_2Cl_2$ (20 mL) was added to precipitate the formed NaBr. The solid was removed by filtration and the solution was evaporated to dryness to afford the crude of the methyl esters mixture (1.70 g, 84%, 1:1 mixture), which was used without further purification. The resulting crude ester was dissolved in

a THF/MeOH mixture (30 mL, 2:1 v/v), cooled to 0 °C, and to this solution was added 1 M NaOH (25 mL). The mixture was stirred for 5 min at 0 °C and then allowed to warm up to RT stirring for 4 h. The THF/MeOH mixture was removed by evaporation and the resulting aqueous phase was washed with $CH_2Cl_2$ (3×20 mL). The aqueous phase was acidified to a pH of 2 with 1 M HCl, and then it was extracted with $CH_2Cl_2$ (3×20 mL). The combined organic phases were washed with 1 M HCl (1×40 mL) and brine (1×40 mL). The resulting organic phase was dried with $MgSO_4$, filtered and evaporated to afford compound **11** (1.04 g, 68%, 1:1 mixture of title compounds). $^1$H NMR (400 MHz, $CDCl_3$) $\delta$ 6.55 – 6.50 (m, 1H), 6.49 – 6.42 (m, 2H), 6.40 – 6.32 (m, 2H), 6.28 – 6.24 (m, 1H), 3.52 – 3.43 (m, 4H), 3.07 – 2.98 (m, 4H). MS calcd for $C_7H_8O_2$ 124.0, found (ESI) 125.0 (M+H+). See Scheme 7.9 and Figure 7.9.

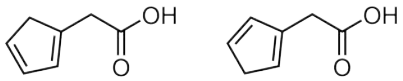


**11**

**Scheme 7.9:** Molecular structure of compound **11**.

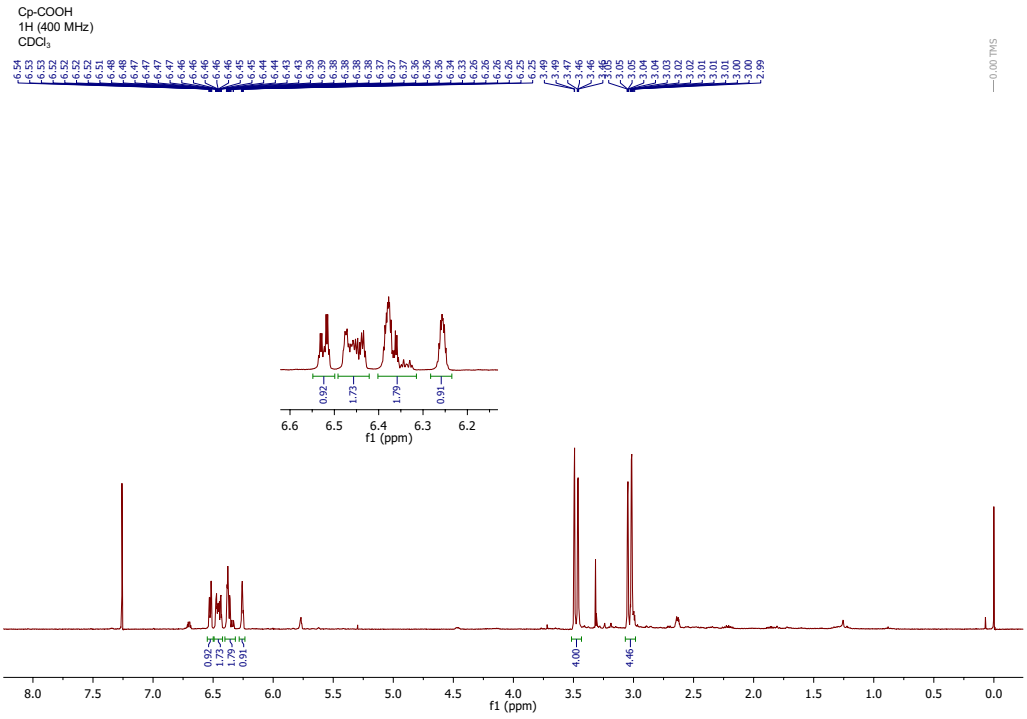


**Figure 7.9:** NMR spectra of compound **11**.

**2,5-dioxopyrrolidin-1-yl-2-(cyclopenta-1,3-dien-1-yl)acetate (12)**

To a solution of compound **11** (150 mg, 1.21 mmol) in THF/$CH_3CN$ (10 mL, 1:1 v/v) was added EDC·HCl (278 mg, 1.45 mmol) and N-hydroxysuccinimide (167 mg, 1.45 mmol) and the mixture was stirred for 16 h at RT. After this time the solvent was evaporated to dryness. The resulting crude was dissolved in $CH_2Cl_2$ (20 mL) and washed with saturated $NaHCO_3$ (2×20 mL), 0.5% w/v citric acid (2×20 mL),

and brine (1×20 mL). The organic phase was dried over $MgSO_4$ and evaporated to obtain the compound 12 (239 mg, 89 mmol), which was used without further purification. $^1$H NMR (400 MHz, $CDCl_3$) $\delta$ 6.87 – 6.82 (m, 1H), 6.44 – 6.38 (m, 1H), 5.99 – 5.95 (m, 1H), 3.05 – 3.00 (m, 2H), 2.87 – 2.81 (m, 4H), 2.70 – 2.65 (m, 2H). MS calcd for $C_{11}H_{11}NO_4$ 221.1, found (ESI) 222.1 (M+H+). See Scheme 7.10 and Figure 7.10.

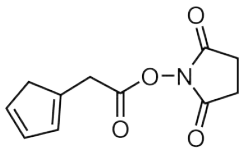

12

**Scheme 7.10:** Molecular structure of compound **12**.

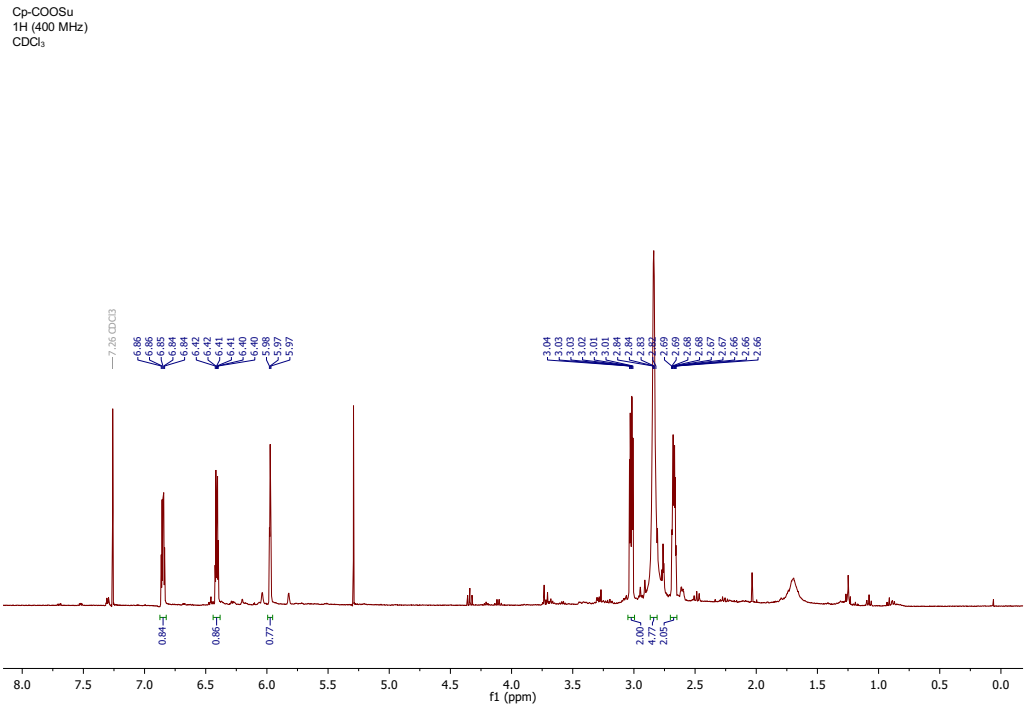


**Figure 7.10:** NMR spectra of compound **12**.

#### 5(6)-carboxyfluorescein-oligoethylene glycol-NHBoc (13)

5(6)-carboxyfluorescein (300 mg, 0.80 mmol), EDC·HCl (168 mg, 0.88 mmol) and N-hydroxysuccinimide (101 mg, 0.88 mmol) were dissolved in dry DMF (10 mL) and the mixture was stirred for 4 h at RT After this time, a solution of 1-(tert-butoxycarbonylamino)-4,7,10-trioxa-13-tridecanamine (281 mg, 0.88 mmol) in dry DMF (1 mL) was added. The resulting mixture was stirred for 3 h at RT. Then, the solvent was evaporated and the crude was purified by flash chromatography on silica using $CH_2Cl_2$ and MeOH as solvents (0 to 5% MeOH in $CH_2Cl_2$), affording compound **13** (453 mg, 84%). $^1$H NMR (400 MHz, $CD_3OD$) $\delta$ 8.41 (dd, J = 1.6, 0.7 Hz, 1H, isomer A), 8.19 (dd, J = 8.0, 1.7 Hz, 1H, isomer A), 8.14 (dd, J = 8.0, 1.4

Hz, 1H, isomer B), 8.07 (dd, J = 8.0, 0.8 Hz, 1H, isomer B), 7.64 (dd, J = 1.4, 0.8 Hz, 1H, isomer B), 7.30 (dd, J = 8.1, 0.7 Hz, 1H, isomer A), 6.69 (d, J = 2.3 Hz, 2H), 6.64 – 6.58 (m, 2H), 6.57 – 6.52 (m, 2H), 3.69 – 3.36 (m, 14H), 3.16 – 3.02 (m, 2H), 1.93 (p, J = 6.4 Hz, 1H), 1.80 (p, J = 6.4 Hz, 1H), 1.74 – 1.59 (m, 2H), 1.46 – 1.37 (m, 9H). MS calcd for $C_{36}H_{42}N_2O_{11}$ 678.3, found (ESI) 679.2 (M+H+). See Scheme 7.11 and Figure 7.11.

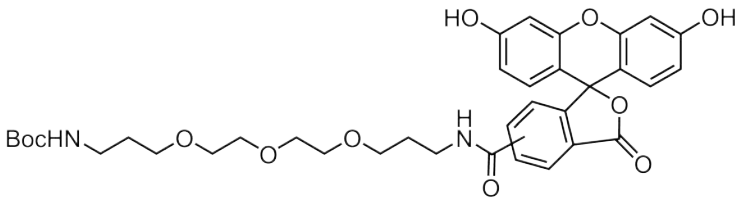


13

Scheme 7.11: Molecular structure of compound **13**.

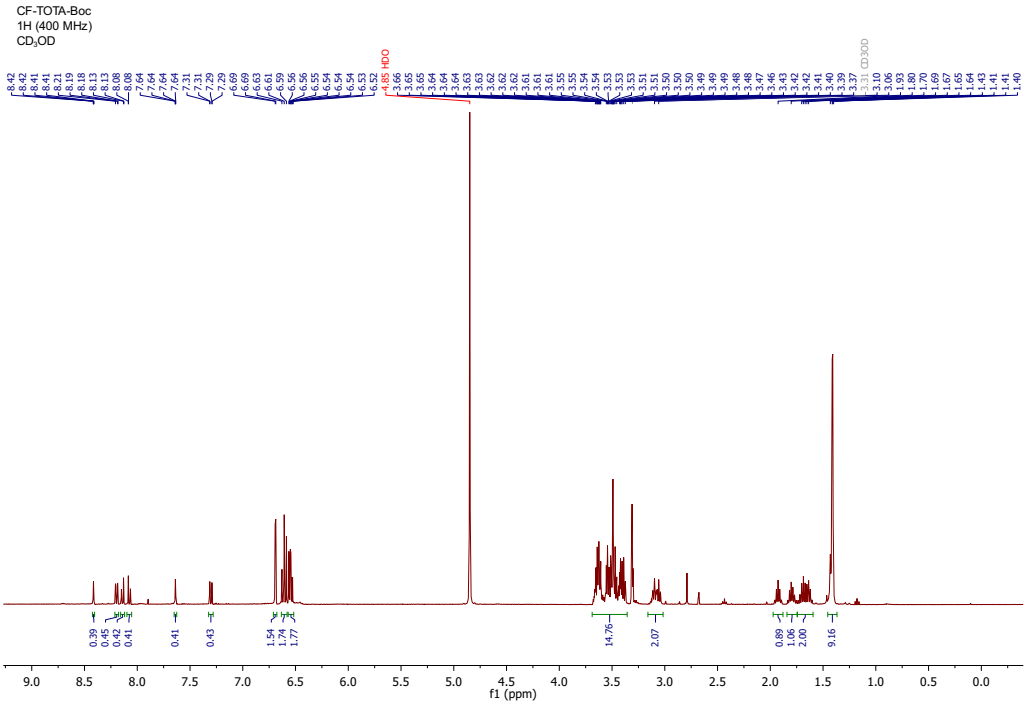


Figure 7.11: NMR spectra of compound **13**.

### 5(6)-carboxyfluorescein-oligoethylene glycol-$NH_3Cl$ (14)

To a solution of compound 13 (441 mg, 0.65 mmol) in dioxane (2 mL) was added a 4 M HCl/dioxane solution (2 mL, 8.0 mmol) and the mixture was stirred for 90 min at RT. Then, the crude was evaporated to dryness to obtain compound **14** (396 mg, 99%), which was used without further purification. $^1$H NMR (400 MHz, D2O) $\delta$ 8.42 (d, J = 1.6 Hz, 1H, isomer A), 8.16 (d, J = 8.2 Hz, 1H, isomer B), 8.04 – 7.98 (m, 2H, isomer A+B), 7.45 (d, J = 1.2 Hz, 1H, isomer B), 7.20 (d, J = 8.0 Hz, 1H, isomer A), 6.93 – 6.83 (m, 2H), 6.78 (dd, J = 12.4, 2.3 Hz, 2H), 6.72 – 6.60 (m, 2H), 3.73 – 3.23 (m, 14H), 3.16 – 3.01 (m, 2H), 2.02 – 1.67 (m, 4H). MS calcd

for $C_{31}H_{34}N_2O_9$ (free amine) 578.2, found (ESI) 579.2 (M+H+), 290.1 ([M+2H+]/2). See Scheme 7.12 and Figure 7.12.

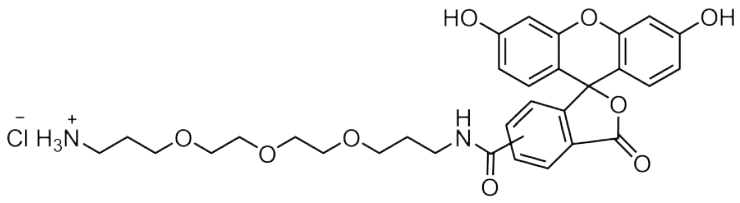

**14**

**Scheme 7.12:** Molecular structure of compound **14**.

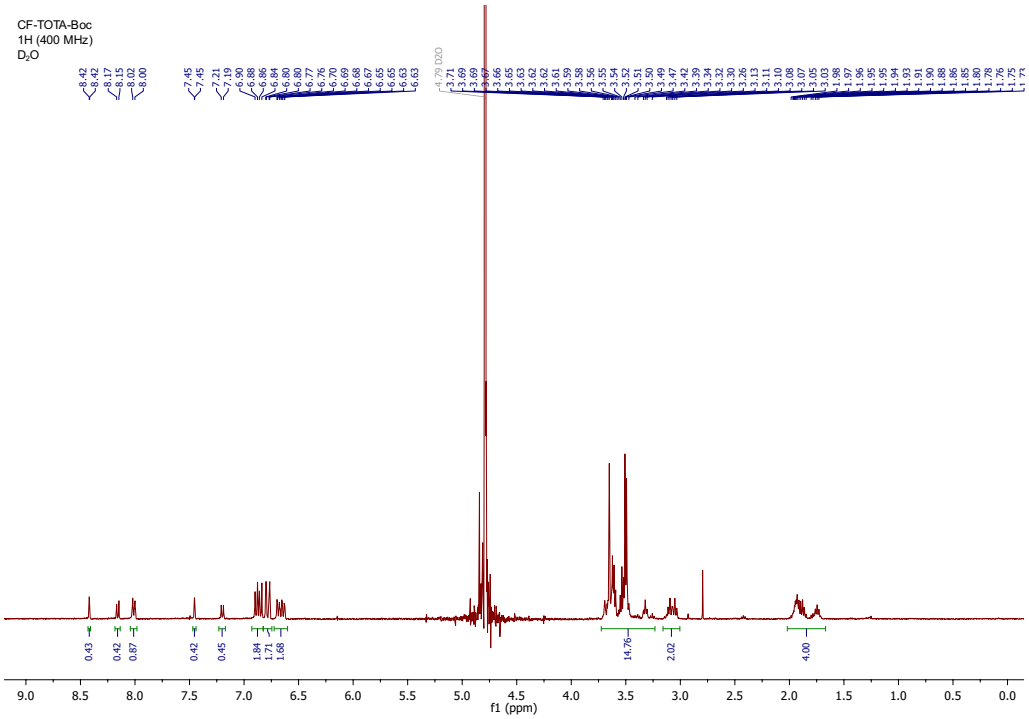


**Figure 7.12:** NMR spectra of compound **14**.

#### 5(6)-carboxyfluorescein-oligoethylene glycol-S-Trt (15)

To a solution of 3-(tritylthio)-propanoic acid (200 mg, 0.57 mmol) in dry DMF (2 mL) was added EDC·HCl (121 mg, 0.63 mmol) and N-hydroxysuccinimide (72.7 mg, 0.63 mmol) and the mixture was stirred for 17 h at RT. After this time, a solution of 14 (321 mg, 0.52 mmol) in dry DMF (1.5 mL) and DIEA (177 µL, 1.04 mmol) was added, and the reaction mixture was stirred for 20 h at RT. Then, the solvent was evaporated and the crude was purified by flash chromatography on silica using $CH_2Cl_2$ and MeOH as solvents (0 to 5% MeOH in CH2Cl2), affording compound **15** (159 mg, 34%). $^1$H NMR (400 MHz, CD3OD) $\delta$ 8.42 (dd, J = 1.6, 0.7 Hz, 1H, isomer A), 8.18 (dd, J = 8.0, 1.7 Hz, 1H, isomer A), 8.13 (dd, J = 8.0, 1.4 Hz, 1H, isomer B), 8.06 (dd, J = 8.0, 0.7 Hz, 1H, isomer B), 7.63 (dd, J = 1.5, 0.7 Hz, 1H, isomer B), 7.41 – 7.13 (m, 15H Trt + 1H isomer A), 6.70 – 6.67 (m, 2H), 6.62 – 6.55 (m, 2H), 6.55 – 6.49 (m, 2H), 3.66 – 3.35 (m, 14H), 3.27 – 3.13 (m, 2H), 2.40 –

2.33 (m, 2H), 2.23 – 2.12 (m, 2H), 1.96 – 1.61 (m, 4H). MS calcd for $C_{53}H_{52}N_2O_{10}S$ 908.3, found (ESI) 909.2 (M+H+). See Scheme 7.13 and Figure 7.13.

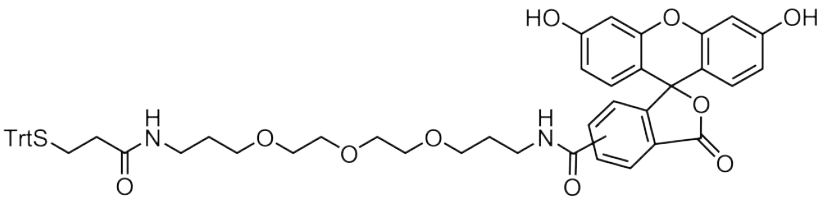


15

Scheme 7.13: Molecular structure of compound **15**.

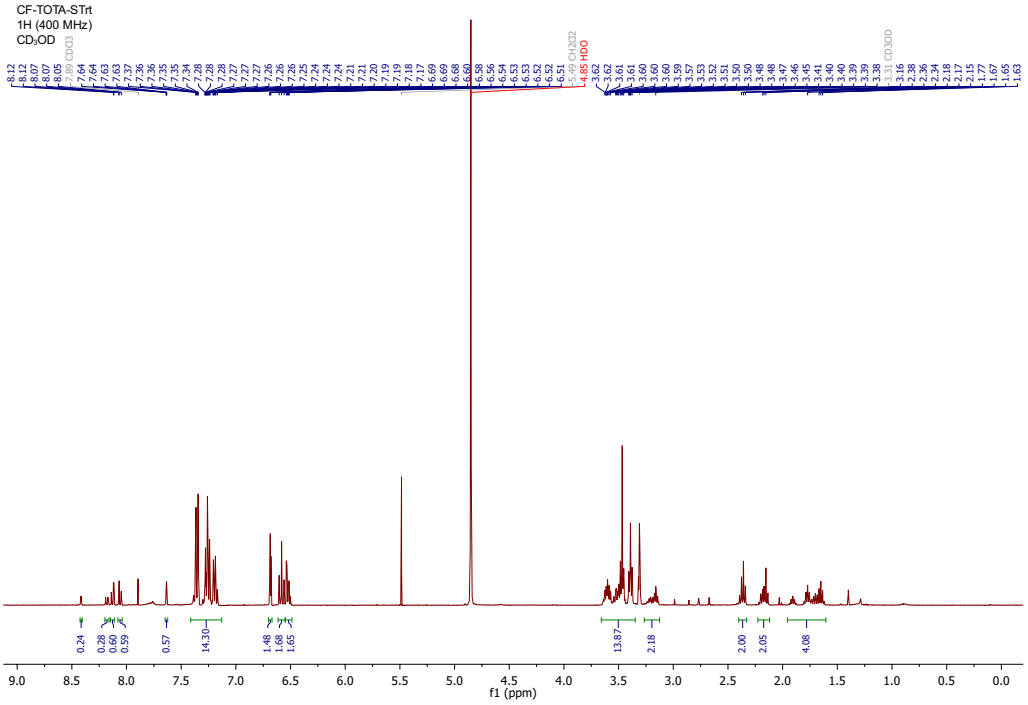


Figure 7.13: NMR spectra of compound **15**.

**5(6)-carboxyfluorescein-oligoethylene glycol-SH (4)**

Compound **15** (144 mg, 0.16 mmol) was dissolved in a mixture of TFA/$CH_2Cl_2$/triisopropylsilane (10 mL, 88:10:2 v/v/v) and the solution was stirred for 1 h at RT. Then, the volume of the mixture was reduced to 5 mL by evaporation and the crude was precipitated into cold diethyl ether (40 mL). After centrifugation of the mixture and removal of the supernatant, the desired compound **4** was isolated (106 mg, 99%). $^1$H NMR (400 MHz, $CD_3OD$) $\delta$ 8.42 (dd, J = 1.6, 0.7 Hz, 1H, isomer A), 8.20 (dd, J = 8.1, 1.6 Hz, 1H, isomer A), 8.14 (dd, J = 8.0, 1.4 Hz, 1H, isomer B), 8.07 (dd, J = 8.0, 0.8 Hz, 1H, isomer B), 7.64 (dd, J = 1.4, 0.8 Hz, 1H, isomer B), 7.30 (dd, J = 8.0, 0.8 Hz, 1H, isomer A), 6.69 (d, J = 2.3 Hz, 2H), 6.61 (t, J = 8.2 Hz, 2H), 6.58 – 6.51 (m, 2H), 3.70 – 3.37 (m, 14H), 3.30 – 3.18 (m, 2H), 2.77 – 2.66 (m, 2H), 2.52 – 2.40 (m, 2H), 1.97 – 1.64 (m, 4H). MS calcd for $C_{34}H_{38}N_2O_{10}S$

666.2, found (ESI) 667.1 (M+H+), 334.1 ([M+2H+] /2). See Scheme 7.14 and Figure 7.14.

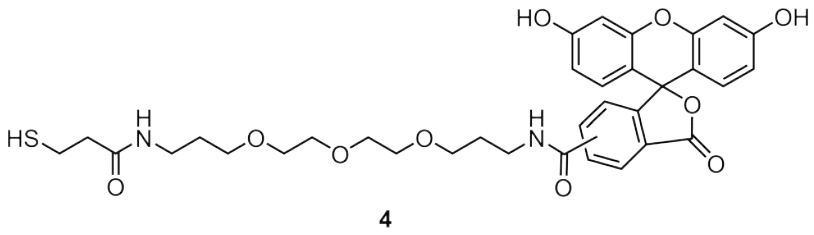


**4**

**Scheme 7.14:** Molecular structure of compound **4**.

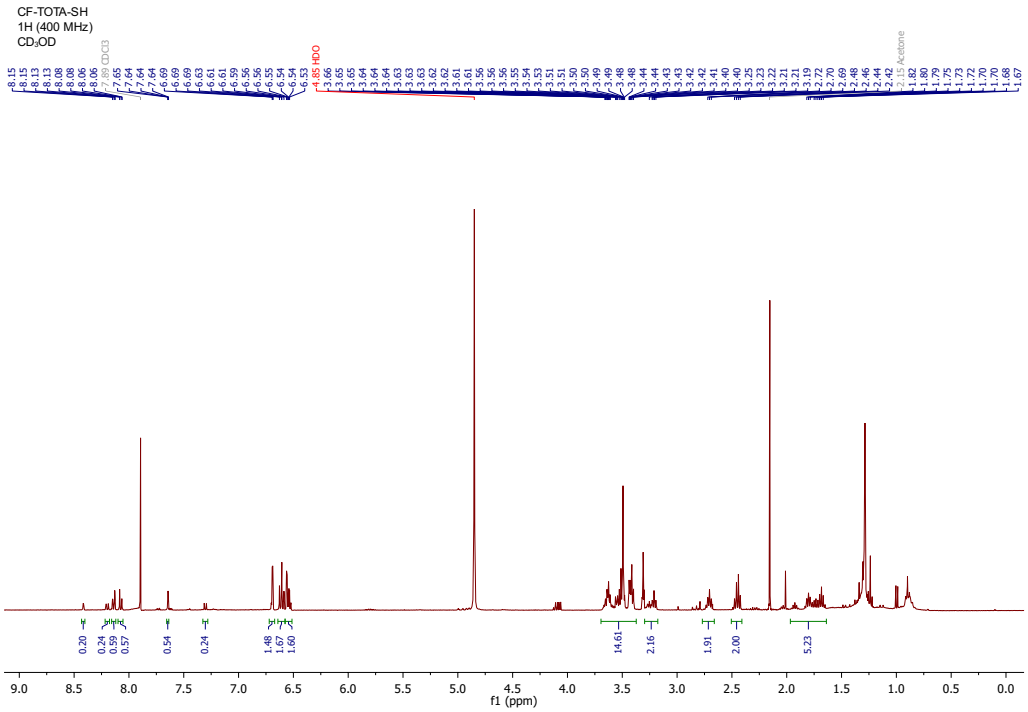


**Figure 7.14:** NMR spectra of compound **4**.

#### 5(6)-carboxyfluorescein-oligoethylene glycol-Cyclopentadiene (3)

To a solution of 14 (262 mg, 0.43 mmol) in dry DMF (10 mL) and DIEA (145 μL, 0.85 mmol) was added a solution of compound **12** (94.2 mg, 0.43 mmol) in dry DMF (3 mL). The resulting mixture was stirred for 16 h at RT. Then, the solvent was evaporated and the crude was purified in two steps, first by flash chromatography on silica using $CH_2Cl_2$ and MeOH as solvents (0 to 6% MeOH in $CH_2Cl_2$), and second by a Waters PorapakTM Rxn RP column (0 to 100% methanol in water) to afford compound 1 (88 mg, 30%). $^1$H NMR (400 MHz, Methanol-d4) $\delta$ 8.43 – 8.38 (m, 1H, isomer A), 8.19 (dd, J = 8.0, 1.5 Hz, 1H, isomer A), 8.13 (dd, J = 8.0, 1.4 Hz, 1H, isomer B), 8.07 (bd, J = 8.0 Hz, 1H, isomer B), 7.65 (bd, J = 1.4 Hz, 1H, isomer B), 7.29 (d, J = 8.0 Hz, 1H, isomer A), 6.69 (d, J = 2.3 Hz, 2H), 6.60 (t, J = 8.0 Hz, 2H), 6.57 – 6.49 (m, 3H), 6.28 – 6.21 (m, 1H), 5.80 – 5.72 (m, 1H), 3.69 – 3.38 (m, 14H), 3.30 – 3.20 (m, 2H), 3.00 – 2.93 (m, 2H), 2.60 – 2.53 (m, 2H), 1.98 –

1.63 (m, 4H). MS calcd for $C_{38}H_{40}N_2O_{10}$ 684.3, found (ESI) 685.3 (M+H+), 343.2 ([M+2H+] /2). See Scheme 7.15 and Figure 7.16.

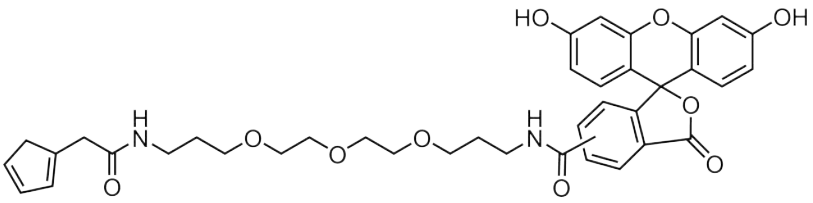


**3**

**Scheme 7.15:** Molecular structure of compound **3**.

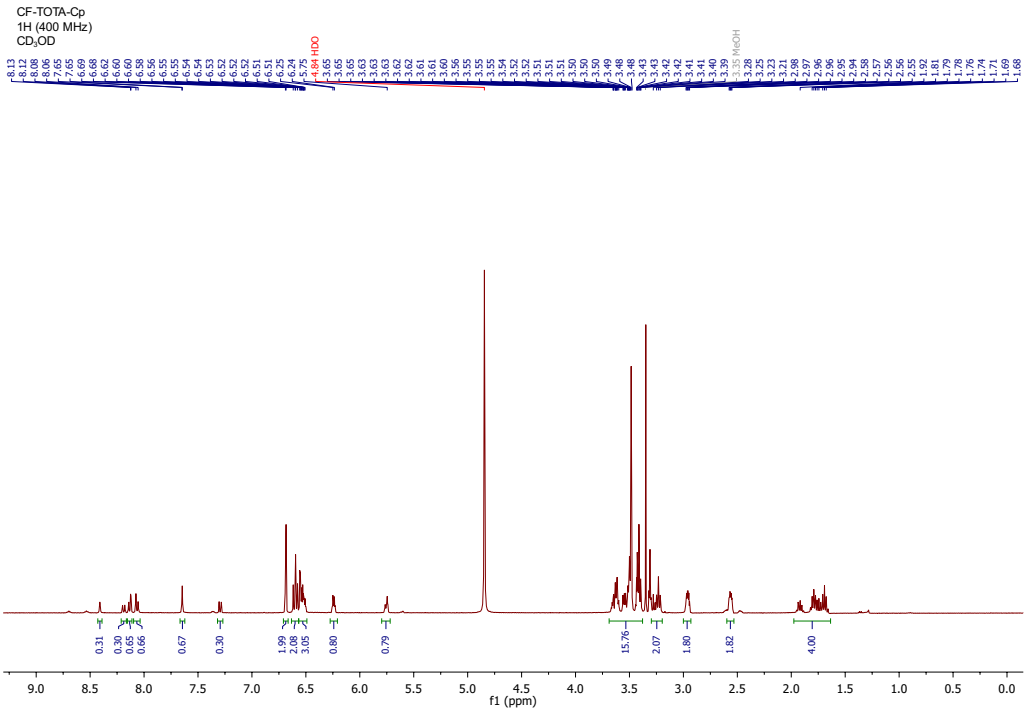


**Figure 7.15:** NMR spectra of compound **3**.

## 7.1.2 SAM Formation

Substrates were prepared by evaporation of titanium (50 nm), as adhesion layer, and gold (100 nm) onto silicon wafers. These were afterwards cut into substrates of $1\times2$ cm. Substrates were cleaned by sonication in isopropanol, acetone, and ethanol (HPLC grade), exposed to ozone for 20 min to get rid of unwanted residues [335] and to activate the gold surface by oxidizing it to a positive charged state [336]. Thereafter, substrates were immersed in absolute ethanol (HPLC grade) for 30 min in order to chemically reduce to zero state (metallic gold) the freshly prepared oxidized gold surfaces [337]. Finally, substrates were dried with a stream of nitrogen and immersed in a solution containing molecules **1** and **2** in a 1:1 molar ratio with a final 1 mM total concentration in absolute ethanol to obtain SAM **S1**. They were left immersed in the solution and under an inert atmosphere overnight.

### 7.1.3 Electrochemical Measurements

Before performing electrochemical measurements, SAMs **S1** were rinsed with absolute ethanol and dried with a stream of nitrogen. SAMs were then electrochemically characterized using CV with an AUTOLAB 204 and the NOVA 1.9 software. A custom built electrochemical cell, adapted from the SVC2 cell (Bio-Logic), with a Pt-wire as the CE, a Ag/AgCl electrode as the RE, and the SAM **S1** on gold as WE was used. The electrolyte used was a 1 M $HClO_4$ aqueous solution, which was purged with argon before performing the experiments. The area exposed to the electrolyte was approximately 1 $cm^2$.

**Figure 7.16:** Picture of the electrochemical setup used, with a connector to be able to immerse the substrate used as the WE.

### 7.1.4 Contact Angle Measurements

CA measurements on SAMs **S1** and **S2** were performed with a volume of 3 μL Milli-Q (MQ) water at RT with a Contact Angle Measuring System DSA 100 from KRÜSS.

### 7.1.5 XPS Measurements

XPS measurements on SAMs **S1**, **S2**, **S3-hexyl**, and **S4-hexyl** were performed with a Phoibos 150 analyzer (SPECS GmbH) under ultrahigh vacuum conditions (base pressure 5×10-10 mbar) with a monochromatic aluminum K alpha X-ray source (1486.74 eV). The energy resolution measured by the fwhm of the Ag 3d5/2 peak for a sputtered silver foil was 0.6 eV. The spot size was 3.5 mm by 0.5 mm.

### 7.1.6 Stimulus Activated Surface Functionalization (Fluorescence)

For the DA surface confined reaction, firstly a voltage of +650 mV for 60 s was applied to SAM **S1** in order to oxidize the HQ groups of the SAM. The resulting

SAM **S2** was then rinsed with MQ-water and immersed in a 20 mM solution of fluorescent Cp-terminated derivative **3** in THF:water (1:1) for 30 minutes to give the SAM **S3-FC**. For the MA surface confined reaction, SAM **S2** was obtained as explained above. Thereafter, it was immersed in a solution of fluorescent thiolated molecule **4** in a mixture of EtOH:water (9:1) to give the SAM **S4-FC**. To optimize the homogeneity of the pattern, different experimental conditions were tested. Specifically, the concentration of molecule **4** was varied from 10 μM to 20 mM and the immersion times ranged from 30 min to overnight. After functionalization, the substrates were rinsed with MQ-water and characterized by fluorescence microscopy.

### 7.1.7 Fluorescence Microscopy

Fluorescein functionalized substrates (**S3-FC** and **S4-FC**) were observed with an Olympus BX51 microscope equipped with a CCD camera Olympus DP20.

## 7.2 Chapter 3

### 7.2.1 SAM Preparation for Cell Adhesion

SAMs with a 1:99 ratio of molecules **2** and **1** (Figure 2.7) and final concentration of 1 mM in absolute ethanol were prepared using substrates consisting of glass coverslips with a 2 nm titanium adhesion layer and a 10 nm layer of gold. SAM formation was achieved by incubation in the mixed thiol solution overnight.

Four SAMs were prepared in order to have two $\mathbf{t_0}$ samples, one sample biofunctionalized via the DA reaction and another one via the MA reaction. A plain glass coverslip was used as positive control, by incubating it with a fibronectin solution (2 μg/mL) during 1 hour.

Therefore, for each experiment, 2 samples were oxidized for 20 seconds using a potential of 0.8 V and these, together with the $\mathbf{t_0}$ samples, were incubated for 1 hour in a 15 mM solution of molecule **3** and molecule **4** (Figure 2.7), in order to perform the DA reaction and the MA reaction, respectively.

### 7.2.2 Cell Culture Protocols for Cell Adhesion Experiments

#### Synthesis of Cp-RGD and SH-RGD

For solid phase peptide synthesis, the general process consists in the synthesis of peptides on a resin by firstly attaching the first amino acid, from the C-terminal residue (carboxyl group), and then proceeding with the peptide sequence construction towards the N-terminal end.

Thereafter, the amino acids are coupled to the resin supported peptide sequence by the alpha amino group and the reactive side chains are protected by a temporary protecting group, normally Boc or Fmoc groups. More concretely, the carboxyl group of the corresponding amino acid must be first activated for its coupling to the resin. After the amino acid is attached, the resin is filtered and washed to remove byproducts and excess of reagents. Afterwards, the Na-$\alpha$-protecting group of the new coupled amino acid is removed, as part of the deprotection process, and the resin is again washed to remove byproducts and excess reagents. Then, the next

amino acid is coupled to the attached one. This cycle is repeated until the peptide sequence is completed and then finally all the protecting groups are removed, the resin is washed and the peptide is cleaved from the resin [338].

Synthetic routes of **Cp-RGD** and **SH-RGD** are shown in Schemes 7.16 and 7.17.

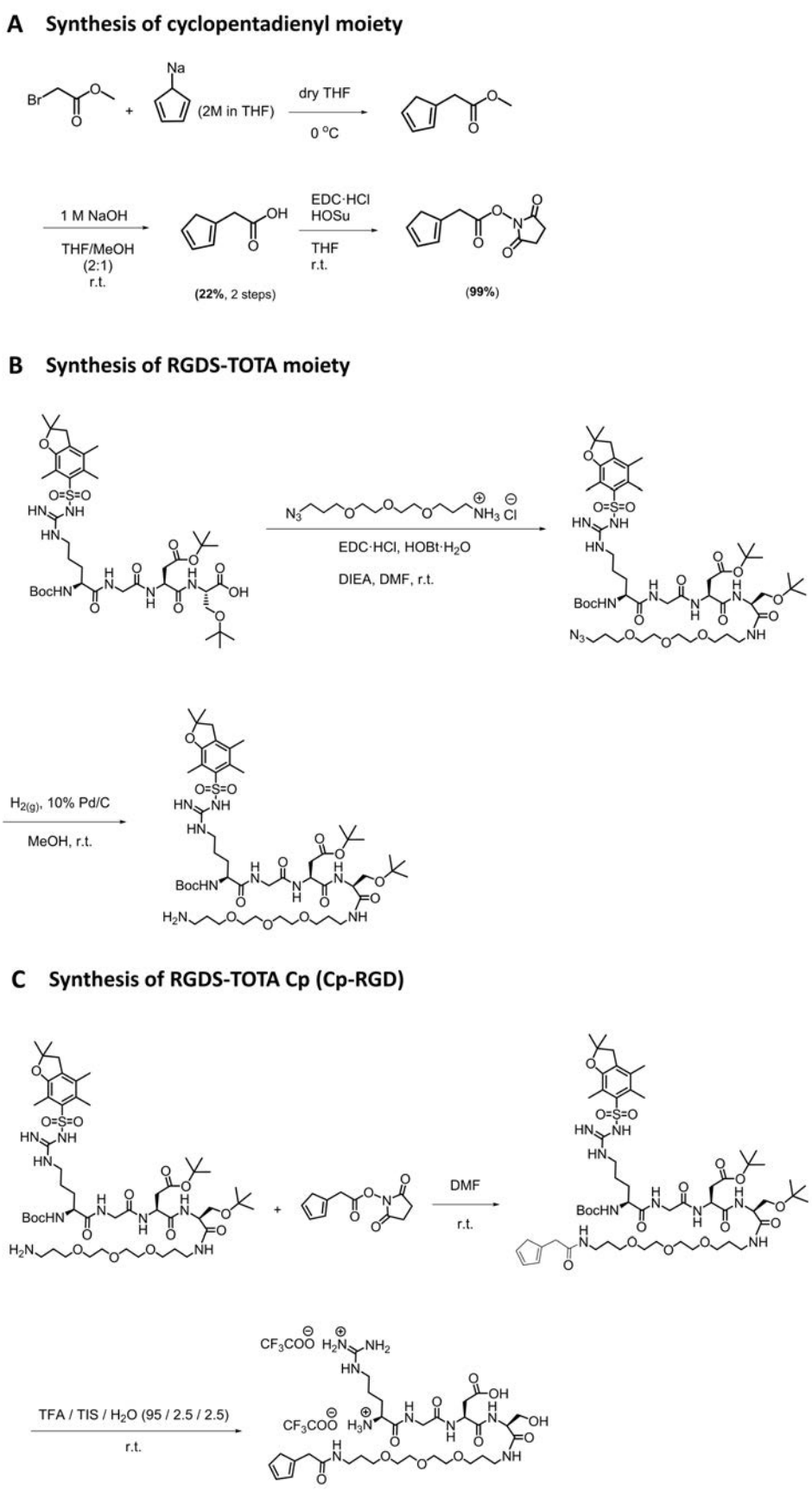


**Scheme 7.16:** Synthetic pathway of **Cp-RGD**. This was carried out by the Combinatorial Chemistry Unit (Technology Platform of the Barcelona Science Park).

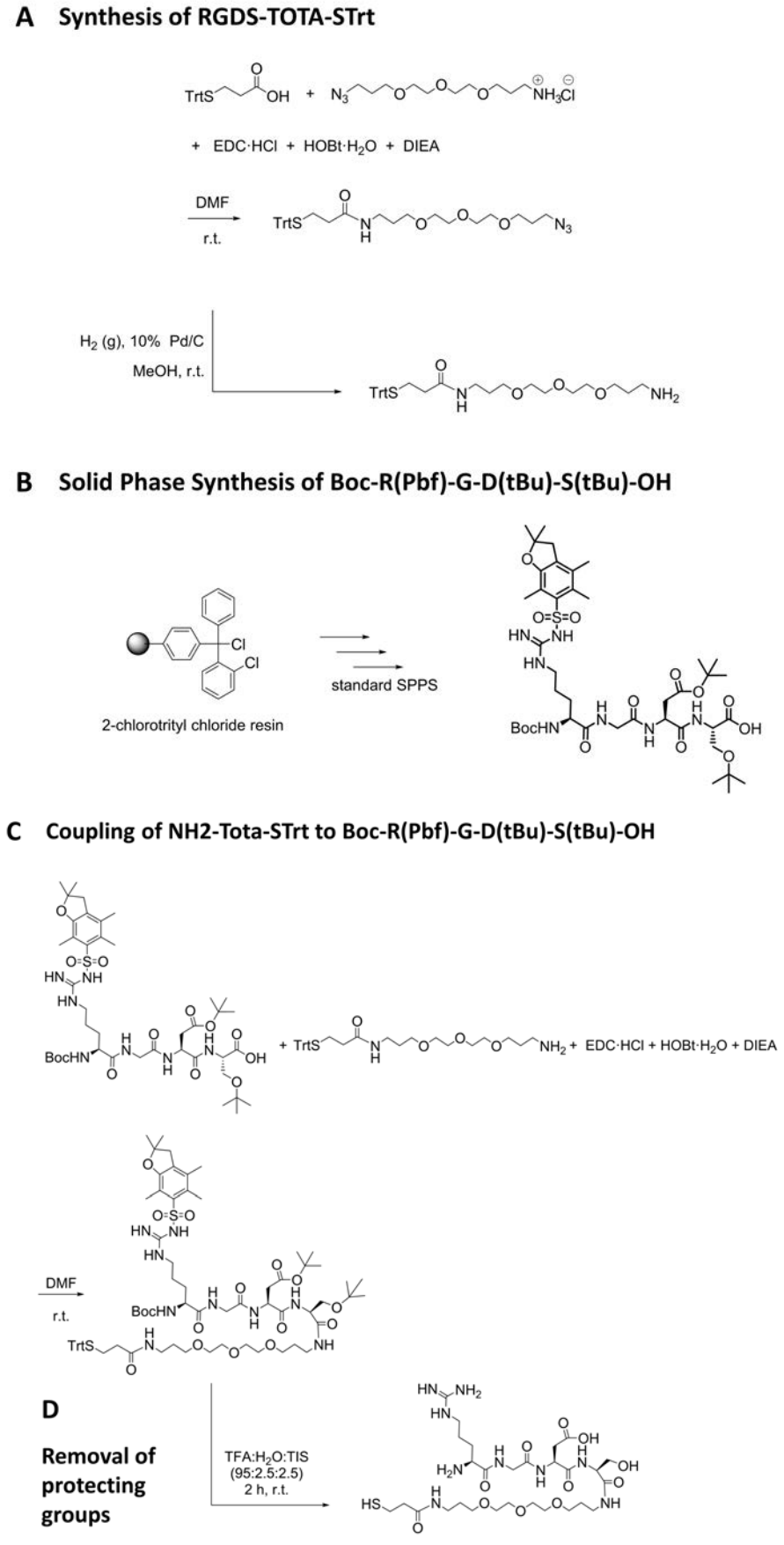


**Scheme 7.17:** Synthetic pathway of **SH-RGD**. This was carried out by the Combinatorial Chemistry Unit (Technology Platform of the Barcelona Science Park).

#### Cell Culture Medium Preparation

Cell culture medium was prepared using Dulbecco's Modified Eagle Medium (DMEM) with 10% FBS and 1% Penicillin Streptavidin.

#### Cell Thawing

A frozen vial containing 1 million cells (Human osteosarcoma cells, U2OS) was introduced into a hot bath during 1-2 minutes to unfreeze. Culture medium (15 mL) was added into a 75 mL flask, together with the content of the vial and was left in the incubator for a couple of days at a temperature of 37 °C and 15 % of $CO_2$.

#### Cell Seeding

The medium was removed and PBS (6 mL) was added and thereafter removed. Tripsin (3 mL) was then added and the flask incubated during 3 minutes at 37 °C and 15% of $CO_2$. Proper detachment of the cells from the flask was checked using the microscope. Therafter, cell medium (6 mL) was added to neutralize the tripsin and all the content was moved into a falcon tube. The tube was centrifuged during 5 minutes at 1400 rpm. The supernatant was removed and the pellet was resuspended in 2-3 mL of cell medium. A 1 to 10 dilution in trypan blue was prepared and cells were counted using a Neubauer chamber.

#### Cell Seeding on Functionalized SAMs

After incubation the substrates were rinsed with MQ-water. Before cell seeding, substrates were rinsed three times with sterile PBS. Thereafter, 45.000 cells were seeded onto each substrate and the wells were filled with cell medium. Substrates were incubated overnight at 37 °C and 15 % of $CO_2$. For cell fixation firstly some drops of 4% PFA were added onto the medium covered substrates, before totally immersing substrates in PFA and fixing the samples during 20 minutes. Finally, substrates were carefully rinsed with PBS.

### 7.2.3 Cell Immunostaining

After cell fixation, cells were permeabilized by adding 0.1% Triton in PBS and treated with a blocking solution (1% bovine serum albumin, BSA, in PBS) for 30 minutes to prevent unspecific binding. After blocking, substrates were incubated 1 hour at RT with a mouse monoclonal anti-paxillin antibody (Sigma-Aldrich, USA) diluted to 1:400.

After incubation with the primary antibody, samples were washed with PBS on a shaker at 50 rpm for 10 minutes, then they were incubated 45 minutes at RT with the secondary antibody Alexa Fluor 488 goat anti-mouse IgG (1:100; Thermo Fisher Scientific, USA) and with Hoechst (1:1000; Thermo Fisher Scientific, USA). Primary and secondary antibodies were diluted in the blocking solution.

Finally, samples were washed with PBS on a shaker for 10 minutes and mounted onto glass slides with ProLong Gold Antifading Mountant (Thermo Fisher Scientific, USA).

### 7.2.4 Confocal Imaging

A Leica TCS SP5 confocal microscope (Leica Microsystems, Germany) was used for image acquisition. A hybrid HyB laser was used for the excitation of both dyes (with wavelengths 488 nm for Alexa 488 and 361 nm for Hoechst). Captures were taken at 20X and 63X (and 1.7 zoom) magnifications in order to obtain both, the general distribution of cells, and more detailed pictures of single or few cells. The images were treated and analyzed using the Image J software, and cell density, cell spreading and focal adhesion area quantification was performed.

### 7.2.5 Confocal Image Analysis Using ImageJ Software

For cell spreading quantification Image J was used to manually delimit cell contour, as shown in Figure 7.17.

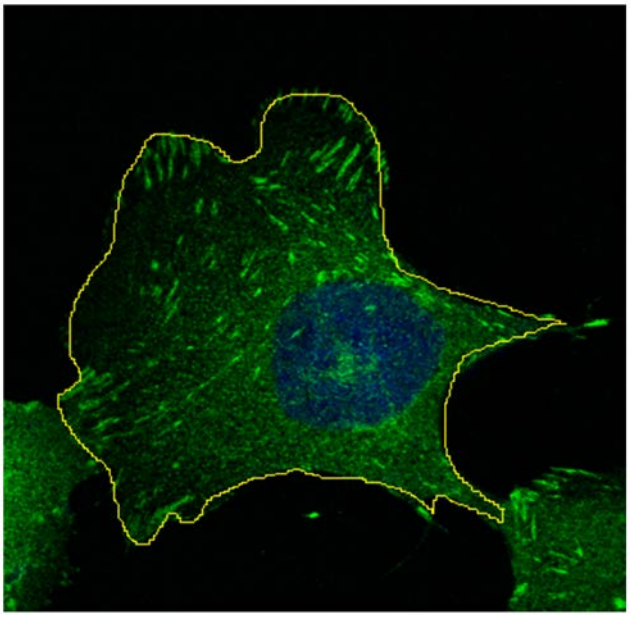

**Figure 7.17:** Example of cell contour delimitation using the Image J software.

In order to be able to quantify the area of FAs per cell or group of cells, the following protocol was used for image processing:

1. Open the image using split channel and keep the green channel.
2. Duplicate the image and start working with the duplicate.
3. Process-enhance contrast-set saturation to 1%.
4. Process-Math-Subtract 30.
5. Process-Subtract Background using sliding paraboloid.
6. Process-Filter-Median 2.0 pixels.

7. Image-Adjust Threshold (255 and 75)-Apply.
8. Analyze-Set Measurements- Tick the following: Area, Intensity density, Area fraction, Limit to threshold, Display label, Decimal places:5.
9. Check the size of the largest and smallest focal adhesion with the magic wand using the ROI manager and measure command.
10. Analyze particles, setting Circularity to 0-1, limit the size of the particles using the data obtained from the ROI manager, show outlines, display results, clear results, summarize, add to manager, exclude on edges and include holes.
11. Superimpose ROIs found on the color image and correct if necessary by deleting or adding more ROIs.
12. From the ROI manager-More-Multi Measure.
13. Export results to spreadsheet.

In some cases if the image had a lot of background, instead of counting particles it was best to use the magic wand to manually select the FAs. See Figure 7.18 for an example.

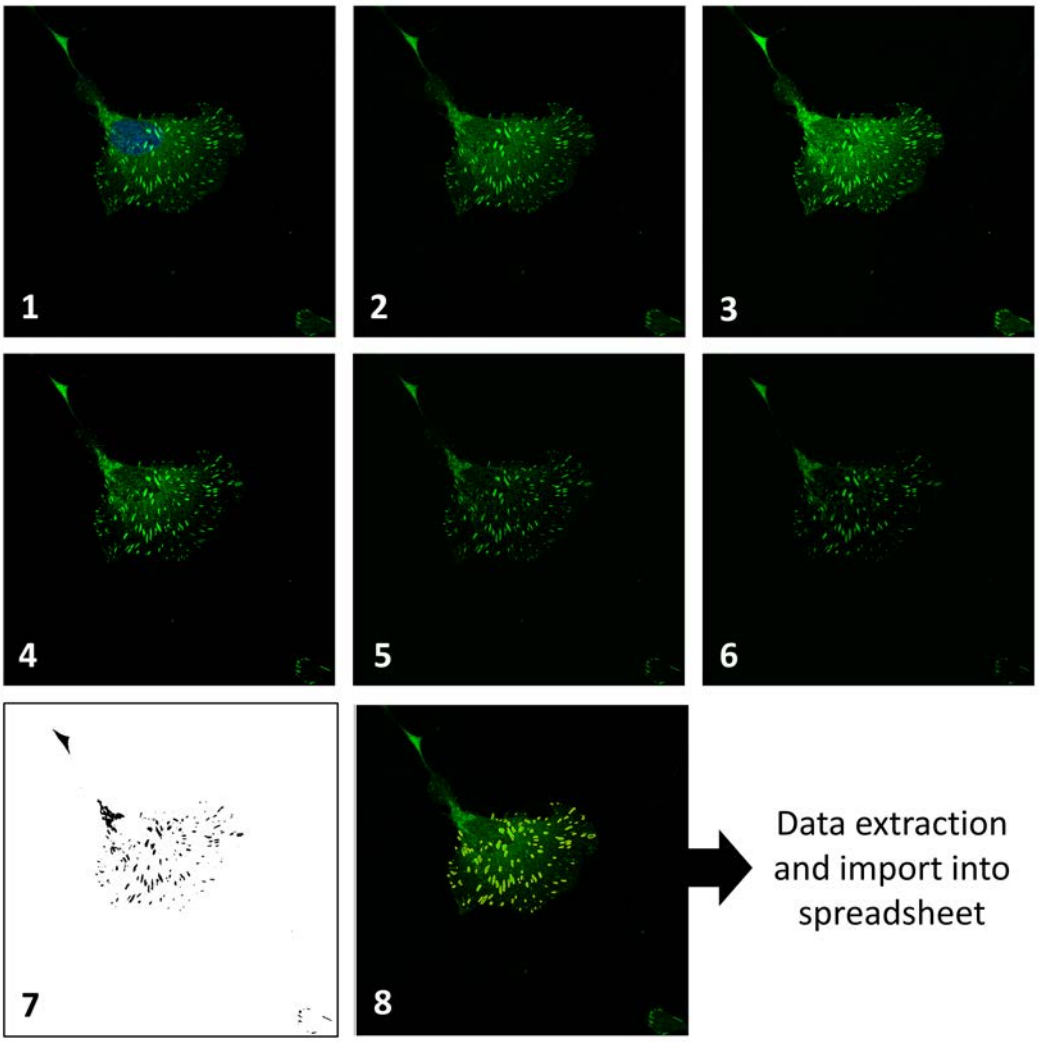


**Figure 7.18:** Example of image treatment (positive control, U2-OS cells on fibronectin coated gold covered coverslips) for extraction of information concerning focal adhesion quantification. (1) Original Image, (2) Green channel, (3) Saturated Image, (4) Image after Math operation, (5) Image after background subtraction, (6) Image after Median Filter, (7) Thresholded Image, (8) ROIs superimposed on RGB image.

### 7.2.6 Experiments with Qk-decorated substrates

#### Synthesis of Molecules

The VEGF mimicking peptide **SH-Qk** was synthesized using standard protocols for solid phase peptide synthesis (Scheme 7.18).

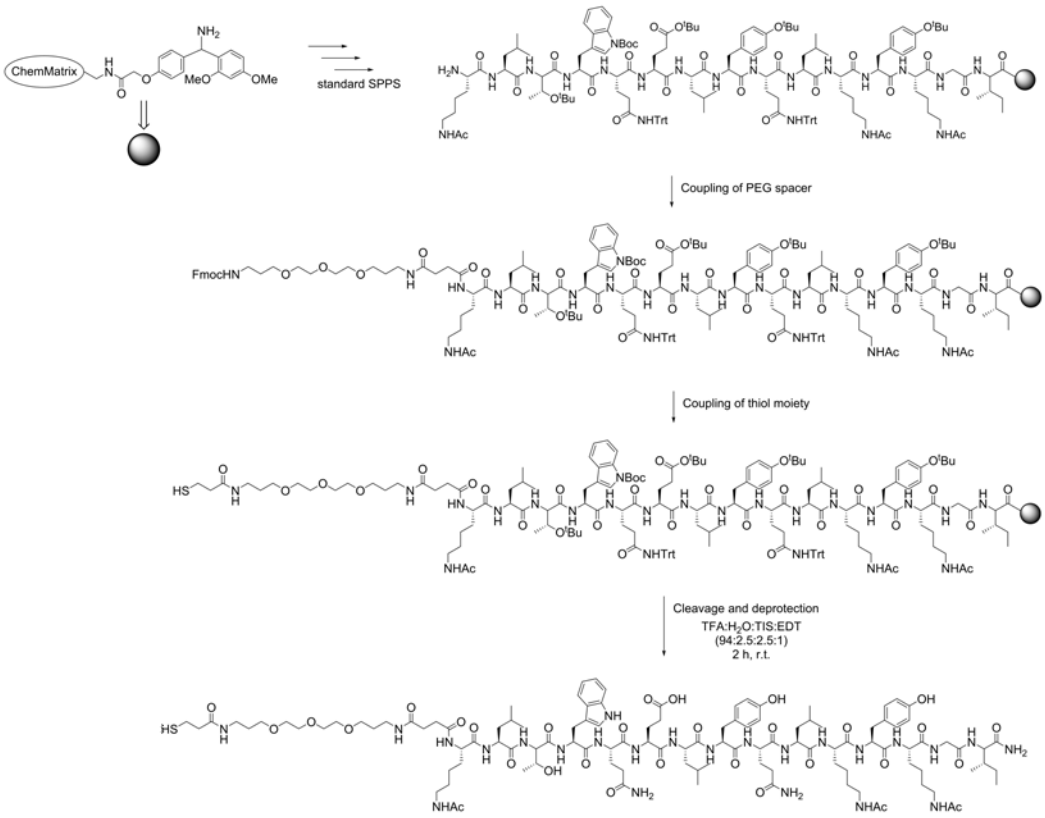


Scheme 7.18: Synthetic pathway of **SH-Qk**. This was carried out by the Combinatorial Chemistry Unit (Technology Platform of the Barcelona Science Park).

### Sample Preparation

**Substrate Cleansing** As done previously, glass coverslips coated with 2 nm of titanium and 10 nm of gold were cleaned using isopropanol, acetone and ethanol (HPLC grade), during 5 minutes in each solvent. Thereafter, substrates were treated with ozone (UVO CLEANER, Model No. 42-220) for 20 minutes an left immersed in ethanol for at least 30 minutes. Prior to functionalization substrates were dried with a nitrogen stream.

### SAM Formation

**S-cRGD: SAMs 1:9 PEG-SH:Qk-SH** Cleaned and dried substrates were coated with an aqueous solution containing **SH-PEG** and **SH-cRGD** in a 1:9 molar ratio with a final concentration of 1 mM.

**S-Qk: SAMs 1:9 PEG-SH:cRGD-SH** Cleaned and dried substrates were coated with an aqueous solution containing **SH-PEG** and **SH-Qk** in a 1:9 molar ratio with a final concentration of 1 mM.

**S-cRGD-Qk: SAMs 1:4.5:4.5 PEG:cRGD-SH:Qk-SH** Cleaned and dried substrates were coated with an aqueous solution containing **SH-PEG**, **SH-cRGD** and **SH-Qk** in a 1:4.5:4.5 molar ratio with a final concentration of 1 mM.

**S-Fibro: Fibronectin coated coverslips** Glass coverslips were coated with a fibronectin solution of 2 μg/mL in MQ-water.

All substrates were functionalized in a humid chamber using the humid chamber setup (Figure 3.8) for 1 hour. A volume 100 μL of thiol solution was used for each sample incubation.

### 7.2.7 Cell Culture Protocols for Tubulogenesis Assay

#### Functionalized Substrate Sterilization

Before proceeding to cell seeding the substrates were sterilized by immersing them in absolute ethanol: each substrate was inserted in petri dish (p60) and 3 mL of ethanol were added to each petri. The ethanol was left to evaporate in a cabin with laminar flow. These were then inserted in a new well plate and sterile PBS was added into each well. After 3 minutes, the PBS was discarded and new sterile PBS containing 4 types of antibiotics was added into each well. The antibiotics used were Hygromicine [100 mg/mL] (InvivoGen) with a concentration of 200 μg/mL, Geneticine [100 mg/mL] (InvivoGen) with a concentration of 200 μg/mL, Puromicine [10 mg/mL] (Gibco) with a concentration of 5 μg/mL and Streptomicine [10000 μg/mL] (Merck) with a concentration of 20000 μg/mL. Substrates were left in this solution overnight.

#### Cell Seeding

Before proceeding to cell seeding, substrates were transferred into a clean p60 and they were immersed in sterile PBS during 20 minutes. Plated HUVEC cells were trypsinized and counted. Substrates were transferred to a 6-well plate and seeded with 750.000 cells, and each well was filled up with 2 mL of cell culture medium (EGM-2, Lonza). Substrates were then incubated during 1.5 hours at a temperature of 37 °C and 5% of $CO_2$. Images were then captured and the cell medium was changed by adding fresh EGM-2. After 5 hours new captures were taken.

### 7.2.8 3D Scaffold: Substrate Mounting onto Matrigel

Previous to mounting the substrates onto the Matrigel films, images were captured for each sample. Substrates were firstly immersed in PBS for approximately 5 minutes. Approximately a volume of 300 mL of cold Matrigel was painted onto an area of the size of the substrates on a p60. After 5 minutes, after the Matrigel had begun to slightly polimerize, substrates were carefully dropped onto the Matrigel layer having the face with the cells attached facing the Matrigel (Figure 3.17). Another 5 minutes were left for the substrate to attach well onto the Matrigel and thereafter around 2-3 mL of EGM-2 cell medium was added into each p60. These were left in the incubator and images were captured after 10 minutes, 5 hours and 18 hours.

### 7.2.9 Viability Assay

The AB (AlamarBlueTM, Biosource) cell viability assay was performed on samples incubated in Matrigel. The cell medium of the p60 dishes with the substrates was discarded and 3 mL of EGM-2 with 10% AB was added to these. As control, a solution of EGM-2 with 10% AB was used. In order to discard existence of contamination, 1 mL of discarded medium was mixed with a solution of EGM-2 with FBS and AB (both at 20%). Also another mL from the discarded medium was centrifuged at 1200 rpm during 5 minutes and the pellet resuspended in 2 mL EGM-2 with AB at 10%. Prepared samples were left in the incubator during 3 hours, at 37 °C and 5% $CO_2$. A volume of 200 μL of each sample was inserted in 96 well plate to read the fluorescence intensity at 590 nm using a microplate reader (Synergy4).

### 7.2.10 Cell Fixation

Before proceeding to cell fixation the AB solution in the p60 petri dishes was discarded and the substrates on Matrigel were rinsed with sterile PBS twice. Thereafter, 4% PFA was added until covering the substrate and these were left immersed in PFA for 40 minutes to fix the cells. After discarding the PFA solution, substrates were immersed in 4 mL of PBS with 0.1% PFA and stored in the fridge at 4 °C until proceeding to their staining.

### 7.2.11 Immunostaining

Substrates in the p60 petri dishes were rinsed twice with sterile PBS and thereafter 3 mL of Triton (0.1% in PBS) was added to each substrate and left for 15 minutes. Substrates were then rinsed once more twice with PBS before adding a solution of 2.5 mL of phalloidin 647 (1:200 in PBS) during 45 minutes while kept protected from the light. Substrates were then rinsed with PBS and 2.5 mL of a Hoechst solution (1:1000 in PBS) was added to each substrate for 10 minutes. These were then rinsed and left in PBS at a temperature of 4 °C until their visualization with the confocal microscope.

### 7.2.12 Imaging

Phase contrast images were taken with an Olympus BX41 and a camera Olympus DP20. Fluorescent images were taken with a Leica TCS SPE (Leica Microsystems), using the 10X dry objective.

## 7.3 Chapter 4

### 7.3.1 SAM Formation

Substrates used consisted in glass coverslips of 22 × 22 mm with a 2 nm titanium adhesion layer and 10 nm of gold. The gold layer was thin enough for the substrates to be translucid. Substrates were cleaned by immersion in isopropanol, acetone and ethanol (HPLC grade), exposed to ozone for 20 minutes and immersed in absolute ethanol (HPLC grade) during 30 minutes. Finally, substrates were dried with a stream of nitrogen and incubated with a solution containing molecules **1** and **2**

(Figure 2.7). Substrates were left in contact with the thiol solution overnight and were rinsed with absolute ethanol before using them further. The ratio between molecules **1** and **2** was varied depending on the sample prepared, but the final concentration was always 1 mM in absolute ethanol.

### 7.3.2 GUV Formation

Bifunctional GUVs were prepared through the electroformation methodology using POPC, DPTTE and Rho-PE (Figure 4.8), all purchased from Avantilipids™. The specific steps followed for the electroformation of GUVs were the following:

- Solutions of lipids in chloroform were prepared from pre-made stock solutions to finally make a solution containing 89% POPC, 10% DPTTE and 1% Rho-PE with a final concentration of 1 mg/mL.
- A few droplets (a total volume of 2 μL) of the lipid solution were placed onto a clean ITO covered glass slide with copper tape connections. These were left to dry under vacuum during 2 hours.
- Thereafter, the ITO-glass slides were sealed with a homologous substrate on top using white clay while (CritoSeal) creating a well inside with a spacer of approximately 2 mm. An aqueous solution of sucrose (315 mM) was added into the well. Glass slides were fitted between the two ITO covered glass slides on each side in order to ensure no contact between the ITO layer and the copper tape to avoid a short circuit (see Figure 4.9).
- The copper tape ends were connected to the function generator and an alternating potential difference was applied of approximately 1 V. This was confirmed with the multimeter. The frequency was set to 10 Hz (T61010 Programmable 10 MHz DDS Function Generator). The setup was mounted on a heating plate since at RT DPTTE is semi-solid. The temperature was set to 70 °C, samples were covered to avoid photobleaching of the fluorophores and they were left under these conditions during 2 hours.
- To check GUV formation a droplet of HEPES buffer (1M HEPES and 150 mM NaCl) (pH=7.42) and a small amount of GUV solution (≈2 μL) were disposed onto a glass slide and observed under the microscope using phase contrast or fluorescence (Figure 7.19).

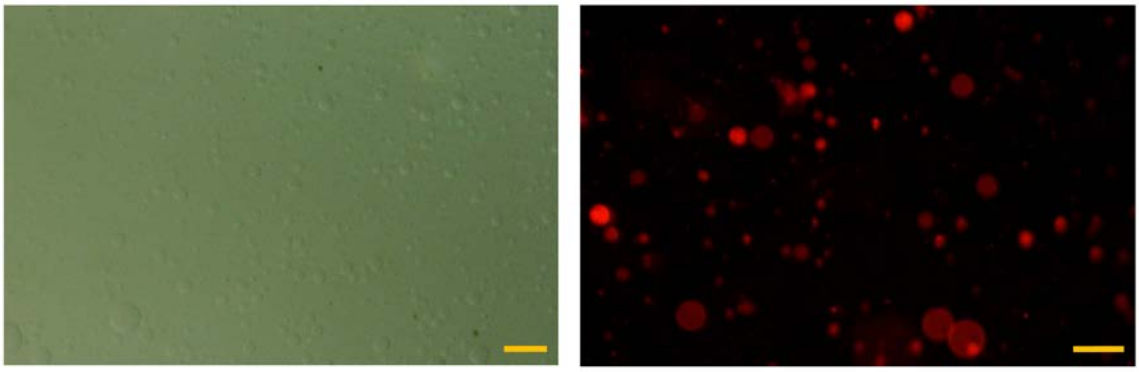


Figure 7.19: (A) Bright field image (scale bar=100 μm) and (B) fluorescence image (scale bar=30 μm) of formed bifunctional GUVs.

### 7.3.3 Sample Preparation

Lipid bilayers were formed by GUV rupture on the prefunctionalized substrates. This was achieved by confining a small volume of HEPES buffer (≈ 100 μL) using a PDMS well in contact with the substrate and adding 10-20 μL of GUV solution. The sample was left incubating for minimum 1 hour and thereafter it was rinsed thoroughly with HEPES buffer.

**Electrochemical Setup** For oxidation of SAM **S1** to **S2** a 3-electrode electrochemical setup was used, the same one described in Section 7.1.3. The electrolyte used was PBS, which was purged with nitrogen before its use. A voltage of 0.8 V during 40 s was applied to ensure the oxidation of the electroactive moieties on surface.

### 7.3.4 FRAP Analysis

The microscope used for imaging and FRAP measurements was an Olympus FV1000 with inverted microscope. The settings for image acquisition and photobleaching were the following: acquisition of 3 pre-bleach images, photobleaching during 2 seconds and acquisition of images to monitor fluorescence recovery every 0.244 seconds during 99.6 seconds to have a total of 400 frames. Images were taken with a 60X water immersion objective and the power of the laser (wavelength=561 nm, TRITC) was set to 100% for photobleaching and 5% for pre- and post-bleaching image acquisition. The radius of the FRAP ROI used was between 5 μm and 7 μm, depending on the sample. At least three FRAP measurements were performed in different patches for every sample.

The fitting of the curves was performed using the Igor plugin developed by Kota Miura (CMCI, EMBL).

## 7.4 Chapter 5

### 7.4.1 Substrate Preparation

#### Patterned Substrates

The substrates used were either glass slides with a 10 nm gold layer and a 2 nm Ti adhesion layer or silicon wafers with a 100 nm gold layer and a 50 nm Ti adhesion layer. Substrates were cut to have an area of 1.5×1 cm. The optimized protocol used to prepare Ni-NTA SAMs and the subsequent immobilization of His-tagged proteins was the following:

1. Substrates were cleaned following the standard protocol, which consisted in immersions in HPLC gradient solvents during 5 minutes: first isopropanol, then acetone, and lastly ethanol.
2. After drying them with the nitrogen gun very carefully, they were exposed to ozone (UVO CLEANER, Model No. 42-220) during 20 minutes.
3. Substrates were then immersed in ethanol during 30 min.
4. For the μCP procedure, the PDMS stamp of interest was cut with a scalpel, rinsed with ethanol and dried off with a stream of nitrogen.
5. A solution of **SH-PEG** (ProChimia Surfaces, Figure 5.4) 1 mM in ethanol was dropped (40 μL) on top of the PDMS stamp. The stamp was then dried off with the nitrogen gun.
6. Substrates were then printed with the inked stamp by carefully placing the stamp on the substrate and leaving them in contact for 2 minutes. An empty and flat petri dish was placed on top of the stamp to increase and homogenize the pressure.
7. The stamp was removed carefully with tweezers and substrates were incubated with 80 μL of **SH-NTA** (ProChimia Surfaces, Figure 5.4) 1 mM in ethanol in a humid chamber during 2 h at RT.
8. Substrates were transferred to a 6-well plate to perform the following immersions:
    - In MQ-water during 5 min (×2).
    - In HEPES buffer solution for 10 min (×1).
    - In 10 mM $NiCl_2$ in HEPES during 30 min at RT.
    - In HEPES for 2 min (×3).
9. Substrates were incubated with the His-tagged protein (His-antimicrobial or His-GFP) in a humid chamber during 1 h at RT.
    - For the preliminary trials, 45 μL of 0.735 mg/mL of His-GFP was used and the petri dish was covered with aluminium foil to avoid photobleaching.

- For the antimicrobial proteins, 50 μL of 0.735 mg/mL and 50 μL of 1.24 mg/mL for soluble antimicrobial protein and antimicrobial IBs, respectively, were used.

10. Samples were immersed in HEPES during 5 min (×2). For the negative control samples, a further treatment with EDTA was performed. EDTA acts as a competitive chelator for NTA, because it cleaves the chelated Ni from NTA to form a Ni-EDTA complex. The effectiveness of this competition lies on the higher stability constant of the Ni-EDTA complex (18.56 in logarithmic) than the Ni-NTA complex (11.26 in logarithmic) [339]. As a consequence, the His-tagged protein can no longer bind to the NTA SAM. The detailed steps were the following:
    - Substrates were immersed in 100 mM EDTA solution (or 10 mM) during 20 minutes and rinsed again with HEPES afterwards.
    - If they were not characterized straight away, substrates were left immersed in HEPES in the fridge at 4 °C.

The pH of both HEPES and EDTA solutions were adjusted before their use to values of 8 and 7.31, respectively, using 0.1 M NaOH and 0.1 M $H_2SO_4$ solutions for the adjustment.

#### Non-patterned Substrates

For non-patterned substrates no μCP was performed, and instead the entire area of the surface was functionalized with NTA.

### 7.4.2 Immunostaining

The immunostaining steps performed were the following:

1. After protein immobilization, substrates were incubated with a solution of primary antibody sPLA2 (E-9) in a ratio of 1:400 in BSA solution (1% in PBS). Each substrate was incubated with 50 μL in a humid chamber for 1 hour.
2. Substrates were rinsed in PBS on the shaker at 50 rpm during 10 minutes.
3. Substrates were incubated with a solution of a second antibody, Alexa mouse 488, in a ratio of 1:100 in BSA solution. Again, each substrate was incubated with 50 μL on parafilm in a dark humid chamber for 45 minutes.
4. Substrates were rinsed in PBS on the shaker at 50 rpm during 10 minutes.
5. Substrates were mounted on glass slides with 50 μL of ProLong Gold Antifade Reagent (Thermo Fisher Scientific, USA). They were left to dry overnight in a dark chamber.
6. After drying they were observed with fluorescence microscopy.

### 7.4.3 Fluorescence Microscopy

The instrument employed for visualization of the samples was an Olympus BX51 microscope equipped with a CCD camera Olympus DP20 for His-GFP samples and an Axio Observer Z1m optical microscope (ZEISS) for the rest of the samples. The software ImageJ was used to extract the intensity profile of the striped pattern. The substrates observed were the following: patterned Ni-NTA-PEG SAMs with immobilized His-GFP and immunostained patterned Ni-NTA-PEG SAMs with immobilized antimicrobial protein (soluble and IBs).

### 7.4.4 Cyclic Voltammetry

A solution of 5 mM of $[Ru(NH_3)_6)]^{3+}$ was prepared in an electrolyte solution consisting of a 50 mM KCl aqueous solution. A platinum wire was employed as the CE and a Ag/AgCl electrode as the RE. The WE was, depending on the measurement, the bare gold substrate, the gold substrate functionalized with an NTA-terminated SAM, the gold substrate with immobilized His-tagged antimicrobial protein (soluble and IBs) and, to compare, His-GFP on the NTA-SAM.

The potentiostat used was an AUTOLAB 204 and the software used for the data acquisition and analysis was Nova 2.3. The scan rate used was 0.1 V/s and the area of the working electrode immersed into the electrolyte solution was around 1.5 $cm^2$.

### 7.4.5 X-Ray Photoelectron Spectroscopy

X-ray photoelectron spectroscopy measurements were performed with a Phoibos 150 analyzer (SPECS GmbH) under ultrahigh vacuum conditions (base pressure 5×10-10 mbar) with a monochromatic aluminum K alpha X-ray source (1486.74 eV). The energy resolution measured by the FWHM of the Ag 3d5/2 peak for a sputtered silver foil was 0.6 eV. The spot size was 3.5 mm by 0.5 mm. Compositional survey and detailed scans (C 1s, O 1s, N 1s, S 2p, and Ni 2p) were acquired. The samples measured were Ni-NTA SAMs on gold with (i) immobilized His-tagged soluble antimicrobial proteins, (ii) immobilized His-tagged antimicrobial IBs, (iii) negative control of immobilized soluble protein (by treatment with EDTA 10 mM), (iv) negative control of immobilized IBs (by treatment with EDTA 100 mM), (v) Ni-NTA SAM, and (vi) NTA SAM. In all substrates, the prepared NTA-SAM was not patterned, which is to say, the incubation with **SH-NTA** was done directly without previous μCP of **SH-PEG**.

### 7.4.6 Atomic Force Microscopy

Surface topography and film thickness were examined by a 5500LS SPM system from Agilent. Images were processed with the Gwyddion software. The samples analyzed had 2 μm striped patterns of novel antimicrobial protein (soluble and IBs) immobilized on Ni-NTA SAMs, and their respective negative controls prepared by immersion in EDTA (100 mM).

### 7.4.7 Antimicrobial Assay

A culture of *Escherichia coli* DH5$\alpha$ was grown overnight reinoculated again in LB + 0.2% glucose, diluted by a factor of 200. The following samples were prepared in triplicate: (i) immobilized antimicrobial soluble proteins on Ni-NTA SAM using 2 different concentrations, (ii) immobilized antimicrobial IBs on Ni-NTA SAM and (iii) NTA-SAM.

Specifically, previously functionalized NTA-Ni substrates were incubated with 20 and 0.5 μM of soluble protein and 1.24 mg/mL of IB protein during 1 hour at RT in a humid chamber. These were then rinsed 2× with buffered potassium phosphate solution (KPi) during 5 minutes, transferred to a sterile well and cell culture medium was added. The samples were incubated overnight at 37 °C.

The supernatant was carefully retrieved and samples were washed 3× with 500 μL of a solution of 0.9% NaCl which had been previously sterilized. Cells were then fixed with 500 μL absolute methanol (MetOH) for 5 minutes. MetOH was then removed and substrates were then dried at 37 °C for 15 minutes. Following, a staining with crystal violet was performed by adding 500 μL of a 1% solution, and letting samples rest for 15 minutes. The supernatant was then retrieved and substrates were washed 3× with water. For absorbance measurements, the stained bacterial films were dissolved with 100 μL of acetic acid (33% in water) and this volume was introduced into an elisa plate. Absorbance was read at 595 nm with a microplate reader (Biorad Model 680 XR reader).

## References

[335] M. Jalal Uddin, M. Khalid Hossain, M. I. Hossain, et al. „Modeling of self-assembled monolayers (SAMs) of Octadecanethiol and Hexadecanethiol on gold (Au) and silver (Ag)“. In: *Results in Physics* 7 (2017), pp. 2289–2295 (cit. on p. 190).

[336] H. Ron and I. Rubinstein. „Alkanethiol Monolayers on Preoxidized Gold. Encapsulation of Gold Oxide under an Organic Monolayer“. In: *Langmuir* 10.12 (1994), pp. 4566–4573 (cit. on p. 190).

[337] Y. Xue, X. Li, H. Li, and W. Zhang. „Quantifying thiol–gold interactions towards the efficient strength control“. In: *Nature Communications* 5.1 (2014), p. 4348 (cit. on p. 190).

[338] J. M. Palomo. „Solid-phase peptide synthesis: an overview focused on the preparation of biologically relevant peptides“. In: *RSC Advances* 4 (62 2014), pp. 32658–32672 (cit. on p. 193).

[339] Inc. Dojindo Molecular Technologies. „Metal Chelates“. In: *Webpage* (Retrieved: December 2018) (cit. on p. 206).

# Annex

## *In situ* Cell Behavior Studies

### Electrochemical Cell Design for *in situ* Cell Culture Studies

In order to be able to study the whole process of adhesion, migration or differentiation in presence of specific immobilized biological ligands a tailored 3-electrode electrochemical cell with certain requirements should be designed and fabricated. Among others, the following specifications should be met:

- An electrochemical setup consisting of a 3-electrode configuration in which the substrate (translucid gold coated coverslip) is the WE, an Ag wire (a chloridized Ag wire) is the pseudo RE and a Pt wire is the CE.
- A setup which allows live cell imaging, implying its compatibility with inverted confocal /fluorescence microscopy. Therefore, dimensions and materials of the electrochemical cell have to be taken into account.
- The electrolyte and the cell media should be able to be confined onto patterned substrates (the area of the PDMS stamp is approximately 0.8 $cm^2$).
- The electrodes should have external and dry connections to the potentiostat. Also, these should to be placed in a practical way that facilitates its use with microscopy imaging in a chamber with controlled temperature and $CO_2$.
- The Ag and Pt electrodes should not touch the substrate nor should touch each other. The Pt wire should have an area immersed in the electrolyte approximately 10 times larger than the Ag wire. The Ag wire ideally should be positioned a few mm from the surface of the substrate (WE).

#### Already Existing Setups

After performing a literature research some similar published setups were found, but related mostly to cell sheet detachment studies. Nevertheless, surely, in-house and custom made electrochemical cells have been created for studying time dependent phenomena with cell cultures. Following, is a brief presentation of the setups reported in the literature that inspired the final design of our setup.

Published in Nature Protocols, a platform developed by Searson's group for triggering cell detachment from patterned electrode arrays by programmed subcellular release was developed and is shown in Figure A1 [71].

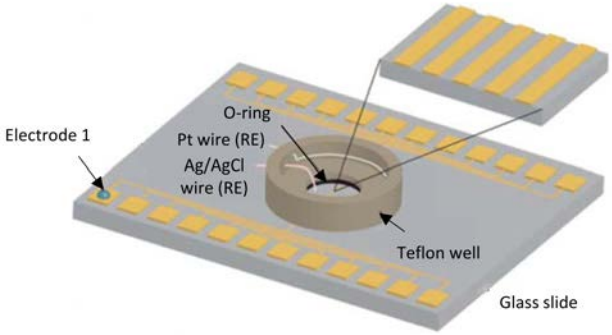


**Figure A1:** Illustration of the subcellular release device (comprising an electrode array and a teflon well) for cell detachment studies developed in the group of Searson. Reproduced from [71].

Another platform for cell detachment studies with an electrochemical control has been developed by Yoon et al. They manufactured an addressable, multifunctional, and reusable platform, termed the biological breadboard (BBB), for spatiotemporal manipulation of cell adhesion and detachment at cellular and subcellular levels (see Figure A2) [76].

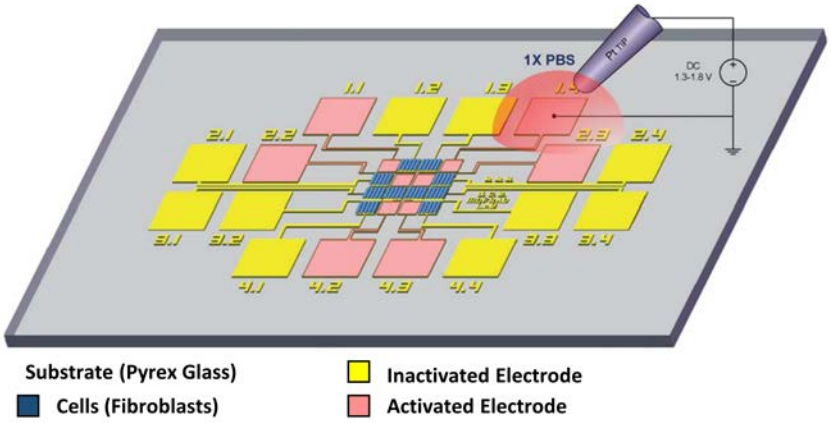


**Figure A2:** The biological breadboard platform (BBB) for the spatiotemporal manipulation of cell adhesion and detachment at cellular and subcellular levels. Schematic representation of the BBB consisting of gold electrodes patterned on a Pyrex substrate. Reproduced from [76].

The group of Fukuda in Japan developed a gold-coated membrane substrate modified with an oligopeptide layer that can be used to grow and subsequently detach a thick cell sheet through an electrochemical reaction (see Figure A3) [74].

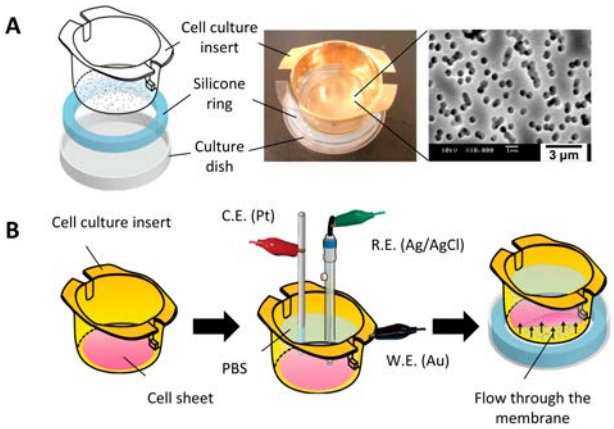


**Figure A3:** The setup used for thick cell detachment with an electrochemical control. (A) SEM image of gold-coated membrane substrate with pores of approximately 0.4 mm in diameter. (B) Procedure for the detachment of cell sheets. Working electrode (WE, gold-coated membrane), reference electrode (RE), and counter electrode (CE). Reproduced from [74].

Also, Fukuda's group developed an electrochemical approach for the fabrication of capillary-like structures, precisely aligned within micrometer distances, whose internal surfaces are covered with vascular endothelial cells [75], see Figure 2.4.

### Our Design

A series of designs have been developed to finally arrive to a final prototype (Figures A4, A5, A6, A7).[1]

[1]This was done with the aid of Miguel Garcia, engineer affiliated to the UPC (Universitat Politècnica de Catalunya).

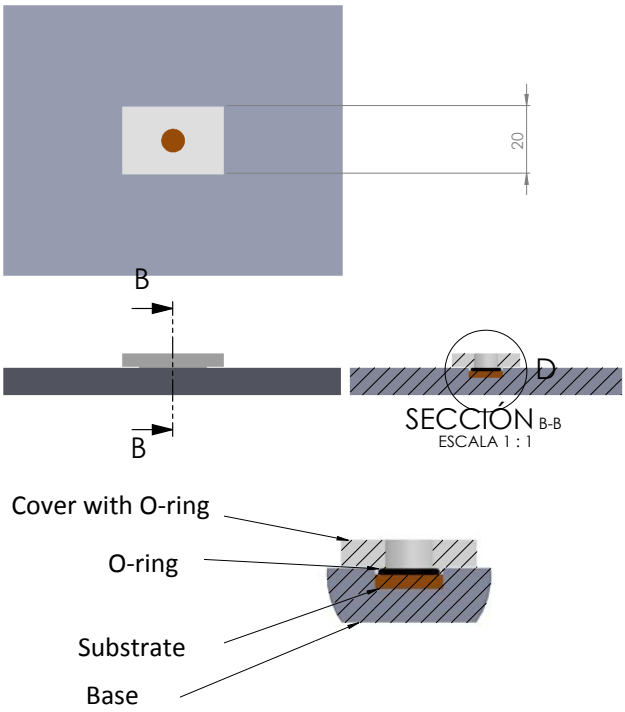


**Figure A4:** Initial design proposed for the setup, missing electrodes and translucid substrate to be able to observe with inverted microscopes.

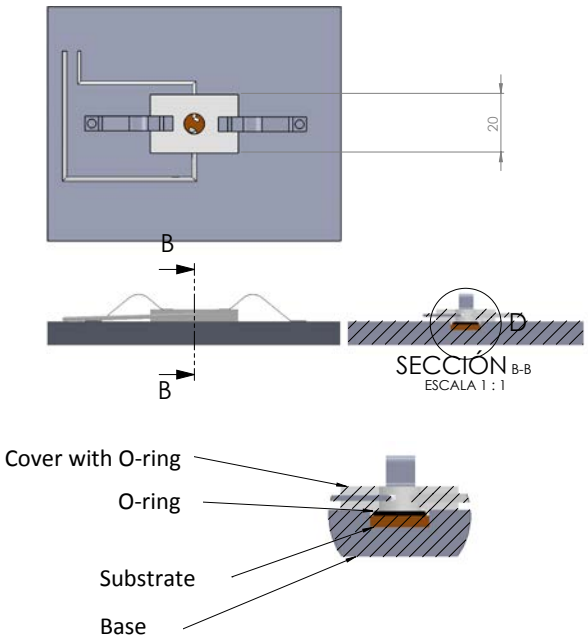


**Figure A5:** Design 2.

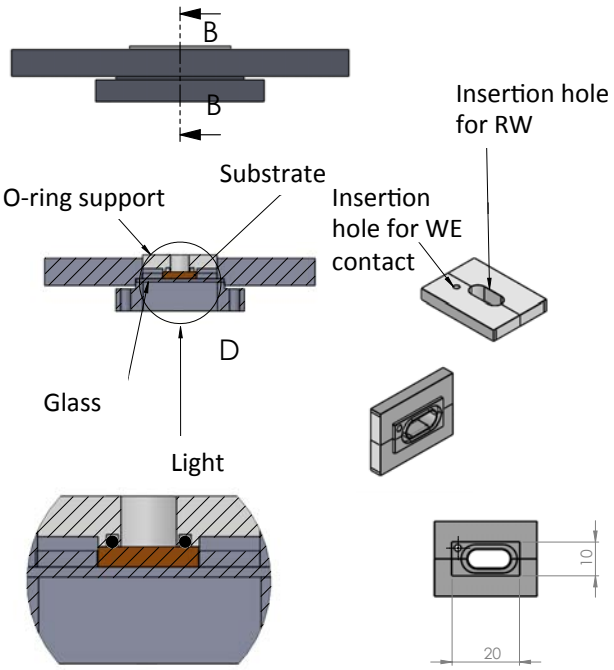


**Figure A6:** Design 3.

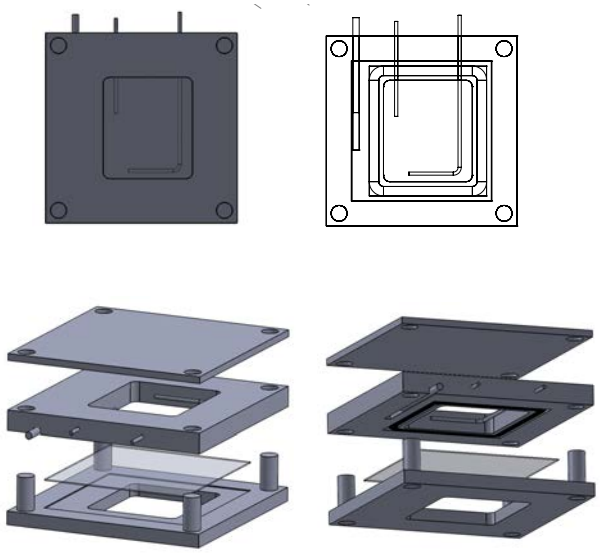

**Figure A7:** Final design of the electrochemical cell for *in situ* cell studies.

# References

[71] B. Wildt, D. Wirtz, and P. C. Searson. „Triggering cell detachment from patterned electrode arrays by programmed subcellular release“. In: *Nature protocols* 5.7 (2010), pp. 1273–1280 (cit. on pp. 28, 29, 211, 212).

[74] J. Enomoto, N. Mochizuki, K. Ebisawa, et al. „Engineering thick cell sheets by electrochemical desorption of oligopeptides on membrane substrates“. In: *Regenerative Therapy* 3 (2016), pp. 24–31 (cit. on pp. 28, 212, 213).

[75] Y. Seto, R. Inaba, T. Okuyama, et al. „Engineering of capillary-like structures in tissue constructs by electrochemical detachment of cells“. In: *Biomaterials* 31.8 (2010), pp. 2209–2215 (cit. on pp. 29, 213).

[76] S.-H. Yoon, J. Chang, L. Lin, and M. R. K. Mofrad. „A biological breadboard platform for cell adhesion and detachment studies“. In: *Lab on a Chip* 11.3555 (2011) (cit. on pp. 29, 212).

# Scientific Contributions

## Publications

Publications within the scope of this thesis:

- **A. R. Kyvik**, C. Luque-Corredera, D. Pulido, et al. „Stimuli-Responsive Functionalization Strategies to Spatially and Temporally Control Surface Properties: Michael vs Diels–Alder Type Additions". In: *The Journal of Physical Chemistry B* 122.16 (2018), pp. 4481–4490.

Publications outside the scope of this thesis:

- M. Souto, V. Díez-Cabanes, L. Yuan, et al. „Influence of the donor unit on the rectification ratio in tunnel junctions based on donor–acceptor SAMs using PTM units as acceptors". In: *Physical Chemistry Chemical Physics* 20.40 (2018), pp. 25638–25647.
- W. I. Tatkiewicz, J. Seras-Franzoso, E. Garcia-Fruitós, et al. „Surface-Bound Gradient Deposition of Protein Nanoparticles for Cell Motility Studies". In: *ACS Applied Materials & Interfaces* 10.30 (2018), pp. 25779–25786.

Publications submitted or in preparation:

- „Control of Diffusion Coefficient in Lipid Bilayers as Cell Membrane Models using an External Electrochemical Stimulus"
- „Cell Adhesion Control via Electrochemically Controlled Interfacial Reactions"
- „Immobilization of a Novel Antimicrobial Protein: a Multi-technique Study"

## Contribution in Scientific Conferences

### Poster

- **A. R. Kyvik**, C. Luque, J. Veciana, I. Ratera. „Dynamic Molecular Bio-Interfaces for Controlled Environments Towards Spatial and Temporal Control of Cell Behavior" NanoBio&Med, Barcelona, Spain, November 2016.

### Oral Presentations

- **A. R. Kyvik**, J. Veciana, K. Sugihara, D. Pulido, M. Royo, J. Guasch and I. Ratera. „Stimuli-Responsive Surfaces for Biological Applications" Bionanomed, Heraklion, Greece, September 2018

- **A. R. Kyvik**, J. Veciana, K. Sugiharay and I. Ratera. „Controlling the diffusion of supported lipid bilayers as cell membrane models in a spatio-temporal manner using a dynamic molecular interface“ Warsaw, Poland, March 2018
- **A. R. Kyvik**, C. Luque-Corredera, D. Pulido, M. Royo, J. Veciana, J. Guasch, K. Sugihara and I. Ratera. „Stimuli-responsive strategies to spatially and temporally control surface functionalization. Application in lipid bilayer immobilization“ Catalan Chemical Society, Barcelona, Spain, January 2018